Title

Interactions with and within mammalian cryptochromes regulate circadian rhythms

Author

Parico, Gian Carlo Guarino

Publication Date

2021

University of California
Santa Cruz

Interactions with and within mammalian cryptochromes regulate circadian rhythms

A dissertation submitted in partial satisfaction
of the requirements for the degree of

DOCTOR OF PHILOSOPHY

in

CHEMISTRY

by

Gian Carlo G. Parico

December 2021

The Dissertation of Gian Carlo G. Parico is approved:

_____
Professor Carrie L. Partch, Advisor

_____
Professor Seth M. Rubin, Chair

_____
Professor Doug Kellogg

_____
Peter F. Biehl
Vice Provost and Dean of Graduate Studies

TABLE OF CONTENTS

LIST OF FIGURES

LIST OF SUPPLEMENTARY FIGURES

LIST OF TABLES

Abstract

Interactions with and within mammalian cryptochromes regulate circadian rhythms

By Gian Carlo G. Parico

Organisms across all kingdoms of life have an internal 24-hour timekeeping mechanism known as circadian rhythms. In mammals, circadian rhythms arise from interlocking transcription-translation feedback loops which include the transcription factor CLOCK:BMAL1 driving the transcription of key repressors such as cryptochrome (CRY1 and CRY2) and period (PER1 and PER2). CRY1 and CRY2 are both similarly composed of a conserved structured domain known as the photolyase homology region (PHR) that is tethered to an intrinsically disordered C-terminal tail. While the PHR is necessary and sufficient to directly interact with CLOCK:BMAL1 to induce repression, the C-terminal tails also play a role in regulating circadian timing. In other CRY homologs such as *Drosophila* CRY, the PHR and C-terminal tail reversibly bind each other to create an autoinhibited conformation.

In this study, we demonstrate how interactions with CRY molecules (e.g. CLOCK interacting with CRY1/2) and interactions within a CRY protein molecule (e.g. the PHR-tail interaction) regulate circadian rhythms interactions. In Chapter 2, we describe how CRY1 and CRY2 play divergent roles in circadian timing due to structural differences in the secondary pockets of CRY1 and CRY2 that lead to differences in how strongly CRY1 or CRY2 interact with CLOCK. In Chapter 3, we determined that the CRY1 C-terminal tail makes an autoinhibitory interaction with the CRY1 PHR and inhibits the CRY1–CLOCK interaction at the secondary pocket. We also found that CRY1Δ11 (a prevalent mutation that extends circadian period and causes delayed sleep phase disorder) enhances the interaction between CRY1 and CLOCK by removing an autoinhibitory region on the CRY1 tail. In Chapter 4, we describe work with collaborators and identify how a cancer-related CRY2 mutation alters circadian timing by weakening the interaction between CRY2 and CLOCK at the secondary pocket. In the final

chapters of this dissertation, we describe how small molecules that target interactions “with and within” CRYs can modulate circadian rhythms.

Acknowledgments

I would like to thank my advisor Carrie Partch for her guidance throughout my years in graduate school. Thank you for helping me grow as a scientist and as a communicator of science (I will never look at fonts and figure colors the same again). I appreciate that you are truly invested in your trainees' personal and academic success and that your enthusiasm for science is very contagious. Thank you for being very understanding of my personal dilemmas as someone who is both a graduate student and a parent of young children. I have also admired you for having gone through the same dilemmas and I am in awe of what you have accomplished. I would also like to acknowledge the other members of my thesis committee, Seth Rubin and Doug Kellogg for their insights on my research project. I would also like to thank Jack Lee for his invaluable help with the NMR aspects of my project.

I would also want to give a big shout out to my former and current labmates (and my fellow neighbors down the hall in the Rubin lab). From random discussions in lab with the GGs, to competitive and creative group costumes at the Halloween party to various shenanigans at research conferences, these will be some of my most cherished memories. I would also like to thank Jenny Fribourgh and Sabrina Hunt for being my science big sisters. Thank you for teaching me all the things.

Finally, I would like to thank my family for their support. I would like to thank my mom and my brothers for being proud of what I have been accomplishing as a graduate student. I would like to thank my wife, Cindy, for understanding why I wanted to return to grad school and why I get so distracted by the science; living another person's dream is one of the most selfless things anybody can do. I would also like to acknowledge my children Miles and Luna. Thank you, kiddos, for always inspiring me to always be better.

The text of this thesis includes a reprint of the following previously published material:

Parico, G. C. G., and C. L. Partch. 2020. 'The tail of cryptochromes: an intrinsically disordered cog within the mammalian circadian clock', *Cell Commun Signal*, 18: 182. DOI: 10.1186/s12964-020-00665-z

Fribourgh, J. L., A. Srivastava, C. R. Sandate, A. K. Michael, P. L. Hsu, C. Rakers, L. T. Nguyen, M. R. Torgrimson, **G. C. G. Parico**, S. Tripathi, N. Zheng, G. C. Lander, T. Hirota, F. Tama, and C. L. Partch. 2020. 'Dynamics at the serine loop underlie differential affinity of cryptochromes for CLOCK:BMAL1 to control circadian timing', *eLife*, 9. DOI: 10.7554/eLife.55275

Parico, G. C. G., I. Perez, J. L. Fribourgh, B. N. Hernandez, H. W. Lee, and C. L. Partch. 2020. 'The human CRY1 tail controls circadian timing by regulating its association with CLOCK:BMAL1', *Proc Natl Acad Sci U S A*, 117: 27971-79. DOI: 10.1073/pnas.1920653117

Chan, A. B., **G. C. G. Parico**, J. L. Fribourgh, L. H. Ibrahim, M. J. Bollong, C. L. Partch, and K. A. Lamia. 2021. 'CRY2 missense mutations suppress P53 and enhance cell growth', *Proc Natl Acad Sci U S A*, 118. DOI: 10.1073/pnas.2101416118

CHAPTER 1: The tail of cryptochromes: an intrinsically disordered cog within the mammalian circadian clock.

The text of this chapter includes a reprint of the following previously published material:

Parico, G. C. G., and C. L. Partch. 2020. 'The tail of cryptochromes: an intrinsically disordered cog within the mammalian circadian clock', *Cell Commun Signal*, 18: 182. DOI: 10.1186/s12964-020-00665-z

Contributions by the co-authors are as follows: G.C.G.P. wrote the manuscript. Both authors edited and approved the final manuscript.

1.1 Abstract

Cryptochrome (CRY) proteins play an essential role in regulating mammalian circadian rhythms. CRY is composed of a structured N-terminal domain known as the photolyase homology region (PHR), which is tethered to an intrinsically disordered C-terminal tail. The PHR domain is a critical hub for binding other circadian clock components such as CLOCK, BMAL1, PERIOD, or the ubiquitin ligases FBXL3 and FBXL21. While the isolated PHR domain is necessary and sufficient to generate circadian rhythms, removing or modifying the cryptochrome tails modulates the amplitude and/or periodicity of circadian rhythms, suggesting that they play important regulatory roles in the molecular circadian clock. In this commentary, we will discuss how recent studies of these intrinsically disordered tails are helping to establish a general and evolutionarily conserved model for CRY function, where the function of PHR domains is modulated by reversible interactions with their intrinsically disordered tails.

1.2 Background

Across the kingdoms of life, the photolyase/cryptochrome family helps organisms respond or adapt to environmental stresses set in place as the sun rises and sets each day. DNA photolyases utilize a flavin adenine dinucleotide (FAD) co-factor to harvest blue light and catalyze the repair of UV-induced DNA lesions such as cyclobutane pyrimidine dimers or pyrimidine-pyrimidone (6-4) photoproducts (1, 2). In contrast to their more ancient photolyase homologs, cryptochrome (CRY) proteins are defined by the loss of DNA repair activity, while they have gained other functions in cell signaling (3). The N-terminal domain of CRY, known as the photolyase homology region (PHR), is structurally similar to photolyase; both are composed of an N-terminal α/β subdomain that forms a secondary pocket that binds an antenna chromophore such as 5,10-methenyl-tetrahydrofolate (MTHF), and a C-terminal helical subdomain that contains the FAD-binding pocket (4-6) (Figure 1.1). Some CRY PHRs, such as those from mammals, do not co-purify with chromophores, while other CRY PHRs from plants, insects or vertebrates do (7-11). Therefore, depending on co-factor binding,

chromophore-binding CRYs have photoreceptive functions while others function independently of light.

One way in which all cryptochromes differ structurally from photolyase is through the acquisition of a C-terminal intrinsically disordered region (IDR) known simply as the CRY tail (Figure 1.1A). In contrast to the highly conserved PHR domain, the tail is highly divergent between CRY paralogs and across different species (3). Changes to the FAD-binding pocket and the evolution of a C-terminal tail in CRYs may be related to their loss of DNA repair activity. For example, the flexible tail of *Drosophila* CRY (dCRY) uses a hydrophobic motif to dock into its FAD-binding pocket in a manner that is similar to the (6-4) photolesion substrate binding to photolyase (7, 8) (Figure 1.1B). In the absence of light, dCRY is maintained in this docked and autoinhibited state, which prevents complex formation of the PHR domain with its clock protein target TIMELESS (dTIM) (12-14) and the E3 ubiquitin ligase JETLAG (15). Light induces photoreduction of the FAD co-factor to alleviate the dCRY PHR-tail interaction, allowing the dCRY PHR domain to regulate the proteasomal degradation of dTIM (16). Since levels of dTIM represent an important state variable of circadian rhythms in *Drosophila*, the dCRY photoreceptor thus entrains circadian rhythms to the environment via light. The photoreceptive function of dCRY is thus mediated by a transition of the dCRY tail from order to disorder (7), suggesting that the dCRY tail exhibits cryptic disorder and unfolds to allow dCRY to perform its function (17). There is now evidence that the presence of an intrinsically disordered C-terminal tail and ability to reversibly bind its respective PHR domain are defining features of CRY function from plants to insects to mammals (14, 18, 19) (Figure 1.1C).

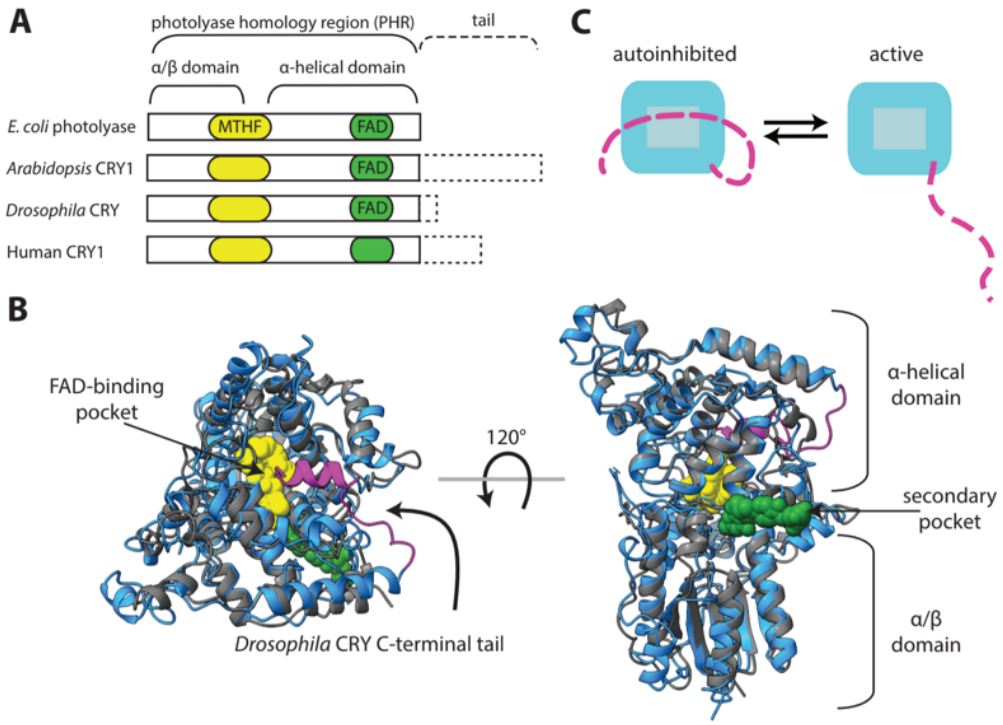

Figure 1.1. The photolyase/cryptochrome PHR domain is highly conserved but the intrinsically disordered C-terminal tail is divergent.

(A) *E. coli* photolyase and the PHR domains of *Arabidopsis* CRY1, *Drosophila* CRY, and human CRY1 (solid rectangle) are highly conserved and share an α/β domain containing a secondary pocket (yellow) that can non-covalently bind a secondary antenna chromophore such as MTHF, and an α-helical domain that contains an FAD-binding pocket (green). Not all CRYs bind both chromophores, and while *Drosophila* CRY binds FAD, human CRY1 does not co-purify with chromophores. Photolyase lacks a C-terminal tail, while cryptochromes from diverse species possess divergent tails (dashed rectangles). ***(B)*** An overlay of the crystal structures of *E. coli* photolyase (PDB 1DNP, gray) and *Drosophila* CRY (PDB 4K03, cyan, tail in magenta) highlighting structural similarities. Both possess an FAD-binding pocket that binds FAD (yellow), and a secondary pocket. The secondary antenna chromophore (MTHF, green) binds to the secondary pocket of photolyase but not *Drosophila* CRY. The C-terminal tail of *Drosophila* CRY (magenta) interacts with the FAD pocket. ***(C)*** Cartoon demonstrating how the PHR-tail (cyan/magenta) interaction yields a reversible autoinhibited state. CRY is in an active state when the PHR domain and tail are unbound from each other.

This commentary aims to discuss recent findings regarding the disordered C-terminal tail in mammalian CRYs and its role in regulating circadian rhythms. In mammals, CRYs serve as light-independent transcriptional repressors in the transcription-translation feedback loop that generates circadian rhythms (20). The heterodimeric transcription factor CLOCK:BMAL1, composed of circadian locomotor output cycles kaput (CLOCK) and brain

and muscle, ARNT-like protein 1 (BMAL1), promotes the transcription of its own repressors, PERIOD (PER1/PER2) and CRY (CRY1/CRY2) (21) (Figure 1.2A). This core feedback loop is interlocked with several interdependent transcriptional feedback loops that collectively regulate approximately 40% of the genome in a circadian manner, giving rise to an oscillation of gene expression with a circadian period of about 24 hours (22) (Figure 1.2B). Because of the widespread nature of circadian transcriptional control, the disruption or alteration of circadian rhythms is linked to metabolic, cardiovascular, psychiatric and sleep-phase disorders (23). For instance, one prevalent human allele affects splicing of the CRY1 tail (*CRY1Δ11*) to cause a form of familial delayed sleep phase disorder (DSPD) (24). Although this recent study provides compelling evidence that the CRY1 tail plays a powerful role in regulating human physiology and behavior, relatively little is known about the mechanism(s) by which the tails regulate cryptochrome function in mammals. While crystal structures have laid the foundation for a mechanistic understanding of how the PHR domains of CRY1 and CRY2 generate and regulate circadian rhythms (7, 10, 25-28), none of these structures have shed light on the role of mammalian CRY tails. Recently, a combination of biochemical studies, innovations in protein NMR spectroscopy, and new chemical biology tools have begun to shed some light on CRY tail function in circadian rhythms.

1.3 Main Text

1.3.1 Mapping CRY function from its PHR domain to its unstructured C-terminal tail.

The CRY PHR domain interacts with two distinct sites on the transcription factor CLOCK:BMAL1 to directly repress its activity. During the day, CLOCK:BMAL1 recruits transcriptional co-activators like CREB-binding protein (CBP) or p300 through the transactivation domain (TAD) on the distal C-terminus of BMAL1 (29, 30). CRY proteins accumulate and enter the nucleus in the evening, allowing the coiled-coil (CC)-helix on the PHR domain to interact directly with the BMAL1 TAD (30, 31) (Figure 1.2C). Competition for mutually exclusive binding sites on BMAL1 allows CRY to sequester the TAD from co-activators; however, the affinity of CRY1 for the TAD is modest, so an additional interaction

that stabilizes CRY recruitment to the transcription factor is required for effective repression (30). Recruitment is mediated by the secondary pocket on the PHR domain, which docks onto the PER-ARNT-SIM (PAS) domain core of CLOCK:BMAL1 (composed of CLOCK PAS-A, CLOCK PAS-B, BMAL1 PAS-A BMAL1 PAS-B), specifically through the CLOCK PAS-B domain (25, 26) (Figure 1.2C). The multivalent binding of CRY to CLOCK:BMAL1 is important, as mutants that decrease affinity for the BMAL1 TAD or CLOCK PAS-B significantly reduce CRY-mediated repression, while mutation of both interfaces completely eliminates repression (32, 33). A few amino acid substitutions fine-tune protein dynamics at the secondary pocket interface between the two mammalian CRY paralogs to contribute to their differential affinity for the PAS domain core (25) and largely confers paralog-specific effects on circadian period (34). Altogether, quantitative analyses of CRY, CLOCK and BMAL1 mutants support an emerging model in which circadian period is correlated with the affinity of CRY for CLOCK:BMAL1—the higher the affinity that CRY has for the CLOCK:BMAL1, the longer circadian period becomes (30).

Even though the CRY PHR domain makes critical contacts with CLOCK:BMAL1 to directly repress its activity, numerous studies over the last decade have demonstrated that the CRY C-terminal tails also contribute to regulation of circadian rhythms. In human CRY1 (hCRY1), the intrinsically disordered C-terminal tail is 95 amino acid residues long, including part of exon 10 and the entire length of exons 11 and 12, while the mouse CRY1 (mCRY1) tail is a bit longer due to a 20 amino acid duplication within exon 10 (Figure 1.3A). The CRY2 tail is a bit shorter at only 80 residues in length and highly divergent in sequence from the CRY1 tail (3). While genetic complementation studies have established that the CRY PHR domain is necessary and sufficient to reconstitute circadian rhythms in *Cry1*$^{-/-}$;*Cry2*$^{-/-}$ cells, the absence of C-terminal tails affects the amplitude and period of reconstituted rhythms (35, 36). Furthermore, swapping the CRY2 tail onto the CRY1 PHR domain is sufficient to shorten circadian period, while swapping the CRY1 tail onto CRY2 lengthens circadian period in

these rescue assays (35), suggesting that sequences encoded by one or both of these tails have the capability to modulate the function of the PHR domains, possibly in different ways.

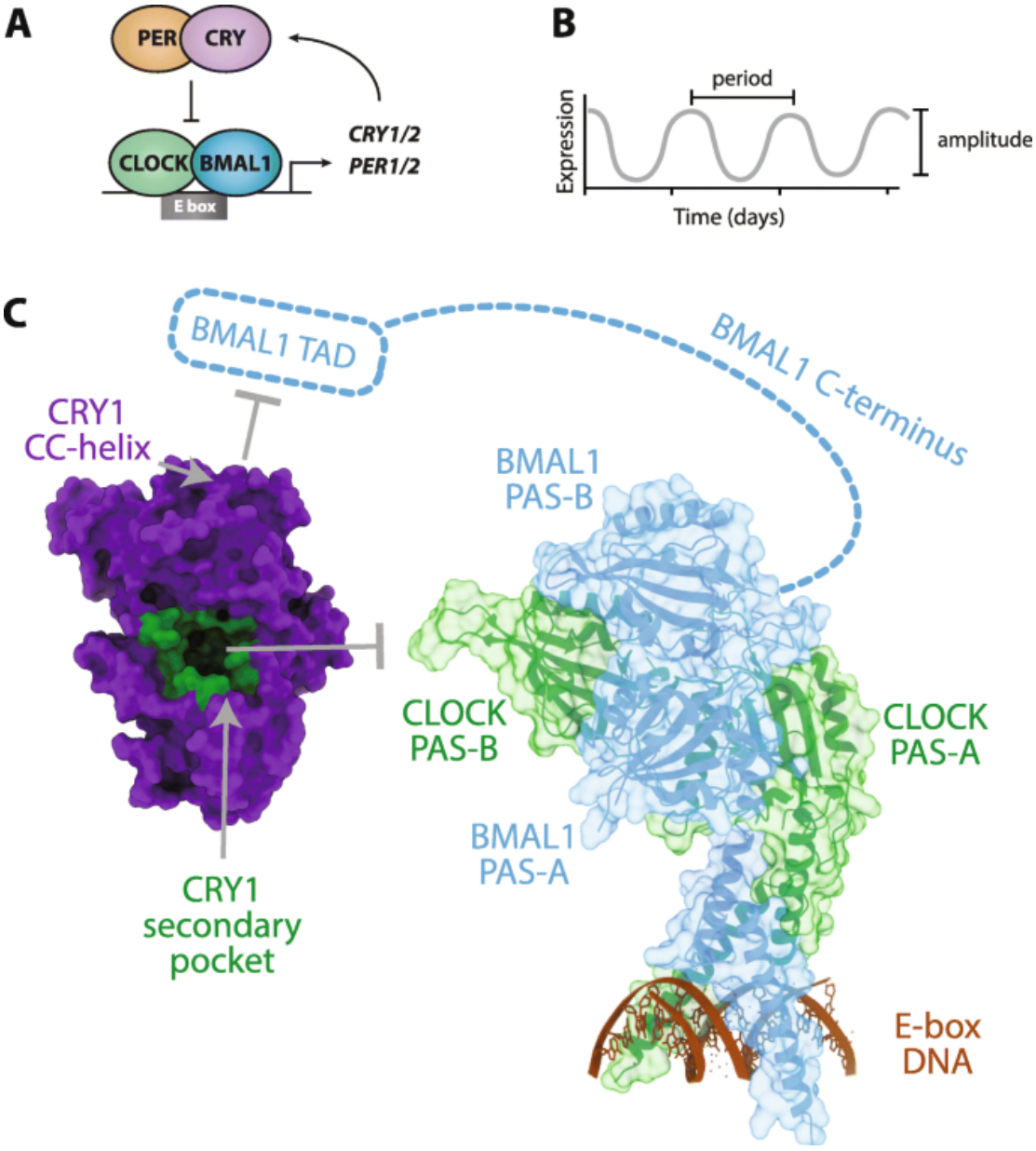

Figure 1.2. Circadian rhythms are driven by interlocked transcription-translation feedback loops to control rhythmic gene expression.

(A) The transcription factor CLOCK:BMAL1 (green/blue) promotes transcription of its repressors PER (light orange) and CRY (purple), which ultimately feedback to bind CLOCK:BMAL1 and induce repression. ***(B)*** The feedback loops result in rhythmic gene

expression on the circadian timescale. The distance between peaks determines the period, while the distance from peak to trough is measured as the amplitude, or the strength of the timekeeping cue. ***(C)*** Crystal structure of CRY1 (PDB 5T5X, purple) and CLOCK:BMAL1 (PDB 4F3L, CLOCK in light green, BMAL1 in cyan) highlighting regions and domains that interact with each other. The CRY1 CC-helix interacts with the BMAL1 TAD (cyan dashed rectangle) on the disordered BMAL1 C-terminus (cyan dashed line) and the CRY1 secondary pocket (dark green) interacts with CLOCK PAS-B. These multivalent interactions between CRY1 and CLOCK:BMAL1 are necessary to induce repression.

Post-translational modifications of both CRY tails also influence circadian rhythms, providing the first clues as to how the function of these intrinsically disordered tails could be regulated *in vivo*. IDPs and IDRs are typically enriched for post-translational modifications and this is most likely due to their accessibility as substrates for modifying enzymes or as binding partners for cell signaling (37). Priming phosphorylation of the CRY2 tail at S557 by the dual specificity tyrosine-phosphorylation-regulated kinase 1A (DYRK1A) and subsequent phosphorylation upstream at S553 by glycogen synthase kinase 3β (GSK-3β) promotes the proteasomal degradation of CRY2 (38, 39). Ablating this phosphorylation with the CRY2 S557A mutant lengthens circadian rhythms *in vivo*, most likely due to stabilization of CRY2 (40). Similarly, phosphorylation at mouse CRY1 at S588 or its corresponding phosphomimetic mutation, S588D, have a stabilizing effect against proteasomal degradation and extend circadian period (41). Stabilization of the CRY1 S588D mutant against proteasomal degradation is likely mediated by decreased association with FBXL3 (42, 43), a substrate adaptor for Skp-Cullin-Fbox (SCF) E3 ligases, and a concomitant increase in association with the deubiquitinase USP7 (also known as the Herpesvirus-associated ubiquitin-specific protease, HAUSP) (43). In addition, phosphorylation of S588 affects the intracellular distribution and rate of nuclear entry of CRY1 (36, 44), which may result from the proximity of S588 to a potential nuclear localization sequence (NLS) on the tail (45). Mutations at this putative NLS, such as the K585A/R586A double mutant, affect cellular distribution of mCRY1 (45); however, it has yet to be determined whether the K585A/R586A mutant influences circadian rhythms. Therefore, the intrinsically disordered tails are regulated

reversibly by phosphorylation to influence the stability and intracellular distribution of cryptochromes.

1.3.2 Night owls provide the first clues for how the CRY1 tail controls human circadian timing.

Recently, the intrinsically disordered tail of CRY1 was linked directly to regulation of circadian timekeeping and delayed sleep phase disorder in humans by discovery of a mutant allele in the *CRY1* gene (24). Delayed sleep phase disorder is characterized by later than normal sleep onset times (a.k.a. night owl behavior), which is often linked to a longer than average circadian period (46). The mutant allele is caused by a single nucleotide polymorphism, *CRY1* c.1657+3A>C, also known as *CRY1Δ11*, that alters the 5' splice site downstream from exon 11 and leads to alternate splicing that removes the 24 amino acids encoded by exon 11 from the disordered tail (24) (Figure 1.3A). The delayed sleep phase disorder phenotype is autosomal dominant and manifests in carriers of the mutant allele, which occurs with a frequency of 0.1% to 0.6% in the human population, and as high as 1 in 75 people in certain populations (24). The discovery of this mutant allele, with its powerful control over circadian rhythms and sleep timing, offered an unprecedented opportunity to explore the mechanism by which the intrinsically disordered tail regulates CRY1 function.

People with the *CRY1Δ11* allele have an increase in the period of their circadian rhythms, which is recapitulated in cellular studies by genetic complementation of the mutant allele in *Cry1*$^{-/-}$;*Cry2*$^{-/-}$ mouse fibroblasts (24). Strikingly, CRY1Δ11 is a more effective transcriptional repressor of CLOCK:BMAL1 than wild-type CRY1, as determined by chromatin occupancy and expression profiles of CLOCK:BMAL1-dependent genes (24). Enhanced repression by the mutant allele could arise from increased stability of the mutant protein, enhanced nuclear entry or retention, and/or tighter binding to CLOCK:BMAL1. Wild-type and mutant proteins exhibited similar stability in cellular assays, but CRY1Δ11 had a moderate increase in nuclear accumulation compared to wild-type protein (24). In addition, CRY1Δ11 appeared to bind CLOCK:BMAL1 more tightly, as determined by enhanced

association with CLOCK:BMAL1 in co-immunoprecipitation assays (24). These findings are consistent with the emerging model that tighter binding of CRY leads to a longer circadian period (30). Because the mutant allele directly modifies only the intrinsically disordered C-terminal tail, and not the PHR domain where cryptochromes have been shown to directly interact with CLOCK:BMAL1, these data suggest that loss of exon 11 relieves some type of autoinhibitory role of the tail between the CRY1 PHR domain and CLOCK:BMAL1, thus making CRY1Δ11 a more effective repressor.

1.3.3 The CRY1 tail serves an autoinhibitory function that controls affinity for CLOCK:BMAL1

Over the last two decades, numerous groups have demonstrated that PHR-tail interactions serve autoinhibitory roles in cryptochromes from other species, such as *Drosophila* (12-14) and *Arabidopsis* (19). Experimental evidence for a direct interaction between the PHR domain of a mammalian CRY and its disordered tail was first published in 2005 (18). A recent study revisited intramolecular interactions of mammalian cryptochromes in more depth with fluorescence polarization (FP) binding assays and nuclear magnetic resonance (NMR) spectroscopy to identify the molecular determinants by which the CRY1 tail directly interacts with its PHR domain (47).

It can be quite challenging to study long IDPs at atomic resolution with conventional protein NMR methods such as the ^{1}H-^{15}N heteronuclear single quantum coherence (HSQC) experiment due to the lack of unique chemical environments in the disordered protein that severely restrict peak dispersion in the ^{1}H dimension of HSQC spectra (18, 47). By contrast, innovative direct ^{13}C-detected experiments such as the ^{13}C-^{15}N CON not only increase peak dispersion, but also allow for detection of proline residues that are typically enriched in IDPs, thus improving biophysical studies of long, native-like IDPs (48). Related ^{13}C-detected triple resonance experiments such as the 3D (HACA)N(CA)NCO and (HACA)N(CA)CON aid in assigning peaks for individual residues for long IDPs (48). The use of CON NMR methods was critical for enabling the identification of residues on the CRY1 tail that exhibit chemical

shift perturbations upon addition of the PHR domain; these residues are primarily centered in short linear motifs in exons 10 and 11, which also correspond to the minimal regions on the tail needed for binding to the PHR domain by FP-based binding assays (47) (Figure 1.3A). This highlights the powerful role that NMR spectroscopy can play in the study of intrinsically disordered proteins by providing atomic resolution data to map binding and quantify the dynamics of IDPs in the absence of crystal structures.

Although NMR mapping studies identified PHR-dependent chemical shift perturbations in exons 10 and 11 of the intact CRY1 tail, exon 11 is necessary and sufficient to complete with CLOCK:BMAL1 binding *in vitro* (47). Given that CLOCK:BMAL1 engages with two distinct binding sites on the CRY1 PHR domain (25, 26, 30), both interactions were explored as potential site(s) of competition; exon 11 clearly competes with the CLOCK PAS-B for the CRY1 secondary pocket, and not the interaction between the CRY1 CC-helix and the BMAL1 TAD (47). Interestingly, exon 11 shares properties with other intrinsically disordered inhibitory modules, such as a similar length (10-40 amino acids) and a susceptibility to being altered in splicing events (49). The mutant allele gives rise to CRY1Δ11 protein, which lacks this autoinhibitory module and binds the transcription factor several-fold tighter (47), thus providing a molecular rationale for increased repression of CLOCK:BMAL1 and *CRY1Δ11*-mediated delayed sleep phase disorder (24).

Compared to both CRY1Δ11 and the isolated PHR domain, full-length CRY1 has a decreased association rate constant (k_{on}) rather than an increased dissociation rate constant (k_{off}) for binding to the PAS domain core of CLOCK:BMAL1 (47). This decrease in k_{on} rather than an increase in k_{off} is seen in other proteins that contain an autoinhibitory domain tethered by a flexible linker (50). Moreover, the decreased k_{on} for CRY1 falls within the diffusion-limited range (10^4 – 10^6 $M^{-1}s^{-1}$) (51), suggesting that the flexible tail interacts transiently with the PHR domain to regulate association with CLOCK:BMAL1. However, it is still not known exactly where on the PHR domain or exon 11 that the two make direct contact. It is possible that the CRY1 tail regulates CLOCK:BMAL1 binding through an allosteric

mechanism, although it seems parsimonious to suggest that exon 11 and CLOCK PAS-B have overlapping binding sites in or near the CRY1 secondary pocket.

1.3.4 Regulation of CRY1 by its disordered tail is influenced by other clock protein factors such as PER2

Other clock protein components, such as the co-repressor PERIOD (PER), also associate with CRY PHR domains to modulate their association with CLOCK:BMAL1 (25, 34). The approximately one-hundred residue-long CRY-binding domain (CBD) of PER2 is also intrinsically disordered, but forms several short helices upon association with CRY1 or CRY2, where it wraps in an extended fashion around the PHR domain in proximity to both the CC-helix and the secondary pocket where CLOCK PAS-B (and possibly CRY1 exon 11) binds (25, 27, 28) (Figure 1.3B). The PER2 CBD efficiently displaces the isolated CRY1 tail from binding to its PHR domain, suggesting that the PER2 CBD and the CRY1 tail have at least some overlap in their binding sites on the PHR domain (47) (Figure 1.3C). While both are intrinsically disordered, PER2 CBD binds to CRY1 with nanomolar affinity (28), while the CRY1 tail binds to its PHR domain with low micromolar affinity in *trans* (47). While the intrinsically disordered PER2 CBD becomes ordered when bound to CRY1 (25, 27, 28), it remains unknown whether the CRY1 tail makes similar conformational changes. If regions of the CRY1 tail undergo an ordered state when bound to the CRY1 PHR, then it can be assumed that the presence of a PER binding partner induces partial unfolding of the CRY1 molecule and awakens the cryptic disorder of the CRY1 tail. The striking ability of PER2 to compete with the tail for the PHR domain suggests a specific window of temporal regulation for regulation of CRY1 by its intrinsically disordered tail. CRY1 is associated with PER proteins, CRY2, and other epigenetic factors in the ~1.9 MDa ‘early’ repressive complex (52), whereas CRY1 represses CLOCK:BMAL1 without PER proteins in the ‘late’ repressive complex at the initiation of each circadian cycle at dawn (53). Therefore, differences in activity between CRY1 and CRY1Δ11 with regards to the autoinhibitory tail may be most pertinent in the context of the ‘late’ repressive complex when PER proteins are absent.

The role for post-transcriptional and post-translational modifications in modulating the CRY1 PHR-tail interaction needs to be explored further. Several DNA-PK-dependent phosphorylation sites have been identified in the CRY1 tail (41) (Figure 1.3A). Of these, two sites flank exon 11 and the third is located at residue S588 (mouse numbering; residue 568 in hCRY1). The role of the two phosphorylation sites near exon 11 has not yet been studied, but the phosphomimetic mutation S588D that stabilizes CRY1 protein, located in exon 12 of the tail, does not affect the affinity between the CRY1 tail and the PHR domain (47). This suggests that any phenotypic effects of the CRY1 S588D mutant in extending CRY1 half-life and circadian period might be independent of the PHR-tail interaction. On the other hand, the S588D mutation could subtly affect the conformation of the CRY1 tail to antagonize access of the ubiquitin ligase FBXL3 to the FAD-binding pocket of the PHR domain to protect CRY1 from proteasomal degradation (42, 43). Finally, there is also a possibility that alternative splicing could regulate CRY1 tail function be deleting exon 11 in a signal or tissue-specific manner. Other IDRs involved in autoinhibition are often regulated by alternate splicing events to modulate protein interactions and cell signaling pathways (49, 54). It remains to be seen whether regulated alternative splicing in a wild-type *Cry1* genetic background could yield CRY1Δ11 protein to modulate circadian timing. The human CRY1Δ11 allele is therefore an example of a permanently altered splicing event in which exon 11 is skipped, thus removing an autoinhibitory module from the tail, and altering the circadian period (24).

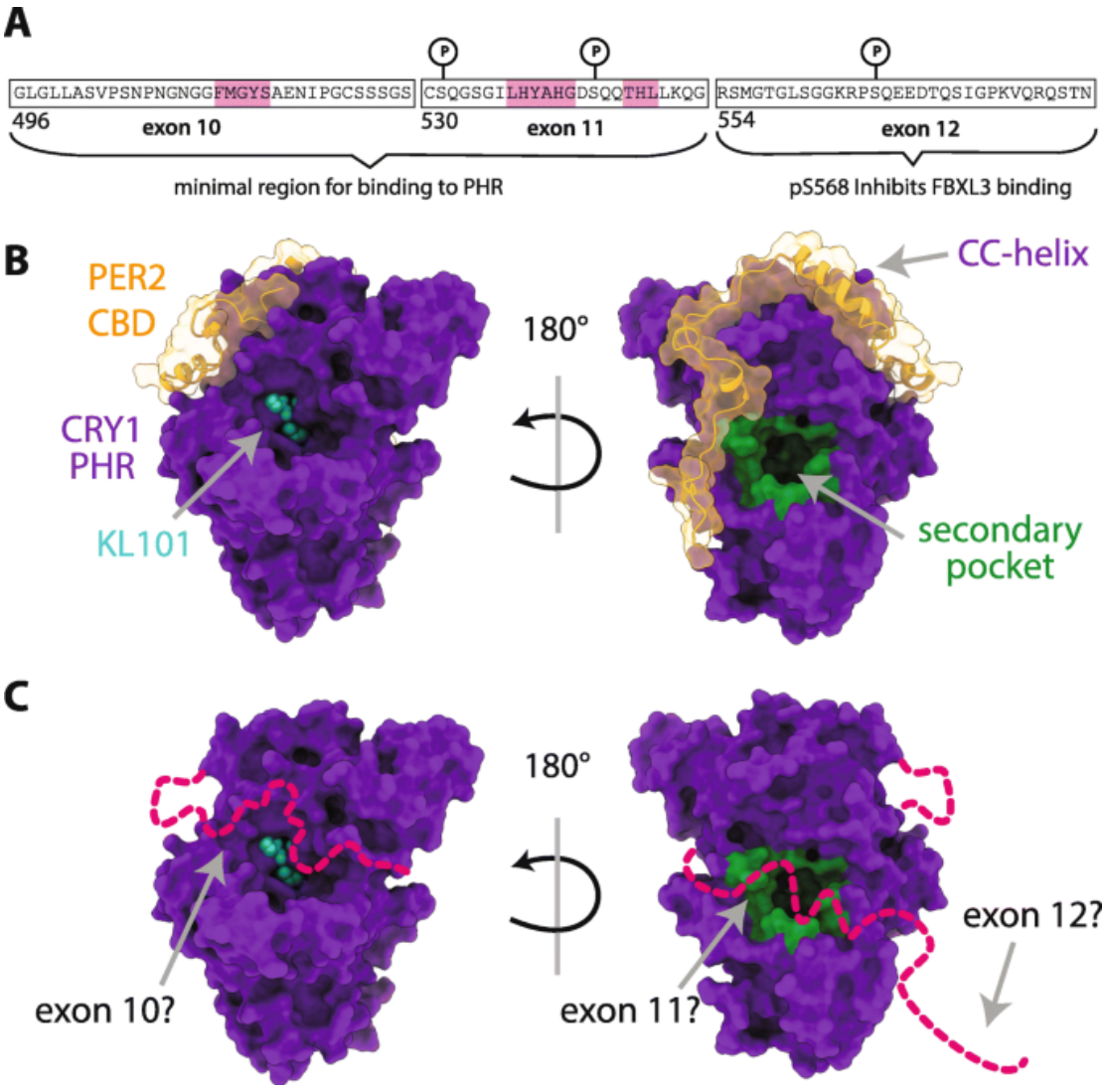

Figure 1.3. The human CRY1 tail regulates multiple sites on the PHR domain

(A) The hCRY1 tail is composed of exons 10 (residues 496-529), exon 11 (residues 530-553), and exon 12 (residues 554-586). NMR chemical shift mapping identified distinct linear motifs in exons 10 and 11 (pink) that may be involved in binding directly to the PHR domain (47). DNA-PK-dependent phosphorylation sites in exons 11 and 12 are marked below a circled 'P' (41). ***(B)*** The PER2 CBD (orange) wraps around the CRY1 PHR domain (purple) near regions where the hCRY1 tail might also interact, such as the CC-helix, FAD-binding pocket (KL101 is a CRY1-selective ligand, cyan) and the secondary pocket (green) in PDBs 6KX6, KL101-bound and 6OF7, PER2 CBD-bound. Thin dashed lines indicate flexible regions on the PHR domain that were missing density. ***(C)*** A possible model for how the tail (magenta) might bind to both the FAD-binding pocket and the secondary pocket on the PHR domain in the absence of PER proteins. Exon 10 has been implicated at binding near the FAD-binding pocket (55), while exon 11 inhibits CLOCK PAS-B binding at the secondary pocket and deletion of exon 12 has no effect on affinity of the tail for the PHR domain (47).

1.3.5 The circadian clock can be modulated by small molecules that rely on CRY tails for their activity

Nearly a decade ago, cryptochromes entered the chemical biology arena with the discovery of KL001, a small molecule that stabilizes CRY half-life by occupying the FAD-binding pocket of CRY to compete with binding of the ubiquitin ligase FBXL3 (10, 56, 57). More recently, Hirota and colleagues identified two new molecules that target CRY1 or CRY2 to extend circadian period by selectively extending the half-life of their respective target (55). Although they similarly bind to the highly conserved FAD-binding pocket of their respective CRY targets, both small molecules require the intrinsically disordered tails for selectivity and the stabilization of cryptochromes in cells (55). To identify how the tails contribute to selectivity, chimeras swapping regions of the tail between CRY1 and CRY2 revealed that the PHR domain-proximal exon 10 is required for selectivity in cells (55). Given that the molecules target the FAD-binding pocket on the opposite side of the PHR domain from the secondary pocket, these data suggest that the short, linear binding motifs identified in exons 10 and 11 may target discrete sites on the PHR domain (Figure 1.3C). Overall, the intrinsically disordered tails of cryptochromes now appear to be compelling new targets for modulating the circadian clock.

1.4 Conclusions

As direct repressors of CLOCK:BMAL1 transcriptional activity, cryptochromes sit at the nexus of circadian rhythms as central regulators of the vast transcriptional network of the mammalian circadian clock (58). With these new insights into cryptochrome structure and dynamics, we are now poised to understand the roles that their intrinsically disordered tails play in fine-tuning circadian timing. Similar to cryptochromes from other species (9, 12, 13, 19), the mammalian CRY1 tail also binds to its PHR domain to form an autoinhibited conformation (47). Identifying the autoinhibitory function of exon 11 and a molecular rationale for *CRY1Δ11*-mediated delayed sleep phase disorder should motivate the development of

inhibitors that to modulate the CRY1–CLOCK interaction at the secondary pocket to restore normal circadian timing (and sleep onset) or reset circadian rhythms (24, 47). Conversely, small molecule ligands that target the FAD-binding pocket to modulate circadian rhythms also appear to suggest an important functional role for CRY tails near the FAD-binding pocket (55).

New insights into the critical role of the CRY1 tail should pave the way for understanding how the divergent intrinsically disordered tails contribute to functional differences between CRY1 and CRY2. For instance, while the respective PHR domains of CRY1 and CRY2 share 80% identity, their tails are highly divergent. Swapping as few as seven residues between the CRY1 and CRY2 PHR domains can make one paralog resemble the other with regards to CLOCK:BMAL1 binding (25, 34). However, to completely recapitulate paralog-specific effects on circadian period, the tails of each paralog also need to be swapped (34), highlighting the remarkable role that these intrinsically disordered regions play in regulation of circadian timing and beyond.

For instance, post-translational modifications of the CRY1 tail help shift the phase of circadian rhythms after DNA damage; exposure to genotoxic stress increases phosphorylation of the mouse CRY1 tail at S588, thus stabilizing CRY1 to extend circadian period length (43). Studying this and other factors that modify or compete for the CRY tails will provide further insights into how intrinsically disordered CRY tails act as signaling hubs to transduce signals between the molecular circadian clock and different pathways.

1.5 References

1. Brash DE, Franklin WA, Sancar GB, Sancar A, & Haseltine WA (1985) Escherichia coli DNA photolyase reverses cyclobutane pyrimidine dimers but not pyrimidine-pyrimidone (6-4) photoproducts. *J Biol Chem* 260(21):11438-11441.
2. Todo T*, et al.* (1993) A new photoreactivating enzyme that specifically repairs ultraviolet light-induced (6-4)photoproducts. *Nature* 361(6410):371-374.

3. Michael AK, Fribourgh JL, Van Gelder RN, & Partch CL (2017) Animal Cryptochromes: Divergent Roles in Light Perception, Circadian Timekeeping and Beyond. *Photochemistry and Photobiology* 93(1):128-140.

4. Brautigam CA*, et al.* (2004) Structure of the photolyase-like domain of cryptochrome 1 from Arabidopsis thaliana. *P Natl Acad Sci USA* 101(33):12142-12147.

5. Huang Y*, et al.* (2006) Crystal structure of cryptochrome 3 from Arabidopsis thaliana and its implications for photolyase activity. *Proc Natl Acad Sci U S A* 103(47):17701-17706.

6. Park HW, Kim ST, Sancar A, & Deisenhofer J (1995) Crystal-Structure of DNA Photolyase from Escherichia-Coli. *Science* 268(5219):1866-1872.

7. Czarna A*, et al.* (2013) Structures of Drosophila Cryptochrome and Mouse Cryptochrome1 Provide Insight into Circadian Function. *Cell* 153(6):1394-1405.

8. Levy C*, et al.* (2013) Updated structure of Drosophila cryptochrome. *Nature* 495(7441):E3-E4.

9. Ozturk N*, et al.* (2009) Comparative photochemistry of animal type 1 and type 4 cryptochromes. *Biochemistry* 48(36):8585-8593.

10. Xing W*, et al.* (2013) SCF(FBXL3) ubiquitin ligase targets cryptochromes at their cofactor pocket. *Nature* 496(7443):64-68.

11. Zoltowski BD*, et al.* (2019) Chemical and structural analysis of a photoactive vertebrate cryptochrome from pigeon. *Proc Natl Acad Sci U S A* 116(39):19449-19457.

12. Busza A, Emery-Le M, Rosbash M, & Emery P (2004) Roles of the Two Drosophila CRYPTOCHROME Structural Domains in Circadian Photoreception. *Science* 304(5676):1503-1506.

13. Dissel S*, et al.* (2004) A constitutively active cryptochrome in Drosophila melanogaster. *Nature Neuroscience* 7(8):834-840.

14. Rosato E*, et al.* (2001) Light-dependent interaction between Drosophila CRY and the clock protein PER mediated by the carboxy terminus of CRY. *Curr Biol* 11(12):909-917.

15. Ozturk N, Selby CP, Annayev Y, Zhong DP, & Sancar A (2011) Reaction mechanism of Drosophila cryptochrome. *P Natl Acad Sci USA* 108(2):516-521.

16. Lin C, Top D, Manahan CC, Young MW, & Crane BR (2018) Circadian clock activity of cryptochrome relies on tryptophan-mediated photoreduction. *Proc Natl Acad Sci U S A* 115(15):3822-3827.

17. Jakob U, Kriwacki R, & Uversky VN (2014) Conditionally and transiently disordered proteins: awakening cryptic disorder to regulate protein function. *Chem Rev* 114(13):6779-6805.

18. Partch CL, Clarkson MW, Ozgür S, Lee AL, & Sancar A (2005) Role of structural plasticity in signal transduction by the cryptochrome blue-light photoreceptor. *Biochemistry* 44(10):3795-3805.

19. Yang HQ*, et al.* (2000) The C termini of Arabidopsis cryptochromes mediate a constitutive light response. *Cell* 103(5):815-827.

20. Griffin EA, Staknis D, & Weitz CJ (1999) Light-independent role of CRY1 and CRY2 in the mammalian circadian clock. *Science (New York, N.Y.)* 286(5440):768-771.

21. Partch CL, Green CB, & Takahashi JS (2014) Molecular architecture of the mammalian circadian clock. *Trends in Cell Biology* 24(2):90-99.

22. Zhang R, Lahens NF, Ballance HI, Hughes ME, & Hogenesch JB (2014) A circadian gene expression atlas in mammals: implications for biology and medicine. *Proceedings of the National Academy of Sciences of the United States of America* 111(45):16219-16224.

23. Bass J & Lazar MA (2016) Circadian time signatures of fitness and disease. *Science* 354(6315):994-999.

24. Patke A*, et al.* (2017) Mutation of the Human Circadian Clock Gene CRY1 in Familial Delayed Sleep Phase Disorder. *Cell* 169(2):203-215.e213.

25. Fribourgh JL*, et al.* (2020) Dynamics at the serine loop underlie differential affinity of cryptochromes for CLOCK:BMAL1 to control circadian timing. *Elife* 9.

26. Michael AK*, et al.* (2017) Formation of a repressive complex in the mammalian circadian clock is mediated by the secondary pocket of CRY1. *Proceedings of the National Academy of Sciences* 114(7):1560-1565.

27. Nangle SN*, et al.* (2014) Molecular assembly of the period-cryptochrome circadian transcriptional repressor complex. *eLife* 3:e03674.

28. Schmalen I*, et al.* (2014) Interaction of circadian clock proteins CRY1 and PER2 is modulated by zinc binding and disulfide bond formation. *Cell* 157(5):1203-1215.

29. Lee Y*, et al.* (2010) Coactivation of the CLOCK-BMAL1 complex by CBP mediates resetting of the circadian clock. *J Cell Sci* 123(Pt 20):3547-3557.

30. Xu H*, et al.* (2015) Cryptochrome 1 regulates the circadian clock through dynamic interactions with the BMAL1 C terminus. *Nature Structural & Molecular Biology* 22(6):476-484.

31. Czarna A*, et al.* (2011) Quantitative Analyses of Cryptochrome-mBMAL1 Interactions MECHANISTIC INSIGHTS INTO THE TRANSCRIPTIONAL REGULATION OF THE MAMMALIAN CIRCADIAN CLOCK. *Journal of Biological Chemistry* 286(25):22414-22425.

32. Kiyohara YB*, et al.* (2006) The BMAL1 C terminus regulates the circadian transcription feedback loop. *Proc Natl Acad Sci U S A* 103(26):10074-10079.

33. Sato TK*, et al.* (2006) Feedback repression is required for mammalian circadian clock function. *Nature genetics* 38(3):312-319.

34. Rosensweig C*, et al.* (2018) An evolutionary hotspot defines functional differences between CRYPTOCHROMES. *Nature Communications* 9(1):1138.

35. Khan SK*, et al.* (2012) Identification of a Novel Cryptochrome Differentiating Domain Required for Feedback Repression in Circadian Clock Function. *Journal of Biological Chemistry* 287(31):25917-25926.

36. Li Y, Xiong W, & Zhang EE (2016) The ratio of intracellular CRY proteins determines the clock period length. *Biochemical and Biophysical Research Communications* 472(3):531-538.

37. Darling AL & Uversky VN (2018) Intrinsic Disorder and Posttranslational Modifications: The Darker Side of the Biological Dark Matter. *Front Genet* 9:158.

38. Harada Y, Sakai M, Kurabayashi N, Hirota T, & Fukada Y (2005) Ser-557-phosphorylated mCRY2 is degraded upon synergistic phosphorylation by glycogen synthase kinase-3 beta. *J Biol Chem* 280(36):31714-31721.

39. Kurabayashi N, Hirota T, Sakai M, Sanada K, & Fukada Y (2010) DYRK1A and glycogen synthase kinase 3beta, a dual-kinase mechanism directing proteasomal degradation of CRY2 for circadian timekeeping. *Mol Cell Biol* 30(7):1757-1768.

40. Hirano A*, et al.* (2014) In vivo role of phosphorylation of cryptochrome 2 in the mouse circadian clock. *Mol Cell Biol* 34(24):4464-4473.

41. Gao P*, et al.* (2013) Phosphorylation of the Cryptochrome 1 C-terminal Tail Regulates Circadian Period Length. *The Journal of Biological Chemistry* 288(49):35277-35286.

42. Liu AC*, et al.* (2007) Intercellular coupling confers robustness against mutations in the SCN circadian clock network. *Cell* 129(3):605-616.

43. Papp SJ*, et al.* (2015) DNA damage shifts circadian clock time via Hausp-dependent Cry1 stabilization. *Elife* 4.

44. Liu N & Zhang EE (2016) Phosphorylation Regulating the Ratio of Intracellular CRY1 Protein Determines the Circadian Period. *Frontiers in Neurology* 7.

45. Chaves I*, et al.* (2006) Functional evolution of the photolyase/cryptochrome protein family: importance of the C terminus of mammalian CRY1 for circadian core oscillator performance. *Mol Cell Biol* 26(5):1743-1753.

46. Jones CR, Huang AL, Ptacek LJ, & Fu YH (2013) Genetic basis of human circadian rhythm disorders. *Experimental Neurology* 243:28-33.

47. Parico GCG*, et al.* (2020) The human CRY1 tail controls circadian timing by regulating its association with CLOCK:BMAL1. *Proc Natl Acad Sci U S A* 117(45):27971-27979.

48. Bastidas M, Gibbs EB, Sahu D, & Showalter SA (2015) A primer for carbon-detected NMR applications to intrinsically disordered proteins in solution. *Concepts in Magnetic Resonance Part A* 44(1):54-66.

49. Trudeau T*, et al.* (2013) Structure and Intrinsic Disorder in Protein Autoinhibition. *Structure* 21(3):332-341.

50. Olsen SK*, et al.* (2004) Insights into the molecular basis for fibroblast growth factor receptor autoinhibition and ligand-binding promiscuity. *Proceedings of the National Academy of Sciences of the United States of America* 101(4):935-940.

51. Zhou H-X & Bates PA (2013) Modeling Protein Association Mechanisms and Kinetics. *Current opinion in structural biology* 23(6).

52. Aryal RP*, et al.* (2017) Macromolecular Assemblies of the Mammalian Circadian Clock. *Molecular Cell* 67(5):770-782.e776.

53. Koike N*, et al.* (2012) Transcriptional Architecture and Chromatin Landscape of the Core Circadian Clock in Mammals. *Science (New York, N.Y.)* 338(6105):349-354.

54. Buljan M*, et al.* (2013) Alternative splicing of intrinsically disordered regions and rewiring of protein interactions. *Current Opinion in Structural Biology* 23(3):443-450.

55. Miller S*, et al.* (2020) Isoform-selective regulation of mammalian cryptochromes. *Nat Chem Biol*.

56. Hirota T*, et al.* (2012) Identification of small molecule activators of cryptochrome. *Science (New York, N.Y.)* 337(6098):1094-1097.

57. Nangle S, Xing W, & Zheng N (2013) Crystal structure of mammalian cryptochrome in complex with a small molecule competitor of its ubiquitin ligase. *Cell Research* 23(12):1417-1419.

58. Takahashi JS (2017) Transcriptional architecture of the mammalian circadian clock. *Nat Rev Genet* 18(3):164-179.

CHAPTER 2: Dynamics at the serine loop underlie differential affinity of cryptochromes for CLOCK:BMAL1 to control circadian timing.

The text of this chapter includes a reprint of the following previously published material:

Fribourgh, J. L., A. Srivastava, C. R. Sandate, A. K. Michael, P. L. Hsu, C. Rakers, L. T. Nguyen, M. R. Torgrimson, **G. C. G. Parico**, S. Tripathi, N. Zheng, G. C. Lander, T. Hirota, F. Tama, and C. L. Partch. 2020. 'Dynamics at the serine loop underlie differential affinity of cryptochromes for CLOCK:BMAL1 to control circadian timing', *eLife*, 9.
DOI: 10.7554/eLife.55275

Contributions by the co-authors are as follows (J.L.F, A.S. and C.R.S contributed equally to this manuscript):

1. J.L.F contributed: Conceptualization, Resources, Formal analysis, Validation, Investigation, Visualization, Writing - original draft, Writing - review and editing.
2. A.S contributed: Conceptualization, Resources, Formal analysis, Validation, Investigation, Visualization, Writing - original draft, Writing - review and editing.
3. C.R.S contributed: Resources, Formal analysis, Validation, Investigation, Visualization, Writing - original draft, Writing - review and editing
4. A.K.M. contributed: Conceptualization, Resources, Investigation
5. P.L.S. contributed: Resources, Investigation
6. C.R contributed.: Resources, Investigation
7. L.T.N contributed: Resources, Data curation
8. M.R.T contributed: Resources, Data curation
9. G.C.G.P contributed: Resources, Data curation
10. S.T. contributed: Resources, Validation
11. N.Z. contributed: Conceptualization, Supervision
12. G.C.L. contributed: Supervision, Funding acquisition, Validation, Visualization, Writing - original draft, Writing - review and editing.
13. T.H contributed: Conceptualization, Supervision, Writing - original draft, Writing - review and editing
14. F.T contributed: Contribution: Conceptualization, Supervision, Funding acquisition, Validation, Visualization, Writing - original draft, Writing - review and editing
15. C.L.P contributed: Conceptualization, Supervision, Funding acquisition, Visualization, Writing - original draft, Project administration, Writing - review and editing

The candidate, Gian Carlo Parico, performed the following contributions for the development of this manuscript: Purified recombinant proteins and collected *in vitro* binding data.

All authors edited and approved the manuscript.

Manuscript acknowledgments:

We would like to thank the beamline staff at 23-ID-D for their assistance during data collection at the Advanced Photon Source. We thank JC Ducom at Scripps Research High Performance Computing and C Bowman at Scripps Research for computational support, as well as B Anderson at the Scripps Research Electron Microscopy Facility for microscopy support. We would like to thank Carla Green for the plasmid encoding the mouse Cry2 7M mutant.

2.1 Abstract

Mammalian circadian rhythms are generated by a transcription-based feedback loop in which CLOCK:BMAL1 drives transcription of its repressors (PER1/2, CRY1/2), which ultimately interact with CLOCK:BMAL1 to close the feedback loop with ~24 hr periodicity. Here we pinpoint a key difference between CRY1 and CRY2 that underlies their differential strengths as transcriptional repressors. Both cryptochromes bind the BMAL1 transactivation domain similarly to sequester it from coactivators and repress CLOCK:BMAL1 activity. However, we find that CRY1 is recruited with much higher affinity to the PAS domain core of CLOCK:BMAL1, allowing it to serve as a stronger repressor that lengthens circadian period. We discovered a dynamic serine-rich loop adjacent to the secondary pocket in the photolyase homology region (PHR) domain that regulates differential binding of cryptochromes to the PAS domain core of CLOCK:BMAL1. Notably, binding of the co-repressor PER2 remodels the serine loop of CRY2, making it more CRY1-like and enhancing its affinity for CLOCK:BMAL1.

2.2 Introduction

The circadian clock links our behavior and physiology to the daily light-dark cycle, providing a timekeeping system that ensures cellular processes are performed at an optimal time of day. At the cellular level, circadian rhythms are driven by a set of interlocked transcription-based feedback loops that take ~24 hr to complete. The basic helix-loop-helix PER-ARNT-SIM (bHLH-PAS) domain-containing transcription factor CLOCK:BMAL1 forms the positive component of the core feedback loop (1). Several CLOCK:BMAL1 target genes (*Per1*, *Per2*, *Cry1*, *Cry2*) constitute the repressive components that close the core feedback loop (2). PER and CRY proteins interact with each other to form a large complex with the kinase CK1δ and enter the nucleus after a delay to bind directly to CLOCK:BMAL1 and inhibit its activity (3, 4). An additional feedback loop comprising the ROR and REV-ERB nuclear receptors controls the rhythmic expression of a subset of genes, including *Bmal1* (5).

Cryptochromes are essential for circadian rhythms, as *Cry1*$^{-/-}$; *Cry2*$^{-/-}$ mice are arrhythmic in constant darkness (6, 7). Despite their high sequence and structural similarity (8), CRY1 and CRY2 appear to have distinct roles in the molecular circadian clock because *Cry1*$^{-/-}$ mice have a short period, while *Cry2*$^{-/-}$ mice have a long period (6, 7). Using a genetic reconstitution assay of *Cry1*$^{-/-}$; *Cry2*$^{-/-}$; *Per2*^{Luc} fibroblasts, we previously showed that tuning CRY1 affinity for CLOCK:BMAL1 can control circadian period (9, 10); notably, the period lengthens when CRY1 binds more tightly to CLOCK:BMAL1, suggesting that the strength of CRY repression contributes to period determination. Consistent with this, CRY1 is a stronger repressor of CLOCK:BMAL1 than CRY2 (11) and a recently discovered allele of CRY1 that enhances its repressive function also lengthens circadian period (12) in humans, providing a conceptual framework to understand why the presence of one CRY or the other influences circadian period.

Another notable difference between the two cryptochromes is the delay in expression of *Cry1* with respect to *Cry2* and the *Per* genes in the core feedback loop (4, 13). The delayed expression of CRY1 is consistent with its recruitment to DNA-bound CLOCK:BMAL1 in two distinct phases: a minor peak at circadian time (CT) 16–20 as part of the large PER-CRY repressive complexes (3, 4), and a major peak later at CT0-4 that is independent of CRY2 and the PER proteins (14). However, the delayed timing of CRY1 expression does not account for its differential regulation of circadian period, because expressing *Cry2* from a minimal *Cry1* promoter that recapitulates this delay in *Cry1*$^{-/-}$; *Cry2*$^{-/-}$; *Per2*^{Luc} fibroblasts or the suprachiasmatic nucleus (SCN) ex vivo still drives CRY2-like short periods (15, 16). These data demonstrate that the differences between CRY1 and CRY2 that influence circadian period are encoded by their protein structure and/or dynamics to influence their repressive function.

What structural features of CRY1 and CRY2 might lead to differential functions in the circadian clock? Both cryptochromes are defined by a highly conserved photolyase homology region (PHR) domain and divergent C-terminal tails that are intrinsically disordered (17).

Deletion or post-translational modification of the unstructured tails can modulate rhythm amplitude and period length (12, 18-20), but the PHR domain is required to generate circadian rhythmicity (21). We recently showed that CRY1 interacts directly with both CLOCK and BMAL1 through two distinct regions on its PHR domain (10, 22) (Figure 2.1A). The CC helix binds directly to the transactivation domain (TAD) of BMAL1 (Figure 2.1B), sequestering it from coactivators to directly repress CLOCK:BMAL1 activity (10, 23). However, repression also relies on the recruitment of CRY1 to the PAS domain core of CLOCK:BMAL1 via the CLOCK PAS-B domain, which docks into the evolutionarily conserved secondary pocket on the CRY1 PHR domain (22).

Here we leverage these insights to identify a key biochemical feature that distinguishes the different repressive capabilities of CRY1 and CRY2. We found that changes in the structure and dynamics of the serine loop, located adjacent to the secondary pocket, allow CRY1 to bind the PAS domain core of CLOCK:BMAL1 with significantly higher affinity than CRY2. Moreover, substitutions in the serine loop and secondary pocket between CRY1 and CRY2 that influence circadian period (16) are sufficient to modulate affinity of the CRY PHR domain for CLOCK:BMAL1. Finally, we found that the CRY-binding domain (CBD) of PER2 differentially remodels the structure of the serine loop of CRY1 and CRY2 to help equalize their affinity for the PAS domain core of CLOCK:BMAL1. These data provide a biochemical rationale linking the repressive function of CRY2 to the PER proteins, as well as explaining how CRY1 can act as a repressor of CLOCK:BMAL1 in the presence or absence of PER proteins.

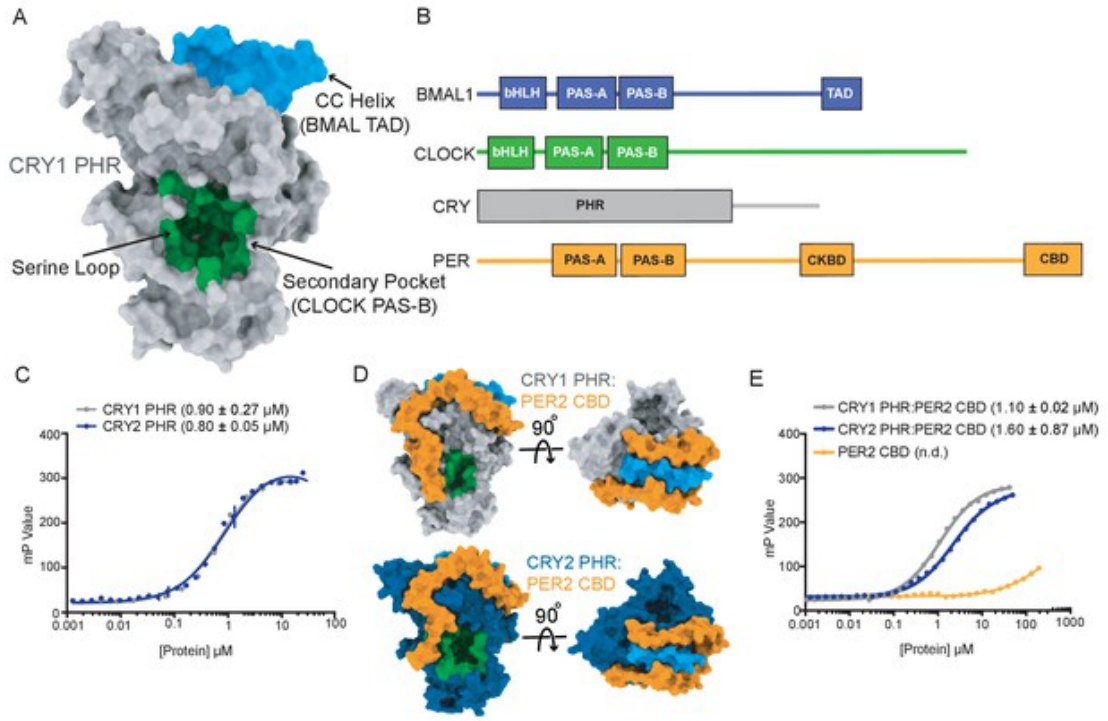

Figure 2.1. CRY1 and CRY2 bind similarly to the BMAL1 transactivation domain.

(A) Crystal structure of the CRY1 PHR domain (PDB: 5T5X) highlighting the CC helix (BMAL1/2 TAD binding interface (blue)) and the secondary pocket (CLOCK PAS-B binding interface (green)). This is the standard orientation of the CRY1 and CRY2 PHR domain used as a reference for all other views. ***(B)*** Domain schematic of core clock proteins. bHLH, basic helix-loop-helix; PAS, PER-ARNT-SIM domain, TAD, transactivation domain; PHR, photolyase homology region; CKBD, Casein Kinase Binding Domain; CBD, CRY-binding domain. ***(C)*** Fluorescence polarization (FP) assay of 5,6-TAMRA-labeled BMAL1 minimal TAD (residues 594–626) binding to CRY1 PHR (gray), replotted from Gustafson et al. (2017), and CRY2 PHR (blue). Mean ± SD data shown from one representative assay of n = 3 independent assays. Binding constants (mean ± SD) derived from n = 3 assays. ***(D)*** Crystal structures of CRY1 PHR:PER2 CBD (PDB: 4CT0) and CRY2 PHR:PER2 CBD (PDB: 4U8H) with the PER2 CBD (orange), CRY1 PHR (gray) and CRY2 PHR (blue), in the standard view and 90° rotated to show the BMAL1 TAD binding interface (blue). ***(E)*** FP assay of 5,6-TAMRA-labeled BMAL1 TAD binding to preformed CRY1 PHR:PER2 CBD (gray), CRY2 PHR:PER2 CBD (blue) or PER2 CBD (orange). Mean ± SD data shown from one representative assay of n = 3 independent assays. Binding constants shown (mean ± SD) were derived from n = 3 assays. n.d., not determined.

2.3 Results

2.3.1 CRY1 and CRY2 bind similarly to the transactivation domain of BMAL1

To begin to understand how CRY1 and CRY2 differ as circadian repressors, we first compared their affinity for the BMAL1 TAD, as sequestration of the TAD from coactivators represents a direct mechanism by which cryptochromes inhibit transcriptional activation by CLOCK:BMAL1 (9, 10). We used a fluorescence polarization (FP)-based binding assay with a TAMRA-labeled BMAL1 TAD probe to demonstrate that CRY1 and CRY2 PHR domains both bind to the TAD with a similar, low micromolar affinity (Figure 2.1C). However, the repressive clock protein complexes that accumulate early in the night contain both CRYs with the associated co-repressor PER proteins (3). Crystal structures of CRY1 and CRY2 PHR domains in their PER2-bound state (24, 25) reveal that the PER2 CBD wraps around the CC helix of both CRYs (Figure 2.1D), coming into close proximity of the BMAL1 TAD binding site (10, 23). To determine if PER2 binding influences the affinity of CRY1 or CRY2 for the BMAL1 TAD, we assessed binding of preformed CRY PHR:PER2 CBD complexes or the PER2 CBD alone to the TAMRA-BMAL1 TAD probe. Despite the intimate association of PER2 with the BMAL-binding site on CRY1 and CRY2, we found that both CRY:PER2 complexes bound the TAD similarly to the free CRYs, while the PER2 CBD displayed negligible affinity for the TAD (Figure 2.1E). These data establish that both CRY proteins have a similar capacity to sequester the TAD, either independently or in complex with the PER2 CBD, to repress CLOCK:BMAL1 activity (10).

2.3.2 CRY1 binds substantially tighter than CRY2 to the PAS domain core of CLOCK:BMAL1

We next focused our attention on the PAS domain core of CLOCK:BMAL1, as we previously showed that the PAS-B domain of CLOCK docks into an evolutionarily conserved secondary pocket on CRY1 (22). Importantly, binding of CRY1 to these two distinct sites on CLOCK and BMAL1 is important for repression, as disruption of either interface hinders

repression by CRY1, while disruption of both interfaces eliminates the ability of CRY1 to act as a repressor for CLOCK:BMAL1 (10, 26).

We initially monitored formation of stable CRY PHR-CLOCK:BMAL1 complexes by gel filtration chromatography using a construct of CLOCK:BMAL1 that contains the structured basic helix-loop-helix DNA-binding domain and tandem PAS domains (bHLH-PAS) that form the structured core of the heterodimer (27). Upon mixing the bHLH-PAS heterodimer with an excess of either CRY1 or CRY2 PHR domain, we observed that only CRY1 could bind CLOCK:BMAL1 tightly enough to co-migrate on the column (Figure 2.2 A,B and Supplementary Figure 2.1), suggesting that there was a substantial difference in affinity of the CRY PHR domains for the PAS domain core of CLOCK:BMAL1. To quantitatively analyze this difference in affinity, we performed bio-layer interferometry (BLI) with the biotinylated tandem PAS-AB domain core of the heterodimer, titrating in free CRY1 or CRY2 PHR domain to assess differences in CRY binding (Figure 2.2C,D). We found that the CRY1 PHR domain binds with a remarkably high affinity (K_d65 ± 6 nM), while CRY2 bound with approximately 20-fold lower affinity (K_d1.2 ± 0.2 μM).

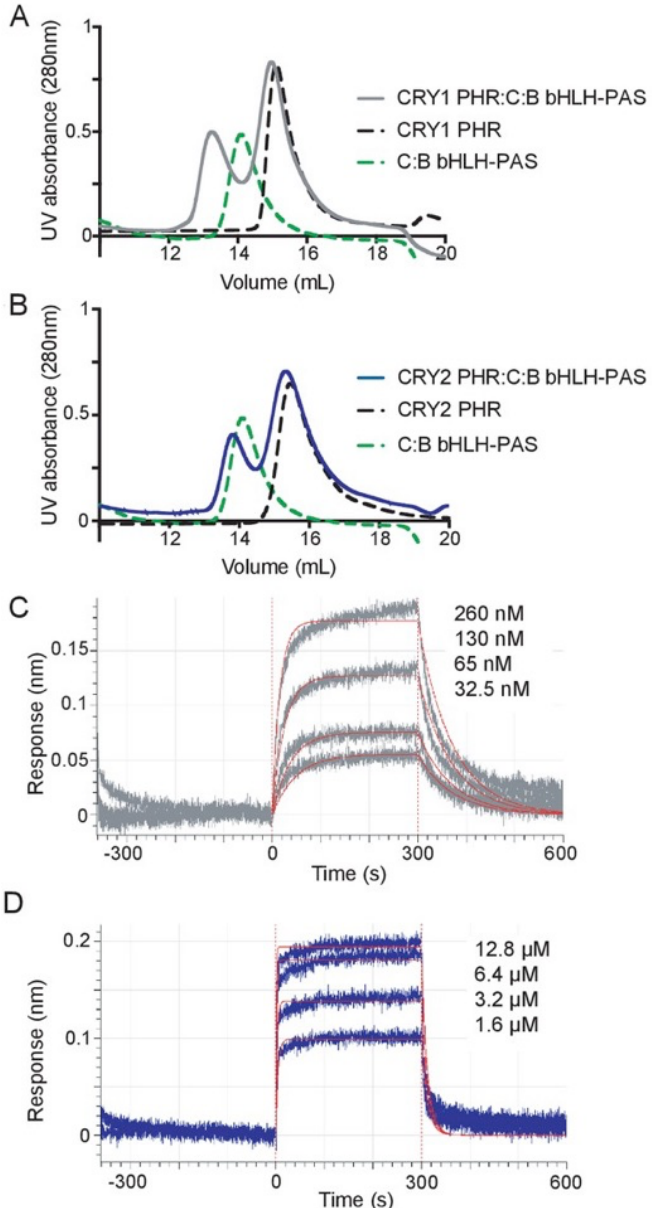

Figure 2.2. CRY1 binds more tightly to PAS domain core of CLOCK:BMAL1 than CRY2.

*(**A**)* Gel filtration analysis of complex formation of CRY1 PHR domain mixed with the CLOCK:BMAL1 (C:B) bHLH-PAS heterodimer. CRY1 PHR domain (black), C:B bHLH-PAS (green), or CRY1 PHR domain incubated with C:B bHLH-PAS (gray) were run on a Superdex 200 10/300 GL column. ***(B)*** Gel filtration analysis of complex formation of CRY2 PHR domain mixed with the CLOCK:BMAL1 (C:B) bHLH-PAS heterodimer. CRY2 PHR domain (black), C:B bHLH-PAS (green), or CRY2 PHR domain incubated with C:B bHLH-PAS (blue) were run on a Superdex 200 10/300 GL column. C-D, BLI data for CRY1 PHR domain (gray, ***(C)*** or CRY2 PHR domain (blue, ***(D)*** binding to immobilized, biotinylated CLOCK:BMAL1 PAS-AB. Inset values represent the concentrations of CRY for individual binding reactions, top to

bottom. Vertical red dashed lines indicate the beginning of association and dissociation. The red solid line is the nonlinear least squares fitting. CRY1 PHR domain K_d = 65 ± 6 nM; CRY2 PHR domain K_d = 1.2 ± 0.2 μM (mean of two independent experiments). Data shown from one representative experiment of n = 2 assays. See Supplementary Figure 2.1 for additional information related to this figure.

The low micromolar affinity of CRY2 for the CLOCK:BMAL1 PAS domain core likely explains its inability to form a stable complex with CLOCK:BMAL1 under the conditions used in this assay. To see if reconstituting the multivalent interactions with CLOCK and BMAL1 could stabilize CRY2 binding to CLOCK:BMAL1, we assayed for stable complex formation in a sample containing the CRY2 PHR domain with a heterodimer containing the truncated CLOCK bHLH-PAS domain and full-length BMAL1 by gel filtration. In contrast to the isolated bHLH-PAS core, the CRY2 PHR domain now co-eluted with the CLOCK:BMAL1 heterodimer, as visualized by SDS-PAGE of the peak fraction (Supplementary Figure 2.1). Therefore, although CRY2 binds with much lower affinity to the PAS core of CLOCK:BMAL1 than CRY1, the addition of a second binding interface with the BMAL1 TAD facilitates stable complex formation with the CRY2 PHR domain. Together, these data suggest that differential affinity of CRY PHR domains for the CLOCK:BMAL1 PAS domain core might underlie their distinctive repressive roles in the circadian clock.

2.3.3 The serine loop differentially gates access to the secondary pocket of CRY1 and CRY2

To explore the structural basis for differential binding of CRY PHR domains to the CLOCK:BMAL1 PAS domain core, we examined existing crystal structures of mouse CRY1 and CRY2 PHR domains (22, 28) to identify sites of structural variability. Despite sharing 80% identity (91% homology) and having PHR domain structures with a Cα Root Mean Square Deviation (RMSD) of 1.4 Å (Figure 2.3A and Supplementary Figure 2.2), molecular dynamics (MD) simulations of the PHR domains revealed that CRY1 exhibits a higher degree of flexibility at the serine loop (Figure 2-3B) and adjacent secondary pocket, which binds to CLOCK PAS-B (22). In addition, another loop (E196-S207) adjacent to the serine loop

showed decreased flexibility in simulations of CRY2 compared to CRY1. Proline residues at positions P219 and P225 in CRY2 replace an aspartate (D201) and serine (S207) in CRY1 at this loop, which could be responsible for the lower flexibility of this region in CRY2. The other side of the PHR domain in both CRYs also contains flexible regions, including the phosphate loop (p-loop) (29) and a proximal loop containing a nuclear localization signal (NLS) (Figure 2.3B and Supplementary Figure 2.2).

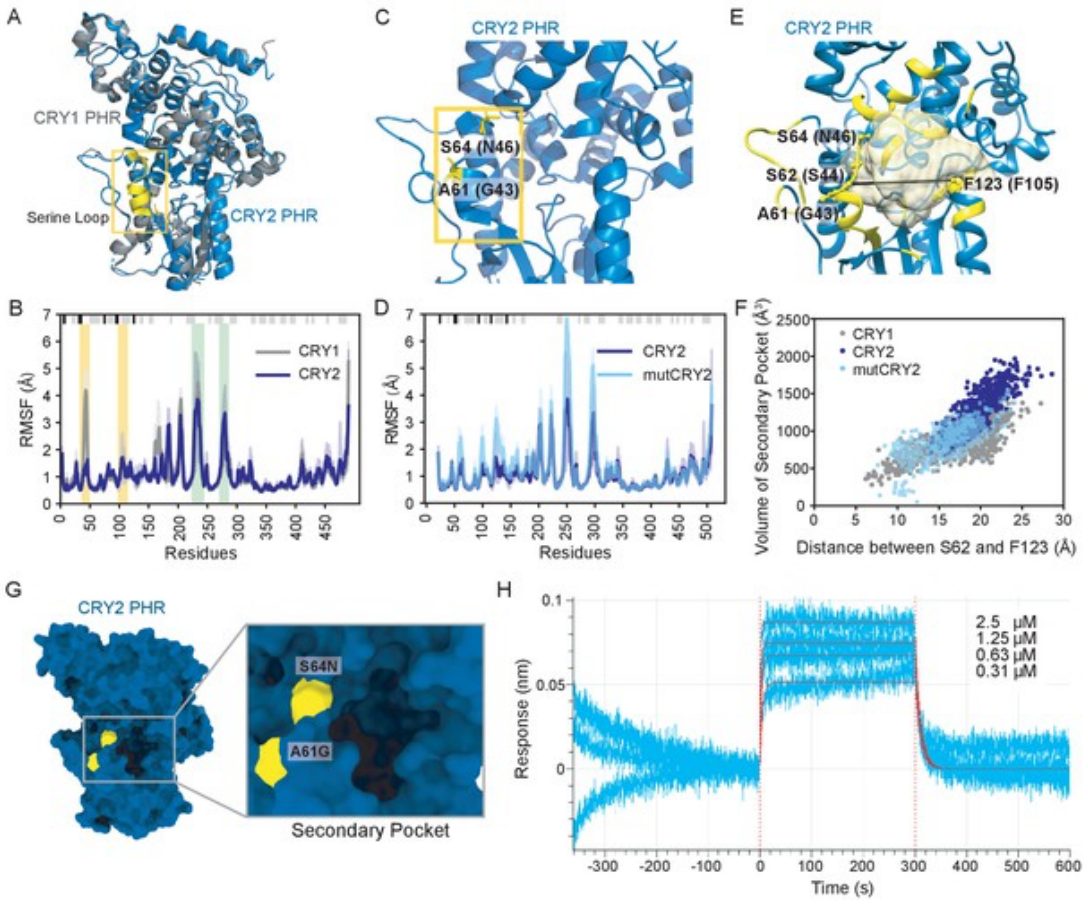

Figure 2.3. Flexibility of the serine loop controls size of the secondary pocket and CLOCK:BMAL1 binding in CRYs.

(A) Structural alignment of CRY1 PHR domain (PDB: 5T5X) and CRY2 PHR domain (PDB: 4I6E). The serine loops are highlighted in yellow and boxed. ***(B)*** Root mean square fluctuation (RMSF) values obtained from MD simulations for Cα atoms of each residue in CRY1 PHR domain (gray) or CRY2 PHR domain (blue) from n = 3 independent runs. The mean RMSF is depicted in dark shades with the variation between minimum and maximum values in light shades. Secondary structure is depicted at the top of the plot (α-helix, gray; β-

strand, black) and residues in the serine loop and p-loop are shaded yellow and green, respectively. ***(C)*** Crystal structure of CRY2 PHR domain (PDB: 4I6E) highlighting two residues that vary from CRY1 on the serine loop adjacent to the secondary pocket. ***(D)*** RMSF values for the wild-type CRY2 PHR domain (dark blue) or mutCRY2 (S64N/A61G, light blue), as above. ***(E)*** Volume of the secondary pocket (yellow cartoon and surface representation) and residues used for distance measurements of the secondary pocket opening in CRY2 (S62 and F123, depicted) or CRY1 (S44 and F105, by conservation). Black line indicates distance measured. ***(F)*** Scatter plot of secondary pocket volume ($Å^3$) versus opening distance between CRY2 S62 and F123 (or S44 and F105 in CRY1). ***(G)*** Surface representation of the CRY2 PHR domain crystal structure (PDB: 4I6E) with the two mutations highlighted in yellow on the serine loop. ***(H)*** BLI data for CRY2 2M PHR domain (blue) binding to immobilized, biotinylated CLOCK:BMAL1 PAS-AB. Inset values represent the concentrations of CRY for individual binding reactions, top to bottom. Vertical red dashed lines indicate the beginning of association and dissociation. Red solid line, nonlinear least squares fitting to a one-site binding model. Calculated K_d for CRY2 2M PHR domain = 343.8 ± 26.9 nM (mean ± SD from n = 2 independent assays). See Supplementary Figure 2.2-4 for additional information related to this figure.

In support of the differential dynamics observed in MD simulations, neither of the two crystal structures of the apo CRY1 PHR domain contain density for the serine loop (22, 30). By contrast, this loop forms a short α-helix in structures of apo or FAD-bound CRY2 (28). Only two amino acids differ between CRY1 and CRY2 in this loop: G43/A61 and N46/S64 (using CRY1/CRY2 numbering, (Figure 2.3C). Since the substitution of alanine for glycine at position 61 likely stabilizes the helical content of CRY2 in this loop (31), we created an in silico mutant of CRY2 swapping in the two CRY1 residues (A61G/S64N, mutCRY2) to see if this would increase flexibility of the serine loop. Comparing the Root Mean Square Fluctuations (RMSF) for wild type and mutCRY2 in MD simulations revealed that flexibility of the serine loop and secondary pocket increased in the mutant (Figure 2.3D), suggesting that minor local perturbations to the serine loop could substantially impact CRY function. Moreover, reconstitution of *Cry1*$^{-/-}$*; Cry2*$^{-/-}$*; Per2*^{Luc} cells with a G43A/N46S CRY1 mutant (swapping CRY2 residues at this site into CRY1) lead to a significantly shorter period than with wild-type CRY1 (16), consistent with a more CRY2-like, weaker repressor activity (32, 33).

To further explore the difference in the conformational ensemble of CRY1 and CRY2, we calculated the Kullback-Leibler (KL) divergence of the phi, psi, and chi1 dihedral angle

distribution for all of the residues (Supplementary Figure 2.2). KL divergence is used to quantitatively describe the differences in the conformational states of residues in two equilibrium ensembles (34). A high KL divergence for a particular residue signifies that its conformational state shows considerable difference between the two ensembles in torsional space. Several residues throughout the CRY1 and CRY2 PHR domains show high KL divergence; in particular, the residues with the highest divergence concentrate in and around the secondary pocket, corresponding to CRY1 residues W52, Q79, D82, Y100, R127, and W390 (Supplementary Figure 2.2). Notably, the comparison of conformational ensembles for wild-type CRY2 and the A61G/N64S CRY1-swapped CRY2 mutant reveals high divergence at the secondary pocket and, to a lesser extent, throughout the rest of the protein (Supplementary Figure 2.2). These data suggest that the effect of substitutions in the secondary pocket that alter its rigidity may extend beyond the secondary pocket to influence the overall dynamical ensemble of CRY PHR domains.

Based on these data, alterations in the structure and dynamics of the serine loop may influence access to the secondary pocket that is located immediately adjacent to this loop. To quantify how variations in the serine loop of CRY1/CRY2 alter the conformational landscape of the secondary pocket, we calculated the volume of the pocket and the distance between center of mass of residue S62 and F123 in CRY2, located on the opposite sides of the pocket (corresponding to S44 and F105 in CRY1), for each of the independent MD trajectories (Figure 2.3E). This analysis revealed an approximately linear relationship between the interatomic distance of the loops that line the secondary pocket and its volume (Figure 2.3F). The overall distribution for CRY2 measurements clustered toward the upper right region of the plot, demonstrating that CRY2 samples a larger pocket volume (1215 ± 275 $Å^3$) as well as having larger opening to the pocket. The distribution of CRY1 measurements revealed a larger variation in distance across the pocket, likely due to the flexibility of the serine loop, but consistently had a smaller pocket volume (876 ± 217 $Å^3$, $p<0.001$, Wilcoxon ranksum test) compared to CRY2. As predicted from its enhanced flexibility, the in silico mutant of the

CRY2 serine loop (i.e., A61G/N64S in mutCRY2) resulted in a significant change in its overall distribution towards a smaller volume of the secondary pocket (868 ± 230 $Å^3$, $p<0.001$, Wilcoxon ranksum test) and shorter distances across the pocket, much like we found for CRY1.

We determined the free energy landscape (FEL) of the PHR domains using the same volumes and distances as reaction coordinates to show that the low energy basin for CRY1 corresponds to the smaller volume and shorter distances as compared to the CRY2 FEL (Supplementary Figure 2.2). In the case of the CRY1-like mutCRY2, the FEL shows a striking similarity to CRY1, with an expanded low energy basin and minimum corresponding to lower values of volume and distance (Supplementary Figure 2.2). We further compared the volume and distances for the frames corresponding to the energy minimum in each FEL (see link for Supplementary file 1a). Here again, the values corresponding to CRY1 and mutCRY2 showed a distinct similarity, whereas CRY2 had a higher value for both volume and distance. These observations suggest that decreasing the flexibility of the serine loop correlates with an increased volume of the secondary pocket, which could play a role in the decreased affinity of CRY2 for the PAS domain core of CLOCK:BMAL1.

We sought to experimentally test if mutations on the serine loop and around the secondary pocket could alter the affinity of CRY2 for the PAS domain core of CLOCK:BMAL1. We first utilized the CRY2 7M mutant (16), which incorporates seven mutations in and around the serine loop and the secondary pocket to swap CRY2 residues with their corresponding residues from CRY1 (Supplementary Figure 2.3). We chose this mutant to characterize biochemically because genetic reconstitution of circadian rhythms in *Cry1*$^{-/-}$; *Cry2*$^{-/-}$; *Per2*^{Luc} cells demonstrated that CRY2 7M was sufficient to largely recapitulate a CRY1-like repression phenotype and period (16). In line with this cell-based observation, we found that the CRY2 7M mutant had a 10-fold enhancement in affinity for the CLOCK:BMAL PAS domain core, as determined by BLI (Supplementary Figure 2.3). To further establish the contribution of substitutions on serine loop to CLOCK:BMAL1 binding,

we purified the CRY2 2M mutant corresponding to mutCRY2 (A61G/N64S) and measured its affinity for the CLOCK:BMAL1 PAS domain core. As predicted by our MD simulations, we found that simply swapping two residues on the serine loop increased CRY affinity for CLOCK:BMAL1 by ~4 fold (Figure 2.3G-H).

To characterize interactions at the serine loop that might be responsible for its conformational diversity, we measured the occurrence of hydrogen bonds formed by loop residues during the MD simulations. A comparison of frequently occurring hydrogen bonds among apo CRY1, CRY2 and mutCRY2 revealed that the serine loop in CRY2 is stabilized primarily by hydrogen bonds *within* the loop residues, as might be expected from the short helical structure present in the starting model. On the other hand, we observed fewer hydrogen bonds within the loop in CRY1 and mutCRY2 trajectories (see link for Supplementary file 1b). Furthermore, we observed that N64 forms hydrogen bonds with D400 and E401 in mutCRY2 that are not frequently seen in the CRY2 simulations. Interestingly, in its native environment, N46 of CRY1 also forms hydrogen bonds with its corresponding residues at these positions (E382 and E383) with high frequency (Supplementary Figure 2.4). Collectively, these results establish that the A61G/N64S substitutions make the CRY2 serine loop behave more like CRY1 and significantly alter its ability to bind CLOCK:BMAL1, helping to differentiate the roles of CRY1 and CRY2 as circadian repressors in the mammalian circadian clock.

2.3.4 The CRY1 serine loop is disordered in the CRY1 PHR:PER2 CBD complex

In addition to binding near the BMAL1 TAD-binding site at the CC helix of CRY1 and CRY2 (Figure 2.1D), the PER2 CBD also wraps around the distal side of the PHR domain to come into close contact with the serine loop (24, 25) (Figure 2.4A). Because of its proximity to the secondary pocket, we wanted to see how PER2 might regulate the affinity of CRY1 or CRY2 for CLOCK:BMAL1. However, the previous crystal structure of a CRY1 PHR:PER2 CBD complex (PDB: 4CT0) revealed that a portion of the PER2 peptide encoded by the expression vector packed against the secondary pocket, resulting in substantial ordering of

the CRY1 serine loop in the secondary pocket (25) (Supplementary Figure 2.5). To see if binding of the PER2 CBD truly alters the serine loop and secondary pocket of CRY1, we determined a crystal structure of the CRY1 PHR:PER2 CBD complex that eliminated this artifact (Figure 2.4 and Supplementary Figure 2.5, see link to Supplementary File 2a). The overall conformation of the PER2 CBD in our structure is highly similar to the previously solved structure (0.76 Å Cα RMSD over PER2 residues 1136–1207). However, we now see that the serine loop maintains most of its flexibility in the PER2-bound state.

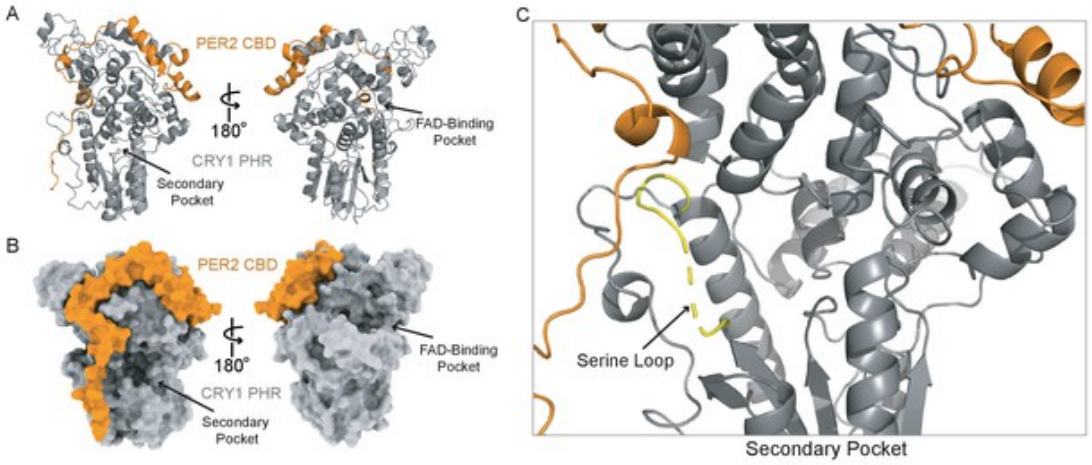

Figure 2.4. A new CRY1 PHR:PER2 CBD crystal structure.

(A-B) Crystal structure of the CRY1 PHR:PER2 CBD complex (PDB: 6OF7) with CRY1 PHR domain (gray) and PER2 CBD (orange). Ribbon and surface representations on the left highlight the secondary pocket, while the FAD binding pocket is shown on the right. ***(C)*** Zoomed in view of the secondary pocket showing the partially ordered serine loop (yellow). See Supplementary Figures 2.5-7 for additional information related to this figure.

To gain further insight into the structural organization of the PER2 CBD:CRY1 PHR:CLOCK PAS-B complex, we generated HADDOCK models of the CRY1 PHR:CLOCK PAS-B domain complex using representative CRY1 structures from the MD simulations (with the serine loop intact) and then superimposed the structures from the two largest and best scoring clusters from HADDOCK onto our CRY1 PHR:PER2 CBD crystal structure (Supplementary Figure 2.6, see also link to Supplementary File 2b). While both models

clearly place the HI loop of the CLOCK PAS-B domain into the secondary pocket of CRY1, they differ in the angular orientation of CLOCK PAS-B with respect to CRY1 by ~30°. We previously observed two similar models of the CRY1 PHR: CLOCK PAS-B complex by HADDOCK, but couldn't resolve the ambiguity between them using low resolution small-angle x-ray scattering data (22). To address this here, we compared simulated electron microscopy projections of these two clusters to reference-free 2D class averages obtained from imaging of a PER2 CBD:CRY1 PHR:CLOCK:BMAL1 complex by cryo-EM (Supplementary Figure 2.6). While the CLOCK PAS-B domain was more flexible relative to the CRY1 PHR domain, the overall position of CLOCK PAS-B in Cluster 1 agrees much better with the experimental data than Cluster 2. Therefore, the integration of computational docking and experimental data support a model of PER2 CBD:CRY1 PHR:CLOCK PAS-B complex.

We previously showed that mutation of W362 to alanine in the HI loop of CLOCK PAS-B reduced binding of the CRY1 PHR and significantly decreased CRY1 repression of CLOCK:BMAL1 in 293 T cells (22). To examine how this mutation quantitatively influences binding of CLOCK to CRY1 and CRY2, we performed BLI-based binding studies using the CLOCK:BMAL1 PAS domain core harboring the W362A CLOCK mutant (Supplementary Figure 2.7The PHR domains of CRY1 and CRY2 both demonstrated a significantly decreased affinity for the mutant PAS domain core, with a K_d for CRY1 of 6.6 ± 2.6 μM, reduced nearly 100-fold from the wild-type PAS domain core, while CRY2 bound with ~10 fold reduced affinity (K_d = 10.2 ± 0.2 μM). These results confirm the requirement for CLOCK PAS-B in interaction of the CLOCK:BMAL1 PAS domain core with both the CRY1 and CRY2 PHR domains, specifically highlighting the critical role of the tryptophan residue on the HI loop of the CLOCK PAS-B domain.

2.3.5 The PER2 CBD remodels the CRY2 serine loop to promote binding to the PAS domain core of CLOCK:BMAL1

A recent study showed that association of CRY2 with PER2 helps it to form a stable complex with CLOCK:BMAL1, while CRY1 can bind stably to CLOCK:BMAL1 either with or without the PER proteins (16), laying the foundation to understand the unique role of CRY1 in the late repressive complex (14, 35). To explore the structural basis for this model, we asked if PER2 binding could regulate affinity of the CRY1 and CRY2 PHR domain for the PAS domain core of CLOCK:BMAL1. Comparing the secondary binding pocket of the apo CRY1 PHR domain structure to our CRY1 PHR:PER2 CBD structure (Figure 2.5A), we observed that PER2 CBD induces a modest structuring at the C-terminal end of the loop (residues 44–47). This reorganization is stabilized by an interaction between S45 on CRY1 and the backbone of Q1135 on the PER2 CBD (Figure 2.5A and Supplementary Figure 2.8). To determine if addition of the PER2 CBD alters binding between the CRY1 PHR domain and CLOCK:BMAL1, we utilized BLI binding assays using preformed CRY:PER2 CBD complexes with the immobilized PAS domain core and found that the CRY1:PER2 CBD complex binds with a ~ 3 fold reduction in affinity (Figure 2.5B and Supplementary Figure 2.9). Therefore, PER2 modestly weakens interaction of the CRY1 PHR domain with the CLOCK:BMAL1 PAS core, suggesting that this modest ordering of the CRY1 serine loop makes docking of the CLOCK PAS-B into the secondary pocket less favorable.

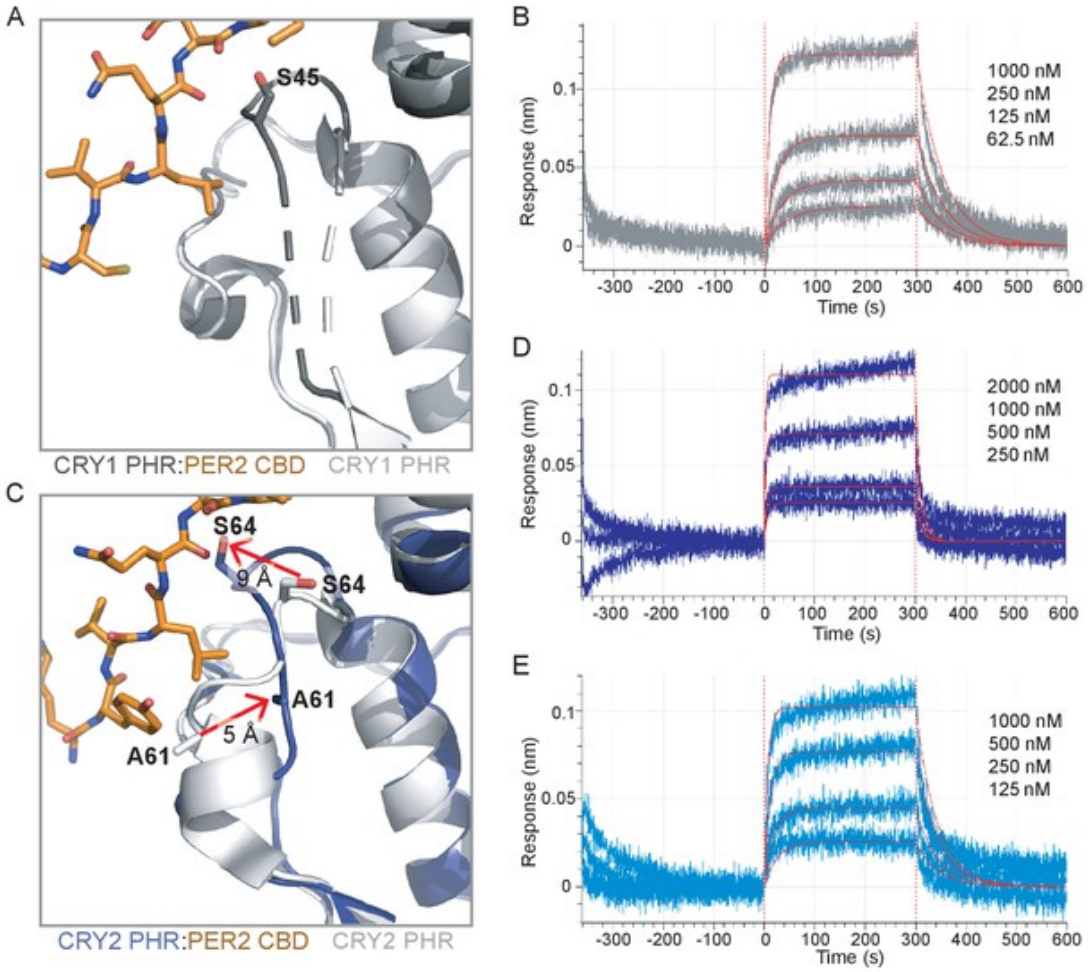

Figure 2.5. The PER2 CBD alters the CRY serine loops to modulate their affinity for the CLOCK:BMAL1 PAS core.

*(**A**)* Comparison of the serine loop from apo CRY1 PHR domain (light gray, PDB: 5T5X) and the CRY1 PHR:PER2 CBD complex (dark gray:orange, PDB: 6OF7). A slight structuring of the C-terminus of the serine loop occurs upon addition of PER2 CBD, while the N-terminus remains flexible (dashed line). *(**B**)* BLI data for the CRY1 PHR:PER2 CBD complex (gray) binding to immobilized, biotinylated CLOCK:BMAL1 PAS-AB. Inset values represent the concentrations of CRY for individual binding reactions, top to bottom. Vertical red dashed lines indicate the beginning of association and dissociation. Red solid line, nonlinear least squares fitting to a one-site binding model. Calculated K_d for CRY1 PHR:PER2 CBD = 196 ± 34 nM (mean ± SD from n = 2 independent assays). (***C***) Comparison of the serine loop from the apo CRY2 PHR domain (light gray, PDB: 4I6E) and the CRY2 PHR:PER2 CBD complex (blue:orange, PDB: 4U8H). *(**D**)* BLI data for the CRY2 PHR:PER2 CBD complex (dark blue) binding to immobilized, biotinylated CLOCK:BMAL1 PAS-AB domains. Calculated K_d for CRY2 PHR:PER2 CBD = 604 ± 29 nM (mean ± SD from n = 2 independent assays). (**E**) BLI data for the CRY2 7M PHR:PER2 CBD complex (light blue) binding to immobilized, biotinylated CLOCK:BMAL1 PAS-AB. Calculated K_d for CRY2 7M PHR:PER2 CBD = 159 ± 66 nM (mean ± SD from n = 2 independent assays). See Supplementary Figure 2.8-10 for additional information related to this figure.

By contrast, our comparison of the apo CRY2 PHR domain structure with the CRY2 PHR:PER2 CBD complex revealed a major structural reorganization of the serine loop induced by PER2 (Figure 2.5C). As described above, the beginning of the serine loop in the apo CRY2 PHR domain is structured with a short α-helix and a stable but extended loop at the end (24, 28). However, in the CRY2 PHR: PER2 CBD complex, the end of the serine loop is stabilized in an alternate position by multiple hydrogen bonds between S64 on CRY2 and A1135 and D1136 of the PER2 CBD (Supplementary Figure 2.8). This interaction moves S64 of CRY2 out of the secondary pocket by ~9 Å (Figure 2.5C), largely mimicking the PER2-dependent interaction and subsequent loop orientation we observed with S45 on CRY1 (Supplementary Figure 2.8). Additionally, the PER2 CBD remodels the N-terminus of the serine loop, causing an unfolding of the short α-helix and a translation of A61 by ~5 Å towards the secondary pocket (Figure 2.5C) Therefore, the addition of PER2 CBD causes the serine loops of CRY1 and CRY2 to take on a largely similar conformation, with the loop in CRY1 becoming more structured and the loop in CRY2 becoming less structured.

Based on the rearrangement of the CRY2 serine loop induced by PER2, we anticipated that PER2 would enhance affinity of CRY2 for the PAS domain core of CLOCK:BMAL1.

We used BLI binding assays to assess binding of a CRY2:PER2 CBD complex to the immobilized PAS domain core of CLOCK:BMAL1 and observed an increase in affinity of CRY2 for CLOCK:BMAL1 by 2-fold (Figure 2.5D). While this is a modest increase in affinity, these data are consistent with the observation that addition of PER2 enhances co-immunoprecipitation of CLOCK:BMAL1 by CRY2 (16). We also probed for a direct interaction of the PER2 CBD with the PAS domain core of CLOCK:BMAL1 by BLI, but observed no detectable binding (Supplementary Figure 2.10), demonstrating that the effect of PER2 CBD is likely due to regulation of the CRY serine loop and not a via direct interaction with CLOCK:BMAL1. These results provide a mechanistic foundation for the model where

formation of a complex with PER2 makes CRY2 a stronger repressor by enhancing its affinity for CLOCK:BMAL1 (16).

Based on the structural and computational analyses presented thus far, we attribute this tighter binding to CLOCK:BMAL1 to the loss of helical structure in the serine loop observed when CRY2 is bound to the PER2 CBD. Therefore, the CRY2 7M mutant, which substitutes CRY1 residues into the serine loop and secondary pocket, might not be expected to exhibit a gain in affinity for CLOCK:BMAL1 in the presence of the PER2 CBD. To test this prediction, we collected BLI binding data on the CRY2 7M PHR domain mutant in the presence of PER2 CBD. In line with our model, the CRY2 7M:PER2 CBD complex behaved more like CRY1 and exhibited a similar drop in affinity for CLOCK:BMAL1 (Figure 2.5E). Altogether, our study establishes that the PER2 CBD tunes affinity of the CRY PHR domains for the PAS domain core of CLOCK:BMAL1 through differential interactions at the serine loop. Notably, when CRY1 or CRY2 are associated with the co-repressor PER2, their affinity for CLOCK:BMAL1 is at its most similar (within a ~ 3 fold difference) compared to the 20-fold difference that we observe with the two proteins in the absence of the PER2 CBD.

2.4 Discussion

Since the identification of core mammalian clock proteins nearly two decades ago, numerous studies have revealed how they work at the network level to generate the transcriptional feedback loop that confers circadian timekeeping (2). However, we still lack a mechanistic understanding of how most clock proteins interact with and/or regulate one another to fulfill their important roles as dedicated molecular ‘cogs’ in the circadian clock. In this study, we integrated biochemistry, structural biology, and computational methods to determine how the association of CLOCK:BMAL1 with CRY1 or CRY2 is differentially regulated by dynamics at the serine loop on their respective PHR domains. In contrast to CRY2, CRY1 has a flexible serine loop adjacent to its secondary pocket on the PHR domain that confers tight binding to the PAS domain core of CLOCK:BMAL1. Substitutions to CRY1 residues at serine loop and/or secondary pocket in CRY2 are sufficient to enhance its

association with the PAS domain core of CLOCK:BMAL1, in line with a previous study showing that these mutants largely recapitulated isoform-dependent changes in circadian period (16). Remarkably, we found that binding of the PER2 CBD remodels the ordered serine loop of CRY2 to enhance its affinity for CLOCK:BMAL1, conferring CRY1-like affinity and dynamics to the serine loop. Therefore, small changes in the structure and dynamics of the serine loop with and without PER2 allow cryptochromes to fine-tune their repressive power by controlling how tightly they bind to CLOCK:BMAL1.

Our data suggest that the differential effect of the PER2 CBD on CRY PHR binding to CLOCK:BMAL1 allows it to serve as a molecular equalizer—PER2 compensates for poorer binding by CRY2 by modestly enhancing its affinity for the transcription factor, while at the same time reducing CRY1 binding to bring the overall affinities of the two cryptochromes for the PAS domain core of CLOCK:BMAL1 to similar levels. This suggests that the actions of CRY1 and CRY2 within the heteromultimeric PER-CRY repressive complexes (3, 4) may be largely similar. The apparent dependency of CRY2 on PER1/2, the PER isoforms that possess a functional CRY-binding domain (36, 37), is consistent with the expression of CRY2 that occurs in phase with the PER proteins. By contrast, the peak expression of CRY1 is delayed by several hours from the other repressors (4, 13). The same temporal profiles are observed in the genome-wide mapping of their DNA occupancy with CLOCK:BMAL1, revealing two distinct waves of repressive complexes: 'early' complexes that contain PER1/2 proteins, their associated kinase CK1δ, CRY2, and some CRY1 with a variety of non-stoichiometrically associated epigenetic regulators (3, 38), and a 'late' complex consisting of CRY1 bound to CLOCK:BMAL1 in the apparent absence of PER proteins (14, 35). The 20-fold increase in affinity of CRY1 that we observed for the PAS domain core of CLOCK:BMAL1 relative to CRY2 therefore likely plays a critical role in its ability to participate in the PER-free 'late' complex, and may also give rise to the CRY1-selective extension of the repression phase observed in the *Fbxl3*^{Afh} mutant (39). Altogether, these data suggest that a

proper balance of the biochemically distinct PER-containing early and PER-free late repressive complexes work together to generate the circadian period of ~24 hr.

Understanding precisely why the more dynamic serine loop helps CRY1 bind to the PAS domain core of CLOCK:BMAL1 awaits determination of a higher resolution structure of the complex. Like many other transcription factors, CLOCK:BMAL1 is a 'malleable machine' (40) and its dynamic nature presents challenges for structure determination, particularly its flexibly tethered, modular PAS domains and disordered regions that play important functional roles (10, 22). From the perspective of cryptochromes, the dynamic nature of the serine loop may be associated with allosteric changes throughout the PHR domain and evolution of transcriptional repressor function. Notably, the secondary pocket in photoreceptive cryptochromes from *Arabidopsis* and *Drosophila* (41, 42), as well as the evolutionarily-related DNA repair enzyme photolyase (43, 44) is considerably smaller in volume, where it binds to small molecule cofactors that facilitate light harvesting (45). The ability of repressor-type cryptochromes to interact with CLOCK PAS-B appears to be deeply rooted in evolution of the metazoan circadian clock, because vertebrate-like cryptochromes that act as transcriptional repressors in insects (46) like the monarch butterfly also depend to the same extent on multivalent interactions with CLOCK PAS-B and the BMAL1 TAD as they do in mammals (10, 26, 47).

The BMAL1 TAD is the primary driver of transcriptional activation by CLOCK:BMAL1 in mammalian and insect systems with repressor-type cryptochromes, as truncation of the TAD decimates CLOCK:BMAL1 activity and leads to arrhythmicity in vivo (44, 47, 48). Sequestration of the TAD by repressor-type cryptochromes allows them to compete with coactivators at a highly conserved and overlapping binding motif in the TAD (9, 10). Strikingly, we did not observe differential binding to the BMAL1 TAD by CRY1 or CRY2, either in the absence or presence of the PER2 CBD. However, it remains to be seen if other regions in the disordered BMAL1 C-terminus (i.e., the G region) (10) or CRY C-termini (17, 23) also participate in CRY binding. This suggests that the changes in CRY affinity for the

PAS domain core of CLOCK:BMAL1 that we observed here underlie the major functional differences between CRY1 and CRY2 that contribute to differential period regulation (6, 7, 15) and the ability of CRY1 to sustain cellular circadian rhythms (33). Therefore, cryptochrome recruitment to the PAS domain core likely represents a key regulatory node in the clock.

2.5 Materials and Methods

2.5.1 Protein expression and purification

Using the baculovirus expression system (Invitrogen), the following constructs were expressed in Sf9 suspension insect cells (Expression Systems): His-tagged mouse CRY1 PHR domain (residues 1–491), CRY2 PHR domain (residues 1–512), CRY2 7M PHR domain (residues 1–512 with the following mutations: A61G, S64N, S394E, V396M, R397K, D400E, F408W), CRY2 2M PHR domain (residues 1–512 with the following mutations: A61G, S64N) CLOCK:BMAL1 bHLH-PAS domains (CLOCK residues 26–395, BMAL1 residues 62–441) or GST-tagged BMAL1 PAS-AB domains (residues 136–441). Sf9 suspension cells were infected with a P3 virus at 1.2 × 10^6 cells per milliliter and grown for 72 hr at 27°C with gentle shaking. Cells were centrifuged at 4°C for 4000 x rpm for 15 min. CRY1, CRY2, CRY2 2M and CRY2 7 M cells were resuspended in 50 mM Tris buffer pH 7.5, 300 mM NaCl, 20 mM imidazole, 10% (vol/vol) glycerol, 0.1% (vol/vol) Triton X-100, 5 mM β-mercaptoethanol and EDTA-free protease inhibitors (Pierce). Cells were lysed using a microfluidizer followed by sonication with a ¼" probe on ice for 15 s on, 45 s off for three pulses at 40% amplitude. Lysate was clarified at 4°C for 19,000 rpm for 45 min. The protein was isolated by Ni^{2+}-nitrilotriacetic acid (Ni-NTA) affinity chromatography (Qiagen). Proteins were eluted with 50 mM Tris buffer pH 7.5, 300 mM NaCl, 250 mM imidazole, 10% (vol/vol) glycerol, and 5 mM β-mercaptoethanol. Proteins were further purified by HiTrap SP cation exchange chromatography (GE Healthcare) and Superdex 75 gel filtration chromatography (GE Healthcare) into 20 mM HEPES buffer pH 7.5, 125 mM NaCl, 5% (vol/vol) glycerol, and 2 mM tris(2-carboxyethyl)phosphine (TCEP).

CLOCK:BMAL1 bHLH-PAS expressing cells were resuspended in 20 mM sodium phosphate buffer pH 8, 15 mM imidazole, 10% (vol/vol) glycerol, 0.1% (vol/vol) Triton X-100 and 5 mM β-mercaptoethanol. Cells were lysed, clarified and Ni-NTA affinity purification was performed as described above. The complex was eluted with sodium phosphate buffer pH 8, 250 mM imidazole, 10% (vol/vol) glycerol and 5 mM β-mercaptoethanol. The complex was further purified by HiTrap Heparin HP affinity column (GE Healthcare) after diluting eluent ~5 fold with 20 mM sodium phosphate buffer pH 7.5, 50 mM NaCl, 2 mM Dithiothreitol, and 10% (vol/vol) glycerol and loaded onto the column. After washing with five column volumes of the above buffer, the complex was then eluted with a gradient 0–100% of 20 mM sodium phosphate buffer pH 7.5, 2 M NaCl, 2 mM Dithiothreitol, and 10% (vol/vol) glycerol. The complex was further purified by Superdex 200 gel filtration chromatography (GE Healthcare) into 20 mM HEPES buffer pH 7.5, 125 mM NaCl, 5% (vol/vol) glycerol, and 2 mM TCEP.

GST-BMAL1 PAS-AB-expressing Sf9 cells were resuspended in 50 mM HEPES buffer pH 7.5, 300 mM NaCl, 5% (vol/vol) glycerol and 5 mM β-mercaptoethanol. Cells were lysed and clarified as described above. The soluble lysate was bound in batch-mode to Glutathione Sepharose 4B (GE Healthcare), then washed and eluted with 50 mM HEPES buffer pH 7.5, 150 mM NaCl, 5% (vol/vol) glycerol and 5 mM β-mercaptoethanol, 25 mM reduced glutathione. The protein was desalted into HEPES buffer pH 7, 150 mM NaCl, 5% (vol/vol) glycerol and 5 mM β-mercaptoethanol using a HiTrap Desalting column (GE Healthcare) and the GST tag was cleaved with GST-TEV protease overnight at 4°C. The cleaved GST-tag and GST-tagged TEV protease was removed by Glutathione Sepharose 4B (GE Healthcare) and the remaining BMAL1 PAS-AB protein was further purified by Superdex 75 gel filtration chromatography (GE Healthcare) into 20 mM HEPES buffer pH 7.5, 125 mM NaCl, 5% (vol/vol) glycerol, and TCEP.

Recombinant baculoviruses expressing GST-CRY2 PHR domain, His-CLOCK bHLH-PAS, and His-BMAL1 full-length were co-infected into monolayer High Five insect cells (Invitrogen) for protein expression. Cells were harvested 48 hr after infection, and lysed in a

buffer containing 40 mM HEPES pH 7.5, 300 mM NaCl, 10% (v/v) glycerol, 5 mM β-mercaptoethanol. Lysed cells were clarified by ultracentrifugation, and the soluble lysate was purified over a glutathione affinity column (GE Healthcare). Bound complex was eluted via overnight on-column TEV cleavage to remove the GST- and His-tags. Eluted material was further purified by a HiTrap Q-HP (GE Healthcare) anion exchange column, followed by a Superdex 200 gel filtration column (GE Healthcare) equilibrated in 20 mM HEPES pH 7.5, 300 mM NaCl, 10% (v/v) glycerol, 1 mM DTT.

The CLOCK PAS-AB (residues 93–395) and PER2 CBD (residues 1095–1215) were expressed in Rosetta2 (DE3) *E. coli*. Protein expression was induced with 0.5 mM isopropyl-β-D-thiogalactopyranoside (IPTG) at an OD_{600} of ~0.8, after which cells were grown for an additional 18 hr at 18°C. Cells were harvested by centrifugation at 4°C for 4000 x rpm for 15 min. For CLOCK PAS-AB (wild-type or W362A mutant), the protein was expressed as a fusion protein with the solubilizing tag His-NusA-XL and an N-terminal biotin acceptor peptide (BAP) (49) C-terminal to the TEV site. Cells were resuspended in 50 mM Tris buffer pH 7.5, 300 mM NaCl, 20 mM imidazole, 10% (vol/vol) glycerol and 5 mM β-mercaptoethanol and lysed by microfluidizer. Lysate was clarified at 4°C for 19,000 rpm for 45 min. The protein was isolated by Ni-NTA affinity chromatography (Qiagen) and eluted with 50 mM Tris buffer pH 7.5, 300 mM NaCl, 250 mM imidazole, 10% (vol/vol) glycerol, and 5 mM β-mercaptoethanol. The protein was then desalted into 50 mM Tris buffer pH 7.5, 150 mM NaCl, 5% (vol/vol) glycerol and 5 mM β-mercaptoethanol, and the His-NusA-XL tag was cleaved with His-TEV protease overnight at 4°C. The cleaved tag and protease were removed by Ni-NTA affinity chromatography (Qiagen) and CLOCK PAS-AB was further purified by Superdex 75 gel filtration chromatography (GE Healthcare) into 20 mM HEPES buffer pH 7.5, 125 mM NaCl, 5% (vol/vol) glycerol, and 2 mM TCEP. PER2 CBD was expressed as a fusion protein with GST and purified as described above. All proteins were flash frozen in small aliquots and stored at −70 °C.

2.5.2 Biotinylation of CLOCK PAS-AB

100 μM BAP-CLOCK PAS-AB (wild-type or W362A mutant) in 20 mM HEPES buffer pH 7.5, 125 mM NaCl, 5% (vol/vol) glycerol, and 2 mM TCEP was incubated at 4 °C overnight with 2 mM ATP, 1 μM GST-BirA [purified from *E. coli* according to a prior protocol (50) and 150 μM biotin]. GST-BirA was removed afterwards with Glutathione Sepharose 4B (GE Healthcare) resin and excess biotin was separated from the labeled protein by Superdex 75 gel filtration chromatography (GE Healthcare) in 20 mM HEPES buffer pH 7.5, 125 mM NaCl, 5% (vol/vol) glycerol, and 2 mM TCEP.

2.5.3 Assembling and verifying protein complexes for binding studies

To assemble CRY PHR:PER2 CBD complexes used for binding studies with CLOCK:BMAL1, a slight molar excess of zinc chloride was added to a 1:1 mix of the PER2 and CRY proteins (24, 25). The assembly and purity of complexes from peak fractions of the Superdex 200 10/300 GL gel filtration column (GE Healthcare) was assessed by SDS-PAGE gel electrophoresis and SimplyBlue SafeStain (Invitrogen) staining before using them in binding assays.

2.5.4 Fluorescence polarization

A peptide of the minimal BMAL1 TAD (residues 594–626) was purchased from Bio-Synthesis with a 5,6-TAMRA fluorescent probe covalently attached to the N terminus. Binding assays with CRY1 PHR domain, CRY1 PHR:PER2 CBD, CRY2 PHR domain and CRY2 PHR:PER2 CBD were performed in 50 mM Bis-Tris Propane buffer pH 7.5, 100 mM NaCl, 2 mM TCEP and 0.05% (vol/vol) Tween-20. The BMAL TAD probe was diluted to a working concentration of 50 nM in assay buffer and binding was monitored by changes in fluorescence polarization with an EnVision 2103 multilabel plate reader (Perkin Elmer) with excitation at 531 nm and emission at 595 nm. Equilibrium binding dissociation constants (K_d) were calculated by fitting the dose-dependent change in millipolarization (mP) to a one-site specific total binding model in Prism 7 (GraphPad). The mP values shown represent the

average of duplicate samples from a representative experiment of n = 3 independent assays. The K_d reported (± SD) is the average of determined from the three independent assays.

2.5.5 Bio-layer interferometry

BLI experiments were performed using an 8-channel Octect-RED96e (ForteBio) with a BLI assay buffer of 20 mM HEPES buffer pH 7.5, 125 mM NaCl, 5% (vol/vol) glycerol and 2 mM TCEP. All experiments began with a reference measurement to establish a baseline in BLI buffer for 120 s. Next, 1.5 µg/mL biotinylated CLOCK:BMAL1 PAS-AB (wild-type or W362A mutant in BLI buffer) was loaded on a streptavidin tip for 300 s at room temperature. Subsequently, a 360 s blocking step was performed with 0.5 mg/mL BSA, 0.02% (vol/vol) Tween, 20 mM HEPES buffer pH 7.5, 125 mM NaCl, 5% (vol/vol) glycerol and 2 mM TCEP. Association was then measured for 300 s for eight different concentrations of the analyte (CRY, CRY:PER2 CBD, PER2 CBD) in a serial dilution starting at approximately 10x the estimated K_d in blocking buffer. Dissociation was measured for 300 s in blocking buffer. Each experiment was repeated with tips that were not loaded with CLOCK:BMAL PAS-AB to provide a reference for non-specific binding to the tip. Data were processed and fit using Octet software v.7 (ForteBio). Before fitting, all datasets were reference-subtracted, aligned on the y-axis and aligned for interstep correction through their respective dissociation steps according to the manufacturer's instructions. For each experiment, at least four different concentrations were used to fit association and dissociation globally using a 1:1 binding model in Octet software v.7 (ForteBio). Ultimately, the goodness of fit was determined using χ^2 and R^2 values according to the manufacturer's instructions.

2.5.6 Molecular dynamics simulations

The crystal structure of apo CRY1 PHR domain (PDB: 5T5X) and apo CRY2 PHR domain (PDB: 4I6E) were prepared for starting models for the molecular dynamics (MD) simulations by modeling non-terminal missing residues using the Prime program (Schrödinger). All crystallographically-defined water molecules were removed from the structures. In order to prepare the system with the in silico mutated CRY2 PHR domain

(A61G/S64N CRY2), the corresponding amino acids were mutated in wild type apo CRY2 PHR domain using UCSF-Chimera (51) and used as starting models. Amber99sb-ildn force field was used for simulation (52). The structures were solvated in a dodecahedron box using TIP3P water molecules. The systems were neutralized and then Na^+ and Cl^- ions were added to maintain a physiological ionic concentration of 0.15 M. Energy minimization was performed for the systems until the maximum force on any atom was less than 1,000 kJ $mol^{-1}nm^{-1}$ in the case of apo CRY1 and CRY2 PHR domains, and 500 kJ $mol^{-1}nm^{-1}$ in the case of the in silico mutated CRY2 PHR domain.

After energy minimization, the systems were equilibrated in an NVT ensemble for 500 ps. The temperature was maintained at 310 K using the modified Berendsen Thermostat (V-rescale) (53). After this, the systems were equilibrated in an NPT ensemble for 500 ps. The pressure was maintained at 1 bar using a Berendsen barostat (54). This was followed by a production run of 500 ns for each system in an NPT ensemble using a Parinello-Rahman barostat (55) and modified Berendsen Thermostat (V-rescale) with the temperature maintained at 310 K and pressure at 1 bar. Three independent simulations were completed for the apo CRY1 PHR domain and apo CRY2 PHR domain systems described in the previous section and two independent simulations were run for the in silico mutated CRY2 PHR domain system. All MD simulations were performed using Gromacs 5 (56).

The trajectories were analyzed using in built functions of Gromacs. RMSD, RMSF, distances and dihedral angles were calculated using gmx rmsd, gmx rmsf, gmx distance and gmx chi programs of Gromacs respectively. UCSF-Chimera (51) was used for molecular visualization. The volume of secondary pocket for 251 equally spaced trajectory frames from each run was calculated using POVME 3.0 (57). The comparison of volumes between CRY1-CRY2 PHR domain and between CRY2-mutCRY2 PHR domains was done by performing Wilcoxon ranksum test as implemented in Scipy (https://www.scipy.org/). Hydrogen bonds were determined for each frame of the MD trajectories using MDTraj (58). The bonds with at least one residue from the serine loop (residues I36/I54 to I49/I67 in CRY1/CRY2) and with

frequency of more than 5000 frames in any trajectory of a particular system were chosen as high frequency hydrogen bonds. The free energy landscape (FEL) was calculated using volume of secondary pocket and distance between center of mass of residue S62 and F123 (S44 and F105 in CRY1), as reaction coordinate. The FEL was calculated by using *gmx sham* utility of Gromacs. For FEL construction the volume and distance were calculated for every 100th frame from each trajectory.

2.5.7 Calculation of Kullback-Leibler (KL) divergence

The KL-divergence or relative entropy has been previously used to quantify the residue wise differences between the ensembles (34, 59, 60). To calculate the KL-divergence between the ensembles using mutinf software (34), we divided each simulation trajectory between 100 ns and 500 ns into 4 blocks of 100 ns each. This gave a total of 12 blocks for apo CRY1 PHR domain and apo CRY2 PHR domain simulations and eight blocks for the in silico mutCRY2 PHR domain. Dihedral angles phi, psi and chi1 were calculated for 5000 equally spaced frames from each block and used as input to calculate KL-divergence. Dividing the trajectories into multiple blocks of sufficiently large number of frames enabled the calculation of bootstrap values, which were used to make a robust estimation of significant differences between the two ensembles. The divergence values greater than the bootstrap values for a given residue suggests that the dynamics of those residues differ significantly between the two ensembles, in terms of side chain rotamer distribution, main chain dihedral angle distribution or both.

2.5.8 Crystallization, data collection and structure determination

The CRY1 PHR:PER2 CBD complex was purified as described above. The protein was concentrated to 4.3 mg/mL and crystalized by sitting-drop vapor diffusion at 22 °C. Crystals formed in a 1:1 ratio of protein to precipitant in 0.2 M $MgCl_2$, 0.1 M Bis-Tris buffer pH 5.5% and 25% (vol/vol) PEG 3350. Crystals were harvested and flash frozen in the reservoir solution with 20% (vol/vol) glycerol before data collection. Data were collected from single crystal at λ = 1.0A, 100 K on Beamline 23-ID-D at the Advanced Photon Source (Argonne,

Illinois, USA). Diffraction images were indexed and scaled using iMosflm (61) and Scala (62) in the CCP4 package (63). Phases were solved by molecular replacement with PHASER (64) using the crystal structure of mouse CRY1 PHR domain in complex with the PER2 CBD (PDB: 4CT0). All reflections were used for refinement except for 5% that were excluded for R_{free} calculations. The structural model was revised in real space with the program COOT (65) based on sigma-A weighted 2Fo-Fc and Fo-Fc electron density maps. Data collection and final refinement statistics are given in Supplementary file 1 Table S1.

2.5.9 Sample preparation for electron microscopy

A complex containing the CLOCK:BMAL1 bHLH-PAS heterodimer bound to an annealed DNA duplex containing the minimal mouse *Per2* E-box (GCG CGG TCA CGT TTT CCA CT) and the CRY1 PHR:PER2 CBD repressor heterodimer was verified from peak fractions of a Superdex 200 10/300 GL gel filtration column (GE Healthcare) and assessed by SDS-PAGE gel electrophoresis and SimplyBlue SafeStain (Invitrogen) staining. The complex was flash frozen and stored at −70 °C. For data collection, the complex was briefly incubated on ice in 20 mM HEPES, 125 mM NaCl, 2 mM TCEP and 1% (vol/vol) glycerol. 2.5 µL of sample was then applied to an UltraAuFoil R1.3/1.3 300-mesh grid (Electron Microscopy Services), which was freshly plasma-cleaned using a Gatan Solarus (75% argon/25% oxygen atmosphere, 15 Watts for 7 s). Grids with applied sample were then manually blotted with filter paper (Whatman No.1) for ~3 s in a 4 °C cold room before plunge freezing in liquid ethane cooled by liquid nitrogen.

2.5.10 Electron microscopy data acquisition

The Leginon automated data-acquisition program (66) was used to acquire all cryo-EM data. Real-time image pre-processing, consisting of frame alignment, contrast transfer function (CTF) estimation and particle picking, were performed using the Appion image-processing pipeline during data collection (67). Image collection was performed using a Thermo Fischer Talos Arctica operating at 200 keV and equipped with a Gatan K2 Summit DED, at a nominal magnification of 36,000X (corresponding to a physical pixel size of 1.15 Å

per pixel). 692 movies were collected, with 48 frames per movie using a total exposure time of 12 s with an exposure rate of 5.2 e^-/pixel/s and total exposure of 47.2 $e^-/Å^2$ (0.98 e^- per frame). A nominal defocus range from −0.8 µm to −1.8 µm was used during data collection.

2.5.11 Electron microscopy image processing

Automated particle picking was conducted using the Difference of Gaussians (DoG) picker (67) to yield 891,700 particle picks. Before particle extraction, CTFFIND4 was used for CTF estimation. Fourier-binned 2 × 2 particles were subjected to reference-free two-dimensional (2D) classification in Relion 3.0 (68) to remove poorly aligning particles and non-particles in the data. A second round of 2D classification in Relion was used to further remove partially denatured or damaged particles and false picks, resulting in 81,257 particles populating 2D classes with strong structural features that were used for analyses (Supplementary Figure 2.6). Attempts to determine a 3D structure of the entire complex were stymied by a strong preferred orientation of the particles in ice.

2.5.12 HADDOCK studies

The cluster representatives obtained after clustering the trajectories were used to dock the PAS-B domain (residues 261–395) of CLOCK (PDB: 4F3L) using HADDOCK 2.2 webserver (69). The active residues used for generating restraints for docking were: D38/D56, P39/P57, F41/F59, R51/R69, G106/G124, R109/R127, F257/F275, E382/D400, E383/E401 for CRY1/CRY2 and G332, H360, Q361, W362, E367 for CLOCK PAS-B as before (22). The passive residues were specified as residues surrounding the active residues. The PAS-B domain of the CLOCK protein was used to dock an ensemble of structures comprised of 15 cluster representatives of apo CRY1 PHR domain and 12 cluster representatives of apo CRY2 PHR domain. A total of 10000, 400 or 400 models were generated, respectively, for the rigid docking, flexible docking and water refinement phase of the docking protocol. The final 400 models were clustered using Fractional Common Contacts (FCC) and sixteen clusters were obtained comprising 360 structures. Out of these sixteen, there were two large clusters with 92 and 80 complexes constituting about 48% of

the clustered structures. The representatives from these two largest clusters were considered for further analysis. Electron microscopy densities were simulated from the atomic models using the 'molmap' function in Chimera, and the densities were low-pass filtered to 8 Å resolution using the 'proc3d' function in EMAN 1.9 (70). Forward projections of each of the two models were generated using the 'project3d' function in EMAN 1.9, and the 'v2' function in EMAN 1.9 was used to compare the projections with the reference-free 2D class averages from RELION.

2.6 Data availability

Diffraction data have been deposited in PDB under the accession code 6OF7.

2.7 Supplementary Figures

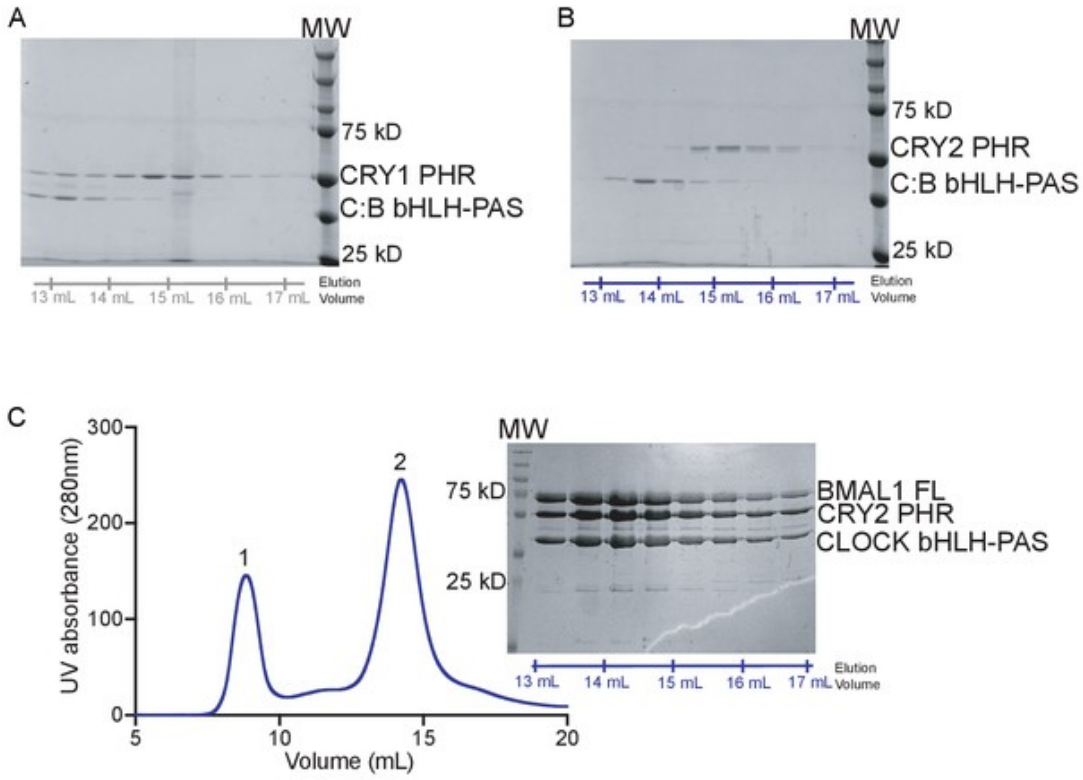

Supplementary Figure 2.1. Gel filtration analysis of CRY1, CRY2 and CLOCK:BMAL bHLH-PAS proteins.

*(**A**)* SDS-PAGE analysis of the peak fractions from the CRY1 PHR incubated with C:B bHLH-PAS (gray) injection on the S200 10/300 GL column (Figure 2A). Elution volume (mL) is marked below the gel. *(**B**)* SDS-PAGE analysis of the peak fractions from the CRY2 PHR incubated with C:B bHLH-PAS (blue) injection on the S200 10/300 GL column (Figure 2B). Elution volume (mL) is marked below the gel. *(**C**)* Chromatographic analysis of complex formation by CRY2 PHR and a heterodimer of CLOCK bHLH-PAS with full-length BMAL1, as above. The addition of the BMAL1 C-terminus resulted in co-elution of CLOCK:BMAL1 with CRY2 PHR in peak 2 (peak 1 contains aggregated protein eluting in the void volume).

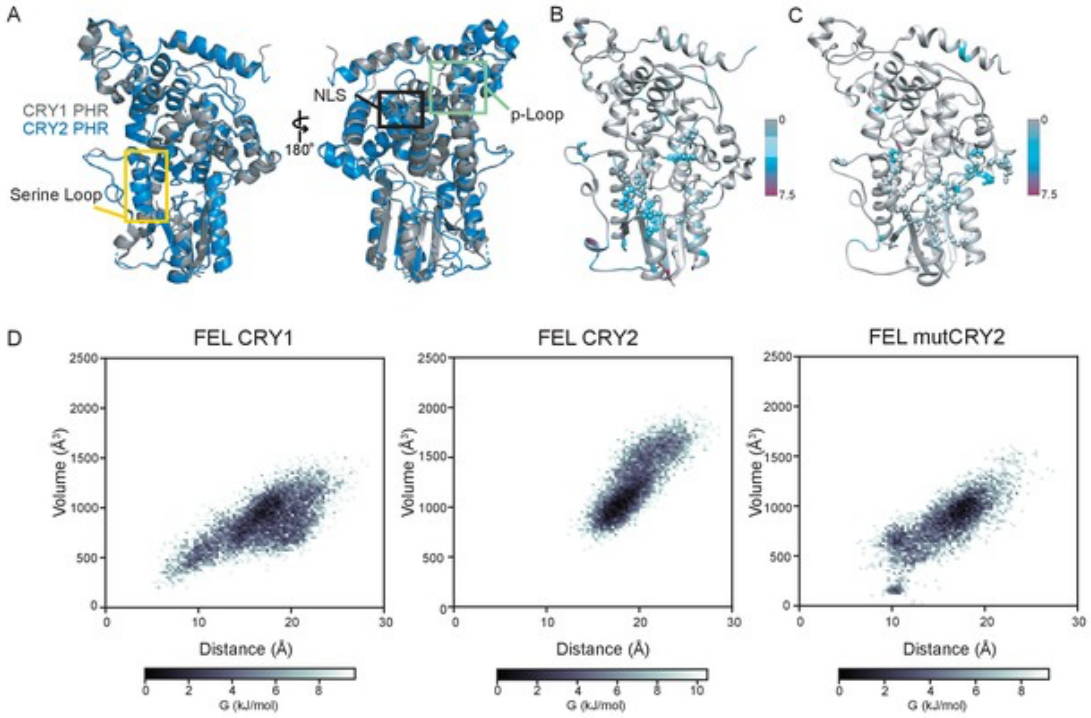

Supplementary Figure 2.2. Kullback-Leibler divergence and Free Energy Landscape of CRY PHR domains.

*(**A**)* Structural alignment of CRY1 PHR (PDB: 5T5X) and CRY2 PHR (PDB: 4I6E). The standard view of CRY with the serine loops highlighted in yellow and boxed (left) and a 180° rotation of the alignment showing the other highly variable regions boxed (right). *(**B**)* KL divergence between CRY1 and CRY2 ensembles. The residues are colored as per the KL divergence. The color bar shows values of the KL divergence corresponding to different colors. *(**C**)* KL divergence between CRY2 and mutCRY2 ensembles. Residues showing high KL divergence near the secondary pocket are displayed in ball and stick representation. *(**D**)* Free energy landscape (FEL) corresponding to the volume and distance at the entrance of secondary pocket for CRY1 (left), CRY2 (middle) and mutCRY2 (right). The colors represent relative energies with minimum being the most populated region of the landscape. See Supplementary file 1 for more information.

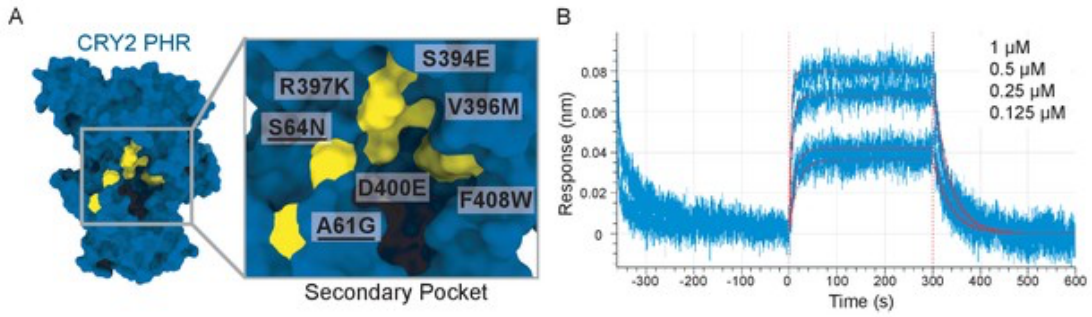

Supplementary Figure 2.3. The CRY2 7M mutant increases affinity for the PAS domain core of CLOCK:BMAL1.

*(**A**)* Crystal structure of CRY2 PHR with the seven mutations (7M) identified in Rosensweig et al. (2018). *(**B**)* BLI data for CRY2 7M (blue) binding to immobilized, biotinylated CLOCK:BMAL1 PAS-AB. Inset values represent the concentrations of CRY for individual binding reactions, top to bottom. Vertical red dashed lines indicate the beginning of association and dissociation. Red solid line, nonlinear least squares fitting to a one-site binding model. Calculated K_d for CRY2 7M PHR = 130 ± 12 nM (mean from n = 2 independent assays).

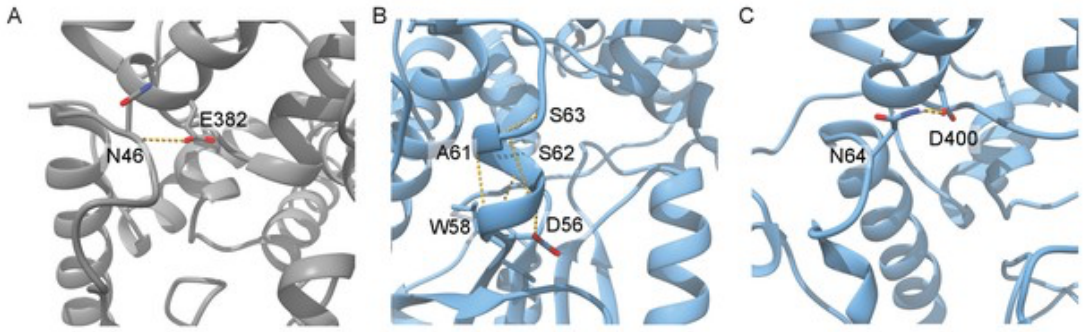

Supplementary Figure 2.4. Analysis of hydrogen bonds in CRY PHR domain serine loops.

*(**A**)* Hydrogen bond (shown in orange) between N46 and E382 seen in the CRY1 simulation with high frequency. *(**B**)* Multiple intra-loop hydrogen bonds in a representative frame from CRY2 simulations. *(**C**)* Hydrogen bond formed between mutated N64 and D400 in one the representative frames from mutated CRY2 simulations. See Supplementary file 1 for more information.

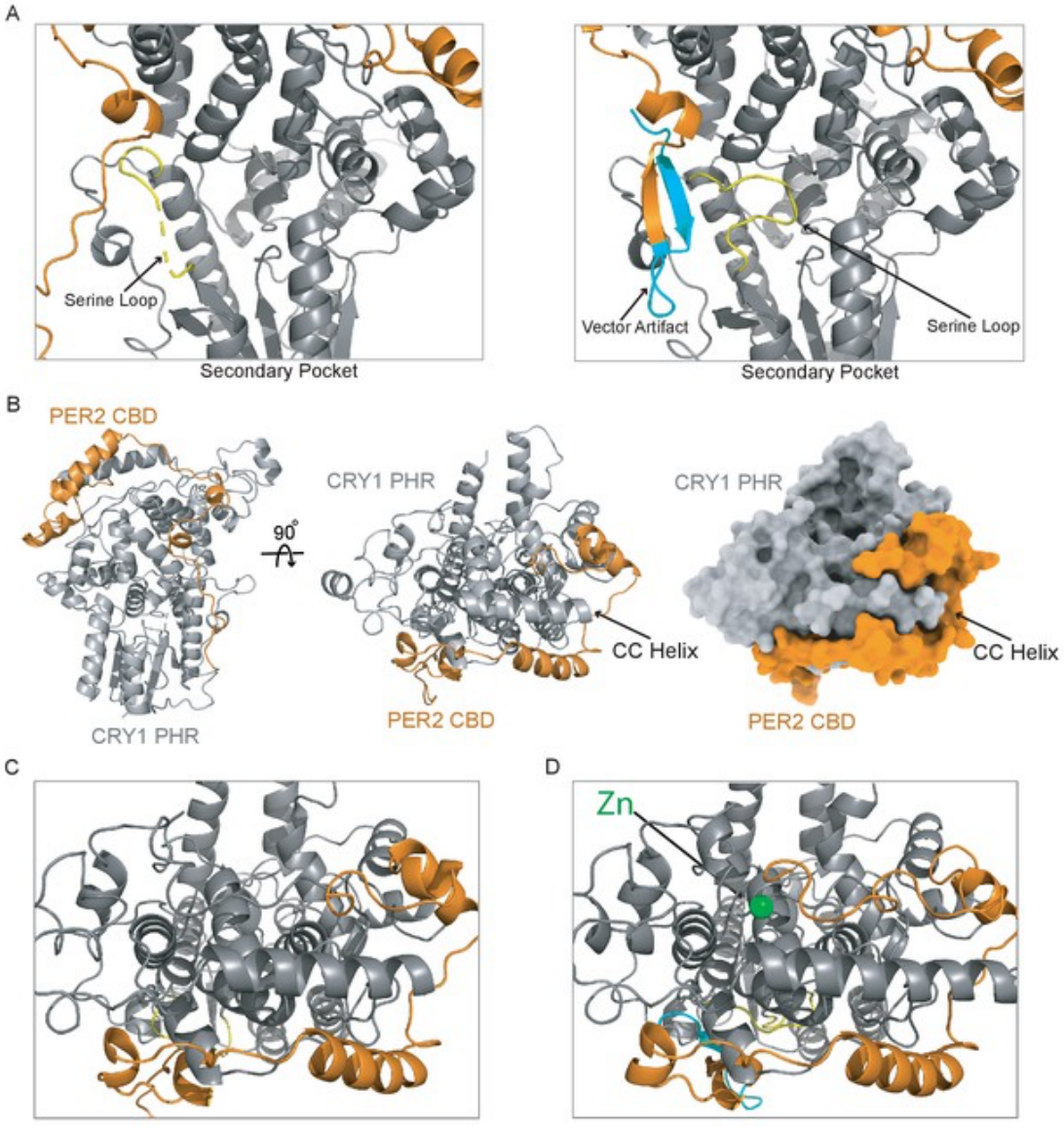

Supplementary Figure 2.5. Additional views of the new CRY1 PHR:PER2 CBD crystal structure.

*(**A**)* Left, zoomed in view of the secondary pocket (CLOCK PAS-B binding site) of our crystal structure (PDB: 6OF7) showing the partially ordered serine loop (yellow). Right, same view of the secondary pocket from the previously published CRY1 PHR:PER2 CBD crystal structure (PDB: 4CT0) (25) with the serine loop (yellow) that is ordered by contact with the vector artifact (cyan). *(**B**)* Crystal structure of CRY1 PHR:PER2 CBD. CRY1 PHR is shown in gray and PER2 CBD is shown in orange. The standard view is shown in ribbon representation (left) and a 90° rotation along the horizontal axis to display the CC helix, where the TAD of BMAL1 binds, is shown in ribbon (middle) and surface (right). *(**C**)* Zoomed in view of the CC helix. *(**D**)* Zoomed in view of the CC helix of the previously solved crystal structure of CRY1 PHR:PER2 CBD (4TC0). CRY1 PHR is shown in gray and PER2 CBD is shown in orange.

The far C-terminus of the CBD of PER is coordinating a zinc ion (green) with CRY1 PHR. The zinc ion and subsequent coordinating residues are missing from the new structure. See Supplementary file 2 for more information.

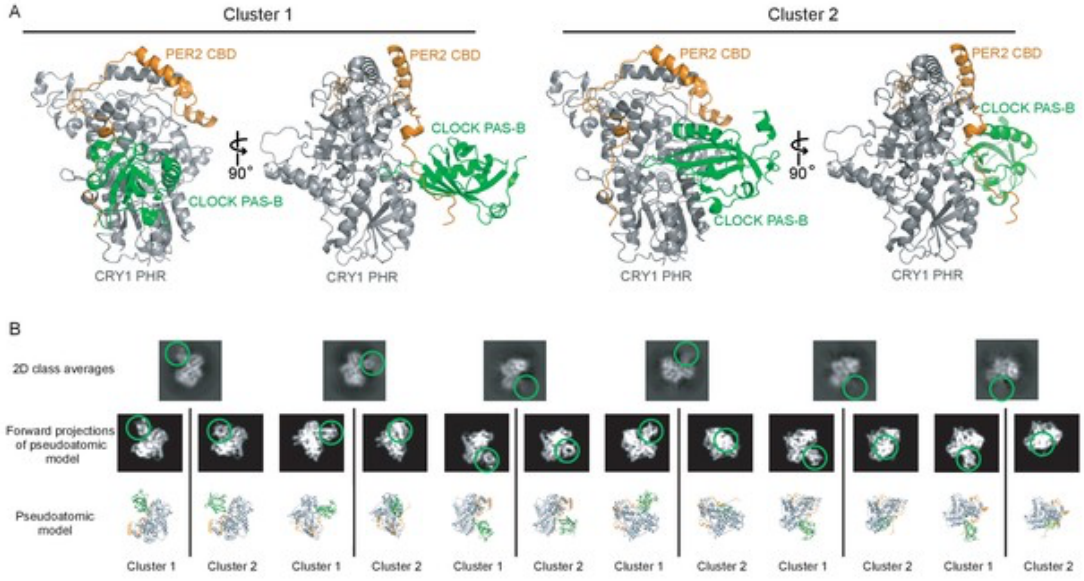

Supplementary Figure 2.6. Representative HADDOCK models of the PER2 CBD:CRY1 PHR:CLOCK PAS-B complex and comparison to 2D class averages from cryo-EM data.

*(**A**)* Representative structures of the top two HADDOCK clusters. Standard views of Cluster 1 (left) and the complex rotated 90° and Cluster 2 (right) are depicted. *(**B**)* Comparison between 2D class averages (top row) from the cryo-EM data and the two pseudoatomic models of CRY PHR:PER2 CBD bound to CLOCK PAS-B generated from HADDOCK (Cluster 1 and Cluster 2). Forward projections (middle row) of the pseudoatomic models (bottom row) were generated to match the angular orientations observed in the experimental data. The general position of the CLOCK PAS-B domain is denoted with a green circle for both 2D class averages and forward projections of the pseudoatomic models. CLOCK PAS-B appears to adopt a range of orientations, leading it to become blurred in some 2D class averages. See Supplementary file 2 for more information.

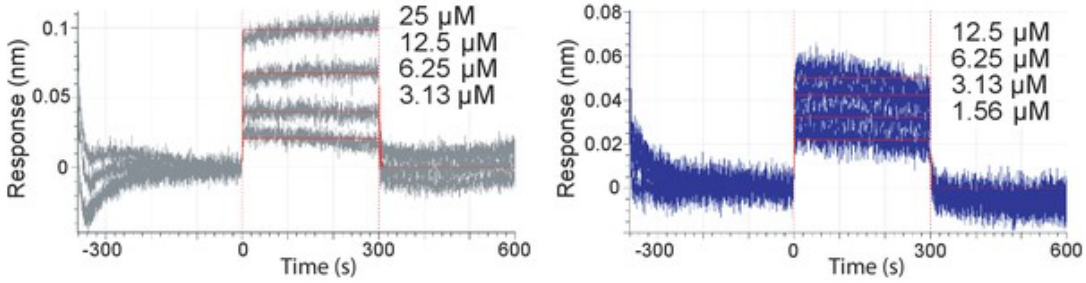

Supplementary Figure 2.7. CRY PHR binding to PAS domain core with CLOCK W362A mutation.

BLI data for CRY1 PHR (gray) or CRY2 PHR (blue) binding to immobilized, biotinylated W362A CLOCK:BMAL1 PAS-AB. Inset values represent the concentrations of CRY for individual binding reactions, top to bottom. Vertical red dashed lines indicate the beginning of association and dissociation. Red solid line, nonlinear least squares fitting to a one-site binding model. Calculated K_d for CRY1 PHR = 6.6 ± 2.6 µM, CRY2 PHR = 10.2 ± 0.2 µM (mean from n = 2 independent assays).

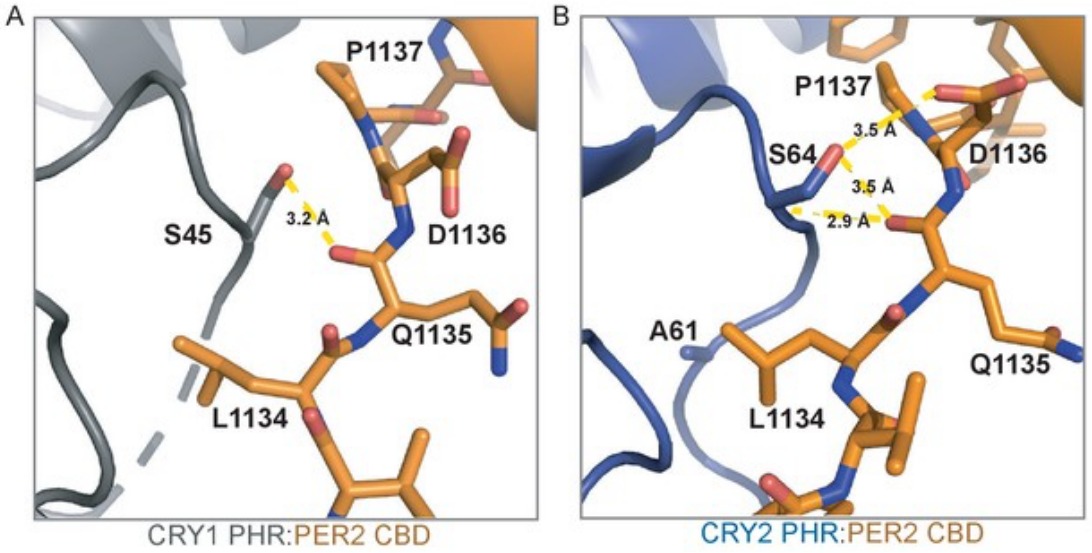

Supplementary Figure 2.8. Binding to PER2 CBD rearranges the serine loops on CRY1 and CRY2.

*(**A**)* Zoomed in view of the serine loop of CRY1 PHR:PER2 CBD (gray:orange). Interaction between Ser45 of CRY1 and the backbone of Gln1135 of PER2 CBD shown with yellow dashed lines. *(**B**)* Zoomed in view of the serine loop of CRY2 PHR:PER2 CBD (blue:orange). Interaction between Ser64 of CRY2 and the backbone of Gln1135 and the side chain of Asp1136 of PER2 CBD shown with yellow dashed lines.

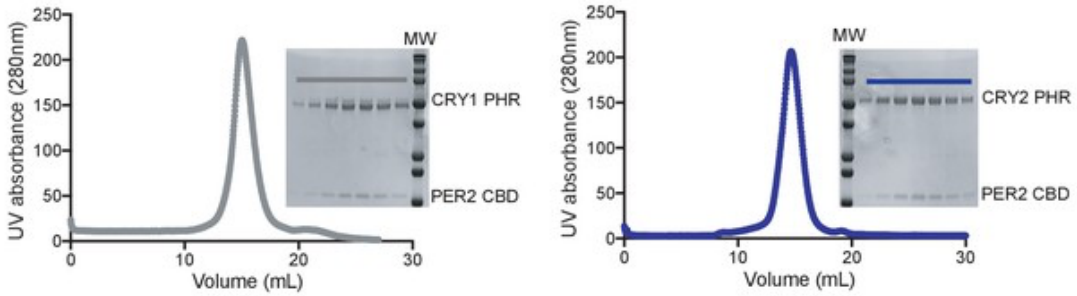

Supplementary Figure 2.9. Formation of stable CRY PHR domain:PER2 CBD complexes for binding studies.

Gel filtration analysis of CRY1 PHR:PER2 CBD (left, gray) and CRY2 PHR:PER2 CBD (right, blue). Complexes were preassembled on ice and then resolved on a S200 10/300 GL column. Peak fractions were analyzed by SDS-PAGE.

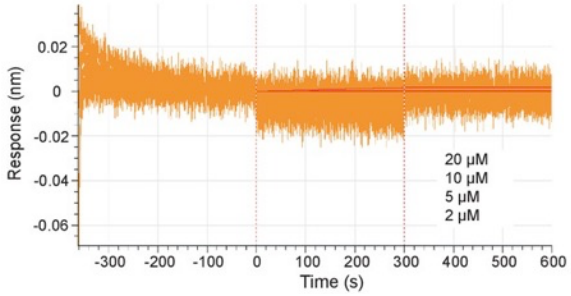

Supplementary Figure 2.10. The PER2 CBD does not bind directly to the PAS domain core of CLOCK:BMAL1.

Processed bio-layer interferometry (BLI) data for PER2 CBD (orange) binding to biotin labeled CLOCK:BMAL PAS-AB. Inset values represent the concentrations of CRY for the individual binding reactions, top to bottom. The red line is the nonlinear least squares fitting. PER2 CBD does not bind to CLOCK:BMAL1 PAS-AB at the concentrations tested.

2.8 Supplementary Files

2.8.1 Supplementary File 1 (Details of molecular dynamics simulations)

This supplementary file contains two tables (1a, 1b) on separate tabs.

https://cdn.elifesciences.org/articles/55275/elife-55275-supp1-v2.xlsx

2.8.2 Supplementary file 2 (Details of the experimental structure and computational docking models)

This supplementary file contains two tables (2a, 2b) on separate tabs.

https://cdn.elifesciences.org/articles/55275/elife-55275-supp2-v2.xlsx

2.9 References

1. Gekakis N*, et al.* (1998) Role of the CLOCK protein in the mammalian circadian mechanism. *Science* 280(5369):1564-1569.

2. Takahashi JS (2017) Transcriptional architecture of the mammalian circadian clock. *Nat Rev Genet* 18(3):164-179.

3. Aryal RP*, et al.* (2017) Macromolecular Assemblies of the Mammalian Circadian Clock. *Molecular Cell* 67(5):770-782.e776.

4. Lee C, Etchegaray JP, Cagampang FR, Loudon AS, & Reppert SM (2001) Posttranslational mechanisms regulate the mammalian circadian clock. *Cell* 107(7):855-867.

5. Preitner N*, et al.* (2002) The orphan nuclear receptor REV-ERBalpha controls circadian transcription within the positive limb of the mammalian circadian oscillator. *Cell* 110(2):251-260.

6. van der Horst GT*, et al.* (1999) Mammalian Cry1 and Cry2 are essential for maintenance of circadian rhythms. *Nature* 398(6728):627-630.

7. Vitaterna MH*, et al.* (1999) Differential regulation of mammalian period genes and circadian rhythmicity by cryptochromes 1 and 2. *Proc Natl Acad Sci U S A* 96(21):12114-12119.

8. Michael AK, Fribourgh JL, Van Gelder RN, & Partch CL (2017) Animal Cryptochromes: Divergent Roles in Light Perception, Circadian Timekeeping and Beyond. *Photochemistry and Photobiology* 93(1):128-140.

9. Gustafson CL*, et al.* (2017) A Slow Conformational Switch in the BMAL1 Transactivation Domain Modulates Circadian Rhythms. *Molecular Cell* 66(4):447-457.e447.

10. Xu H*, et al.* (2015) Cryptochrome 1 regulates the circadian clock through dynamic interactions with the BMAL1 C terminus. *Nature Structural & Molecular Biology* 22(6):476-484.

11. Griffin EA, Staknis D, & Weitz CJ (1999) Light-independent role of CRY1 and CRY2 in the mammalian circadian clock. *Science (New York, N.Y.)* 286(5440):768-771.

12. Patke A*, et al.* (2017) Mutation of the Human Circadian Clock Gene CRY1 in Familial Delayed Sleep Phase Disorder. *Cell* 169(2):203-215.e213.

13. Ukai-Tadenuma M*, et al.* (2011) Delay in feedback repression by cryptochrome 1 is required for circadian clock function. *Cell* 144(2):268-281.

14. Koike N*, et al.* (2012) Transcriptional Architecture and Chromatin Landscape of the Core Circadian Clock in Mammals. *Science (New York, N.Y.)* 338(6105):349-354.

15. Edwards MD, Brancaccio M, Chesham JE, Maywood ES, & Hastings MH (2016) Rhythmic expression of cryptochrome induces the circadian clock of arrhythmic suprachiasmatic nuclei through arginine vasopressin signaling. *Proc Natl Acad Sci U S A* 113(10):2732-2737.

16. Rosensweig C*, et al.* (2018) An evolutionary hotspot defines functional differences between CRYPTOCHROMES. *Nature Communications* 9(1):1138.

17. Partch CL, Clarkson MW, Ozgür S, Lee AL, & Sancar A (2005) Role of structural plasticity in signal transduction by the cryptochrome blue-light photoreceptor. *Biochemistry* 44(10):3795-3805.

18. Gao P*, et al.* (2013) Phosphorylation of the Cryptochrome 1 C-terminal Tail Regulates Circadian Period Length. *The Journal of Biological Chemistry* 288(49):35277-35286.

19. Li Y, Xiong W, & Zhang EE (2016) The ratio of intracellular CRY proteins determines the clock period length. *Biochem Biophys Res Commun* 472(3):531-538.

20. Liu N & Zhang EE (2016) Phosphorylation Regulating the Ratio of Intracellular CRY1 Protein Determines the Circadian Period. *Frontiers in Neurology* 7.

21. Khan SK*, et al.* (2012) Identification of a Novel Cryptochrome Differentiating Domain Required for Feedback Repression in Circadian Clock Function. *Journal of Biological Chemistry* 287(31):25917-25926.

22. Michael AK*, et al.* (2017) Formation of a repressive complex in the mammalian circadian clock is mediated by the secondary pocket of CRY1. *Proceedings of the National Academy of Sciences* 114(7):1560-1565.

23. Czarna A*, et al.* (2011) Quantitative analyses of cryptochrome-mBMAL1 interactions: mechanistic insights into the transcriptional regulation of the mammalian circadian clock. *J Biol Chem* 286(25):22414-22425.

24. Nangle SN*, et al.* (2014) Molecular assembly of the period-cryptochrome circadian transcriptional repressor complex. *eLife* 3:e03674.

25. Schmalen I*, et al.* (2014) Interaction of circadian clock proteins CRY1 and PER2 is modulated by zinc binding and disulfide bond formation. *Cell* 157(5):1203-1215.

26. Sato TK*, et al.* (2006) Feedback repression is required for mammalian circadian clock function. *Nature genetics* 38(3):312-319.

27. Huang N*, et al.* (2012) Crystal structure of the heterodimeric CLOCK:BMAL1 transcriptional activator complex. *Science (New York, N.Y.)* 337(6091):189-194.

28. Xing W*, et al.* (2013) SCF(FBXL3) ubiquitin ligase targets cryptochromes at their cofactor pocket. *Nature* 496(7443):64-68.

29. Ode KL*, et al.* (2017) Knockout-Rescue Embryonic Stem Cell-Derived Mouse Reveals Circadian-Period Control by Quality and Quantity of CRY1. *Mol Cell* 65(1):176-190.

30. Czarna A*, et al.* (2013) Structures of Drosophila Cryptochrome and Mouse Cryptochrome1 Provide Insight into Circadian Function. *Cell* 153(6):1394-1405.

31. Lopez-Llano J, Campos LA, & Sancho J (2006) Alpha-helix stabilization by alanine relative to glycine: roles of polar and apolar solvent exposures and of backbone entropy. *Proteins* 64(3):769-778.

32. Hirota T*, et al.* (2012) Identification of small molecule activators of cryptochrome. *Science (New York, N.Y.)* 337(6098):1094-1097.

33. Liu AC*, et al.* (2007) Intercellular coupling confers robustness against mutations in the SCN circadian clock network. *Cell* 129(3):605-616.

34. McClendon CL, Hua L, Barreiro A, & Jacobson MP (2012) Comparing Conformational Ensembles Using the Kullback-Leibler Divergence Expansion. *J Chem Theory Comput* 8(6):2115-2126.

35. Partch CL, Green CB, & Takahashi JS (2014) Molecular architecture of the mammalian circadian clock. *Trends in Cell Biology* 24(2):90-99.

36. Miyazaki K, Mesaki M, & Ishida N (2001) Nuclear entry mechanism of rat PER2 (rPER2): role of rPER2 in nuclear localization of CRY protein. *Mol Cell Biol* 21(19):6651-6659.

37. Yagita K*, et al.* (2002) Nucleocytoplasmic shuttling and mCRY-dependent inhibition of ubiquitylation of the mPER2 clock protein. *The EMBO journal* 21(6):1301-1314.

38. Kim JY, Kwak PB, Gebert M, Duong HA, & Weitz CJ (2015) Purification and analysis of PERIOD protein complexes of the mammalian circadian clock. *Methods Enzymol* 551:197-210.

39. Anand SN*, et al.* (2013) Distinct and separable roles for endogenous CRY1 and CRY2 within the circadian molecular clockwork of the suprachiasmatic nucleus, as revealed by the Fbxl3(Afh) mutation. *The Journal of neuroscience : the official journal of the Society for Neuroscience* 33(17):7145-7153.

40. Fuxreiter M*, et al.* (2008) Malleable machines take shape in eukaryotic transcriptional regulation. *Nat Chem Biol* 4(12):728-737.

41. Brautigam CA*, et al.* (2004) Structure of the photolyase-like domain of cryptochrome 1 from Arabidopsis thaliana. *Proc Natl Acad Sci U S A* 101(33):12142-12147.

42. Levy C*, et al.* (2013) Updated structure of Drosophila cryptochrome. *Nature* 495(7441):E3-4.

43. Hitomi K*, et al.* (2009) Functional motifs in the (6-4) photolyase crystal structure make a comparative framework for DNA repair photolyases and clock cryptochromes. *Proc Natl Acad Sci U S A* 106(17):6962-6967.

44. Park HW, Kim ST, Sancar A, & Deisenhofer J (1995) Crystal structure of DNA photolyase from Escherichia coli. *Science* 268(5219):1866-1872.

45. Sancar A (2003) Structure and function of DNA photolyase and cryptochrome blue-light photoreceptors. *Chem Rev* 103(6):2203-2237.

46. Zhu H*, et al.* (2005) The two CRYs of the butterfly. *Curr Biol* 15(23):R953-954.

47. Zhang Y, Markert MJ, Groves SC, Hardin PE, & Merlin C (2017) Vertebrate-like CRYPTOCHROME 2 from monarch regulates circadian transcription via independent repression of CLOCK and BMAL1 activity. *Proc Natl Acad Sci U S A* 114(36):E7516-E7525.

48. Kiyohara YB*, et al.* (2006) The BMAL1 C terminus regulates the circadian transcription feedback loop. *Proc Natl Acad Sci U S A* 103(26):10074-10079.

49. Beckett D, Kovaleva E, & Schatz PJ (1999) A minimal peptide substrate in biotin holoenzyme synthetase-catalyzed biotinylation. *Protein Sci* 8(4):921-929.

50. Fairhead M & Howarth M (2015) Site-specific biotinylation of purified proteins using BirA. *Methods Mol Biol* 1266:171-184.

51. Pettersen EF*, et al.* (2004) UCSF Chimera--a visualization system for exploratory research and analysis. *J Comput Chem* 25(13):1605-1612.

52. Lindorff-Larsen K*, et al.* (2010) Improved side-chain torsion potentials for the Amber ff99SB protein force field. *Proteins* 78(8):1950-1958.

53. Bussi G, Donadio D, & Parrinello M (2007) Canonical sampling through velocity rescaling. *J Chem Phys* 126(1):014101.

54. Berendsen HJC, Postma JPM, van Gunsteren WF, DiNola A, & Haak JR (1984) Molecular dynamics with coupling to an external bath. *The Journal of Chemical Physics* 81(8):3684-3690.

55. Parrinello M & Rahman A (1981) Polymorphic Transitions in Single-Crystals - a New Molecular-Dynamics Method. *J Appl Phys* 52(12):7182-7190.

56. Abraham MJ*, et al.* (2015) GROMACS: High performance molecular simulations through multi-level parallelism from laptops to supercomputers. *SoftwareX* 1-2:19-25.

57. Wagner JR*, et al.* (2017) POVME 3.0: Software for Mapping Binding Pocket Flexibility. *J Chem Theory Comput* 13(9):4584-4592.

58. McGibbon RT*, et al.* (2015) MDTraj: A Modern Open Library for the Analysis of Molecular Dynamics Trajectories. *Biophys J* 109(8):1528-1532.

59. Moffett AS, Bender KW, Huber SC, & Shukla D (2017) Allosteric Control of a Plant Receptor Kinase through S-Glutathionylation. *Biophys J* 113(11):2354-2363.

60. Rapp C, Snow S, Laufer T, & McClendon CL (2013) The role of tyrosine sulfation in the dimerization of the CXCR4:SDF-1 complex. *Protein Sci* 22(8):1025-1036.

61. Battye TGG, Kontogiannis L, Johnson O, Powell HR, & Leslie AGW (2011) iMOSFLM: a new graphical interface for diffraction-image processing with MOSFLM. *Acta Crystallographica Section D* 67(4):271-281.

62. Evans P (2006) Scaling and assessment of data quality. *Acta Crystallogr D Biol Crystallogr* 62(Pt 1):72-82.

63. Winn MD*, et al.* (2011) Overview of the CCP4 suite and current developments. *Acta Crystallogr D Biol Crystallogr* 67(Pt 4):235-242.

64. Adams PD*, et al.* (2010) PHENIX: a comprehensive Python-based system for macromolecular structure solution. *Acta Crystallographica Section D* 66(2):213-221.

65. Emsley P, Lohkamp B, Scott WG, & Cowtan K (2010) Features and development of Coot. *Acta Crystallogr D Biol Crystallogr* 66(Pt 4):486-501.

66. Suloway C*, et al.* (2005) Automated molecular microscopy: the new Leginon system. *J Struct Biol* 151(1):41-60.

67. Voss NR, Yoshioka CK, Radermacher M, Potter CS, & Carragher B (2009) DoG Picker and TiltPicker: software tools to facilitate particle selection in single particle electron microscopy. *J Struct Biol* 166(2):205-213.

68. Scheres SH (2012) RELION: implementation of a Bayesian approach to cryo-EM structure determination. *J Struct Biol* 180(3):519-530.

69. van Zundert GCP*, et al.* (2016) The HADDOCK2.2 Web Server: User-Friendly Integrative Modeling of Biomolecular Complexes. *J Mol Biol* 428(4):720-725.

70. Ludtke SJ, Baldwin PR, & Chiu W (1999) EMAN: semiautomated software for high-resolution single-particle reconstructions. *J Struct Biol* 128(1):82-97.

CHAPTER 3: The human CRY1 tail controls circadian timing by regulating its association with CLOCK:BMAL1

The text of this chapter includes a reprint of the following previously published material:

> **Parico, G. C. G**., I. Perez, J. L. Fribourgh, B. N. Hernandez, H. W. Lee, and C. L. Partch. 2020. 'The human CRY1 tail controls circadian timing by regulating its association with CLOCK:BMAL1', *Proc Natl Acad Sci U S A*, 117: 27971-79. DOI: 10.1073/pnas.1920653117

Contributions by the co-authors are as follows: G.C.G.P., H.-W.L., and C.L.P. designed research; G.C.G.P., I.P., J.L.F., B.N.H., and H.-W.L. performed research; G.C.G.P., I.P., J.L.F., and B.N.H. contributed new reagents/analytic tools; G.C.G.P., I.P., J.L.F., and H.-W.L. analyzed data; G.C.G.P. and C.L.P. wrote the paper; and C.L.P. supervised project and secured funding.

The candidate, Gian Carlo Parico, performed the following contributions for the development of this manuscript: designed and performed research; contributed new reagents/analytic tools; analyzd data; and wrote the paper.

All authors edited and approved of the manuscript.

Manuscript Acknowledgments

We thank Scott Showalter (Penn State) and Isabella Felli (University of Florence) for pulse sequences and advice on ^{13}C-detected CON NMR experiments.

3.1 Abstract

Circadian rhythms are generated by interlocked transcription-translation feedback loops that establish cell-autonomous biological timing of ~24-hours. Mutations in core clock genes that alter their stability or affinity for one another lead to changes in circadian period. The human CRY1Δ11 mutant lengthens circadian period to cause Delayed Sleep Phase Disorder (DSPD), characterized by a very late onset of sleep. CRY1 is a repressor that binds to the transcription factor CLOCK:BMAL1 to inhibit its activity and close the core feedback loop. We previously showed how the PHR (photolyase homology region) domain of CRY1 interacts with distinct sites on CLOCK and BMAL1 to sequester the transactivation domain from coactivators. However, the Δ11 variant alters an intrinsically disordered tail in CRY1 downstream of the PHR. We show here that the CRY1 tail, and in particular the region encoded by exon 11, modulates the affinity of the PHR domain for CLOCK:BMAL1. The PHR-binding epitope in exon 11 is necessary and sufficient to disrupt the interaction between CRY1 and the subunit CLOCK. Moreover, PHR-tail interactions are conserved in the paralog CRY2 and reduced when either CRY is bound to the circadian co-repressor PERIOD2. Discovery of this autoregulatory role for the mammalian CRY1 tail and conservation of PHR-tail interactions in both mammalian cryptochromes highlights functional conservation with plant and insect cryptochromes, which also utilize PHR-tail interactions to reversibly control their activity.

3.2 Introduction

Circadian rhythms coordinate behavior and physiology with the 24-hour solar day. At the molecular level, over 40% of the genome is temporally regulated in a circadian manner (1). In the core transcription/translation feedback loop of the clock, the heterodimeric transcription factor CLOCK:BMAL1 (CLOCK, circadian locomotor cycles kaput; BMAL1, brain and muscle ARNT-like protein 1) promotes transcription of its own repressors, period (PER1/2) and cryptochrome (CRY1/2) (2). Cryptochromes facilitate the direct interaction of PER-CRY repressive complexes with CLOCK:BMAL1 (3) and sequester the transactivation

domain (TAD) of BMAL1 from coactivators to directly inhibit its activity (4). We previously showed that changing the affinity of CRY1 for the BMAL1 TAD can alter circadian timing (4, 5), presumably by shortening or lengthening the duration of repression in the feedback loop. Similarly, missense mutations within other core clock genes that alter their stability or activity can change the circadian period (6-12). Variants that shorten circadian period correlate with the earlier sleep/wake times associated with Advanced Sleep Phase Disorder (ASPD), while DSPD is characterized by a longer than normal circadian period (>24.2 hours) and later than normal sleep/wake times (13).

One form of familial DSPD arises from a variant of CRY1 (CRY1Δ11) that is as prevalent as 1 in 75 in certain populations (14). CRY1Δ11 disrupts a splice site leading to the in-frame deletion of exon 11, thus removing 24 residues within the disordered C-terminal tail of CRY1. While only the PHR domain of CRY1 is necessary to reconstitute circadian rhythms in Cry1–/–;Cry2–/–;*Per2*^{Luc} cells (15), the tails can modulate the period and/or amplitude of cycling, as evidenced by reconstitution assays using chimeras swapping the CRY1 and CRY2 tails (15-17) or assessing post-translational modifications like phosphorylation in the tail (18-20). Mechanistically, the CRY1 PHR binds directly to both CLOCK (3, 21) and BMAL1 (4, 5, 22) subunits as well as the CRY-binding domain (CBD) of PER2 (23) to form the central linchpin of vertebrate circadian repressive complexes (24). This suggests that the CRY1Δ11 variant, which enhances both the co-immunoprecipitation with CLOCK:BMAL1 and the transcriptional repressive state in cells (14), may alleviate an interaction between the CRY1 tail and PHR domain to increase its affinity for CLOCK:BMAL1.

Here, we identify an autoinhibitory role for exon 11 of the CRY1 tail in regulating its association with CLOCK:BMAL1, and therefore, CRY1 control of the molecular circadian clock. We show that the CRY1 C-terminal tail interacts directly with its PHR domain; using biochemical analyses and solution NMR spectroscopy, we discovered that exon 11 comprises one of two linear epitopes in the tail that bind to the PHR. Exon 11 is necessary and sufficient to compete with the PAS-B domain of CLOCK for binding to CRY1. Consistent

with this, full-length CRY1 has decreased affinity for the PAS domain core of CLOCK:BMAL1 compared to CRY1Δ11 or the isolated PHR domain. Notably, PHR-tail interactions are conserved in the paralog CRY2 and formation of a stable complex between the CRY-binding domain (CBD) of PER2 and the PHR domain of CRY1 or CRY2 interferes with PHR-tail interactions. These data point towards a conserved role for cryptochrome C-terminal tails as regulators of CRY function via direct interaction with the PHR domain.

3.3 Results

3.3.1 The CRY1 tail binds directly to the CRY1 PHR.

We used fluorescence polarization (FP) assays to explore binding of a fluorescently labeled human CRY1 tail to the PHR domain in *trans* (Figure 3.1A). The resulting binding curve is consistent with single-site protein-ligand binding and fits to an equilibrium dissociation constant (K_D) of about 5 μM (Figure 3.1B,C). The Δ11 version of the hCRY1 tail interacts with about four-fold lower affinity, demonstrating that exon 11 plays an important role in binding the PHR domain (Figure 3.1B,C). A peptide encoding the isolated exon 11 also binds to the PHR domain, but with lower affinity similar to that of the Δ11 tail, suggesting that additional sites on the CRY1 tail contribute to PHR binding.

Using an exon-based truncation analysis of the tail, we determined that exons 10 and 11 comprise the minimal binding region of the hCRY1 tail for the PHR domain (Figure 3.1B,C). The mouse CRY1 tail, which contains a short repeat insertion within exon 10, binds to its PHR with a similar affinity to the human tail (Supplementary Figure 3.1). Finally, our data suggest that exon 12 does not enhance affinity for the PHR domain (Figure 3.1B,C). This was surprising since post-translational modification within the region encoded by exon 12 apparently regulates the interaction of CRY1 with its E3 ubiquitin ligase to influence circadian rhythms (19, 20). Phosphorylation of S588 in exon 12 of mouse CRY1 (S568 in humans) after DNA damage increases its stability, as does the corresponding phosphomimetic mutation S588D (18-20). Consistent with our observation that exon 12 does

not appear to contribute to PHR binding; we found no change in affinity of the S588D CRY1 tail for the PHR domain (Supplementary Figure 3.1C,D).

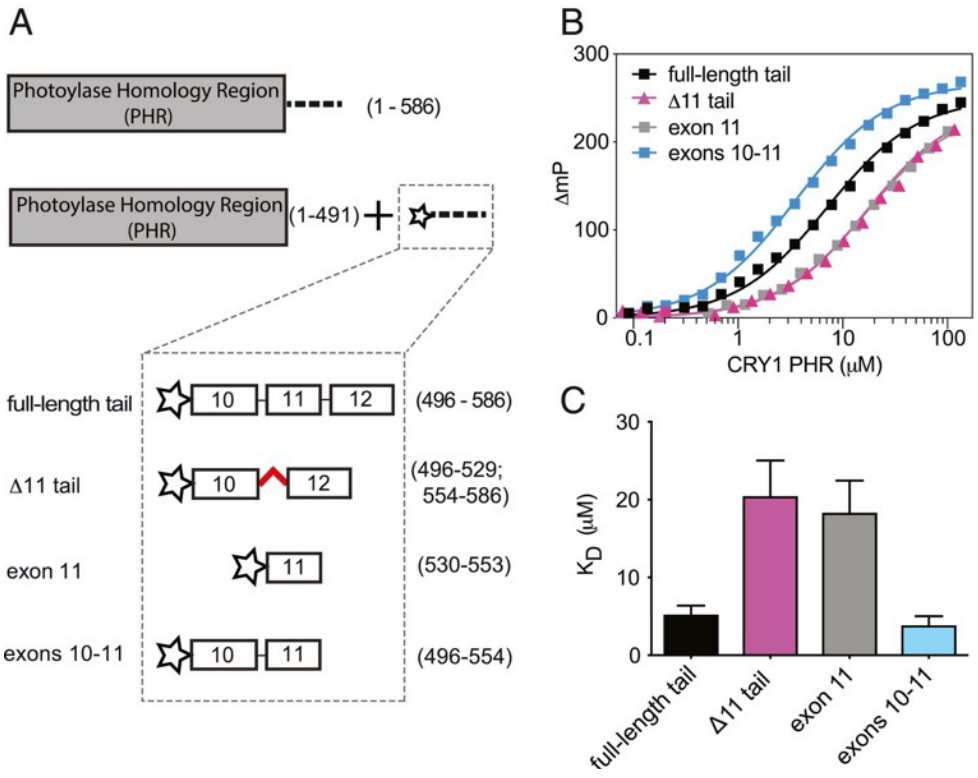

Figure 3.1. Exons 10 and 11 in the CRY1 tail are required for PHR binding

(A), Domain architecture of full-length human CRY1 and the constructs used in FP experiments, comprising the PHR (residues 1-491, gray box) and tail (residues 492-586, dashed line) with various truncations; the N-terminal fluorescein (FAM) label is depicted as a star. ***(B)*** FP binding curves of fluorescently labeled human tail constructs to the CRY1 PHR. Plot shows the mean representative binding curves of duplicate samples ± sd (of n = 3 independent assays). Curve represents fit to one-site binding (Prism). ***(C)*** Affinities of FAM-tail constructs for the PHR derived from FP binding assays (n = 3 independent assays ± sd).

3.3.2 NMR Spectroscopy maps PHR-binding epitopes in the CRY1 tail.

To further map the PHR-binding epitopes on the tail, we used nuclear magnetic resonance (NMR) spectroscopy. Backbone-based ^{1}H-^{15}N HSQC experiments probe the chemical environment of all non-proline residues as individual peaks; however, these spectra exhibit severe peak overlap in the case of long intrinsically disordered proteins (IDPs) such as the CRY1 tail (Figure 3.2A) (25, 26). To circumvent this problem, we turned to ^{13}C carbon-detected methods such as the ^{13}C-^{15}N CON to increase peak dispersion and therefore, our resolution, on this IDP (27). The CON spectrum of the CRY1 tail exhibited excellent peak dispersion that allowed us to visualize and unambiguously assign 81% of the backbone chemical shifts (Figure 3.2B).

To probe the role of exon 11 in the CRY1 tail/PHR interaction, we added unlabeled CRY1 PHR domain to the ^{13}C,^{15}N-labeled CRY1 tail and monitored chemical shift perturbations in the tail. We were limited to some degree by the solubility and stability of the CRY1 PHR domain under our NMR conditions, but under equimolar concentrations of tail and PHR, we identified a number of peaks that exhibited PHR-dependent changes indicative of binding (Figure 3.2B,C). Another advantage of carbon-detected methods is their ability to visualize proline chemical shifts, often enriched in IDPs, that cannot be detected using standard ^{1}H-^{15}N HSQC spectra (Figure 3.2C,D). For the most part, we observed broadening at select peaks within the ^{13}C,^{15}N-labeled CRY1 tail upon binding to the PHR, likely due to the large size of the PHR domain (~55 kDa) (Figure 3.2B,C,E). However, some clusters of peaks in exon 10 and 11 demonstrated changes in chemical shift (Figure 3.2F), including a hydrophobic patch in exon 10 that is composed of the motif Phe-Met-Gly-Tyr and several histidines in exon 11 that are conserved (Figure 3.2 G-K and Supplementary Figure 3.2). These same peaks are also broadened relative to the rest of the tail, suggesting that these residues are hotspots for interacting with the PHR (Figure 3.2E). An exon-based analysis of peak broadening demonstrates that it occurs to the highest extent in exons 10-11, and to a

lesser degree in exon 12 (Figure 3.2L), corroborating our FP data that the minimal binding region on the tail for interacting with the PHR domain lies within exons 10-11.

We also utilized the NMR data to probe structural characteristics of the isolated CRY1 tail. The narrow proton chemical shift dispersion and overlap of peaks in the ^{1}H-^{15}N HSQC spectrum is representative of a typical IDP (Figure 3.2A), in agreement with circular dichroism data of the CRY1 tail (28). Although the computational algorithm PONDR predicts that the CRY1 tail is highly disordered, it suggested that there may be some propensity for structure within an ordered 'minimum' centered around the sequence encoded by exon 11 (Figure 3.2M) (29); these local, ordered minima have been implicated as linear binding epitopes within other IDPs (30). However, a quantitative comparison of CRY1 tail NMR data to the chemical shift index (CSI) (31) revealed that the entire tail lacks secondary structure in the absence of the PHR domain (Figure 3.2N). Further studies could identify if any regions in the tail, such as exon 11, might adopt secondary structure upon binding to the PHR domain.

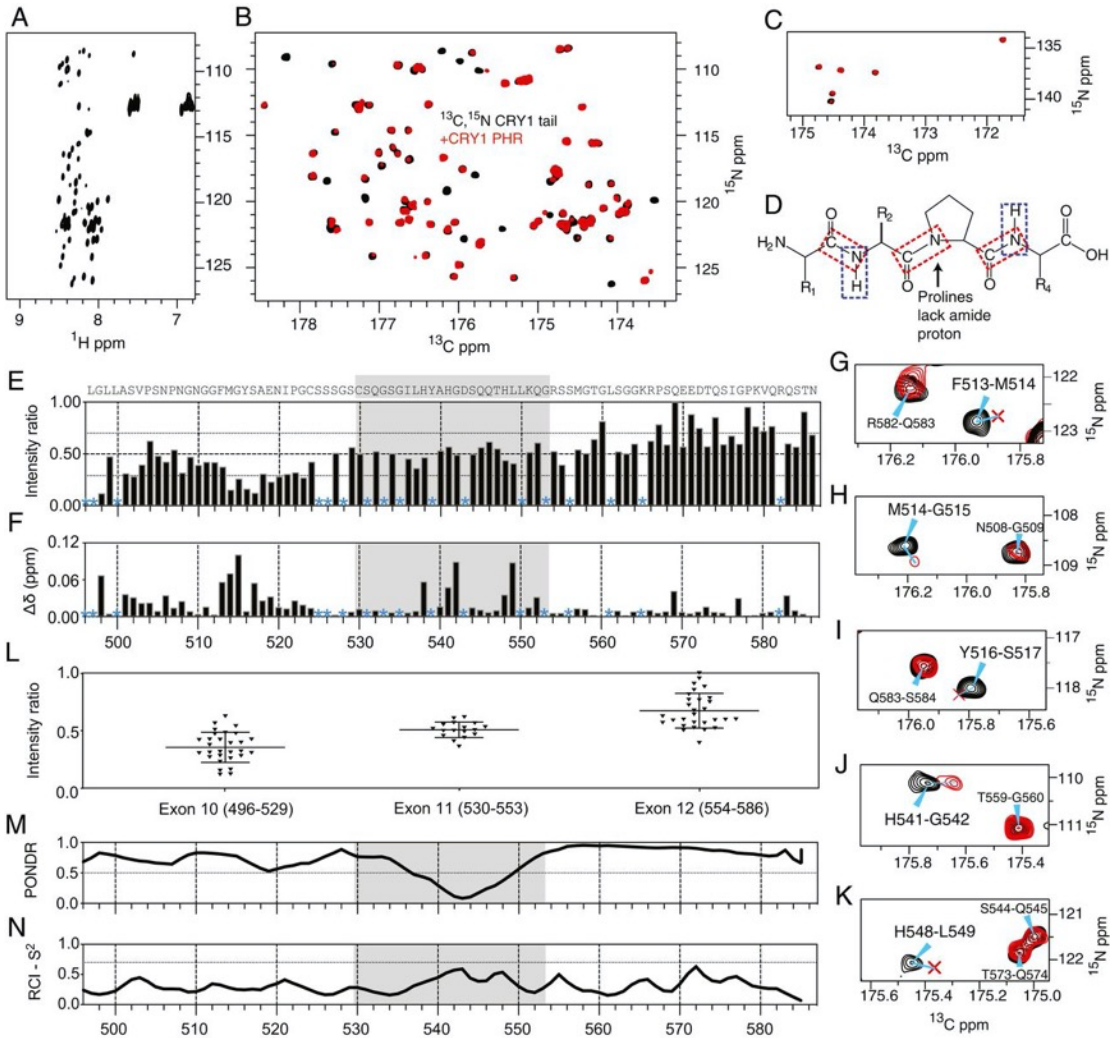

Figure 3.2. NMR spectroscopy maps the PHR binding site on the CRY1 tail

(A) ^{1}H-^{15}N HSQC spectrum of the isolated ^{15}N-labeled CRY1 tail at 120 μM. ***(B)*** ^{13}C-^{15}N CON spectra of the ^{13}C, ^{15}N-labeled CRY1 tail at 120 μM alone (black) or in the presence of 120 μM CRY1 PHR (red) ***(C)*** Proline-specific region of the ^{13}C-^{15}N CON spectrum of the ^{13}C, ^{15}N-labeled CRY1 tail ± CRY1 PHR (as in panel B). ***(D)*** Schematic of proline-containing peptide backbone, highlighting the correlations visualized by ^{1}H-^{15}N HSQC (blue box) or ^{13}C-^{15}N CON (red box). ***(E-F)***, Relative intensity (E) and chemical shift perturbation (Δδ, F) of the ^{13}C, ^{15}N-labeled CRY1 tail upon addition of equimolar CRY1 PHR. Asterisk, unassigned or overlapping peaks excluded from the analysis. Exon 11 is represented by a gray box. In E, dashed horizontal line represents the mean intensity ratio ($I_{tail+PHR}/I_{tail\ alone}$), while the dotted lines represent sem. Peaks are referred to by the number of the nitrogen of the ^{13}C-^{15}N peptide bond. ***(G-K)***, Zoom in on ^{13}C-^{15}N CON spectra peaks (^{13}C carbonyl of F513, M514, Y516, H541, H548 respectively) that are severely broadened or perturbed upon addition of CRY1 PHR. Residues along a C-N bond point to their corresponding peaks with a cyan arrow and severely broadened peaks with intensities below the base contour level are labeled with a red 'x'. ***(L)*** NMR intensity ratios ($I_{tail+PHR}/I_{tail\ alone}$) grouped by exon (mean ratio per exon ± sd). ***(M)*** PONDR prediction of a disorder in the CRY1 tail with an ordered minimum in Exon

11. ***(N)*** Random coil index (RCI) predicts lack of secondary structure (model-free parameter $S^2 < 0.7$) from NMR chemical shift assignments.

3.3.3 Exon 11 is necessary and sufficient to regulate the interaction between CRY1 and CLOCK.

Given that exon 11 plays an important role in the interaction between the CRY1 tail and its PHR domain, we next wanted to determine how it could regulate binding between the CRY1 PHR and CLOCK:BMAL1. There are two distinct interfaces for interaction with the CLOCK:BMAL1 heterodimer on the CRY1 PHR: the coiled-coil (CC) helix of CRY1 binds to the transactivation domain (TAD) of BMAL1 (4, 28), while the secondary pocket of CRY1 binds directly to CLOCK PAS-B (Figure 3.3A) (3, 21). We established FP-based binding assays for the PHR domain using fluorescently labeled BMAL1 TAD (4) or CLOCK PAS-B (Supplementary Figure 3.2A-F), allowing us to form complexes of the PHR with either target and determine the ability of exogenous tail to compete for interaction on the PHR domain in *trans*. Titrating CRY1 tail into a CRY1 PHR:BMAL1 TAD complex did not result in any changes in fluorescence polarization, demonstrating that the CRY1 tail does not play a role in regulating the interaction between the CRY1 PHR and the BMAL1 TAD (Figure 3.3B). However, titrating the CRY1 tail to a CRY1 PHR:CLOCK PAS-B complex caused a dose-dependent decrease in FP signal to levels observed with the isolated CLOCK PAS-B, demonstrating that the tail could displace CLOCK PAS-B from the CRY1 PHR domain (Figure 3.3C).

To determine a role for exon 11 in displacement of CLOCK PAS-B from the CRY1 PHR, we asked whether a peptide comprising the isolated exon 11 could also displace CLOCK PAS-B from the CRY1 PHR. As shown in Figure 3C, exon 11 also competed CLOCK PAS-B from the PHR domain, albeit with a modest reduction in efficiency relative to the full-length tail (tail IC_{50}=0.72 ± 0.66 μM, exon 11 IC_{50}=1.43 ± 1.06 μM). By contrast, the Δ11 tail had no effect on the CRY1 PHR:CLOCK PAS-B complex (Figure 3.3C). Therefore, exon 11 is necessary and sufficient to regulate the interaction between CLOCK PAS-B and the CRY1

PHR domain. Exon 11 shares sequence attributes with other intrinsically disordered inhibitory modules (idIM) involved in autoinhibition, which have a mean length of 24 ± 13 residues (exon 11 is 24 residues) and are often modified in splicing isoforms (32). Since the Δ11 tail cannot displace CLOCK PAS-B, it appears that although exon 10 contributes to PHR binding, it does not play a direct role in regulating the interaction between the CRY1 PHR domain and CLOCK PAS-B. This is consistent with data suggesting that residues encoded by exon 10 region bind near the FAD-binding pocket on CRY1, distal from the secondary pocket where CLOCK binds (33).

One prediction of our model is that both CRY1Δ11 and the tail-less CRY1 PHR domain should have higher affinity for the PAS domain core of CLOCK:BMAL1 relative to full-length CRY1. We used biolayer interferometry (BLI) to quantitatively assess CRY1 binding to the immobilized PAS domain core comprising the tandem PAS-AB domain heterodimer. Importantly, our previous studies demonstrated that association with CRY1 absolutely depends on CLOCK PAS-B docking into the secondary pocket of CRY1 (3, 21). We tracked the binding kinetics (association and dissociation) of CRY1 over time (Figure 3.3D-E and Supplementary Figure 3.3K) to confirm that both CRY1Δ11 and the isolated PHR have a higher affinity for the CLOCK:BMAL1 PAS domain core than full-length CRY1 (Figure 3.3F). Analysis of the kinetic binding data suggested that the decrease in affinity of full-length CRY1 for CLOCK is due to a modest decrease in the association rate (k_{on}) (Figure 3.3G) rather than an increase in the dissociation rate (k_{off}) (Figure 3.3H), consistent with other proteins that have autoinhibitory domains (34, 35). Furthermore, the kinetic association rate k_{on} between full-length CRY1 and the PAS domain core of CLOCK:BMAL1 PAS-AB (4.73×10^4 $M^{-1}s^{-1}$) still falls within the typical diffusion-limited regime (10^4 – 10^7 $M^{-1}s^{-1}$), rather than the conformational change-limited regime ($<10^4$ $M^{-1}s^{-1}$) suggesting that formation of the autoinhibitory complex of CRY1 occurs transiently (36). We also measured the equilibrium binding response relative to the concentration of CRY1 titrant (Figure 3.3I and Supplementary Figure 3.3L) to observe that CRY1Δ11 and the PHR domain both have a higher affinity than

full-length CRY1 (Figure 3.3J). Therefore, both kinetic and steady-state analyses show that CRY1Δ11 and the CRY1 PHR domain have similar affinities for CLOCK, thus emphasizing the essential role of the tail, and exon 11 in particular, as an autoinhibitory module that regulates CRY1 association with CLOCK:BMAL1.

Cells expressing CRY1Δ11 exhibit gene expression profiles consistent with stronger repression of CLOCK:BMAL1 (14). To confirm that the enhanced affinity of CRY1Δ11 for CLOCK directly enhances its ability to repress transcriptional activation by CLOCK:BMAL1, we performed *Per1-luc* luciferase reporter assays in HEK293T cells (Figure 3.3K). CRY1 is already a potent repressor of CLOCK:BMAL1 and its multivalent interactions with CLOCK and BMAL1 subunits can partially compensate for changes in affinity at only one of the binding sites (4, 21, 37); therefore, we used a series of *Clock* or *Bmal1* mutants that reduce affinity between CRY1 and CLOCK:BMAL1 at either the PAS domain core (*Clock* W362A) or the BMAL1 TAD (*Bmal1* L606A/L607A or the 619X truncation), reasoning that stronger binding by CRY1Δ11 would rescue repression. Indeed, expression of CRY1Δ11 consistently led to significantly increased repression, not only with wild-type CLOCK:BMAL1, but also with CLOCK and BMAL1 mutants (Figure 3.3K), even though CRY1Δ11 was expressed to the same extent as full-length CRY1 (Figure 3.3L). Therefore, by enhancing CRY1 affinity for CLOCK at the PAS domain core, the Δ11 allele serves as a better repressor of CLOCK:BMAL1.

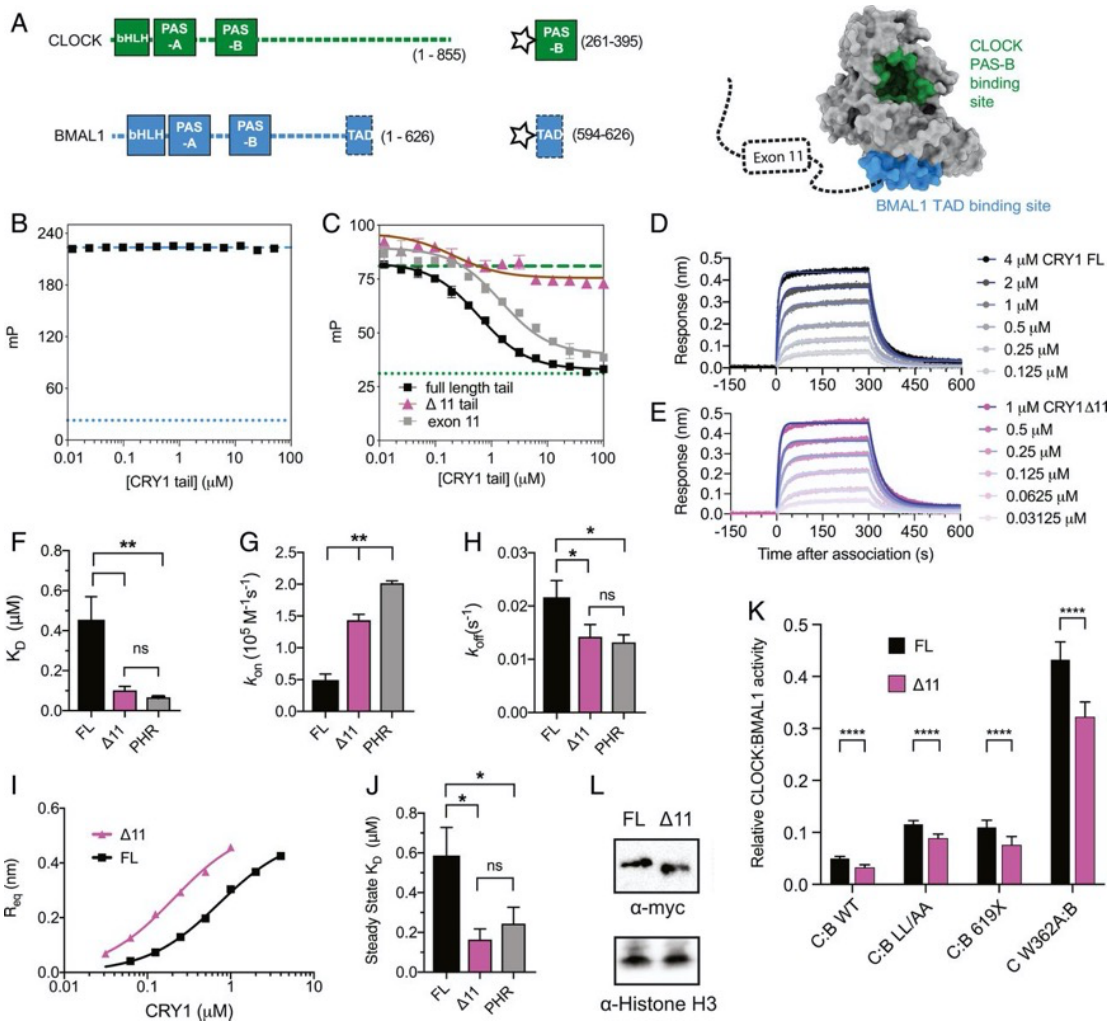

Figure 3.3. Exon 11 competes with CLOCK PAS-B to reduce CRY1 affinity for CLOCK:BMAL1

(A) Domain architecture of CLOCK and BMAL1. Starred constructs represent those used for FP assays. Right, CLOCK (green) and BMAL1 (blue) binding sites mapped onto the CRY1 PHR (PDB: 5T5X). ***(B)*** FP-based equilibrium competition assay in which the CRY1 tail (black) is titrated into a mixture of 4 μM CRY1 PHR and 20 nM fluorescently labeled BMAL1 TAD probe. Mean FP signal (n =13 points from same plate as tail titration) of 4 μM CRY1 PHR with BMAL1 TAD probe is denoted by a dashed cyan line and the mean FP signal of isolated BMAL1 TAD probe is denoted by a dotted cyan line. Data represent mean ± sd from one representative assay (of n = 3). ***(C)*** Competition assay in which CRY1 tail (black), exon 11 (gray), or the Δ11 tail (magenta) is titrated into a mixture of 4 μM CRY1 PHR and 20 nM fluorescently labeled CLOCK PAS-B probe. Mean FP signal (n =14 points from same plate as titration) of 4 μM CRY1 PHR CLOCK PAS-B probe is denoted by a dashed green line and the mean FP signal of isolated CLOCK PAS-B probe is denoted by a dotted green line. Data represent mean ± sd from one representative assay (of n = 3). Curves represent fit to one-site competitive binding model (Prism). ***(D-E),*** BLI sensorgram for biotinylated CLOCK:BMAL1 PAS-AB titrated with full-length CRY1 (E, gray to black) or CRY1Δ11 (pink to

magenta). Model fit to association and dissociation over time represented by thin blue line. ***(F-H)***, Fits for K_D, k_{on} and k_{off} from kinetic analysis of BLI data. **P* < 0.05; ***P* < 0.01 determined by one-way unpaired ANOVA and Tukey's multiple comparison test. Non-significant differences (p > 0.05) is denoted by "ns". ***(I)***, Steady-state analysis of BLI response versus CRY1 full-length (black) or CRY1Δ11 (magenta) concentration (from data in panel D and E, respectively). Plot shows the mean representative binding curves of samples (of n = 3 independent assays). Curve represents fit to one-site binding (Prism). ***(J)***, Fits for K_D from steady-state analysis of BLI data. **P* < 0.05; ***P* < 0.01 determined by one-way unpaired ANOVA and Tukey's multiple comparison test. Non-significant differences (p > 0.05) is denoted by "ns". ***(K)***, Per1-Luc assay in HEK293T cells with plasmids encoding hCry1 WT-Flag-Myc-His (black) or hCRY1 Δ11-Flag-Myc-His (magenta) with Clock WT (C) or Clock W362A, and Bmal1 WT (B), L606A L607A (LL/AA) or 619x. Relative activity is normalized to each Clock-Bmal1 construct (set to 1) in the absence of Cry1. Error bars, s.d of 11 measurements across 3 assay repeats *****P* < 0.0001 compared by two-tailed *t* test. ***(L)***, Western blots showing expression of transiently transfected CRY protein (α-Myc) or a Histone H3 loading control.

3.3.4 PER2 attenuates the CRY1 PHR-tail interaction.

ChIP-sequencing data of native clock proteins in mouse liver throughout the day revealed that CRY1 participates in two temporally distinct repressive complexes on DNA (38): an 'early' complex at circadian time (CT) 16-20, when CRY1 is also found in large, heterogeneous complexes with CRY2, PER proteins and other epigenetic regulators (39), and a 'late' complex at CT0-4 where CRY1 is bound to CLOCK:BMAL1 in the absence of other core clock proteins (24, 40, 41). Therefore, CRY1 has a distinct role in the clock, in line with studies showing that it is critical for sustaining cellular circadian rhythms in dissociated SCN neurons (42), and that it can work as a repressor both with PER proteins and independently of them (24, 40, 41).

Crystal structures reveal that the CBD of PER2 wraps around the CRY PHR domain to make contacts near both of the CLOCK and BMAL1 binding sites (Figure 3.4A) (3, 23, 43) . Given that exon 11 can displace CLOCK PAS-B from the CRY1 secondary pocket, we wanted to see if the PER2 CBD could affect interaction of the tail with the CRY1 PHR domain. First, we examined binding of the fluorescently labeled tail to either CRY1 PHR or a preformed CRY1 PHR:PER2 CBD complex, and found that PER2 decreased tail binding on the PHR domain by at least 10-fold (Figure 3.4B). By contrast, the presence of the tail in full-length CRY1 did not affect the affinity between CRY1 and the PER2 CBD (Figure 3.4C).

Therefore, even though the tail is tethered and thus present at a higher localized effective concentration, the PER2 CBD binds to CRY with low nanomolar affinity (23) and is able to outcompete the tail for binding to the PHR domain. We further tested this hypothesis by titrating the PER2 CBD into a preformed complex of the CRY1 PHR with its fluorescently labeled tail to show that the PER2 CBD efficiently displaced the CRY1 tail from the CRY1 PHR domain (Figure 3.4D). Therefore, binding of the PER2 CBD and the CRY1 tail to the PHR domain appear to be mutually exclusive. This suggests that regulation of CRY1 function in the clock by exon 11 is most likely to occur in the late repressive complex at CT0-4 when CRY1 represses CLOCK:BMAL1 independently of PER proteins (24, 38).

3.3.5 PHR-tail interactions are conserved in CRY2.

Unlike CRY1, circadian repressive complexes that contain CRY2 obligately contain PER proteins (38). Although the CRY1 and CRY2 tails are highly divergent in sequence, their PHR domains are highly conserved with 80% identity (Supplementary Figure 3.4). Therefore, we sought to determine how the PHR-tail interactions identified earlier in CRY2 (26) compare in affinity to CRY1 and if they too are affected by PER binding. We performed an FP binding assay with fluorescently labeled CRY2 tail and PHR domain to find that the CRY2 tail binds to its PHR with an affinity similar to that of CRY1 (CRY2 tail K_D = 7.53 ± 3.49 μM; CRY1 tail K_D = 4.81 ± 0.95 μM) (Figure 3.4E). Interestingly, we found that the fluorescently labeled CRY1 tail also bound to the CRY2 PHR domain with similar affinity (Supplementary Figure 3.4C), suggesting that tail binding site(s) on the PHR domains may be conserved between the two paralogs. Furthermore, we found that the PER2 CBD similarly reduced affinity of the CRY2 tail for its PHR domain (Figure 3.4E) and that inclusion of the tail in full-length CRY2 had no effect on PER2 CBD binding (Figure 3.4F). Altogether, these data demonstrate that PHR-tail interactions are a conserved biochemical property of mammalian cryptochromes and that PER2 binding competes with the disordered tails of both CRY1 and CRY2 for binding to the PHR domain.

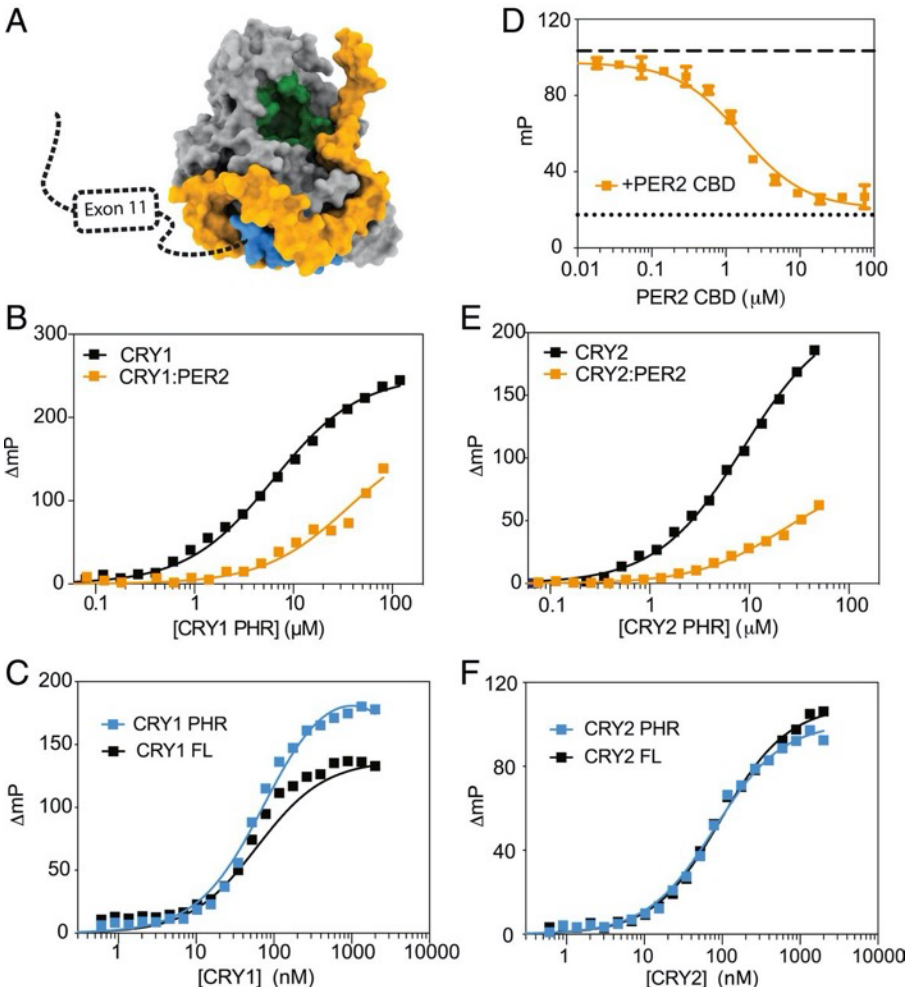

Figure 3.4. PER2 competes with the CRY1 tail for binding to the PHR domain

(A) Crystal structure of the CRY1 PHR:PER2 CBD complex (PDB: 4CT0) illustrating the proximity of PER2 CBD (PER2 1095-1215, orange) to the CLOCK (green) and BMAL1 (blue) binding sites on the CRY1 PHR (gray). ***(B)*** FP binding curves of fluorescently labeled human tail to the CRY1 PHR (black) or a CRY1 PHR:PER2 CBD complex (orange). Plot shows the mean representative binding curves of duplicate samples ± sd (of n = 3 independent assays). Curve represents fit to one-site binding (Prism). ***(C)*** FP binding curves of fluorescently labeled PER2 CBD to the CRY1 PHR (cyan) or full-length CRY1 (black). Plot shows the mean representative binding curves of duplicate samples ± sd (of n = 3 independent assays). Curve represents fit to one-site binding (Prism) with PER2 CBD binding to the CRY1 PHR at K_D= 64.8 ± 24.9 nM and PER2 CBD binding to CRY1 FL at K_D= 75.3 ± 3.7 nM. ***(D)*** FP-based equilibrium competition assay in which PER2 CBD (orange) is titrated into a mixture of 4 μM CRY1 PHR and 20 nM fluorescently labeled CRY1 tail probe. Mean FP signal (n =13 points from same plate as PER2 CBD titration) of 4 μM CRY1 PHR and 20 nM CRY1 tail probe is denoted by a dashed black line and the mean FP signal of isolated CRY1 tail probe is denoted by a dotted black line. Data represent mean ± sd from one representative assay (of n = 3). For assays with displacement, curves represent fit to one-site competitive binding model (Prism). ***(E)*** FP binding curves of fluorescently labeled human tail to the CRY2 PHR (black) or a CRY2 PHR:PER2 CBD complex (orange). Plot shows the mean representative

binding curves of duplicate samples ± sd (of n = 3 independent assays). Curve represents fit to one-site binding (Prism). ***(F)*** FP binding curves of fluorescently labeled PER2 CBD to the CRY2 PHR (cyan) or full-length CRY2 (black). Plot shows the mean representative binding curves of duplicate samples ± sd (of n = 3 independent assays). Curve represents fit to one-site binding (Prism). with PER2 CBD binding to the CRY2 PHR at K_D = 70.5 ± 7.8 nM and PER2 CBD binding to CRY2 FL at K_D= 99.8 ± 15 nM.

3.4 Discussion

The human *Cry1Δ11* allele lengthens circadian period and consequently delays the release of melatonin and onset of sleep associated with Delayed Sleep Phase Disorder. Mechanistically, the change in circadian period is likely due to enhanced repression by the CRY1Δ11 mutant that was reported in cellular studies (14). We demonstrate here that exon 11 is necessary and sufficient to regulate CRY1 affinity for the PAS domain core of CLOCK:BMAL1, leading to an increase in repression. Although the change in K_D for CLOCK:BMAL1 upon deletion of exon 11 is relatively modest (~4-fold), this is similar to what has been observed in other proteins upon removal of analogous autoinhibitory domains (44, 45). Moreover, we previously showed that tuning CRY1 affinity for the BMAL1 TAD over a similar range of K_Ds elicited comparable changes in period in cellular circadian rhythms (4, 5), providing compelling evidence that the change in affinity of CRY1 for CLOCK:BMAL1 measured here underlies physiologically relevant effects on human circadian rhythms.

Our discovery that the disordered tail of CRY1 binds directly to its PHR domain provides a framework to begin to understand how truncations, substitutions, and post-translational modifications of the CRY1 tail influence circadian period (15-20). While exon 11 controls affinity for CLOCK:BMAL1, our NMR studies also identified a PHR-binding epitope upstream in exon 10, consistent with our exon-based truncation studies showing that exons 10-11 comprise the core PHR-binding motif. Although the DNA damage-dependent phosphorylation of S588 (pS588) or a phosphomimetic mutation (S588D) downstream in exon 12 both regulate proteasomal degradation of CRY1 (18-20), we saw no effect of the phosphomimetic mutant on affinity of the tail for the PHR domain. The stabilizing effect of

pS588 or S588D may be related to an interaction between the CRY1 tail and the Herpes virus-associated ubiquitin-specific protease (HAUSP, a.k.a. USP7), which promotes deubiquitination of CRY1 (20). Identifying how the tail binds to regulatory proteins like HAUSP and where it docks on the PHR domain will provide key insight into its regulation of CRY1 stability and circadian rhythms.

Although both cryptochromes serve as transcriptional repressors of CLOCK:BMAL1, genetic deletion of CRY1 or CRY2 in mice leads to dramatically different circadian periods. Loss of the stronger repressor, CRY1, leads to a short period, while loss of the weaker repressor, CRY2, gives rise to a long period (46, 47). Consistent with this, the intracellular ratio of cryptochromes can define the repressive potential of the negative arm of the molecular clock to contribute to period generation (16). Remarkably, differences in their repressive power of cryptochrome isoforms is defined by biochemical differences in the secondary pocket on their PHR domains and their respective C-terminal tails; swapping several pocket residues and the tails is sufficient to confer CRY2-like repression and clock timing to CRY1 and vice versa (17). Isoform-specific differences in protein dynamics at the secondary pocket contribute to a 20-fold difference in affinity for the PAS domain core of CLOCK:BMAL1 between CRY1 and CRY2 (3). However, it was not clear until now how the disordered tails of cryptochromes might figure into regulation of CRY function in the molecular clock. This work demonstrates how PHR-tail interactions in CRY1 converge on regulation of CLOCK:BMAL1 binding at the secondary pocket of CRY1. PHR-tail interactions likely regulate CRY2 as well, since the disordered tail of CRY2 tail also binds its PHR domain (26) and post-translational modifications in the tail regulate CRY2 stability (48). Collectively, these data demonstrate that there is much more to learn about these cryptic regulatory domains and how they influence circadian rhythms.

This work reveals a general mechanism for CRY regulation that is apparently conserved from human CRY1 to cryptochromes from *Arabidopsis* and *Drosophila*, where C-terminal tails bind to their respective PHR domains to create autoinhibited states

(Supplementary Figure 3.5) (26, 28, 49-52). In this respect, the CRY1Δ11 mutant appears to functionally mimic *Drosophila* CRY mutants that are constitutively active due to removal of their autoinhibitory C-terminal tail (49-51). However, unlike cryptochromes from *Arabidopsis* and *Drosophila* that use blue light to regulate the PHR-tail interaction (26, 28, 49, 53), mammalian cryptochromes do not co-purify with flavin (54) or respond to blue light in their roles as transcriptional repressors (55). As an alternative to regulation by phototransduction, our data suggest that the association of other proteins (56) or post-translational modifications (18-20) likely play direct roles in regulating the CRY1 PHR-tail interaction (Supplementary Figure 3.5). Use of a flexibly tethered autoinhibitory domain to tune CRY1 activity in the clock is also consistent with a growing appreciation that intrinsically disordered regions offer a powerful means to modulate protein activity via regulated alternate splicing (57).

3.5 Materials and Methods

3.5.1 Expression and purification of recombinant proteins.

All CRY1 tail constructs (full length human CRY1 tail, residues 496-586; human CRY1 exon 11, residues 530-553; Δ11 tail, residues 496-586 missing residues 530-553; human CRY1 exons 10-11, residues 496–553; mouse CRY1 tail, residues 496-606) and other proteins such as PER2 CBD (human PER2 residues 1095-1215), CLOCK PAS-B (mouse CLOCK residues 261-395), and Biotin Acceptor Peptide (BAP)-tagged CLOCK PAS-AB (mouse CLOCK residues 93-395) were expressed using *Escherichia coli* (*E. coli*) Rosetta2 (DE3) cells. Sortase A and BirA were expressed in BL21 (DE3) *E. coli*. Proteins were expressed as a fusion to the solubilizing tags GST (for BirA), His_6-GST (for CRY1 and PER2 constructs), His_6-NusA-XL (for CLOCK PAS-B and BAP-tagged CLOCK PAS-AB), or His_6 (for Sortase A). Protein expression was induced at 37°C with 0.5 mM isopropyl-β-D-thiogalactopyranoside (IPTG) at an OD_{600} of ~0.8 and grown for an additional 16 hours at 18°C. Cells were centrifuged at 4°C at 3200 x g, reconstituted in 50 mM Tris pH 7.5, 300 mM NaCl, 5% (vol/vol) glycerol and 5 mM β-mercaptoethanol (BME) and lysed using a

microfluidizer followed by brief sonication. After clarifying lysate on a centrifuge at 4°C at 140,500 x g for 1 hour, protein was captured using Ni-NTA affinity chromatography (Qiagen) or Glutathione Sepharose 4B resin (GE Life Sciences). After capturing protein on the relevant affinity chromatography resin, the affinity and solubility tags (e.g. His_6-GST, His_6, or GST) were cleaved using GST-TEV (on Glutathione resin) or His_6-TEV protease (on Ni-NTA resin) at 4°C overnight. Cleaved protein was then collected from the flow-through after overnight TEV cleavage. Sortase A and CRY1 tail constructs were further purified using size exclusion chromatography (SEC) in 50 mM Tris, pH 7.5, 150 mM NaCl, 10% (vol/vol) glycerol. GST-BirA was further purified using SEC in 50 mM Tris, pH 8.0, 300 mM NaCl, 1 mM dithiothreitol (DTT), 5% (vol/vol) glycerol. All other proteins (e.g. CLOCK PAS-B, CLOCK PAS-AB) were further purified using SEC in 20 mM HEPES pH 7.5, 125 mM NaCl, 5% (vol/vol) glycerol, and 2 mM Tris(2-carboxyethyl)phosphine (TCEP). For long-term storage, small aliquots of these proteins were frozen in liquid nitrogen and stored at -70°C.

BMAL1 PAS-AB (mouse BMAL1 residues 136-441) and all CRY1 constructs containing the PHR domain (mouse CRY1 PHR, residues 1-491; full-length mouse CRY1, residues 1-606; full-length human CRY1, residues 1-586; human CRY1 Δ11, residues 1-586 Δ530-553; mouse CRY2 PHR, residues 1-512; full-length mouse CRY1, residues 1-592) were expressed in Sf9 suspension insect cells (Expression systems) using the baculovirus expression system. His_6-tagged versions of CRYs were cloned into pFastBac HTa vectors that were later transduced into baculovirus. We used P3 virus to infect Sf9 cells at 1.2 x 10^6 cells per milliliter, which were grown for 72 hours at 27°C before harvesting.

CRY-expressing cells were centrifuged at 4°C at 3200 x g, resuspended in 50 mM Tris pH 7.5, 300 mM NaCl, 5% (vol/vol) glycerol and 5 mM BME and lysed in low concentrations of detergent (0.01% (vol/vol) Triton X-100), Pierce Protease Inhibitor EDTA-free tablets (1 tablet/50mL, Thermo Scientific), and 1 mM phenylmethylsulfonyl fluoride (PMSF) using a microfluidizer followed by brief sonication. After clarifying lysate on a centrifuge at 4°C at 140,500 x g for 1 hour, protein was captured using Ni-NTA affinity chromatography (Qiagen).

Protein was further purified using ion exchange chromatography preceding SEC into CRY buffer (20 mM HEPES pH 7.5, 125 mM NaCl, 5% (vol/vol) glycerol, and 2 mM TCEP). CRY protein preps were stored on ice at 4°C or frozen in small aliquots and subjected to only one freeze/thaw cycle. If kept on ice, full-length (or Δ11) CRY proteins were used for experiments within 36 hours of purification to minimize proteolysis of the tail, while PHR domains were used within 7 days.

BMAL1 PAS-AB expressing cells were resuspended in BMAL1 resuspension buffer (50 mM HEPES buffer pH 7.5, 300 mM NaCl, 5% (vol/vol) glycerol and 5 mM BME). Cells were lysed and clarified as described above. The soluble lysate was bound in batch-mode to Glutathione Sepharose 4B (GE Healthcare), then washed in BMAL1 resuspension buffer and eluted with 50 mM HEPES buffer pH 7.5, 150 mM NaCl, 5% (vol/vol) glycerol and 5 mM BME, 25 mM reduced glutathione. The protein was desalted into 50 mM HEPES buffer pH 7, 150 mM NaCl, 5% (vol/vol) glycerol and 5 mM BME using a HiTrap Desalting column (GE Healthcare) and the GST tag was cleaved with GST-TEV protease overnight at 4°C. The cleaved GST-tag and GST-tagged TEV protease was removed by Glutathione Sepharose 4B (GE Healthcare) and the remaining BMAL1 PAS-AB protein was further purified by Superdex75 SEC (GE Healthcare) into 20 mM HEPES buffer pH 7.5, 125 mM NaCl, 5% (vol/vol) glycerol, and 2 mM TCEP. Purified BMAL1 PAS-AB was mixed with biotinylated CLOCK PAS-AB (below) to generate the heterodimer for binding assays.

3.5.2 Biotinylation and reconstitution of Biotin-CLOCK:BMAL1 PAS-AB.

For the biotinylation reaction, 100 μM BAP-CLOCK PAS-AB in 20 mM HEPES pH 7.5, 125 mM NaCl, 5% (vol/vol) glycerol, and 2 mM TCEP was incubated at 4˚C overnight with 2 mM ATP, 1 μM GST-BirA and 150 μM biotin. GST-BirA was removed after the reaction using Glutathione Sepharose 4B (GE Healthcare) resin and excess biotin was separated from the labeled protein by SEC. Biotin-CLOCK:BMAL1 PAS-AB heterodimer was reconstituted after labeling by adding equimolar BMAL1 PAS-AB to biotinylated CLOCK PAS-AB and verifying

complex formation by SEC. Biotinylated heterodimer was quick frozen in liquid nitrogen for long-term storage at -80°C.

3.5.3 Fluorescent labeling.

For shorter peptides such as CRY1 exon 11, BMAL1 TAD, and the Sortase A recognition motif, we purchased commercially synthesized peptides with N-terminal cysteines conjugated to tetramethylrhodamine (TAMRA) 5-maleimide fluorophore or a fluorescein 5-maleimide fluorophore. To fluorescently label recombinantly expressed proteins and peptides, we utilized Sortase A-mediated reactions (58) between an N-terminally fluorescein-labeled (or TAMRA-labeled) Sortase A recognition motif peptide (FAM-LPETGG) and our protein of interest (e.g., CRY1 tail or CLOCK PAS-B). CLOCK PAS-B were labeled right after purification via SEC (i.e., without a freeze/thaw cycle). Reactions were carried out in 50 mM Tris, pH 7.5, 150 mM NaCl, and 10 mM $CaCl_2$ using 5 μM His_6-Sortase A and 3-5x molar excess of the fluorescently labeled Sortase A recognition motif peptide relative to the protein to be labeled. Labeled protein was purified from the reaction mixture using Ni-NTA affinity chromatography (Qiagen) and/or followed by SEC. Labeled protein was characterized by fluorescent imaging on an SDS-PAGE gel using a Typhoon imager (GE Healthcare). Extent of labeling was measured through spectrophotometry and calculated using the following equation:

$$\%_{labeled} = \frac{A_{dye}}{\varepsilon_{dye} \times \left(\frac{A_{280} - \left(A_{dye} \times CF\right)}{\varepsilon_{protein}}\right)}$$

where A_{dye} is the absorbance at the maximum absorption wavelength (555 nm for TAMRA and 494 nm for fluorescein), ε_{dye} is the extinction coefficient of the dye (65,000 M^{-1} cm^{-1} for TAMRA and 68,000 M^{-1} cm^{-1} for fluorescein), and the CF is a correction factor that adjusts for the amount of absorbance at 280 nm contributed by the dye (59). We also measured molecular weights of fluorescent probe using a SciEx QTOF mass spectrometer. All probes were labeled with at least 60% efficiency.

3.5.4 Fluorescence polarization.

All FP assays were performed in 50 mM Bis-Tris Propane pH 7.5, 100 mM NaCl, 0.05% (vol/vol) Tween, 2 mM TCEP. For direct binding assays, varying amounts of CRY protein was mixed with 0.02 μM of a fluorescently labeled tail construct. Reactions were incubated for 10 minutes at room temperature. For displacement assays, 0.02 μM fluorescently labeled probe (BMAL1 TAD, CLOCK PAS-B, or hCRY1 tail) were incubated with 4 μM CRY1 PHR for 3 hours on ice. Varying amounts of unlabeled CRY tail constructs were mixed with this reaction and incubated for 10 minutes at room temperature. Fluorescence polarization measurements were measured on a Perkin Elmer EnVision 2103 Multilabel plate reader with excitation at 485 nm and emission at 535 nm. The equilibrium dissociation constant (K_D) and extent of non-specific binding was calculated by fitting millipolarization level (mp) to a one-site total model in GraphPad Prism using averaged mp values from assays with duplicate samples. IC_{50} values were calculated from displacement assays by fitting the mp level to a one-site competitive binding model in GraphPad Prism, with averaged mp values from assays with duplicate samples. Data shown are from one representative experiment (± sd) of three independent assays.

3.5.5 NMR spectroscopy.

All experiments were performed on a Bruker Avance 800 MHz spectrometer equipped with cryogenic probes. Spectra shown for experiments were collected using 20 mM MES buffer pH 6.8, 100 mM NaCl, 4 mM TCEP, 1 mM EDTA, and 10% (vol/vol) D_2O at 298 K. Spectra were processed using nmrPipe and analyzed with Sparky and CCPNMR (60-62). The backbone assignment of the human CRY1 tail was accomplished using standard NH-edited triple-resonance experiments (HN(CA)CO, HNCO, HNCACB, CBCA(CO)NH) and four-dimensional carbon detection methods such as (HACA)N(CA)CON and (HACA)N(CA)NCO (27). We were able to assign 79 non-ambiguous peaks out of 97 possible residues on the CON spectra. Chemical shift perturbation (Δδ) or the change in 2D CON peak position was calculated using the following equation:

$$\Delta\delta = \sqrt{\left(N\Delta_{ppm}\alpha\right)^2 + \left(CO\Delta_{ppm}\right)^2}$$

where Δ_{ppm} is the change in chemical shift and a value of N = 0.3 was used to normalize between ^{15}N and ^{13}C chemical shift ranges (63).

3.5.6 Biolayer interferometry.

All BLI experiments were performed using an 8-channel Octet-RED96e (ForteBio). All BLI experiments were performed in BLI assay buffer (20 mM HEPES pH 7.5, 125 mM NaCl, 5% (vol/vol) glycerol, 2 mM TCEP). For experiments containing full-length CRY1 or CRY1Δ11, we added 0.5 mM EDTA to the BLI buffer. For each experiment, we used 8 streptavidin biosensor tips (ForteBio). All experiments began with reference measurements using unloaded streptavidin tips to establish a baseline in BLI buffer, after which non-specific CRY1 association was measured for 5 minutes in wells containing 2-fold serial dilutions of CRY1 (*e.g.* 4 μM, 2 μM, 1 μM, 0.5 μM, 0.25 μM, etc.) or a reference sample well containing no CRY, and then dissociation was subsequently measured for 5 minutes in wells containing BLI buffer. After measuring our initial reference, we repeated the same assay with fresh tips that were loaded with 1.5 – 3 μg/mL biotinylated CLOCK:BMAL PAS-AB dimer using BLI buffer that contained no BSA or Tween-20. Data were processed and fitted using Octet software v.7 (ForteBio). Before fitting, all datasets were reference-subtracted, aligned on the y-axis through their respective baselines, aligned for interstep correction through their respective dissociation steps, and finally smoothened using Savitzy-Golay filtering. For each experiment, at least 4 different concentrations were used to fit association and dissociation globally over the full range of the experiment using a 1:1 binding model in Octet software v.7 (ForteBio). Goodness of fit was determined with $\chi 2$ and R2 tests that conform to the manufacturer's guidelines.

3.5.7 Cellular Assays.

Per1-Luc reporter-gene assays investigating repression by CRY1 were performed as before (4). Briefly, plasmids were transfected into HEK293T cells (ATCC) in a 48-well plate in

duplicate with LT-1 transfection reagent (Mirus) at the indicated concentrations: 5 ng pGL3 *Per1-Luc* reporter, 100 ng each pSG5 Flag-*Bmal1* and pSG5 His_6-Flag-*Clock*, and 50 ng pcDNA4B *Cry1*-Flag-Myc-His_6 (wild-type or Δ11) with empty pcDNA4 vector used to normalize total plasmid concentrations to 800 ng/well. Cells were harvested 30 h after transfection with luciferase-compatible 1X Passive Lysis Buffer (NEB) and luciferase activity was assayed with Bright-Glo luciferin reagent (Promega) on an EnVision plate reader (Perkin Elmer). Statistical tests were performed on aggregated data from n = 3 independent assays using two-sided, two-tailed Student's t-tests.

Protein expression of CRY1 full-length and Δ11 was assessed by western blotting after transfection of 200 ng of either construct into HEK293T cells in a 12-well plate. Cells were harvested 48 h later and equal volumes of cell lysate were resolved on a 7.5% SDS-PAGE and transferred to a nitrocellulose membrane. CRY protein was detected using the anti-myc (9E10) antibody (purified in-house from the (9E10) hybridoma line purchased from the Developmental Studies Hybridoma Bank, University of Iowa). Histone H3 (1G1) antibody was used as a loading control (cat. # sc-517576, Santa Cruz Biotechnology) and both were detected with a rabbit anti-mouse IgG-horseradish peroxidase conjugate (cat. # sc-358914, Santa Cruz Biotechnology) and Clarity chemiluminescence reagents (Bio-Rad) using a ChemiDoc XRS+ CCD imager (Bio-Rad). Data are representative of n = 2 experiments with duplicate samples.

3.6 Depositions

The NMR chemical shift assignments for the human CRY1 tail have been deposited in the Biological Magnetic Resonance Bank database with accession number 27988.

3.7 Supplementary Figures

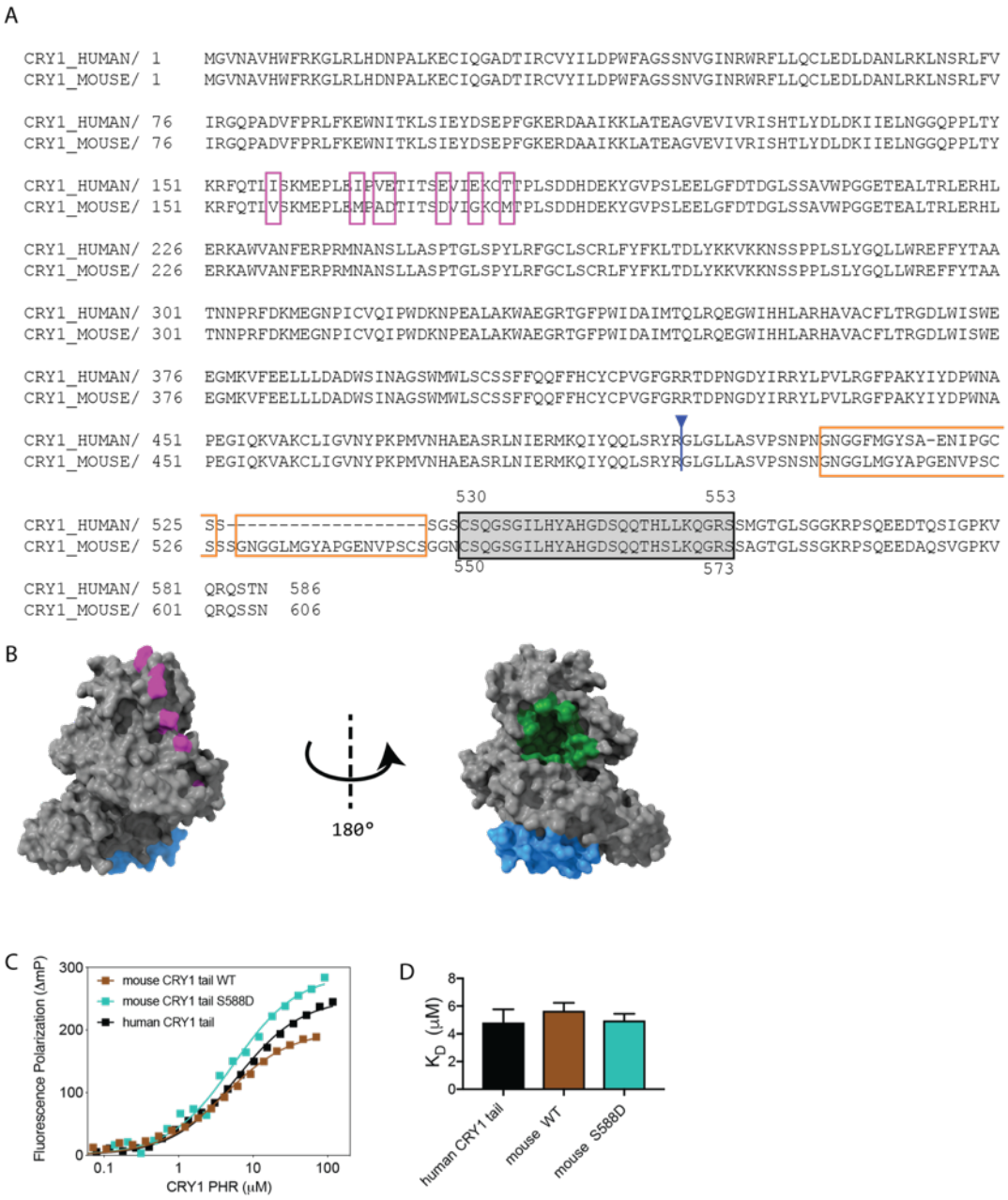

Supplementary Figure 3.1. Human CRY1 and mouse CRY1 are highly conserved

(A) Sequence alignment of human CRY1 and mouse CRY1. Only 7 residues differ between human and mouse CRY1 PHR (highlighted in purple). The CRY1 tail constructs used in this study start from residue 496 (blue arrow). The mouse CRY1 tail differs from the human CRY1 tail through a repeat insertion at residues at 529 - 546 (highlighted in orange) upstream of exon 11 (gray box, residues 530-553 in human CRY1 and residues 550-573 in mouse CRY1). ***(B)*** Residues that differ between human and mouse CRY1 PHR are highlighted on the mouse CRY1 PHR crystal structure (PDB ID 5T5X). Non-identical residues (pink) do not

overlap with either the CLOCK PAS-B binding site (green) or the BMAL1 TAD binding site (blue). ***(C)*** FP binding curves of fluorescently labeled CRY1 tail constructs to the CRY1 PHR. Plot shows the mean representative binding curves of duplicate samples ± sd (of n = 3 independent assays). Curve represents fit to one-site binding (Prism). ***(D)*** Affinities of FAM-tail constructs for the PHR derived from FP binding assays (n = 3 independent assays ± sd).

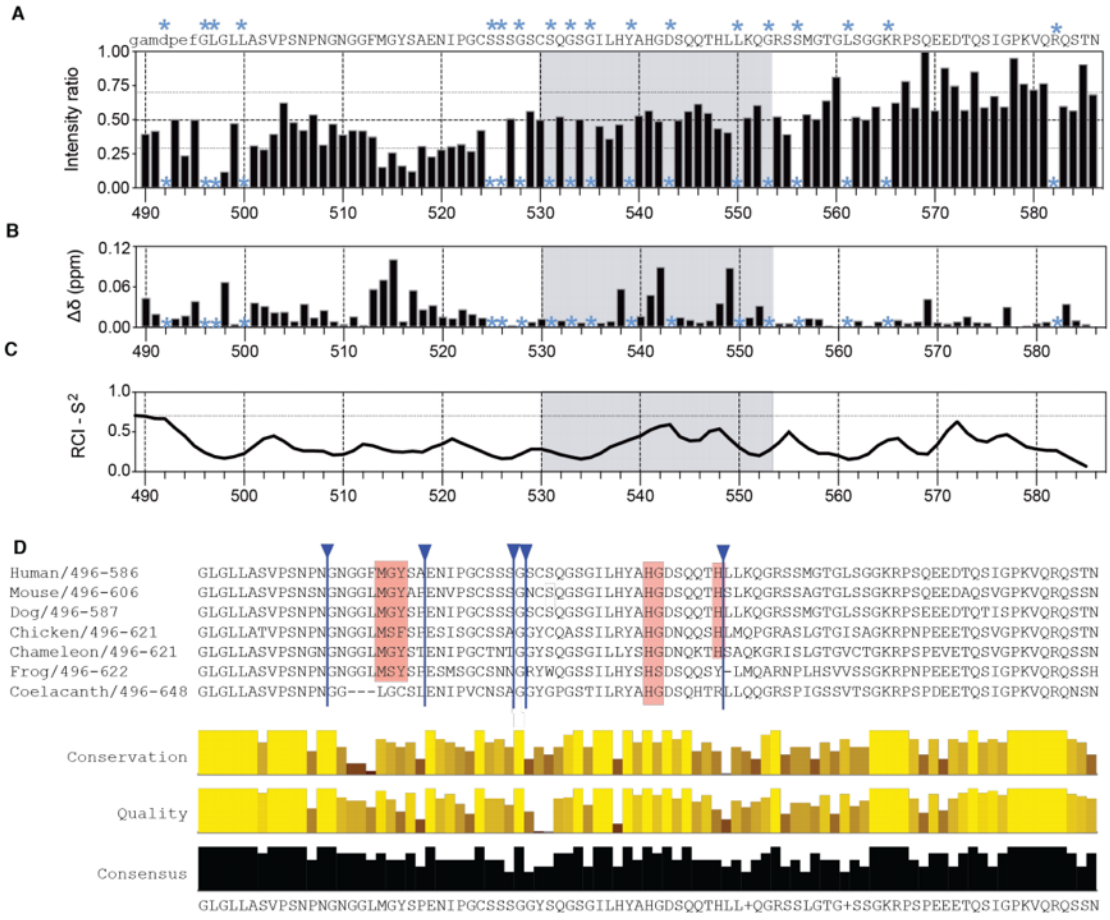

Supplementary Figure 3.2. NMR spectroscopy maps the PHR binding site on the CRY1 tail to conserved residues

(A-B) Relative intensities (A) and chemical shift perturbations (Δδ, B) in the ^{13}C, ^{15}N-labeled CRY1 tail including residual vector sequence on protein (lower case) upon addition of equimolar CRY1 PHR. Asterisk, unassigned or overlapping peaks excluded from the analysis. Exon 11 is represented by a gray box. In A, dashed horizontal line represents the mean intensity ratio ($I_{tail+PHR}/I_{tail}$ alone), while the dotted lines represent sem. Peaks are referred to by the number of the nitrogen of the ^{13}C-^{15}N peptide bond. ***(C)*** CSI prediction of the lack of secondary structure from NMR data (S^2 < 0.7). ***(D)*** Sequence alignment and conservation of CRY tail sequences: human (Uniprot ID Q16526); mouse (P97784); Dog (E2RMX4); Chicken (Q8QG61); Chameleon (G1KQX0); Frog (F7B4K1); Coelacanth (H3AHZ5). Potential hotspot residues mapped by NMR are conserved (red box). Insertions that do not align to the human CRY1 tail sequence are hidden and marked by blue arrows: first blue arrow from the left (Chicken residues 509-510; Chameleon residues 509-510; Frog residues 509-510; Coelacanth residue 518); second blue arrow (Mouse residue 519; Dog residue 519; Chicken residue 521; Chameleon residue 521; Frog residue 521; Coelacanth residue 518); third blue arrow (Mouse residues 529-547; Chicken residues 531-500; Chameleon residues 531-550; Frog residues 531-550; Coelacanth residues 528-547); fourth blue arrow (Chicken residues 552-563; Chameleon residues 552-563; Frog residues 552-

565; Coelacanth residues 549-588); fifth blue arrow (Coelacanth residues 609-610). Conservation score was calculated by Clustal Omega.

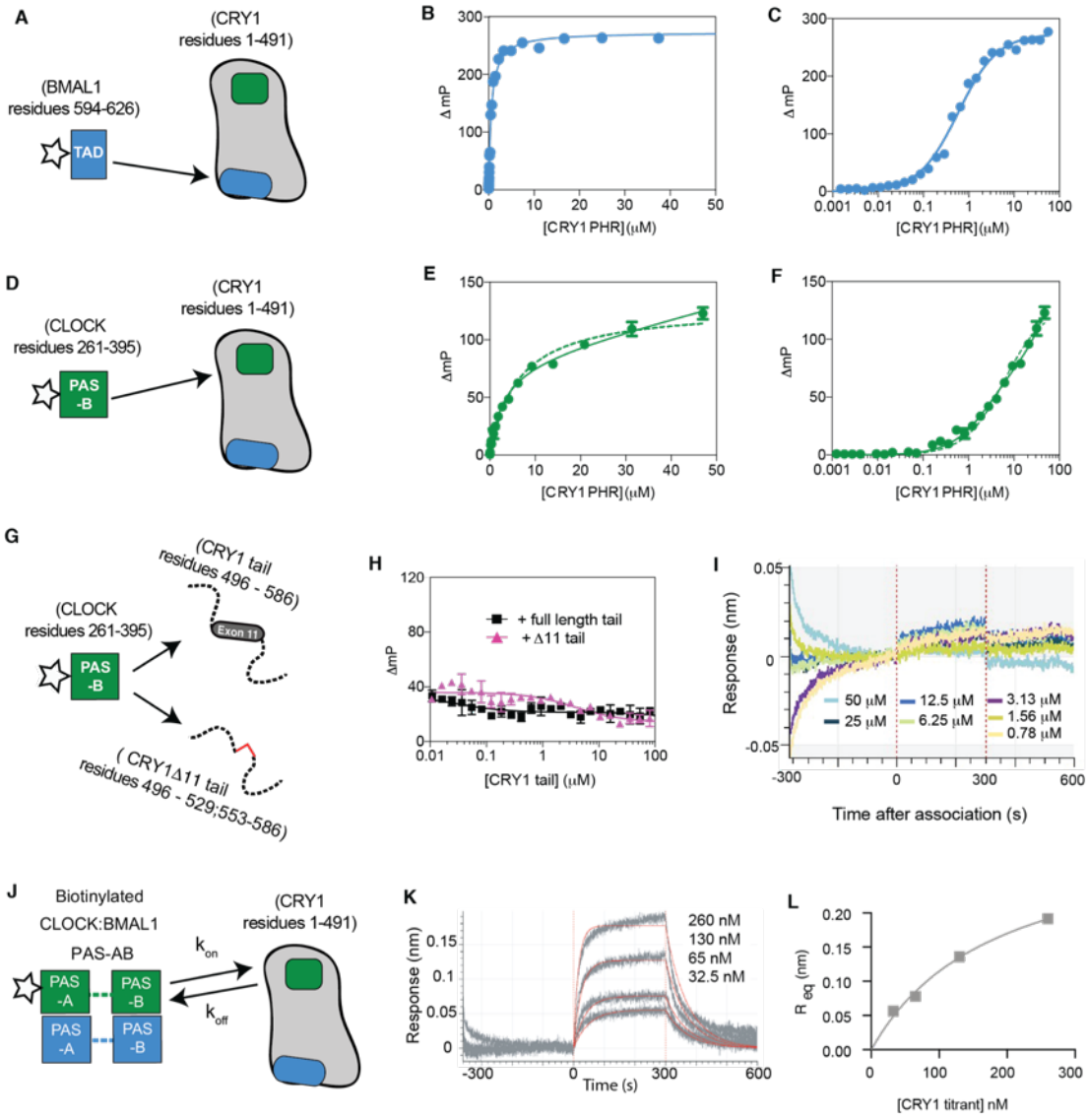

Supplementary Figure 3.3. CRY1 PHR interacts with CLOCK:BMAL1 at distinct sites

(A) The BMAL1 TAD (blue rectangle; fluorescent label, star) binds to the CC-helix (blue cylinder) of the CRY1 PHR (gray). ***(B-C)*** FP binding curves of fluorescently labeled BMAL1 TAD to the CRY1 PHR in linear scale B and logarithmic scale C. Data fitted to a single site-specific binding model. ***(D)*** CLOCK PAS-B (green square; fluorescent label, star) binds to the secondary pocket (green rounded square) of the CRY1 PHR (gray). ***(E-F)*** FP binding curves of fluorescently labeled CLOCK PAS-B to the CRY1 PHR in linear scale E and logarithmic scale F. Data fitted to both single site specific binding model (dashed green line) but some degree of non-specific binding was accounted for by fitting to a single site total model (solid green line). ***(G)*** CLOCK PAS-B (green square; fluorescent label, star) does not bind to the CRY1 tail (dashed line). ***(H)*** FP binding curves of fluorescently labeled CLOCK PAS-B to the full-length tail (black squares) and Δ11 tail (magenta triangles) in logarithmic scale depicting insignificant changes in FP upon titration of CRY1 tail. Plots show the mean

representative binding curves of duplicate samples ± sd (of n = 3 independent assays) and were fitted on GraphPad Prism. ***(I)*** BLI sensogram for biotinylated CLOCK:BMAL1 PAS-AB titrated with CRY1 tail. ***(J)*** CLOCK:BMAL1 PAS-AB (CLOCK, green; BMAL1, blue; biotin, star) binds with CRY1 PHR (gray) through an interaction between CLOCK PAS-B and the secondary pocket (green rounded square). ***(K)*** BLI sensogram for biotinylated CLOCK:BMAL1 PAS-AB titrated with CRY1 PHR (gray). Model fit represented by a thin red line. Fitted K_D is 65 ± 6 nM with an association rate (k_{on}) of 2.01 ± 0.4 x 10^5 M^{-1} s^{-1} and a dissociation rate (k_{off}) of 1.31± 0.1 x 10^{-2} s^{-1} (3). ***(L)***,Steady-state analysis of BLI response versus CRY1 PHR concentration (from data in panel K). Curve represents fit to one-site binding (Prism).

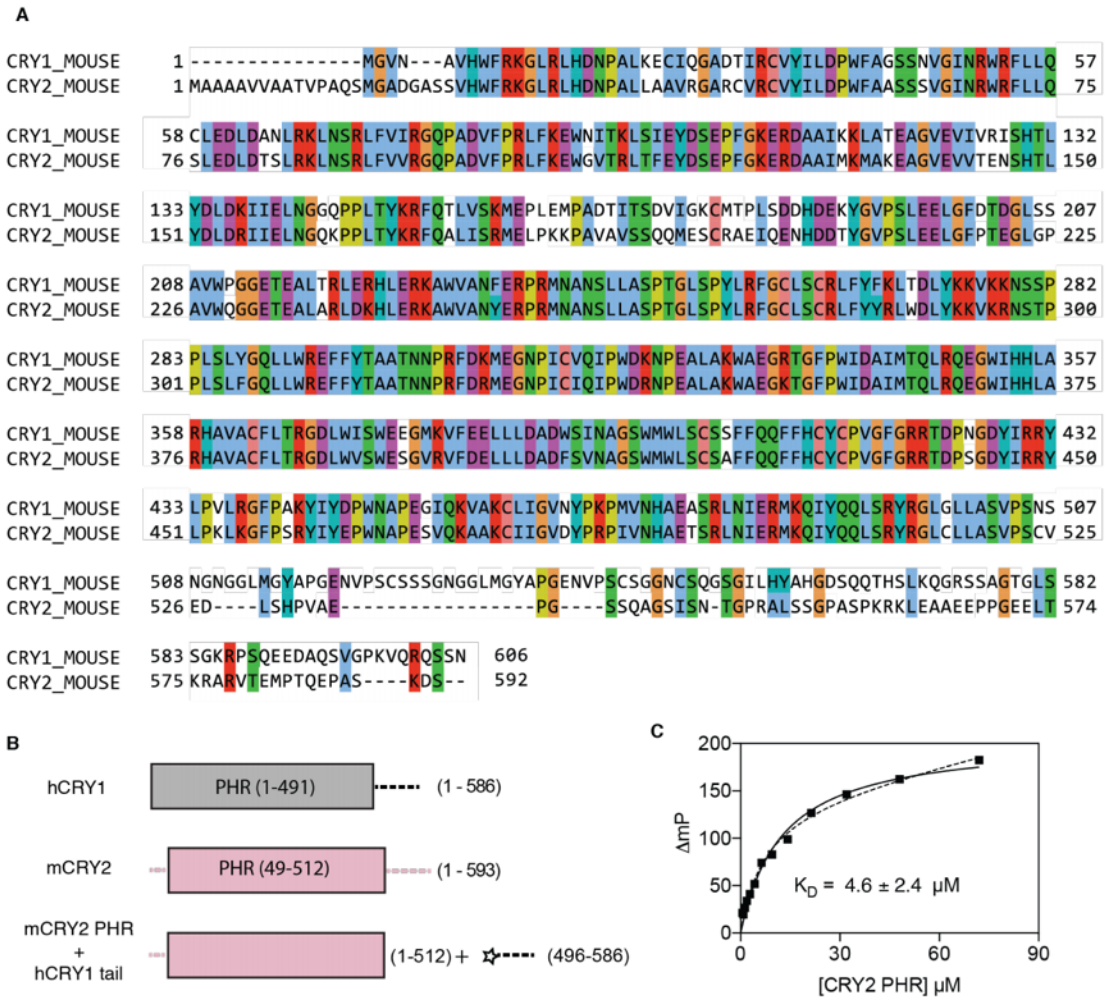

Supplementary Figure 3.4. The CRY1 and CRY2 tails are divergent but functional conservation allows the CRY2 PHR to bind to the CRY1 tail

(A) Sequence alignment and conservation of mouse CRY1 (Uniprot ID P97784) and mouse CRY2 (Q9R194) sequences. Similar amino acids between CRY1 and CRY2 are colored as such hydrophobics (blue); positively charged (red); negatively charged (purple); polar (green); cysteines (pink); glycines (orange); prolines (yellow); and histidines and tyrosines (cyan). Divergent sequences are not colored, and alignment gaps are represented by a dash. ***(B)*** Schematics for CRY1 and CRY2 domain architecture and CRY2 PHR binding to the CRY1 tail. ***(C)*** FP binding curve of fluorescently labeled CRY1 tail to the CRY2 PHR in linear. Data fitted to both single-site specific binding model (solid black line) but some degree of non-specific binding was accounted for by fitting to a single site total model (dashed black line).

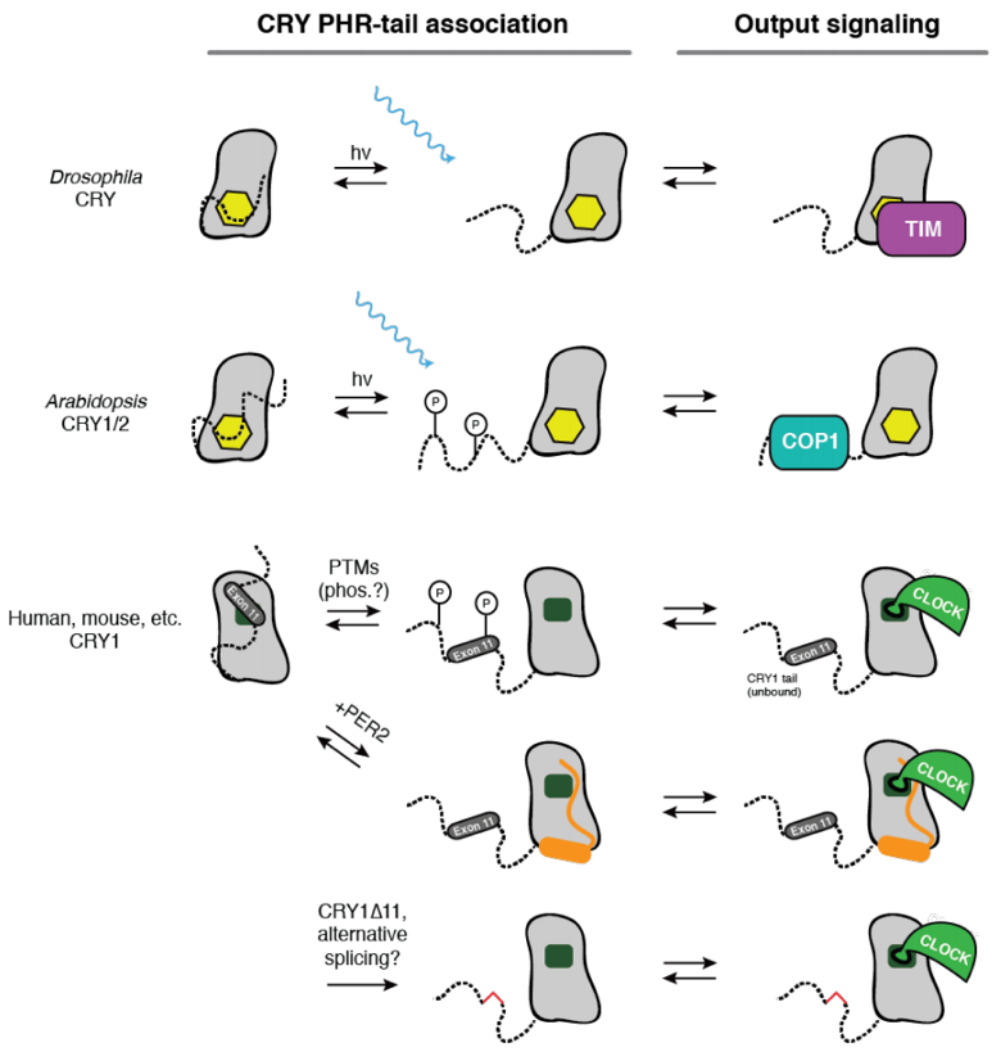

Supplementary Figure 3.5. The C-terminal of CRY reversibly interacts with its respective PHR to create an autoinhibited state

In Drosophila, the cryptochrome tail (dashed line) interacts with a flavin within the cofactor pocket (yellow) of its respective PHR (gray). Blue light induces the release of the tail from its respective PHR thus allowing an interaction between the CRY PHR and circadian regulator Timeless (purple). In Arabidopsis, the cryptochrome tail (dashed line) also interacts with a flavin within the cofactor pocket (yellow) of its respective PHR (gray). Blue light induces the release of the tail from its respective PHR and phosphorylation of the tail (circled P) thus allowing an interaction between the CRY tail and COP1 (cyan). In mammals, the CRY1 tail possibly interacts with the secondary pocket (dark green) of its respective PHR (gray). Post-translational modifications such as phosphorylation (circled P), or the association of other proteins such as PER2 (orange) could regulate the interaction between the tail and the PHR. When the tail is not bound to the PHR, the secondary pocket is open for binding to the CLOCK PAS-B domain (light green). Gene variants or alternative splicing events that remove exon 11 (red line) could possibly modulate the tail/PHR interaction.

3.8 References

1. Zhang R, Lahens NF, Ballance HI, Hughes ME, & Hogenesch JB (2014) A circadian gene expression atlas in mammals: implications for biology and medicine. *Proceedings of the National Academy of Sciences of the United States of America* 111(45):16219-16224.

2. Partch CL, Green CB, & Takahashi JS (2014) Molecular architecture of the mammalian circadian clock. *Trends in Cell Biology* 24(2):90-99.

3. Fribourgh JL*, et al.* (2020) Dynamics at the serine loop underlie differential affinity of cryptochromes for CLOCK:BMAL1 to control circadian timing. *Elife* 9.

4. Xu H*, et al.* (2015) Cryptochrome 1 regulates the circadian clock through dynamic interactions with the BMAL1 C terminus. *Nature Structural & Molecular Biology* 22(6):476-484.

5. Gustafson CL*, et al.* (2017) A Slow Conformational Switch in the BMAL1 Transactivation Domain Modulates Circadian Rhythms. *Molecular Cell* 66(4):447-457.e447.

6. Godinho SI*, et al.* (2007) The after-hours mutant reveals a role for Fbxl3 in determining mammalian circadian period. *Science* 316(5826):897-900.

7. Hirano A*, et al.* (2016) A Cryptochrome 2 mutation yields advanced sleep phase in humans. *eLife* 5.

8. Hirano A*, et al.* (2013) FBXL21 regulates oscillation of the circadian clock through ubiquitination and stabilization of cryptochromes. *Cell* 152(5):1106-1118.

9. Militi S*, et al.* (2016) Early doors (Edo) mutant mouse reveals the importance of period 2 (PER2) PAS domain structure for circadian pacemaking. *Proc Natl Acad Sci U S A* 113(10):2756-2761.

10. Toh KL*, et al.* (2001) An hPer2 phosphorylation site mutation in familial advanced sleep phase syndrome. *Science (New York, N.Y.)* 291(5506):1040-1043.

11. Xu Y*, et al.* (2005) Functional consequences of a CKIdelta mutation causing familial advanced sleep phase syndrome. *Nature* 434(7033):640-644.

12. Xu Y*, et al.* (2007) Modeling of a Human Circadian Mutation Yields Insights into Clock Regulation by PER2. *Cell* 128(1):59-70.

13. Jones CR, Huang AL, Ptacek LJ, & Fu YH (2013) Genetic basis of human circadian rhythm disorders. *Exp Neurol* 243:28-33.

14. Patke A*, et al.* (2017) Mutation of the Human Circadian Clock Gene CRY1 in Familial Delayed Sleep Phase Disorder. *Cell* 169(2):203-215.e213.

15. Khan SK*, et al.* (2012) Identification of a Novel Cryptochrome Differentiating Domain Required for Feedback Repression in Circadian Clock Function. *Journal of Biological Chemistry* 287(31):25917-25926.

16. Li Y, Xiong W, & Zhang EE (2016) The ratio of intracellular CRY proteins determines the clock period length. *Biochem Biophys Res Commun* 472(3):531-538.

17. Rosensweig C*, et al.* (2018) An evolutionary hotspot defines functional differences between CRYPTOCHROMES. *Nature Communications* 9(1):1138.

18. Gao P*, et al.* (2013) Phosphorylation of the Cryptochrome 1 C-terminal Tail Regulates Circadian Period Length. *The Journal of Biological Chemistry* 288(49):35277-35286.

19. Liu N & Zhang EE (2016) Phosphorylation Regulating the Ratio of Intracellular CRY1 Protein Determines the Circadian Period. *Frontiers in Neurology* 7.

20. Papp SJ*, et al.* (2019) DNA damage shifts circadian clock time via Hausp-dependent Cry1 stabilization. *eLife* 4.

21. Michael AK*, et al.* (2017) Formation of a repressive complex in the mammalian circadian clock is mediated by the secondary pocket of CRY1. *Proceedings of the National Academy of Sciences* 114(7):1560-1565.

22. Czarna A*, et al.* (2011) Quantitative analyses of cryptochrome-mBMAL1 interactions: mechanistic insights into the transcriptional regulation of the mammalian circadian clock. *J Biol Chem* 286(25):22414-22425.

23. Schmalen I*, et al.* (2014) Interaction of circadian clock proteins CRY1 and PER2 is modulated by zinc binding and disulfide bond formation. *Cell* 157(5):1203-1215.

24. Chiou YY*, et al.* (2016) Mammalian Period represses and de-represses transcription by displacing CLOCK-BMAL1 from promoters in a Cryptochrome-dependent manner. *Proc Natl Acad Sci U S A* 113(41):E6072-E6079.

25. Kosol S, Contreras-Martos S, Cedeño C, & Tompa P (2013) Structural Characterization of Intrinsically Disordered Proteins by NMR Spectroscopy. *Molecules* 18(9):10802-10828.

26. Partch CL, Clarkson MW, Ozgür S, Lee AL, & Sancar A (2005) Role of structural plasticity in signal transduction by the cryptochrome blue-light photoreceptor. *Biochemistry* 44(10):3795-3805.

27. Bastidas M, Gibbs EB, Sahu D, & Showalter SA (2015) A primer for carbon-detected NMR applications to intrinsically disordered proteins in solution. *Concepts in Magnetic Resonance Part A* 44(1):54-66.

28. Czarna A*, et al.* (2013) Structures of Drosophila Cryptochrome and Mouse Cryptochrome1 Provide Insight into Circadian Function. *Cell* 153(6):1394-1405.

29. Fuxreiter M, Simon I, Friedrich P, & Tompa P (2004) Preformed structural elements feature in partner recognition by intrinsically unstructured proteins. *Journal of Molecular Biology* 338(5):1015-1026.

30. Pancsa R & Fuxreiter M (2012) Interactions via intrinsically disordered regions: What kind of motifs? *IUBMB Life* 64(6):513-520.

31. Hafsa NE, Arndt D, & Wishart DS (2015) CSI 3.0: a web server for identifying secondary and super-secondary structure in proteins using NMR chemical shifts. *Nucleic Acids Res* 43(W1):W370-377.

32. Trudeau T*, et al.* (2013) Structure and Intrinsic Disorder in Protein Autoinhibition. *Structure* 21(3):332-341.

33. Miller S*, et al.* (2020) Isoform-selective regulation of mammalian cryptochromes. *Nat Chem Biol*.

34. Kasahara K, Shiina M, Higo J, Ogata K, & Nakamura H (2018) Phosphorylation of an intrinsically disordered region of Ets1 shifts a multi-modal interaction ensemble to an auto-inhibitory state. *Nucleic Acids Res* 46(5):2243-2251.

35. Olsen SK*, et al.* (2004) Insights into the molecular basis for fibroblast growth factor receptor autoinhibition and ligand-binding promiscuity. *Proceedings of the National Academy of Sciences of the United States of America* 101(4):935-940.

36. Zhou H-X & Bates PA (2013) Modeling Protein Association Mechanisms and Kinetics. *Current opinion in structural biology* 23(6).

37. Sato TK*, et al.* (2006) Feedback repression is required for mammalian circadian clock function. *Nature genetics* 38(3):312-319.

38. Koike N*, et al.* (2012) Transcriptional Architecture and Chromatin Landscape of the Core Circadian Clock in Mammals. *Science (New York, N.Y.)* 338(6105):349-354.

39. Aryal RP*, et al.* (2017) Macromolecular Assemblies of the Mammalian Circadian Clock. *Molecular Cell* 67(5):770-782.e776.

40. Stratmann M, Stadler F, Tamanini F, van der Horst GT, & Ripperger JA (2010) Flexible phase adjustment of circadian albumin D site-binding protein (DBP) gene expression by CRYPTOCHROME1. *Genes Dev* 24(12):1317-1328.

41. Ye R*, et al.* (2014) Dual modes of CLOCK:BMAL1 inhibition mediated by Cryptochrome and Period proteins in the mammalian circadian clock. *Genes Dev* 28(18):1989-1998.

42. Liu AC*, et al.* (2007) Intercellular coupling confers robustness against mutations in the SCN circadian clock network. *Cell* 129(3):605-616.

43. Nangle SN*, et al.* (2014) Molecular assembly of the period-cryptochrome circadian transcriptional repressor complex. *eLife* 3:e03674.

44. Regan MC*, et al.* (2013) Structural and dynamic studies of the transcription factor ERG reveal DNA binding is allosterically autoinhibited. *Proceedings of the National Academy of Sciences* 110(33):13374-13379.

45. Currie SL*, et al.* (2017) Structured and disordered regions cooperatively mediate DNA-binding autoinhibition of ETS factors ETV1, ETV4 and ETV5. *Nucleic Acids Research* 45(5):2223-2241.

46. van der Horst G*, et al.* (1999) Mammalian Cry1 and Cry2 are essential for maintenance of circadian rhythms. *Nature* 398(6728):627-630.

47. Vitaterna M*, et al.* (1999) Differential regulation of mammalian period genes and circadian rhythmicity by cryptochromes 1 and 2. *Proc Natl Acad Sci U S A* 96(21):12114-12119.

48. Kurabayashi N, Hirota T, Sakai M, Sanada K, & Fukada Y (2010) DYRK1A and glycogen synthase kinase 3beta, a dual-kinase mechanism directing proteasomal degradation of CRY2 for circadian timekeeping. *Mol Cell Biol* 30(7):1757-1768.

49. Busza A, Emery-Le M, Rosbash M, & Emery P (2004) Roles of the Two Drosophila CRYPTOCHROME Structural Domains in Circadian Photoreception. *Science* 304(5676):1503-1506.

50. Dissel S*, et al.* (2004) A constitutively active cryptochrome in Drosophila melanogaster. *Nature Neuroscience* 7(8):834-840.

51. Rosato E*, et al.* (2001) Light-dependent interaction between Drosophila CRY and the clock protein PER mediated by the carboxy terminus of CRY. *Curr Biol* 11(12):909-917.

52. Zoltowski BD*, et al.* (2011) Structure of full-length Drosophila cryptochrome. *Nature* 480(7377):396-399.

53. Levy C*, et al.* (2013) Updated structure of Drosophila cryptochrome. *Nature* 495(7441):E3-E4.

54. Xing W*, et al.* (2013) SCF(FBXL3) ubiquitin ligase targets cryptochromes at their cofactor pocket. *Nature* 496(7443):64-68.

55. Griffin EA, Staknis D, & Weitz CJ (1999) Light-independent role of CRY1 and CRY2 in the mammalian circadian clock. *Science (New York, N.Y.)* 286(5440):768-771.

56. Cal-Kayitmazbatir S*, et al.* (2020) CRY1-CBS binding regulates circadian clock function and metabolism. *FEBS J*.

57. Buljan M*, et al.* (2013) Alternative splicing of intrinsically disordered regions and rewiring of protein interactions. *Current Opinion in Structural Biology* 23(3):443-450.

58. Theile CS*, et al.* (2013) Site-specific N-terminal labeling of proteins using sortase-mediated reactions. *Nature Protocols* 8(9):1800-1807.

59. Anonymous (2011) Calculate dye:protein (F/P) molar ratios. *Thermo Scientific. Tech Tip #31* TR0031.7(TR0031.7).

60. Delaglio F*, et al.* (1995) NMRPipe: A multidimensional spectral processing system based on UNIX pipes. *Journal of Biomolecular NMR* 6(3):277-293.

61. Goddard TD & Kneller DG (2017) SPARKY 3. in *SPARKY 3* (Universitty of California, San Francisco).

62. Vranken WF*, et al.* (2005) The CCPN data model for NMR spectroscopy: development of a software pipeline. *Proteins* 59(4):687-696.

63. Lawrence CW, Bonny A, & Showalter SA (2011) The disordered C-terminus of the RNA polymerase II phosphatase FCP1 is partially helical in the unbound state. *Biochemical and Biophysical Research Communications* 410(3):461-465.

CHAPTER 4: CRY2 missense mutations suppress P53 and enhance cell growth

The text of this chapter includes a reprint of the following previously published material:

Chan, A. B., **G. C. G. Parico**, J. L. Fribourgh, L. H. Ibrahim, M. J. Bollong, C. L. Partch, and K. A. Lamia. 2021. 'CRY2 missense mutations suppress P53 and enhance cell growth', *Proc Natl Acad Sci U S A*, 118. DOI: 10.1073/pnas.2101416118

Contributions by the co-authors are as follows: A.B.C., C.L.P., and K.A.L. designed research; A.B.C., G.C.G.P., and J.L.F. performed research; A.B.C. contributed new reagents/analytic tools; A.B.C., G.C.G.P., J.L.F., L.H.I., M.J.B., C.L.P., and K.A.L. analyzed data; and A.B.C. and K.A.L. wrote the paper.

The candidate, Gian Carlo Parico, performed the following contributions for the development of this manuscript: purified recombinant proteins and collected and analyzed *in vitro* binding data.

All authors edited and approved of the manuscript.

Manuscript Acknowledgments

We thank Drs. Hiroki Ueda, Carla Green, Tsuyoshi Hirota, Clark Rosensweig, Anne-Laure Huber, Megan Vaughan, Anna Kriebs, and Marie Pariollaud, and Ms. Rebecca Mello for helpful discussions and/or gifting us critical reagents. The results published here are, in whole or in part, based on data generated by the TCGA Research Network. We thank Toni Thomas, Judy Valecko, and Yolanda Slivers for administrative assistance.

4.1 Abstract

Disruption of circadian rhythms enhances cancer risk. Mammalian cryptochromes (CRY1 and CRY2) are circadian transcriptional repressors that are related to DNA repair enzymes. While CRYs lack DNA repair activity, they modulate the transcriptional response to DNA damage, and CRY2 can promote SKP1 cullin 1-F-box $(SCF)^{FBXL3}$-mediated ubiquitination of c-MYC and other targets. Here, we characterize five mutations in CRY2 observed in human cancers in The Cancer Genome Atlas. We demonstrate that two orthologous mutations of mouse CRY2 (D325H and S510L) accelerate the growth of primary mouse fibroblasts expressing high levels of c-MYC. Neither mutant affects steady state levels of overexpressed c-MYC, and they have divergent impacts on circadian rhythms and on the ability of CRY2 to interact with SCF^{FBXL3}. Unexpectedly, stable expression of either CRY2 D325H or of CRY2 S510L robustly suppresses P53 target-gene expression, suggesting that this may be the primary mechanism by which they influence cell growth.

4.2 Introduction

Circadian rhythms entrain many aspects of physiology to the daily solar cycle (1). Mammalian circadian rhythms are generated by a cell-autonomous molecular clock based on a transcription-translation feedback loop (TTFL): a heterodimer of circadian locomotor output cycles kaput (CLOCK) and brain and muscle ARNT-like protein 1 (BMAL1) drives transcription of their own repressors period (PER1, PER2, and PER3) and cryptochrome (CRY1 and CRY2). The F-box and leucine-rich repeat proteins 3 (FBXL3) and 21 (FBXL21) are substrate adaptors for S phase kinase-associated protein 1 (SKP1)-cullin 1 (CUL1)-F-box protein (SCF) E3 ubiquitin ligases that stimulate CRY ubiquitination and degradation and contribute to circadian rhythms (2-8).

In addition to driving circadian rhythms, clock components transmit temporal information to other physiological processes (1, 9-11). For example, CRY1/2 suppress the activity of several non-circadian transcription factors (11-17), thereby influencing their susceptibility to activation in a time-of-day-dependent manner. In the case of c-MYC and

Early 2 factor (E2F) family members, this suppression is driven by stimulated proteolysis (12, 16), in which CRY2 acts as a co-factor to recruit c-MYC or E2F family members to the SCF^{FBXL3} complex to promote ubiquitination and subsequent degradation.

Mammalian CRYs evolved from bacterial light-activated DNA repair enzymes also known as photolyases, but lack DNA-repair activity and light sensitivity (18). Several studies have identified molecular links between CRYs and cancer-related pathways (19). The CRY photolyase homology region (PHR) comprises most of the protein, excluding the disordered C-terminal tail (CTT). The PHR includes a flavin adenine dinucleotide (FAD) binding pocket, a secondary pocket [analogous to the antenna chromophore-binding pocket of photolyases (20)], and a coiled-coil (CC) just upstream of the CTT. FBXL3 and FBXL21 interact with the FAD binding pocket of CRYs; a C-terminal tryptophan in each of these F-box proteins occupies the FAD binding site (2-8). Similarly, a tryptophan in the disordered loop that connects helices H and I (i.e., the HI loop) of CLOCK interacts with the secondary pocket of CRY1 (21). Sequence differences between CRY1 and CRY2 surrounding the secondary pocket have a major influence on their differential binding affinity for CLOCK:BMAL1 (22, 23) and their divergent influence on circadian period (23). The CC helix of CRY1 interacts with both PER2 and with the transcriptional activation domain (TAD) of BMAL1 and likely reduces the association of BMAL1 with co-activators (24-26). The CTTs in CRY1 and CRY2 are highly divergent both from the C-termini of CRYs in other organisms and from each other. The CTTs contain many phosphorylation sites, which modulate stability (27-30), are regulated by DNA damage signaling (29, 30), and influence circadian timing (31).

The circadian and cell cycles influence each other (9, 32-35), and several studies have demonstrated that environmental or genetic disruption of circadian rhythms alters cancer development (36). Regarding the repressive arm of the TTFL and the period and cryptochrome proteins, previous studies have reported mixed results regarding how their disruption impacts cancer progression. In p53-deficient mice, loss of both Cry1 and Cry2 reduces tumor formation and increases survival (37). By contrast, in wild-type (WT) mice,

loss of both Cry1 and Cry2 increases the development of liver tumors spontaneously and in response to either whole-body radiation or treatment with diethylnitrosamine (38-40). Furthermore, contradictory findings appear with irradiated Per2-deficient mice; while several studies have reported enhanced tumor formation upon deletion of mutation of PER2 (38, 39, 41-45), another study found that irradiated Per2-deficient mice are not tumor prone (46). Further investigation is needed to understand the influence of genetic backgrounds, age, and tumor-driving stimuli on these outcomes.

We previously demonstrated that genetic deletion of *Cry2* renders cells more susceptible to transformation by diverse oncogenic insults (16), and we and others found that Cry2-deficient cells accumulate more DNA damage (30, 47), which could impact cell growth. Here, we investigate five missense mutations in CRY2 that have each been observed in multiple human tumors, selected based on their predicted impacts on the interactions between CRY2, FBXL3, and c-MYC. Expression of WT CRY2, but not of two of the mutant mouse orthologues studied here, suppresses the growth of c-MYC-transformed *Cry2*$^{-/-}$ fibroblasts (16). One of the mutants, human CRY2 S532L (mouse CRY2 S510L), exhibits greatly reduced association with FBXL3 as predicted. In contrast, the human CRY2 D347H mutation (mouse CRY2 D325H) does not impact the association of CRY2 with FBXL3 or c-MYC. Instead, we found that it reduces the ability of CRY2 to interact with and repress the CLOCK:BMAL1 heterodimer, and, therefore, it cannot support circadian rhythms in fibroblasts. To gain insight into common effects of the mouse CRY2 D325H and S510L mutations, we globally sequenced RNA prepared from cells expressing wildtype or mutant CRY2 in combination with c-MYC. This unbiased analysis revealed that both CRY2 missense mutations that accelerate transformation by c-MYC robustly reduce the expression of P53 target genes, suggesting that these mutations influence cell growth by suppressing P53.

4.3 Results

4.3.1 Missense mutation of CRY2 alters cell growth in a context-dependent manner

We used cBioPortal (48, 49) (last accessed November 13, 2020) to identify recurrent missense mutations in CRY2 reported in human tumor samples in The Cancer Genome Atlas PanCancer Atlas studies (Figure 4.1 and Supplementary Figure 4.1). We selected five mutations to investigate based on 1) their frequency of observation in diverse tumor types (when cBioPortal was first accessed in August 2016), and 2) their surface-exposed locations on the three-dimensional structure of CRY2 in close proximity to the CRY2:FBXL3 interface and the phosphate-binding loop where c-MYC interacts with CRY2 (Figure 4.1A), suggesting that these mutations may affect the interactions between CRY2, FBXL3, and c-MYC.

Malignant cells must replicate indefinitely (50). To investigate the potential for mutant CRY2 to influence cell proliferation, we monitored cell numbers over ten days after sparsely plating *Cry2*$^{-/-}$ mouse embryonic fibroblasts (MEFs) expressing either c-MYC or short hairpin RNA (shRNA) targeting P53 in combination with wildtype or mutant CRY2. Cells expressing elevated c-MYC proliferated more quickly, consistent with the well-established role of MYC in promoting entry into S phase (51). Stable expression of wildtype CRY2 slowed proliferation of *Cry2*$^{-/-}$ fibroblasts expressing c-MYC and tended to slow the growth of P53-depleted cells (Figure 4.1 and Supplementary Figure 4.1B-C). While the impact of CRY2 expression on proliferation was reduced by several of the mutations examined, the high variability and small effect size made it difficult to measure significant differences in this assay. Intriguingly, cells expressing CRY2 S414R seemed to proliferate more slowly in the context of P53 depletion.

Figure 4.1. Missense mutations in CRY2 alter cell growth.

(A) Three-dimensional structure of mouse CRY2 (orange) and FBXL3 (light pink) (Protein Data Bank ID: 4I6J). The location and numbering of amino acids orthologous to missense mutations found in TCGA are depicted in blue, with the relevant mutations in human CRY2 indicated in parentheses. Magenta shading on CRY2 indicates the phosphate binding loop that interacts with c-MYC. ***(B and C)*** Quantitation of crystal violet staining of colonies formed by *Cry2*$^{-/-}$ MEFs stably expressing c-MYC (B) or shRNA targeting P53 (C) after plating at low density. Bars represent mean ± SEM for quantification of staining from four biological replicates each analyzed in triplicate, with individual measurements for each replicate depicted by a unique symbol type: open or filled square, open or filled circle. Each condition was compared with controls that were plated in wells on the same plates (see also SI Appendix, Figs. S3 and S4). *P ≤ 0.05, ****P ≤ 0.0001 by two-way ANOVA with Tukey's multiple comparison test.

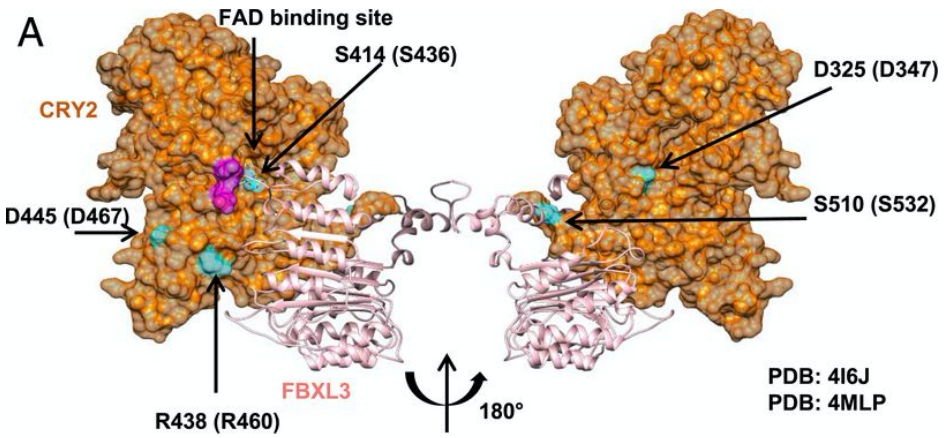
A
FAD binding site
S414 (S436)
D325 (D347)
CRY2
D445 (D467)
S510 (S532)
FBXL3
R438 (R460)
180°
PDB: 4I6J
PDB: 4MLP

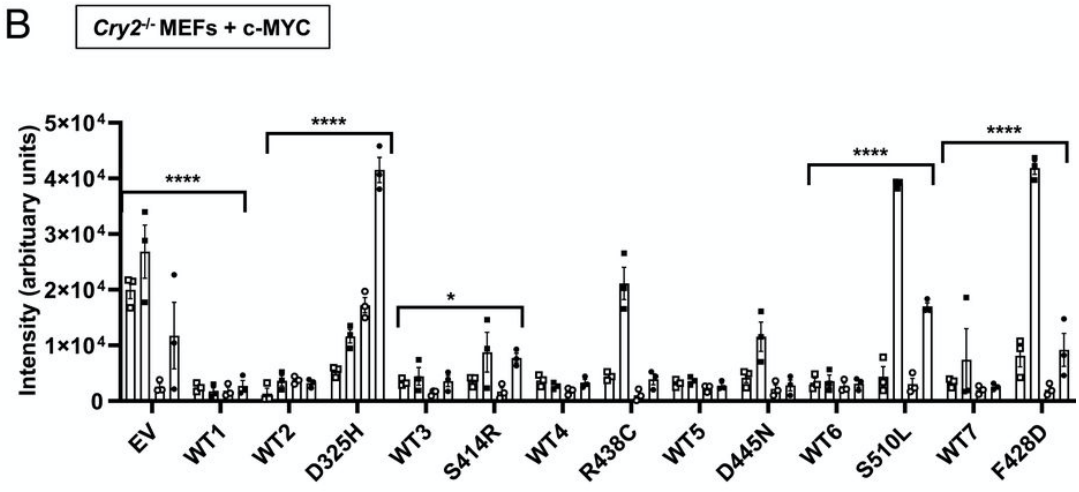
B
Cry2-/- MEFs + c-MYC
Intensity (arbitrary units)
5×10^4
4×10^4
3×10^4
2×10^4
1×10^4
0
****
****
*
****
****
EV
WT1
WT2
D325H
WT3
S414R
WT4
R438C
WT5
D445N
WT6
S510L
WT7
F428D

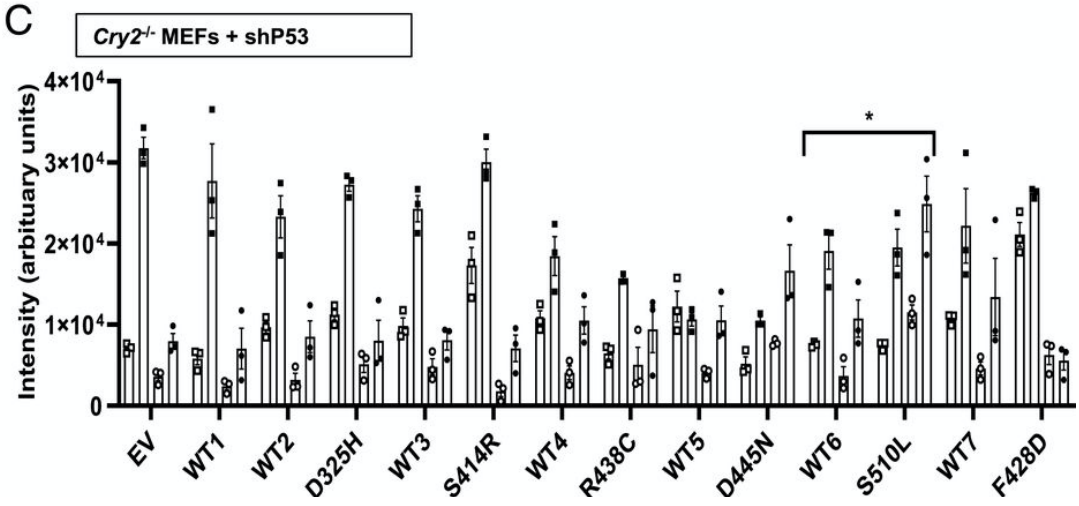
C
Cry2-/- MEFs + shP53
Intensity (arbitrary units)
4×10^4
3×10^4
2×10^4
1×10^4
0
*
EV
WT1
WT2
D325H
WT3
S414R
WT4
R438C
WT5
D445N
WT6
S510L
WT7
F428D

Two-dimensional (2D) colony formation tests cells' ability to survive and grow under limited paracrine signaling conditions. We previously demonstrated that *Cry2*$^{-/-}$ fibroblasts form colonies much more efficiently than matched wildtype cells in the context of either *c-MYC* overexpression or depletion of *p53*. Notably, this phenomenon was most robust in primary fibroblasts that were maintained in culture only for very few passages (16), perhaps due to accelerated accumulation of DNA damage in *Cry2*$^{-/-}$ cells (30). To study the impact of CRY2 missense mutations, we generated *Cry2*$^{-/-}$ fibroblasts stably expressing either c-MYC or shRNA targeting P53 and then further manipulated those lines to stably express wildtype or mutant CRY2. The process of generating the cell lines and growing a sufficient number to plate multiple replicates required performing colony formation assays after 10-12 passages. In this context, we found that wildtype CRY2 consistently suppresses colony growth in c-MYC-expressing *Cry2*$^{-/-}$ MEFs (Figure 4.1B) but the tendency for CRY2 to suppress colony formation in P53-depleted cells was less robust (Figure 4.1C). Consistent with our previous studies (16), a mutant that abolishes the interaction between CRY2 and FBXL3 (F428D) (2) fails to suppress colony growth of c-MYC-expressing cells (Figure 4.1B). Each of the cancer-associated missense mutants of CRY2 that we examined tended to be somewhat less effective at suppressing colony formation in c-MYC expressing cells compared to WT CRY2 but most had a mild impact. Strikingly, mouse CRY2 D325H and S510L consistently failed to suppress colony growth in c-MYC expressing cells (Figure 4.1B and Supplementary Figure 4.1D). In the context of *P53* depletion, expression of CRY2 S510L slightly enhanced colony formation, but neither WT nor mutant CRY2 had a major impact on colony formation of P53-depleted cells under the conditions tested (Figure 4.1C and Supplementary Figure 4.1E). Protein levels of the CRY2 missense mutants varied across biological replicates, likely due to heterogeneity of genome-integration sites within the stable-cell population, and did not have consistent effects on c-MYC protein accumulation in the *Cry2*$^{-/-}$ c-MYC–expressing cells (Supplementary Figure 4.2).

4.3.2 CRY2 missense mutations alter protein-protein interactions

To determine whether the observed impact of CRY2 missense mutations on cell growth could be explained by altered interaction with SCF complexes and/or with c-MYC, we examined the interactions of wildtype and mutant CRY2 with FBXL3, FBXL21, and c-MYC. Human CRY2 S436R, R460C, and S532L each exhibits decreased interactions with FBXL3 and FBXL21 compared to WT CRY2 (Figure 4.2A,B), though their impact is more subtle than that of the CRY2 F428D mutant, which was established from structural studies to critically disrupt interaction with FBXL3 (2) (Supplementary Figure 4.3A,B). None of the mutants consistently affected interactions with c-MYC (Supplementary Figure 4.3C).

Since FBXL3 and FBXL21 are primary determinants of CRY stability (2-8), we hypothesized that the half-lives of CRY2 S436R, R460C, and S532L would be increased due to their reduced interaction with FBXL3 and FBXL21. We generated tools to express fusion proteins in which luciferase is appended to the caryboxyl terminus of WT or mutant CRY2 (CRY2::LUC) in AD293 cells to measure the impact of each mutation on CRY2 stability. Contrary to expectations, each of the missense mutations studied reduces the half-life of the CRY2::LUC fusion protein (Figure 4.2C and Supplementary Figure 4.3F-H). This assay may not accurately reflect CRY2 half-life under physiological conditions, given that the fusion protein may behave differently than CRY2 alone, as well as the probability that expression of the fusion protein alters the stoichiometry of CRY2, endogenous F-box proteins, and/or other components that regulate CRY2 stability *in vivo*. Nevertheless, we did not observe consistent alterations in the steady state accumulation of either CRY2 or c-MYC under the conditions in which cell growth properties were impacted by mutant CRY2 (Supplementary Figure 4.2).

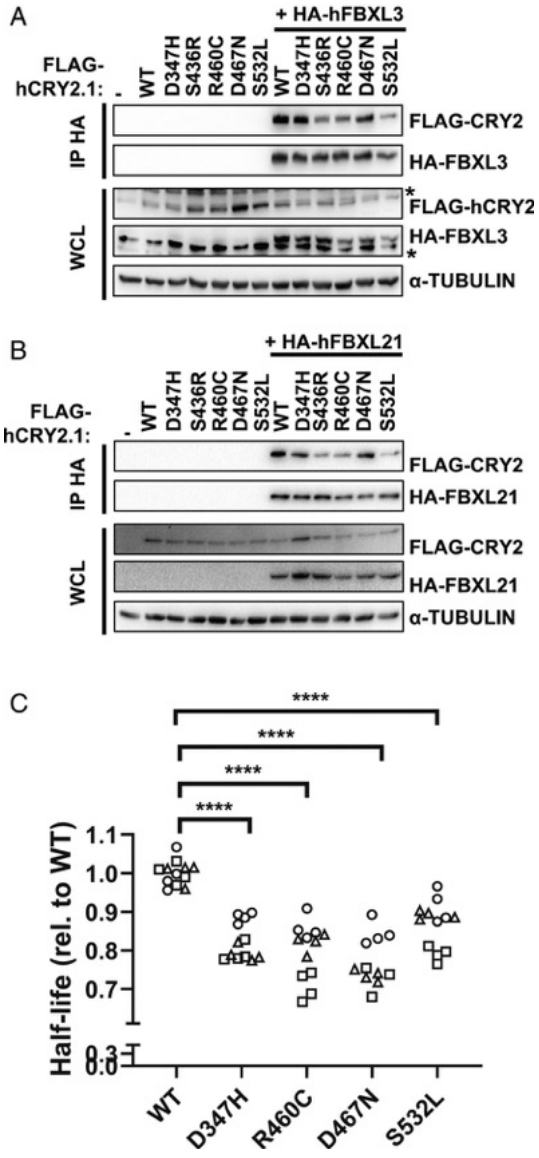

Figure 4.2. CRY2 S436R, R460C, and S532L exhibit reduced interaction with F-box proteins.

(A-B) Proteins detected by immunoblot (IB) following HA immunoprecipitation (IP) or in whole-cell lysates (WCL) from HEK293T cells expressing the indicated plasmids with the indicated tags. * denotes nonspecific band. ***(C)*** Half-life of CRY2-Luciferase fusions proteins containing the indicated missense mutations in CRY2 expressed in AD293 cells. Each symbol represents the half-life calculated from fitting luminescence data recorded continuously after addition of cycloheximide to an exponential decay function. Data represent three independent experimental replicates indicated by different symbols, each performed in quadruplicate. ****P ≤ 0.0001 by two-way ANOVA with Tukey's multiple comparison test.

Within the core circadian clock mechanism, CRYs directly repress CLOCK and BMAL1 in the presence or absence of PERs (52, 53). Several studies have suggested that disruption of circadian rhythms may contribute to tumor development (36). So, we examined whether the five selected tumor-associated CRY2 mutants exhibit altered interaction with core clock components. Indeed, several of the missense mutations under investigation reduced the recruitment of CRY2 to the CLOCK:BMAL1 heterodimer. Most strikingly, the interaction of human CRY2 D347H with CLOCK in the presence of BMAL1 was almost undetectable (Figure 4.3A). The ability of overexpressed CRY2 to interact with endogenous BMAL1 recapitulated the pattern of interaction with overexpressed CLOCK in the presence of overexpressed BMAL1, suggesting that these mutants may influence the interaction of CRY2 with the CLOCK:BMAL1 heterodimer under physiological conditions (Figure 4.3 and Supplementary Figure 4.4A). Importantly, none of the mutations examined had any effect on the interactions of CRY2 with overexpressed PER1 or PER2 (Figure 4.3 and Supplementary Figure 4.4B,C), suggesting that the decreased interaction of CRY2 D347H with CLOCK in the presence of BMAL1 is due to local disruptions in the structure rather than a global alteration of protein fold. The analogous mutations in human CRY1 (D307H) and mouse CRY2 (D325H) similarly impacted their interactions with CLOCK and BMAL1 (Figure 4.3B,C).

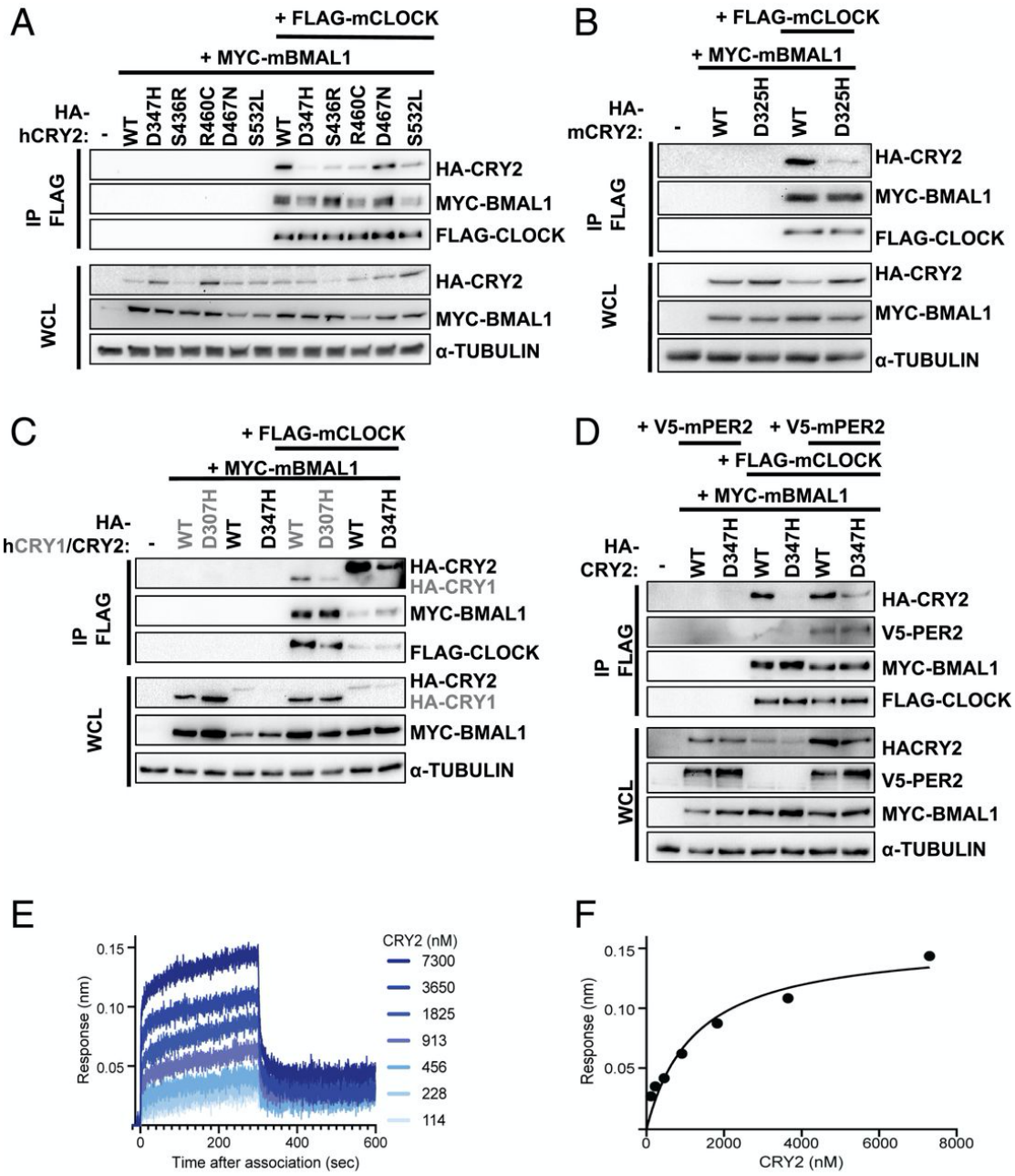

Figure 4.3. CRY2 D347H, S436R, R460C, and S532L exhibit reduced interaction with CLOCK.

(A–D) Proteins detected by IB following IP of the FLAG tag or in WCL from HEK293T cells expressing the indicated plasmids. ***(E)*** Representative BLI binding data of mouse CRY2 D325H PHR domain binding to the CLOCK:BMAL1 PAS domain core (PAS-AB domain heterodimer) immobilized on streptavidin tips. ***(F)*** Equilibrium analysis of the BLI data in E fit to a one-site binding model. KD = 1.8 ± 0.4 μM from two independent BLI experiments.

The interaction of PER2 with CRY2 was previously shown to enhance its ability to coimmunoprecipitate with CLOCK:BMAL1 (22, 23) resulting from an approximately two-fold decrease in the KD of the CRY2 PHR domain for the PAS domain core of CLOCK:BMAL1 in vitro (22). Consistent with this, co-expression of PER2 enables detection of CRY2 D347H in complex with CLOCK:BMAL1, although the mutant binds less robustly than wildtype CRY2 (Figure 4.3D). Given that relatively modest changes in affinity impact the ability of CRY2 to coimmunoprecipitate with CLOCK:BMAL1 from cells, we used biolayer interferometry (BLI) to determine how the CRY2 D325H mutation influences the affinity of the mouse CRY2 PHR domain for the PAS domain core of CLOCK:BMAL1 *in vitro* (Figure 4.3E). The D325H mutation decreased the affinity by 1.5-fold compared to wildtype CRY2 (22) for a K_D of 1.8 ± 0.4 μM (Figure 4.3F), helping to explain the reduced interaction of these proteins in cellular extracts.

4.3.3 CRY2 D347H does not repress CLOCK:BMAL1

Given that CRY2 D347H exhibits reduced interaction with CLOCK in the presence of BMAL1, we predicted that it would be a less effective repressor of CLOCK:BMAL1 transcriptional activity. In U2OS cells, transient overexpression of CLOCK and BMAL1 enhances the expression of luciferase driven by the *Per2* promoter (Figure 4.4A,B). CRY2 dose-dependently decreases the bioluminescent signal, indicating repression of the CLOCK:BMAL1 heterodimer by CRY2 as expected. A previous study demonstrated that CRY2 G351D is unable to repress CLOCK:BMAL1 (54); we have recapitulated that finding and use CRY2 G351D as a control in our assay. Four CRY2 missense mutants (S436R, R460C, D467N, S532L) examined behave indistinguishably from WT CRY2 in this assay. However, consistent with its impact on the interaction of CRY2 with CLOCK and BMAL1 in a co-immunoprecipitation assay, CRY2 D347H does not repress CLOCK:BMAL1 when all three are overexpressed in U2OS cells (Figure 4.4B)

Figure 4.4. CRY2 D347H neither represses CLOCK/BMAL1 nor supports circadian rhythms.

(A) Schematic diagram of the luciferase assay performed in B. ***(B)*** Luminescence detected from U2OS cells expressing Per2-Luciferase and the indicated additional plasmids (mCherry, mCh). Data are represented as mean ± SEM and are normalized to the gray bar and CLOCK-BMAL1 alone. Triangles on the x-axis indicate increasing amounts of CRY WT or mutant transfected, 2 or 5 ng. ****P ≤ 0.0001 by Student's t test versus CLOCK-BMAL1 alone in GraphPad Prism 9. ***(C)*** Schematic diagram of rhythmicity rescue assay in *Cry1*$^{-/-}$*;Cry2*$^{-/-}$ MEFs. ***(D)*** Periods of *Cry1, Cry2* WT, or mutant or control (no Cry transfected) across three independent experiments (open circles, triangles, or squares) with six technical replicates in each. Periods calculated using the Lumicycle analysis program using running-average background subtraction and fitting to a damped sine wave by least mean squares method. Replicates for which the best-fit damped sine had period >40 h and/or goodness of fit <80% were considered arrhythmic and are indicated as 0 on the graph. ***(E)*** Periods of the mutants that showed rhythmicity (R438C and S510L). Data represent mean ± SEM of two independent experiments with two to six replicates each as indicated by filled circles in the graph. ***P ≤ 0.001, ****P ≤ 0.0001 by one-way ANOVA using Dunnett's multiple comparisons in GraphPad Prism 9. ***(F)*** Background-subtracted data generated from continuous recording of luciferase activity from *Cry1*$^{-/-}$*;Cry2*$^{-/-}$ fibroblasts transfected with *Per2-Luciferase* and *WT Cry1* (gray), or WT (black) or mutant (as indicated) *Cry2*. Note that, because the background signal decreases exponentially over time, the background-subtracted signal falls below zero. Data represent mean bioluminescence for two to six replicates from a representative of at least two experiments.

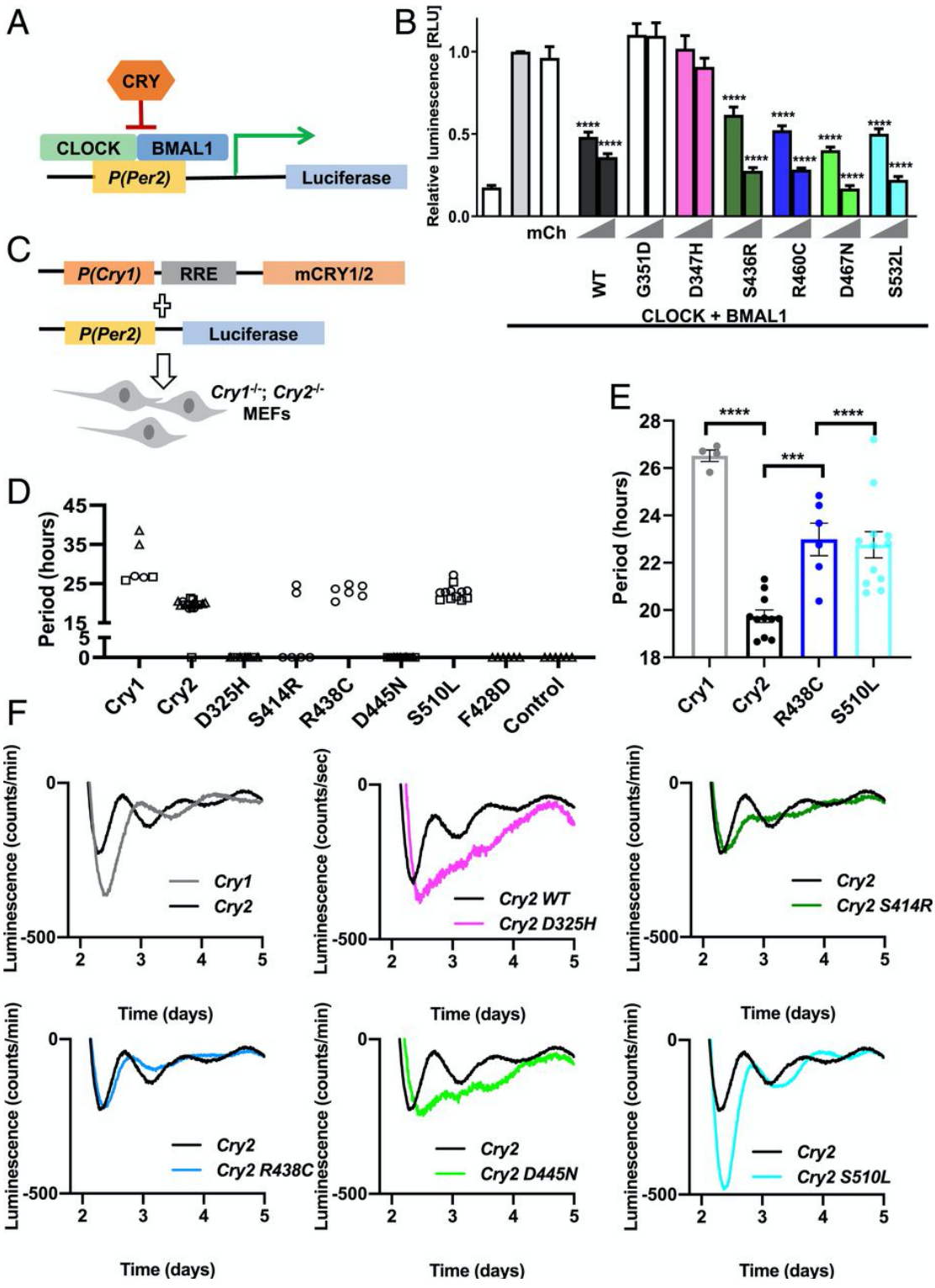
A
CRY
CLOCK
BMAL1
P(Per2)
Luciferase
B
Relative luminescence [RLU]
1.0
0.5
0.0
mCh
WT
G351D
D347H
S436R
R460C
D467N
S532L
CLOCK + BMAL1
C
P(Cry1)
RRE
mCRY1/2
P(Per2)
Luciferase
Cry1-/-; Cry2-/-
MEFs
D
Period (hours)
45
35
25
15
5
0
Cry1
Cry2
D325H
S414R
R438C
D445N
S510L
F428D
Control
E
Period (hours)
28
26
24
22
20
18
****
***
****
Cry1
Cry2
R438C
S510L
F
Luminescence (counts/min)
Luminescence (counts/sec)
0
-500
2
3
4
5
Time (days)
Cry1
Cry2
Cry2 WT
Cry2 D325H
Cry2
Cry2 S414R
Cry2
Cry2 R438C
Cry2
Cry2 D445N
Cry2
Cry2 S510L

To examine whether cancer-associated missense mutations in CRY2 alter the ability of CRY2 to sustain endogenous circadian rhythms, we used the rhythmicity rescue assay developed in ref. (55). In this assay, arrhythmic *Cry1*$^{-/-}$;*Cry2*$^{-/-}$ MEFs (56) are transiently transfected with a plasmid encoding destabilized luciferase under the control of the *Per2* promoter, in combination with CRY1 or CRY2 under the control of elements derived from the endogenous *Cry1* promoter and first intron. Expression of WT CRY1 (55) or CRY2 (23) under these conditions enables rhythmic expression of the luciferase reporter with long or short periodicity characteristic of *Cry2*$^{-/-}$ or *Cry1*$^{-/-}$ MEFs, respectively. Continuous recording of luciferase activity enables precise measurement of the period of the resulting rhythmic luciferase expression, which allows sensitive detection of perturbations of those rhythms.

Using this system, we found that all of the cancer-associated missense mutations tested impair the ability of CRY2 to sustain short period circadian rhythms of luciferase expression driven by the *Per2* promoter (Figure 4.4D-F and Supplementary Figure 4.5). Consistent with its inability to repress CLOCK:BMAL1 transcriptional activity, orthologous mouse CRY2 D325H was unable to rescue rhythms. Unexpectedly, CRY2 D445N also failed to support circadian expression of *Per2-luciferase* despite having minimal impact on the interaction of CRY2 with either FBXL3/21 or CLOCK:BMAL1. Expression of CRY2 R438C or S510L resulted in longer periods than those observed with expression of WT CRY2. CRY2 S414R sustained detectable rhythms in only one-third of replicates and those rhythms also had a longer period than observed with WT CRY2, similar to those supported by CRY2 R438C and S510L.

4.3.4 CRY2 mutants that fail to suppress colony formation repress P53 target gene expression

Because neither their impact on protein-protein interactions nor their ability to rescue circadian rhythms distinguished the two CRY2 mutants that fail to suppress two-dimensional colony growth in c-MYC expressing fibroblasts (D325H and S510L) (Figure 4.5 and Supplementary Table 4.1), we took an unbiased approach to examine their influence on global gene expression in those cells. We sequenced RNA from *Cry2*$^{-/-}$ MEFs overexpressing c-MYC and either an empty vector (EV, Control), or WT or mutant CRY2 plated at a low or high density. Gene Set Enrichment Analysis (GSEA) (57) revealed dramatic suppression of a hallmark set of P53 target genes (58) in cells expressing either CRY2 D325H (FDR = 0.004) or S510L (FDR = 0.01) compared with those expressing WT CRY2 (Figure 4.5A,B,E,F,K,L and Supplementary Figure 4.6). Expression of the transcript encoding P53 (Trp53) is decreased in cells expressing CRY2 D325H or S510L (Supplementary Figure 4.7A), but P53 protein levels do not seem to be affected (Supplementary Figure 4.7B). This suggests that the decreased expression of the Trp53 transcript in D325H and S510L does not explain the reduced expression of P53 target genes. Instead, the reduction in Trp53 mRNA is likely a consequence of decreased P53 activity, since it has been reported to regulate its own expression (59).

Figure 4.5. mCRY2 D325H and mCRY2 S510L suppress transcription in the P53 pathway.

(A–J) GSEA enrichment plots *(A–D, and J)* and heat maps representing the top 15 up- or down-regulated transcripts of the leading edge that were driving the enrichment score (ES) (E–I) for the hallmark gene sets representing the P53 pathway (A, B, E, and F), hypoxia pathway (C, D, G, and H), or E2F target genes (I and J). In A–D and J, the top portion shows the running ES for the gene set as the analysis walks down the ranked list. The middle portion shows where the members of the gene set appear in the ranked list of genes. The bottom portion shows the value of the ranking metric as you move down the list of ranked genes. The ranking metric measures a gene's correlation with a phenotype. Here, the phenotypes are defined as the cell lines stably expressing WT or mutant (D325H or S510L). In E–I, red, high expression; blue, low expression. ***(K–Q)*** Extracted gene-expression profiles of the indicated genes from the RNA-seq data. Light red, low-density plating; light blue, high-density plating.

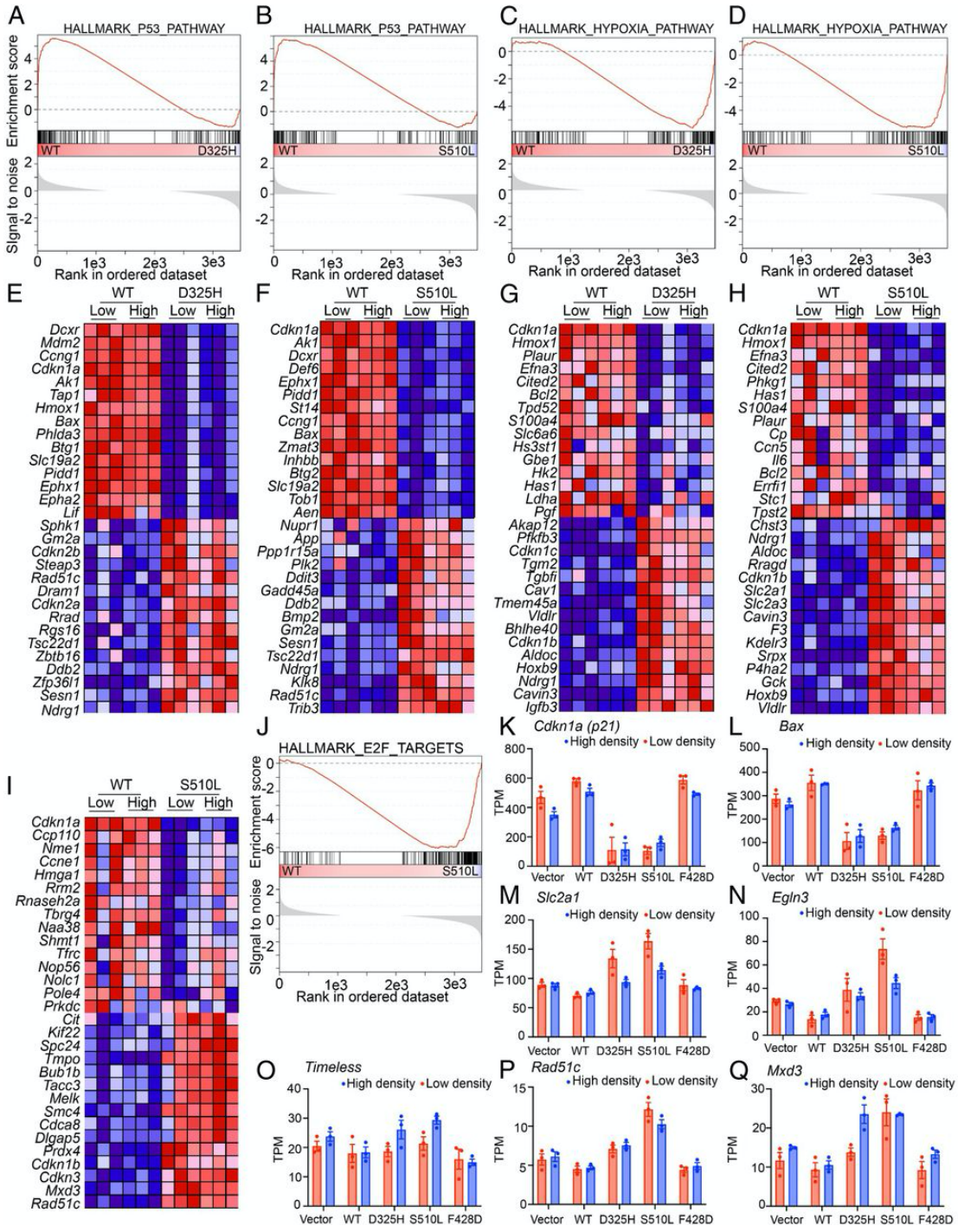
A
HALLMARK_P53_PATHWAY
Enrichment score
Signal to noise
WT
D325H
Rank in ordered dataset
B
HALLMARK_P53_PATHWAY
WT
S510L
C
HALLMARK_HYPOXIA_PATHWAY
WT
D325H
D
HALLMARK_HYPOXIA_PATHWAY
WT
S510L
E
WT
D325H
Low High Low High
Dcxr
Mdm2
Ccng1
Cdkn1a
Ak1
Tap1
Hmox1
Bax
Phlda3
Btg1
Slc19a2
Pidd1
Ephx1
Epha2
Lif
Sphk1
Gm2a
Cdkn2b
Steap3
Rad51c
Dram1
Cdkn2a
Rrad
Rgs16
Tsc22d1
Zbtb16
Ddb2
Zfp36l1
Sesn1
Ndrg1
F
WT
S510L
Low High Low High
Cdkn1a
Ak1
Dcxr
Def6
Ephx1
Pidd1
St14
Ccng1
Bax
Zmat3
Inhbb
Btg2
Slc19a2
Tob1
Aen
Nupr1
App
Ppp1r15a
Plk2
Ddit3
Gadd45a
Ddb2
Bmp2
Gm2a
Sesn1
Tsc22d1
Ndrg1
Klk8
Rad51c
Trib3
G
WT
D325H
Low High Low High
Cdkn1a
Hmox1
Plaur
Efna3
Cited2
Bcl2
Tpd52
S100a4
Slc6a6
Hs3st1
Gbe1
Hk2
Has1
Ldha
Pgf
Akap12
Pfkfb3
Cdkn1c
Tgm2
Tgbfi
Cav1
Tmem45a
Vldlr
Bhlhe40
Cdkn1b
Aldoc
Hoxb9
Ndrg1
Cavin3
Igfb3
H
WT
S510L
Low High Low High
Cdkn1a
Hmox1
Efna3
Cited2
Phkg1
Has1
S100a4
Plaur
Cp
Ccn5
Il6
Bcl2
Errfi1
Stc1
Tpst2
Chst3
Ndrg1
Aldoc
Rragd
Cdkn1b
Slc2a1
Slc2a3
Cavin3
F3
Kdelr3
Srpx
P4ha2
Gck
Hoxb9
Vldlr
I
WT
S510L
Low High Low High
Cdkn1a
Ccp110
Nme1
Ccne1
Hmga1
Rrm2
Rnaseh2a
Tbrg4
Naa38
Shmt1
Tfrc
Nop56
Nolc1
Pole4
Prkdc
Cit
Kif22
Spc24
Tmpo
Bub1b
Tacc3
Melk
Smc4
Cdca8
Dlgap5
Prdx4
Cdkn1b
Cdkn3
Mxd3
Rad51c
J
HALLMARK_E2F_TARGETS
Enrichment score
Signal to noise
WT
S510L
Rank in ordered dataset
K
Cdkn1a (p21)
High density
Low density
TPM
Vector
WT
D325H
S510L
F428D
L
Bax
M
Slc2a1
N
Egln3
O
Timeless
P
Rad51c
Q
Mxd3

Given that P53 is a key mediator of growth suppression, reduced expression of P53 target genes in cells expressing CRY2 D325H or S510L with concomitant overexpression of c-MYC suggests that reduced P53 activity may be a critical effector of the CRY2 mutants' impact on the growth of c-MYC–expressing cells. To understand whether regulation of P53 is required for the influence of CRY2 on colony formation in c-MYC–overexpressing cells, we used shRNA to deplete P53 or Luciferase (control) in cells that also express c-MYC and WT or mutant CRY2 (Supplementary Figure 4.8). As expected, depleting P53 robustly increases colony formation in c-MYC–expressing cells (Supplementary Figure 4.8A). Consistent with the idea that CRY2 suppression of colony formation in cells overexpressing c-MYC involves regulation of P53, expression of WT CRY2 is less effective at suppressing colony formation in P53-depleted cells. However, in contrast to *Cry2*$^{-/-}$ cells in which P53 is depleted by shRNA without overexpression of c-MYC (Figure 4.1C), expression of WT CRY2 consistently suppresses colony formation in these cells in which c-MYC overexpression is combined with shRNA-mediated depletion of P53 (Supplementary Figure 4.8A). Intriguingly, reduced P53 expression does not significantly impact colony formation in *Cry2*-deficient cells or in those expressing CRY2 S510L when compared with shLuc (Supplementary Figure 4.8B), suggesting that P53 activity may be already suppressed in those cells even when P53 protein is present.

While the effect was less robust than the observed suppression of the P53 pathway, we also measured significantly increased expression of the hallmark hypoxia gene network (FDR = 0.016 or 0.05, Figure4.5C,D,G,H,M,N and Supplementary Figure 4.6). Finally, consistent with our demonstration that CRYs cooperate with SCF^{FBXL3} to regulate E2F protein accumulation (12), E2F target gene expression was elevated in cells expressing CRY2 S510L (which exhibits decreased interaction with FBXL3), when plated at high density (FDR = 0.21 including only high density samples,

Figure 4.5I,J,O,P,Q and Supplementary Figure 4.6). Taken together, these data suggest that CRY2 D325H and S510L are unable to suppress colony formation of *Cry2*$^{-/-}$ MEFs overexpressing c-MYC due to overlapping functional impairments, including suppression of the P53 transcriptional network.

4.4 Discussion

Most missense mutations reported in The Cancer Genome Atlas (TCGA) have an unknown functional impact on the cancers in which they are found. Although missense mutations in *CRY2* are rare in TCGA, human genome-sequencing data spanning six global and eight sub-continental ancestries (60) demonstrate that core clock genes, including *CRY2*, are resistant to mutation in healthy somatic tissues, suggesting that recurrent cancer-associated mutations in these genes may be functionally important. Several lines of evidence indicate that *CRY2* may play a role in preventing tumor development. In a variety of cancers, *CRY2* expression is significantly reduced compared to matched normal tissues (16, 61). Furthermore, inactivation or reduced expression of *CRY2* is strongly associated with altered activity of established oncogenic or tumor suppressive pathways (61). Here, we demonstrate that two cancer-associated mutations in *CRY2* (D347H and S532L, using numbering for human *CRY2*) prevent CRY2-mediated suppression of colony growth in the context of c-MYC overexpression in *Cry2*$^{-/-}$ fibroblasts.

Several molecular mechanisms have been proposed to explain the apparent inhibition of tumor development by CRY2 (19). For example, CRY2 can cooperate with SCF^{FBXL3} to stimulate ubiquitination and subsequent degradation of c-MYC (16), the DNA damage activated protein kinase TLK2 (62), E2F family members (12), and likely other proteins. CRY2 S532L exhibits decreased interaction with FBXL3 and FBXL21, and this likely contributes to the elevated expression of E2F target genes in cells expressing CRY2 S532L. However, disrupted interaction with FBXL3/21 may not be sufficient to prevent CRY2 from suppressing colony formation because the S436R and R460C mutations, which had a similar impact on the ability of CRY2 to interact with FBXL3/21, can suppress colony formation. We cannot

exclude the possibility that quantitative differences in the impacts of these mutations on CRY2-FBXL3/21 affinity underlie their diverse functional impacts on cell growth. Conversely, CRY2 D347H fails to suppress colony formation but does not prevent CRY2 from interacting with its F-box–protein partners. Thus, disruption of the CRY2-FBXL3 interaction is not required for loss of CRY2 suppression of colony formation in the context of c-MYC overexpression.

CRY2 D347H exhibits reduced interaction with and an inability to repress CLOCK:BMAL1, and cannot sustain circadian rhythms of *Per2-luciferase* expression in *Cry1*$^{-/-}$;*Cry2*$^{-/-}$ fibroblasts.

The secondary pocket of CRYs provides an extensive interaction surface for the CLOCK PAS-B domain that plays a critical role in the stable recruitment of cryptochromes to CLOCK:BMAL1 (22, 23). The electrostatic surface of the CRY secondary pocket is mostly negatively charged, while the HI loop of the CLOCK PAS-B domain that docks into this pocket is positively charged (21) suggesting that electrostatic attraction could help to support the CRY-CLOCK interaction. Notably, D347 is located on the edge of the secondary pocket of CRY2, providing a rationale for how the mutation from aspartic acid (D) to histidine (H) could contribute to reduced affinity of the CRY2 mutant for CLOCK:BMAL1. Given that differences in the affinity of CRY1 and CRY2 define their ability to stably interact with CLOCK:BMAL1 and repress its activity (22, 23), the D437H mutation represents another example of how a modest change in binding at this critical interface can manifest as a substantial change in CRY function in the clock.

Disrupted circadian rhythms increase cancer risk in humans and increase tumor formation in a variety of genetically engineered mouse models of cancer (36). The inability of the mouse ortholog of CRY2 D347H to suppress colony formation in c-MYC expressing fibroblasts supports the contention that circadian rhythms play a protective role against tumorigenesis. However, as for the role of CRY2 in promoting SCF$^{FBXL3/21}$-mediated protein turnover, loss of the ability to sustain circadian rhythms is not sufficient to prevent

suppression of colony formation since the CRY2 D467N ortholog (D445N) suppresses colony formation but cannot support cell-autonomous rhythms. The inability of CRY2 D445N to sustain circadian rhythms despite its seemingly normal interaction with and repression of CLOCK:BMAL1 suggests that it must disrupt some other aspect of the concerted and periodic interaction with other endogenous proteins (63), appropriate degradation (3, 5, 7), or other post-translational regulation within the clock mechanism. We cannot exclude the possibility that the impact of the CRY2 mutants examined could differ in the presence of WT CRY1 and/or CRY2 both of which are likely present in tumor samples where the mutations occur in a single copy. Taken together, the impacts of the five missense mutations in CRY2 on cell growth, circadian rhythms, and interaction with FBXL3/21 suggest that disruption of core clock function or circadian proteolysis may contribute to enhanced cell growth, but neither is sufficient nor required for loss of growth suppression by CRY2. We measured global RNA expression patterns to identify functional impacts shared by the two mutations with the greatest impact on cell growth. This analysis revealed a striking suppression of a P53 transcriptional network and concomitant elevation of hypoxia target genes in cells expressing mutant CRY2. We do not exclude the possibility that multiple mechanisms contribute to the failure of CRY2 D325H and S510L to suppress colony growth.

We previously demonstrated that CRY1 is stabilized and CRY2 is destabilized in response to DNA damage (30). Furthermore, transcriptional activation of at least some P53 target genes is blunted in *Cry2*$^{-/-}$ cells and sustained in *Cry1*$^{-/-}$ cells following DNA damage (30). PER2, which cooperates with CRYs to repress transcriptional activation of the CLOCK:BMAL1 heterodimer, stabilizes P53 by inhibiting its MDM2-mediated ubiquitination and degradation (64-66). These mechanisms could be at play, but further investigation will be required to understand how CRY2 D325H and CRY2 S510L suppress P53 target gene expression.

Elevated expression of hypoxia-regulated transcripts can enhance cell survival under stressful conditions and contribute to tumorigenesis (67-69). We and others recently

demonstrated that CRY1 and CRY2 suppress both the protein accumulation and transcriptional activation of HIF1α and HIF2α (70, 71). HIFs are closely related to CLOCK and BMAL1 (72) and we and others have shown that BMAL1 dimerizes with HIF1α (70, 73, 74). Given that the CRY2 D325H mutation reduces its association with and repression of CLOCK:BMAL1, it may also influence repression of HIF1α/BMAL1 by altering protein-protein interactions, although it is unclear whether the interaction of CRYs with HIFs involves the secondary pocket. In contrast, the CRY2 S510L mutation may enhance hypoxia target gene expression by preventing CRY-mediated suppression of HIF1α protein accumulation.

E2Fs are a family of transcription factors that regulate G1-to S-phase progression in the cell cycle (75). The expression of E2F target genes is elevated in cells expressing CRY2 S510L but not in those expressing CRY2 D325H. This distinction likely reflects reduced $SCF^{FBXL3/21}$-mediated turnover of E2F family members (12) in the presence of CRY2 S510L which exhibits reduced association with FBXL3 and FBXL21. The additional elevation of E2F target genes in combination with suppression of P53 likely contributes to the greater impact of CRY2 S510L in cell growth and colony formation assays.

Over the past decade, several small molecules that target CRYs have been identified and some are under development for therapeutic use in metabolic disease and cancer (76-80). Intriguingly, one of these (TH301) forms a hydrogen bond with the serine in CRY1 analogous to CRY2 S414 and selectively increases the half-life of CRY2 (and not of CRY1), presumably by reducing its interaction with FBXL3 (79). The disordered C-terminal tail (CTT) of CRY2 was required for the impact of TH301 on CRY2 stability suggesting that an intramolecular interaction between the CTT and the globular photolyase homology region (PHR), which contains the FAD binding pocket in which S414 is located. The apparently greater impact of the CRY2 mutant (D325H) to decrease interaction with CLOCK:BMAL1 in cells compared to the modest difference in affinity between the wildtype and D325H mutant CRY2 PHR for the BMAL1:CLOCK PAS domain core *in vitro* may also be explained by

participation of the CTT. Improved understanding of the molecular mechanisms connecting circadian clocks, and CRYs in particular, to cancer-driving networks will inform efforts for further development of CRY-modulating compounds and other strategies to combat the increased incidence of metabolic disease, cancer, and other pathologies associated with chronic circadian disruption.

4.5 Materials and Methods

4.5.1 Cell culture

HEK 293T and U2OS cells were purchased from the American Type Culture Collection (ATCC). Littermate wildtype and Cry2$^{-/-}$ mouse embryonic fibroblasts (MEFs) were generated from embryos collected from Cry2+/− female mice on day E12.5-13.5 after fertilization by Cry2+/- male mice (initially generated by Dr. Aziz Sancar, University of North Carolina) (81)). The original cells prepared from embryos are considered Passage 0. Each time the cells are subcultured (passaged, a.k.a. split) the passage number is increased by one. Experiments using these cells were performed in cells that were passaged no more than 12 times. *Cry1*$^{-/-}$*;Cry2*$^{-/-}$ MEFs were generated by Andrew Liu, University of Florida, Gainesville, FL, and Hiroki Ueda, University of Tokyo, Tokyo, Japan and the RIKEN Quantitative Biology Center, Osaka, Japan (55) and were gifted to us. AD293 cells were gifted to us by Dr. Steve Kay, University of Southern California, Los Angeles, CA. Cell culture methods were the same as in (12). Fetal Bovine Serum (FBS) was purchased from Thermo Fisher (cat # 16000044). All transfections were carried out using linear polyethylenimine (PEI; Polysciences cat. #23966-2) by standard protocols.

4.5.2 Immunoprecipitation and western blotting

Methods were the same as in ref. (12). Antibodies for Western Blots were anti-FLAG polyclonal (Sigma, St. Louis, MO, cat # F7425), anti-V5 polyclonal (Bethyl Labs, Montgomery, TX, cat # A190–120A), anti-HA polyclonal (Sigma, St. Louis, MO, cat # H6908), anti-α-TUBULIN (Sigma, St. Louis, MO, cat # T5168), anti-LAMIN A (Sigma, St. Louis, MO, cat # L1293), CRY1-CT and CRY2-CT as described in ref. (82), anti-cMYC (Abcam cat #

ab32072), anti-P53 (Leica biosystems, Wetzlar, Germany, cat # CM5), anti-P53 (Santa Cruz Biotechnology, Inc, Dallas, TX, cat # sc-126) (used in S2 G,H), anti-MYC (for MYC tag) (Sigma, St. Louis, MO, cat # C3956), anti-phospho-P53 (S15) (Cell Signaling Technology, Danvers, MA, cat # 9284) .

4.5.3 Plasmids

pcDNA3-2xFlag-mCRY2, pcDNA3-HA-FBXL3, pcDNA3-human c-MYC-V5 are as described previously (16). FBXL3 was replaced with human FBXL3 cDNA and human CRY2 cDNA was cloned in to a pCDNA3.1-based HA or 2xFLAG-epitope tagged vector using standard methods. CRY2/CRY1 TCGA mutations were made using Q5 Site-Directed Mutagenesis (New England Biolabs Inc., Ipswich, MA, cat # E0554S). psPAX plasmid (Addgene, Watertown, MA, plasmid 12260) and pMD2.G plasmid (Addgene. Watertown, MA, plasmid 12259) deposited by Dr. Didier Trono, and used for infection, were purchased from Addgene . Watertown, MA. pCL-AMPHO was purchased from Novus Biologicals Littleton, CO (cat # NBP2-29541). MLH-shLuciferase, MLH-shP53 pBABE-Puro, pWZL hygro HRASV12 were gifts from Dr. Tyler Jacks. pcDNA3-2xFlag-mBMAL1, pcDNA3-2xFlag-CLOCK, and pGL2-Per2-luciferase were gifts from Charles Weitz, Department of Neurobiology, Harvard Medical School, Boston. pCMX βgalactosidase was a gift from Dr. Ron Evans, Gene Expression Laboratory, The Salk Institute for Biological Studies, La Jolla. pMU2-P(Cry1)-(intron336)-Cry1/2-Myc, modified with a C-terminal MYC tag was gifted to us by Dr. Carla Green as in ref. (23) and the modified using Q5 Site-Directed Mutagenesis (New England Biolabs Inc., Ipswich, MA, cat # E0554S) to create the CRY2 TCGA mutants. p3XFLAG-CMV14-CRY1-LUC was gifted to us from Dr. Tsuyoshi Hirota as in (77) and modified using Q5 Site-Directed Mutagenesis (New England Biolabs Inc., Ipswich, MA, cat # E0554S) to replace CRY1 with human CRY2 and the CRY2 TCGA mutants.

4.5.4 Generation of viruses and stable cell lines

Lentiviral or retroviral shRNA or stable overexpression constructs were produced by transient transfections in HEK293T cells using psPAX, PMD2.G, or pCL-AMPHO packaging

plasmids for virus generation. Viral supernatants were harvested 48hours after transfection and then filtered through a 0.45μm filter. Viral supernatant was combined with media and 6μg/mL polybrene (Sigma, St. Louis, MO, cat # 107689-10G) and then added to parental cell lines. After 16hrs, the media was changed into selection media – containing 2μg/mL puromycin (Sigma, St. Louis, MO, cat # P9620-10ML), 75μg/mL hygromycin (Sigma, St. Louis, MO, cat # H3274-1G), 5μg/mL blasticidin (Invivogen, San Diego, CA, cat # ant-bl-1). Selection media was replaced every 2-3 days until selection was complete (as judged by death of mock-infected cells, 4 days to 2 weeks).

4.5.5 Proliferation and 2-D colony formation assays

For proliferation assays, cells were plated at 5000 cells/well in triplicate in a 6-well plate and counted every 2 days for 10 days via hemocytometer. Two independent experiments were performed. For 2-D colony formation assays, cells were plated 150 cells/well of a 6-well plate in triplicate and grown for 11-18 days prior to fixing and staining with crystal violet. To stain, media was aspirated, washed with 1xPBS, then fixed with 100% methanol (Sigma, St. Louis, MO, cat # 179337-4X4L) for 10min and then removed, then stained with 20% methanol and 0.05% crystal violet (Sigma, St. Louis, MO, cat # C3886-25 g) for 20min and then removed, plates were rinsed in DI-H2O and imaged. Three independent experiments were performed.

4.5.6 Real-time bioluminescence rhythmicity rescue assays

Cry1$^{-/-}$;*Cry2*$^{-/-}$ cells (from Dr. Hiroki Ueda, University of Tokyo and the RIKEN Quantitative Biology Center) were plated at 4 x 105 per 3.5 cm dish and transfected the same day with FuGene 6 (Promega, Madison, WI, cat # E2311) according to the manufacturer's protocol. Assays were performed as in ref. (23) with the following minor modifications: Cells were transfected with 6 μg Per2-luciferase and 150 ng of pMU2- P(Cry1)-(intron336)-Cry1/2-Myc expressing wildtype CRY1 or CRY2 or CRY2 containing the TCGA mutations. After 72 hours, media was replaced and cells were synchronized with media containing 1mM dexamethasone and 100 μM D-luciferin. After the 2 hours, the media was replaced with

media containing DMEM, 5% FBS, 1% penicillin-streptomycin, 15 mM Hepes, pH 7.6, and 100 μM D-luciferin. Plates were then sealed and placed in the Lumicycle as in ref. (23) Data were analyzed using the Lumicycle Analysis software package (Actimetrics, Inc.). The first two days of recording were discarded, and background signal calculated as the running average of 24 hours surrounding each point were subtracted from the raw data. (Note that because the background signal decreases exponentially over time, this results in the background-subtracted signal dropping below zero). Baseline subtracted data were further corrected for background noise as in ref. (23). Period, phase, amplitude, and damping rate were then calculated by fitting the remaining data to a damped sine wave by a least mean squares method for each plate of cells. Samples were considered arrhythmic if the goodness of fit for the damped sine wave was <80% or if the period of the best fit sine wave was greater than 40 hours. The cells used in these assays were a generous gift from Dr. Hiroki Ueda, University of Tokyo and the RIKEN Quantitative Biology Center. The passage number of the cells that we received was unknown and they are likely spontaneously immortalized. We used the cells within seven (Supplementary Figure 4.3A), four (Supplementary Figure 4.3A,C), or eight additional passages (Supplementary Figure 4.3E)

4.5.7 Protein degradation assay

Assay was performed as in (7) (77) using AD293 cells with slight modifications. AD293 cells were transiently transfected using PEI. 24hrs after transfection, the media was changed to selection media 750μg/mL Neomycin (G418 Sulfate) (Mirus Bio, Madison, WI, cat # MIR5920). Media was changed ever 2-3 days until selection was complete (as judged by death of mock-infected cells, 4 days to 2 weeks). The stable cell lines were plated at 2x106cells/ 35mm cell culture dish (VWR, Radnor, PA, cat # 82050-538). After 24hrs, media was changed into luciferase recording media (DMEM, 5% FBS, 1% penicillin-streptomycin, 15 mM Hepes, pH 7.6, and 100 μM D-luciferin) for 1 hour then cycloheximide (CHX) (Fisher Scientific, Hampton, NH, cat # 50255724) was added at a final concentration of 100μg/ml diluted in serum free media. Plates were sealed with vacuum grease (Dow Corning high

vacuum grease; VWR, Radnor, PA, cat #59344-055) and glass cover slips (Fisher Scientific Hampton, NH, Cat # 22038999; 40CIR-1,) and placed into the Lumicycle 32 from Actimetrics, Inc. (Wilmette, IL). Data were recorded for 24hrs using the Actimetrics Lumicycle. Data Collection software and analyzed/exported using Actimetrics Lumicycle Analysis program. Half-life was obtained by one phase exponential decay fitting with Prism software (GraphPad Software, Graphpad Holdings, LLC, San Diego, CA).

4.5.8 Luciferase Assays

Luciferase assays were performed with U2OS cells as in ref. (13). U2OS cells were plated at 10,000 cells/well in 96-well plates with six replicates per condition After 8 hr, U2OS cells were transfected with 35 ng pGL2- Per2-luciferase, 5 ng β-galactosidase, 0.5 ng BMAL1, 1.5 ng CLOCK, and 0.01–0.05 ng CRY2/mutants/mCherry. All low-concentration plasmid dilutions were prepared fresh immediately before transfection. The following day, medium was replaced. The following day luciferase activity was measured using the britelite plus Reporter Gene Assay System (Perkin-Elmer, Waltham, MA, cat. #6066761) according to the manual, followed by measuring β-galactosidase activity measurement using 2-Nitrophenyl β-D-galactopyranoside (Sigma, St. Louis, MO, cat #N1127) as substrate.

4.5.9 Mice

Cry1$^{-/-}$*; Cry2*$^{-/-}$ mice from which *Cry2*$^{-/-}$ primary MEFs were derived were from Dr. Aziz Sancar (1) (81). All animal care and treatments were in accordance with Scripps Research guidelines and regulations for the care and use of animals. All procedures involving experimental animals were approved by the Scripps Research Institutional Animal Care and Use Committee (IACUC) under protocol #10-0019.

4.5.10 RNA-sequencing

Cry2$^{-/-}$ primary MEFs stably overexpressing c-MYC and EV, WT, D325H, S510L, or F428D were plated in biological triplicate, two wells per replicate, in 6-well plates at two plating densities – 150 cells/ well (low) or 500 cells/ well (high). The cells from two wells were combined and collected for RNA extraction 11 days (high) and 14 days (low) after plating.

RNA was extracted using RNeasy mini kit (Qiagen, Hilden, Germany, cat # 74106) according to the manufacturer's protocol. The QIAGEN RNase-Free DNase Set was used for on-column DNA digestion according to the manufacturer's protocol (Qiagen, Hilden, Germany, cat # 79256). Total RNA samples were sent to BGI Group, Beijing, China, for library preparation and sequencing. Reads (single-end 50bp at a sequencing depth of 20 million reads per sample) were generated by BGISEQ-500. Primary data will be available from gene expression omnibus under accession number GSE165647.

4.5.11 RNA-seq analysis

Kallisto (https://pachterlab.github.io/kallisto/) was used to align to the reference transcriptome (ftp://ftp.ensembl.org/pub/current_fasta/mus_musculus/cdna/) and estimate transcript abundance. GenePattern (https://www.genepattern.org/use-genepattern), Gene Set Enrichment Analysis (GSEA) (57), and differential expression analysis (DESeq2) (using R (https://www.r-project.org/)) were used to analyze the RNA-seq data for differentially expressed genes and to find suppressed or enriched gene sets across samples.

4.5.12 Protein expression and purification

His-tagged mouse CRY2 D325H PHR domain (residues 1-512) was expressed in Sf9 suspension insect cells (Expression Systems, Davis, CA) infected with a P3 baculovirus at 1.2 X 106 cells per milliliter and grown for 72 hours at 27°C with gentle shaking. Cells were centrifuged at 4°C for 4000 x rpm for 15 minutes and resuspended in 50 mM Tris buffer pH 7.5, 300 mM NaCl, 20 mM imidazole, 10% (vol/vol) glycerol, 0.1% (vol/vol) Triton X-100, 5 mM β-mercaptoethanol and EDTA-free protease inhibitors (Pierce, Waltham, Massachusetts,). Cells were lysed using a microfluidizer followed by sonication with a ¼" probe on ice for 15 seconds on, 45 seconds off for three pulses at 40% amplitude and lysate was clarified at 4°C for 19,000 rpm for 45 minutes. CRY2 protein was isolated by Ni2+-nitrilotriacetic acid (Ni-NTA) affinity chromatography (Qiagen, Hilden, Germany) following elution with 50 mM Tris buffer pH 7.5, 300 mM NaCl, 250 mM imidazole, 10% (vol/vol) glycerol, and 5 mM β-mercaptoethanol. The protein was further purified by HiTrap HP cation

exchange chromatography (GE Healthcare, Chicago, IL) and Superdex 75 gel filtration chromatography (GE Healthcare, Chicago, IL) into 20 mM HEPES buffer pH 7.5, 125 mM NaCl, 5% (vol/vol) glycerol, and 2 mM tris(2-carboxyethyl)phosphine (TCEP). The CLOCK:BMAL1 PAS domain core was purified and biotinylated as reported in (10) (22).

4.5.13 Bio-layer interferometry (BLI)

BLI experiments were performed using an 8-channel Octect-RED96e (ForteBio, Fremont, CA) with a BLI assay buffer of 20 mM HEPES buffer pH 7.5, 125 mM NaCl, 5% (vol/vol) glycerol and 2 mM TCEP. All experiments began with a reference measurement to establish a baseline in BLI assay buffer for 120 seconds. Next, 1.5 µg/mL biotinylated CLOCK:BMAL1 PAS-AB was loaded on streptavidin tips for 300 seconds at room temperature. Subsequently, a 360 second blocking step was performed with 0.5 mg/mL BSA, 0.02% (vol/vol) Tween, 20 mM HEPES buffer pH 7.5, 125 mM NaCl, 5% (vol/vol) glycerol and 2 mM TCEP. Association was measured for 300 seconds with 7 concentrations in a serial dilution of the CRY2 mutant in blocking buffer, and then dissociation was measured for 300 seconds in blocking buffer. Each experiment was repeated with tips that were not loaded with CLOCK:BMAL PAS-AB to provide a reference for non-specific binding to the tip and two independent replicates of the BLI experiment were done. Before fitting, all datasets were reference-subtracted, aligned on the y-axis and for interstep correction through their respective dissociation steps according to the manufacturer's instructions (ForteBio, Fremont, CA). Data were processed in steady state mode to extract concentration-dependent changes of CRY2 binding to CLOCK:BMAL1 and fit to a one-site binding model using Prism 8.0 (GraphPad, San Diego, CA).

4.6 Supplementary Tables

Mutation in hCRY2	Cancer Type(s)	Suppress 2D colonies in *Cry2*$^{-/-}$ + MYC	Interaction with FBXL3/21	Interaction with CLOCK in the presence of BMAL1	CLOCK/ BMAL1 repressor	Rhythmicity rescue assay
D347H	Bladder	**No**	+++	-	-	-
S436R S436N	Colorectal, Breast	Yes	+	++	+++	-/Long τ
R460C R460H	Colorectal, Stomach	Yes	+	++	+++	Long τ
D467N D467V	Colorectal, Bladder	Yes	+++	+++	+++	-
S532L	Stomach, Melanoma, Head and neck	**No**	+	+++	+++	Long τ

Supplementary Table 4.1.

Table summarizing data from this paper. The first column shows point mutants that we studied in detail in black font and other mutations observed at the same location in grey font. For columns four and five, the number of +'s indicates strength of interaction and - indicates no detectable interaction as determined by coIP. For column six, + indicates repressor of CLOCK/BMAL1 in a dose dependent manner in a luciferase assay, - indicates no repression of CLOCK/BMAL1. For column seven, - indicates arrhythmic; ***τ,*** period.

4.7 Supplementary Figures

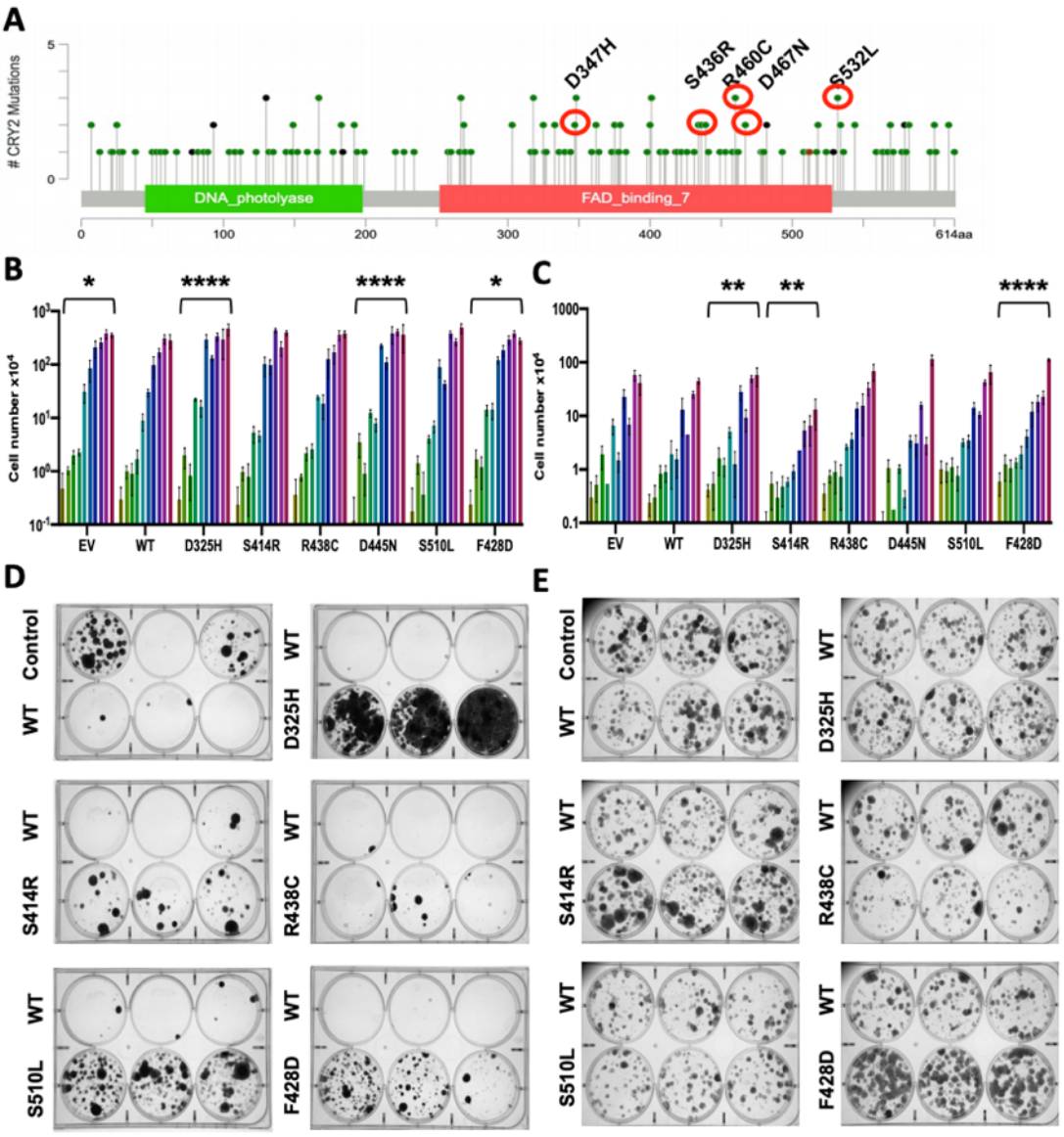

Supplementary Figure 4.1.

(A) Lollipop diagram from cbioPortal (last accessed November 13, 2020) indicating location and frequency of mutations in CRY2 in tumor samples included in The Cancer Genome Atlas (TCGA). The missense mutations we chose to study in this paper are circled in red. ***(B,C)*** Proliferation data expressed as cell number x104 across ten days starting at day two for *Cry2*$^{-/-}$ MEFs stably expressing c-MYC (B) or shRNA targeting P53 (C) with additional stable expression of empty vector (EV, control), or wildtype or mutant CRY2 as indicated. Data represent mean ± SEM for two independent experiments (adjacent bars) with three technical triplicates each. *p≤0.05, **p≤0.01, ****p≤0.0001 by two-way ANOVA with Tukey's multiple comparison test. ***(D,E)*** Examples of raw images from one of four biological replicates in Figures 1B and 1C, respectively.

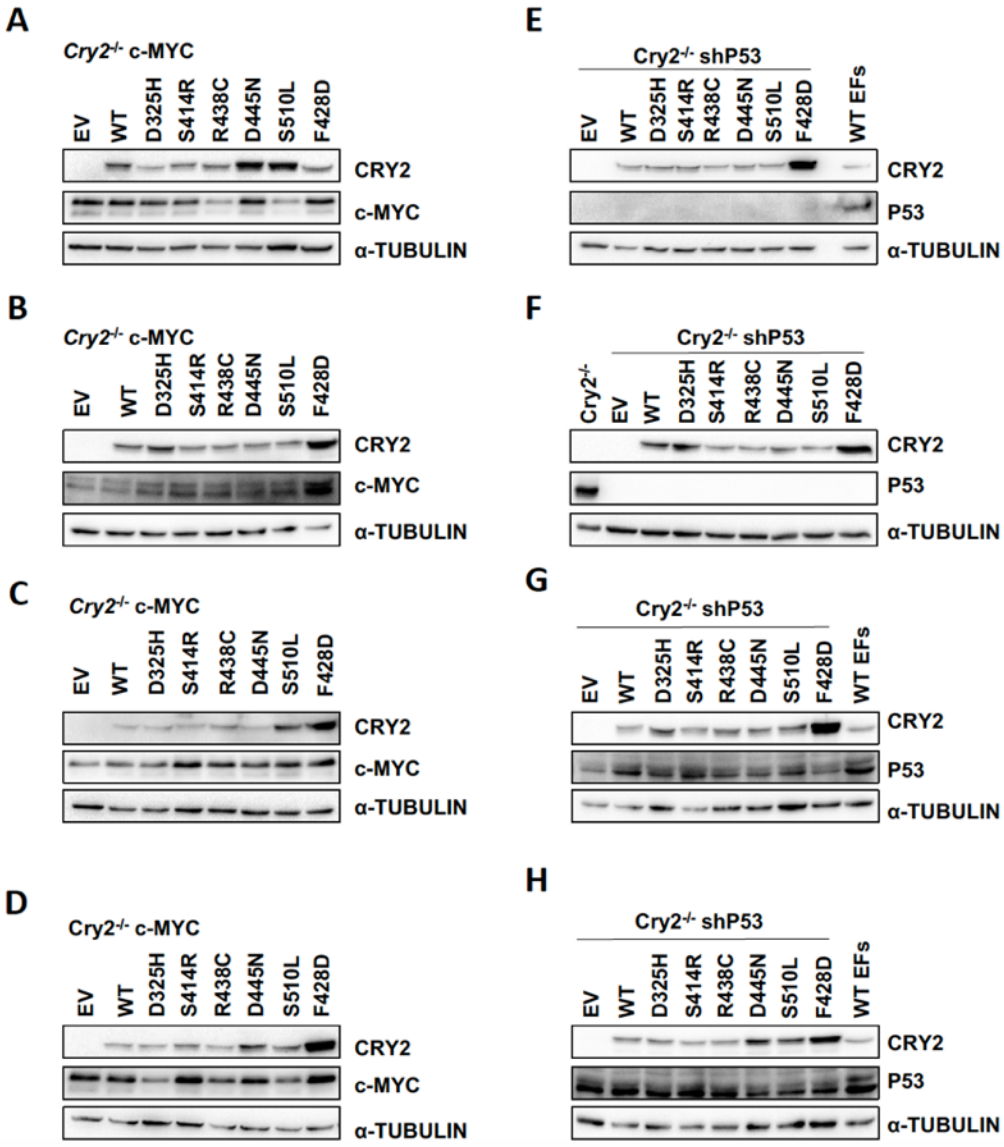

Supplementary Figure 4.2

(A-D, E-H) Lysates from cells plated in parallel used in Figure 1B and C, respectively. Proteins detected by immunoblot (IB) for the indicated proteins from *Cry2*$^{-/-}$ cells overexpressing the CRY2 missense mutations and c-MYC or shRNA targeting P53, respectively. EV, empty vector, control. WT EFs, Wildtype ear fibroblasts, control. Note: In (E,F) and (G,H) the antibodies used to detect P53 were Leica anti-P53 CM5 and Santa Cruz anti-P53, DO-1, respectively.

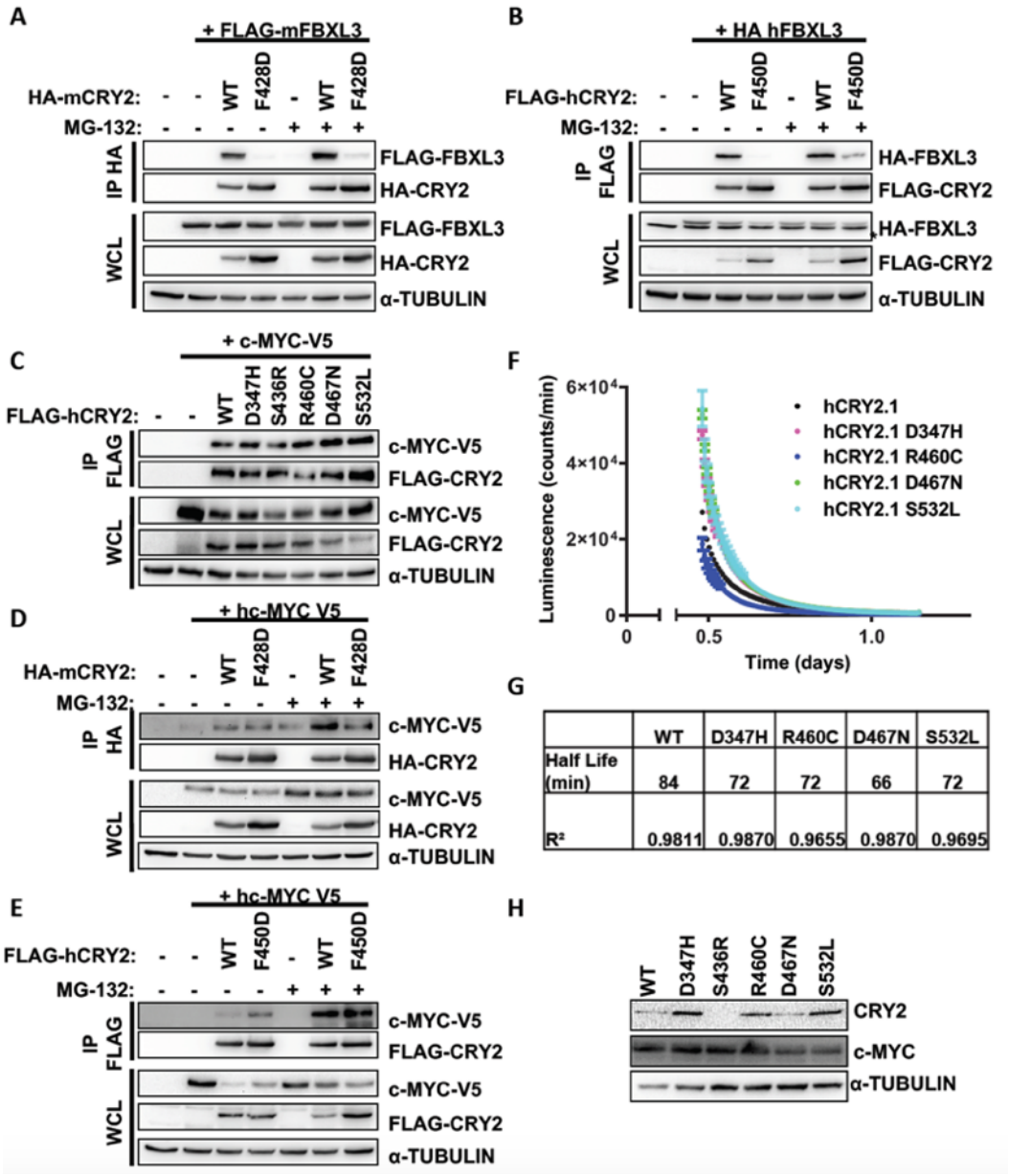

	WT	D347H	R460C	D467N	S532L
Half Life (min)	84	72	72	66	72
R^2	0.9811	0.9870	0.9655	0.9870	0.9695

Supplementary Figure 4.3

(A,B) Proteins detected by immunoblot (IB) following immunoprecipitation (IP) of HA (A) or FLAG (B) epitope tags from whole cell lysates (WCL) of HEK293T cells expressing the indicated plasmids. Samples were treated with vehicle (-, DMSO) or 10μM MG-132 (+) for four hours. ***(C-E)*** Proteins detected by immunoblot (IB) following IP of FLAG (C,E) or HA (D) or in whole cell lysates (WCL) from HEK293T cells expressing the indicated plasmids with the indicated tags. For (D,E) samples were treated with vehicle (DMSO) or 10μM MG-132 (+) for four hours. ***(F)*** Raw luminescence curves from one of three independent experiments in Figure 2C represented as mean ± SEM. ***(G)*** Half-lives (minutes) and R2 values are indicated from one-phase exponential curve fitting of data in (A) using Graph Pad Prism 9. ***(H)*** Western blots of lysates from cells in (F) blotted for the indicated proteins.

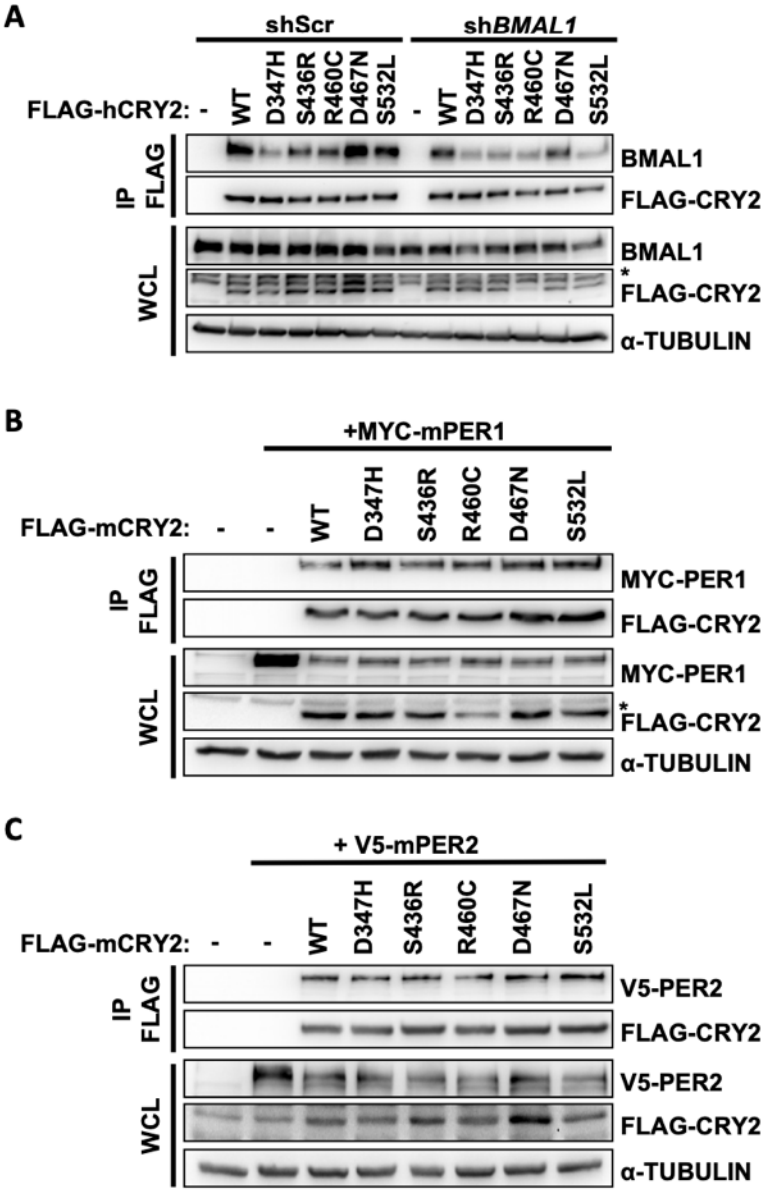

Supplementary Figure 4.4

(A-C) Proteins detected by immunoblot (IB) following IP of the FLAG tag or in whole cell lysates (WCL) from HEK293T cells expressing the indicated plasmids. In (A) cells were treated with either knockdown using a control “scrambled” shRNA (shScr) or shRNA targeting Bmal1 (shBMAL1). * denotes non-specific band.

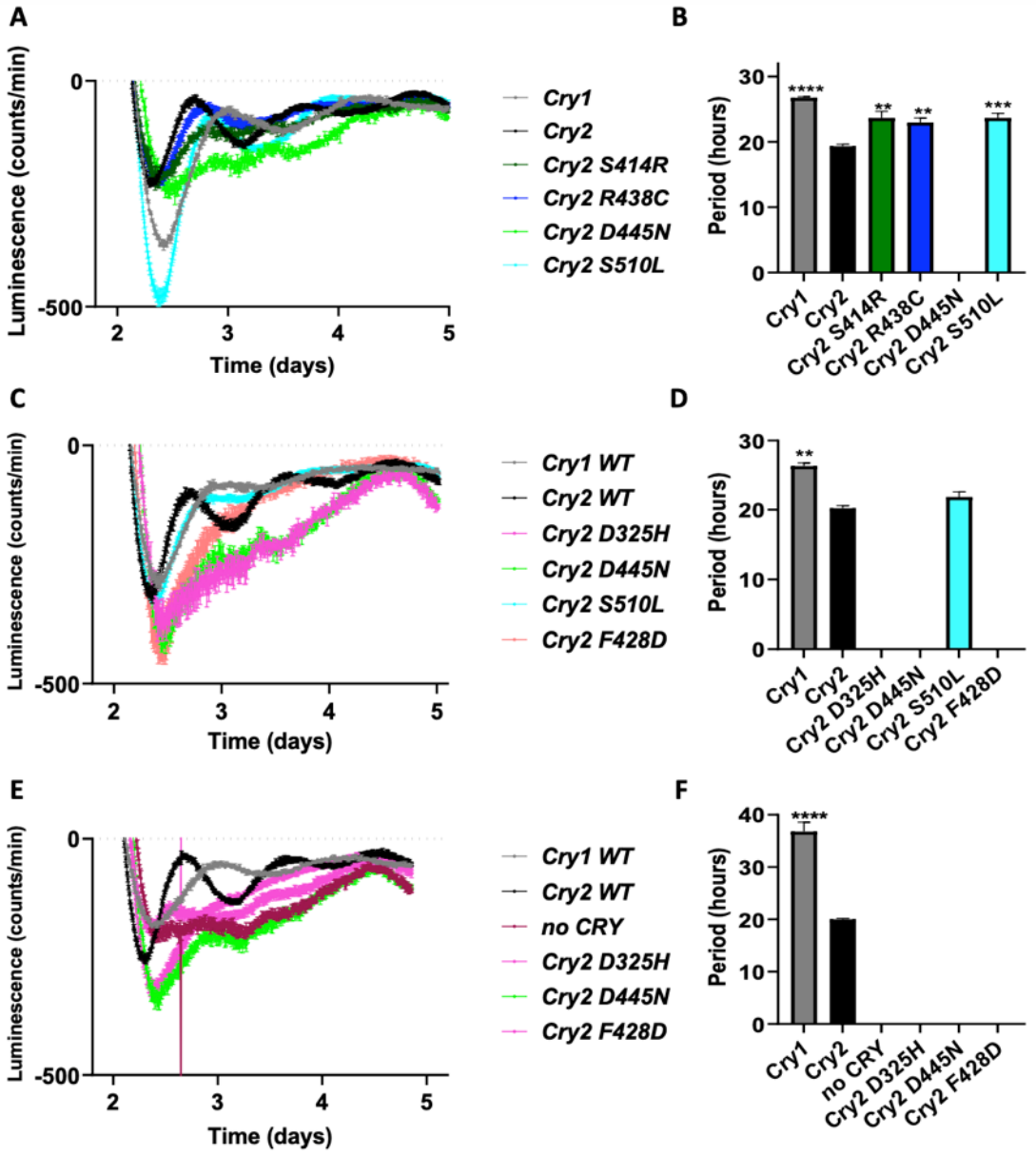

Supplementary Figure 4.5

(A-F) Raw luminescence traces and periods from Figure 4D-F grouped as they were performed together. **p≤0.01, ***p≤0.001, ****p≤0.0001 by two-way ANOVA with Tukey's multiple comparisons versus Cry2 in GraphPad Prism 9.

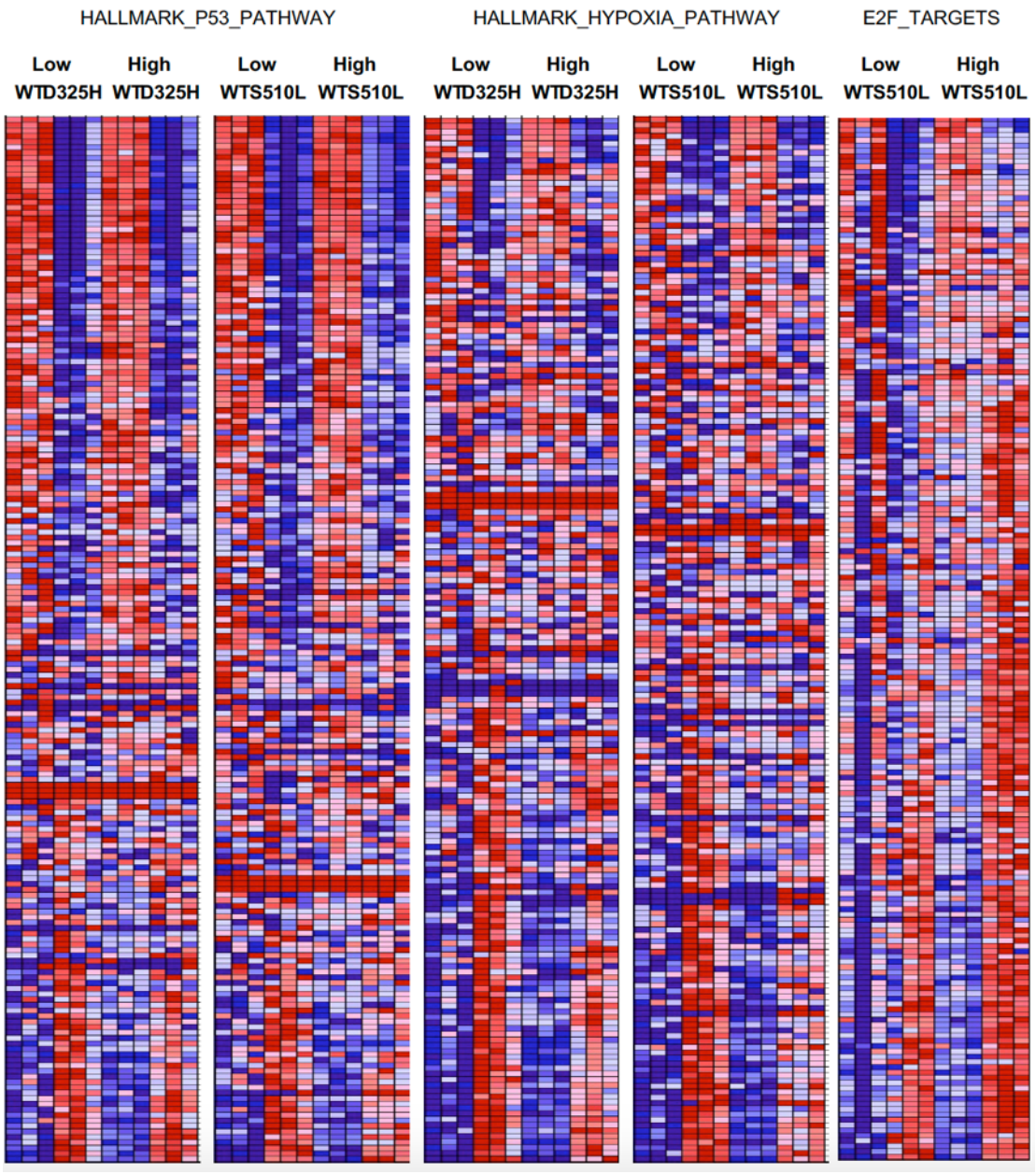

Supplementary Figure 4.6

Heatmaps from RNA-sequencing representing all transcripts included in each gene set. Red, high expression; Blue low expression.

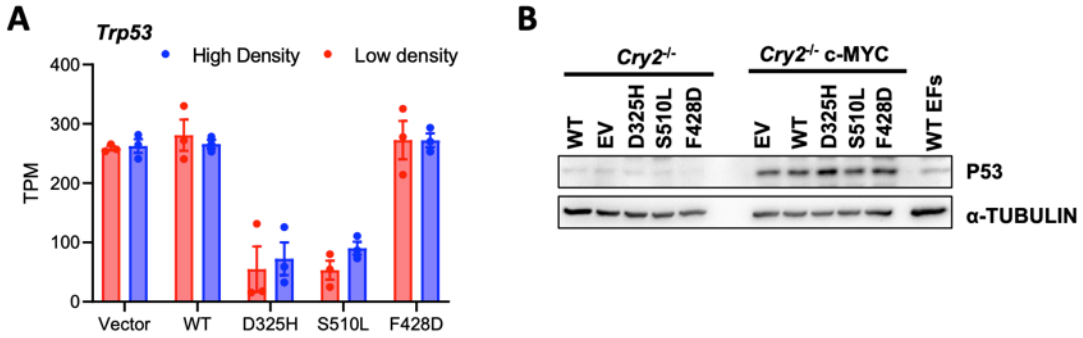

Supplementary Figure 4.7

(A) Extracted gene expression profiles of the indicated genes from the RNA-sequencing data. Light red, low density plating; light blue, high density plating. ***(B)*** Proteins detected by immunoblot (IB) for the indicated proteins from *Cry2*$^{-/-}$ cells overexpressing the CRY2 missense mutations with or without concomitant overexpression of c-MYC as indicated. WT EFs, wildtype ear fibroblasts. EV, empty vector, control.

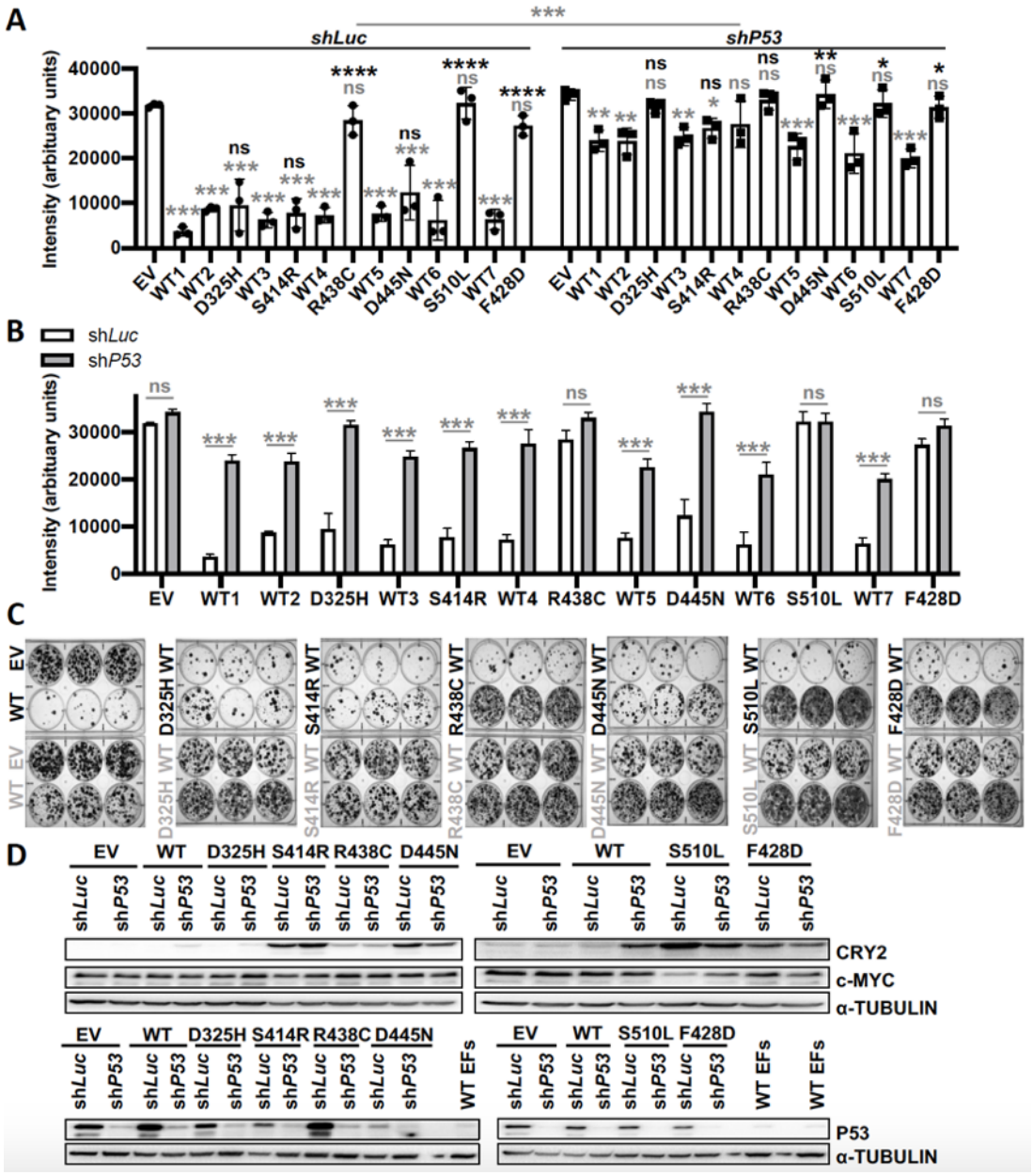

Supplementary Figure 4.8

(A,B) Quantitation of colonies formed by *Cry2*$^{-/-}$ MEFs stably expressing c-MYC and shRNA targeting Luciferase (*shLuc*) or P53 (*shP53*). Note that (A) and (B) present the same data, arranged differently. Bars represent mean ± s.e.m. for quantitation of staining from technical triplicates. In (A) *p≤0.05, **p≤0.01, ***p≤0.001 vs EV (gray font) or vs WT control (black font), or *shLuc* vs *shP53* main effect as indicated, or (B) ***p<0.001 by two-way ANOVA with Dunnett's multiple comparisons test. EV (empty vector, control). ***(C)*** Raw images of data shown in (A) *shLuc* in black; *shP53* in gray. ***(D)*** Proteins detected by immunoblot (IB) for the indicated proteins from cells in (A). WT EFs, wildtype ear fibroblasts, control.

4.8 References

1. Bass J (2012) Circadian topology of metabolism. *Nature* 491(7424):348-356.

2. Xing W*, et al.* (2013) SCF(FBXL3) ubiquitin ligase targets cryptochromes at their cofactor pocket. *Nature* 496(7443):64-68.

3. Godinho SI*, et al.* (2007) The after-hours mutant reveals a role for Fbxl3 in determining mammalian circadian period. *Science* 316(5826):897-900.

4. Busino L*, et al.* (2007) SCFFbxl3 controls the oscillation of the circadian clock by directing the degradation of cryptochrome proteins. *Science* 316(5826):900-904.

5. Siepka SM*, et al.* (2007) Circadian mutant Overtime reveals F-box protein FBXL3 regulation of cryptochrome and period gene expression. *Cell* 129(5):1011-1023.

6. Dardente H, Mendoza J, Fustin JM, Challet E, & Hazlerigg DG (2008) Implication of the F-Box Protein FBXL21 in circadian pacemaker function in mammals. *Plos One* 3(10):e3530.

7. Hirano A*, et al.* (2013) FBXL21 regulates oscillation of the circadian clock through ubiquitination and stabilization of cryptochromes. *Cell* 152(5):1106-1118.

8. Yoo SH*, et al.* (2013) Competing E3 ubiquitin ligases govern circadian periodicity by degradation of CRY in nucleus and cytoplasm. *Cell* 152(5):1091-1105.

9. Kowalska E*, et al.* (2013) NONO couples the circadian clock to the cell cycle. *Proc Natl Acad Sci U S A* 110(5):1592-1599.

10. Hunt T & Sassone-Corsi P (2007) Riding tandem: circadian clocks and the cell cycle. *Cell* 129(3):461-464.

11. Koike N*, et al.* (2012) Transcriptional architecture and chromatin landscape of the core circadian clock in mammals. *Science* 338(6105):349-354.

12. Chan AB, Huber AL, & Lamia KA (2020) Cryptochromes modulate E2F family transcription factors. *Sci Rep* 10(1):4077.

13. Kriebs A*, et al.* (2017) Circadian repressors CRY1 and CRY2 broadly interact with nuclear receptors and modulate transcriptional activity. *Proc Natl Acad Sci U S A* 114(33):8776-8781.

14. Lamia KA (2011) Cryptochromes mediate rhythmic repression of the glucocorticoid receptor. *Nat.* 480.

15. Jang H*, et al.* (2016) SREBP1c-CRY1 signalling represses hepatic glucose production by promoting FOXO1 degradation during refeeding. *Nat Commun* 7:12180.

16. Huber AL*, et al.* (2016) CRY2 and FBXL3 Cooperatively Degrade c-MYC. *Mol Cell* 64(4):774-789.

17. Jordan SD*, et al.* (2017) CRY1/2 Selectively Repress PPARdelta and Limit Exercise Capacity. *Cell Metab* 26(1):243-255 e246.

18. Partch CL & Sancar A (2005) Photochemistry and photobiology of cryptochrome blue-light photopigments: the search for a photocycle. *Photochem Photobiol* 81(6):1291-1304.

19. Chan AB & Lamia KA (2020) Cancer, hear my battle CRY. *J Pineal Res* 69(1):e12658.

20. Sancar A (2003) Structure and function of DNA photolyase and cryptochrome blue-light photoreceptors. *Chem Rev* 103(6):2203-2237.

21. Michael AK*, et al.* (2017) Formation of a repressive complex in the mammalian circadian clock is mediated by the secondary pocket of CRY1. *Proc Natl Acad Sci U S A* 114(7):1560-1565.

22. Fribourgh JL*, et al.* (2020) Dynamics at the serine loop underlie differential affinity of cryptochromes for CLOCK:BMAL1 to control circadian timing. *Elife* 9.

23. Rosensweig C*, et al.* (2018) An evolutionary hotspot defines functional differences between CRYPTOCHROMES. *Nature Communications* 9(1):1138.

24. Schmalen I*, et al.* (2014) Interaction of circadian clock proteins CRY1 and PER2 is modulated by zinc binding and disulfide bond formation. *Cell* 157(5):1203-1215.

25. Nangle SN*, et al.* (2014) Molecular Assembly of the Period-Cryptochrome Circadian Transcriptional Repressor Complex. *Elife* 3.

26. Xu H*, et al.* (2015) Cryptochrome 1 regulates the circadian clock through dynamic interactions with the BMAL1 C terminus. *Nat Struct Mol Biol* 22(6):476-484.

27. Harada Y, Sakai M, Kurabayashi N, Hirota T, & Fukada Y (2005) Ser-557-phosphorylated mCRY2 is degraded upon synergistic phosphorylation by glycogen synthase kinase-3 beta. *J Biol Chem* 280(36):31714-31721.

28. Kurabayashi N, Hirota T, Sakai M, Sanada K, & Fukada Y (2010) DYRK1A and glycogen synthase kinase 3beta, a dual-kinase mechanism directing proteasomal degradation of CRY2 for circadian timekeeping. *Mol Cell Biol* 30(7):1757-1768.

29. Gao P*, et al.* (2013) Phosphorylation of the cryptochrome 1 C-terminal tail regulates circadian period length. *J Biol Chem* 288(49):35277-35286.

30. Papp SJ*, et al.* (2015) DNA damage shifts circadian clock time via Hausp-dependent Cry1 stabilization. *Elife* 4.

31. Parico GCG*, et al.* (2020) The human CRY1 tail controls circadian timing by regulating its association with CLOCK:BMAL1. *Proc Natl Acad Sci U S A* 117(45):27971-27979.

32. Matsuo T*, et al.* (2003) Control mechanism of the circadian clock for timing of cell division in vivo. *Science* 302(5643):255-259.

33. Geyfman M*, et al.* (2012) Brain and muscle Arnt-like protein-1 (BMAL1) controls circadian cell proliferation and susceptibility to UVB-induced DNA damage in the epidermis. *Proc Natl Acad Sci U S A* 109(29):11758-11763.

34. Hong CI*, et al.* (2014) Circadian rhythms synchronize mitosis in Neurospora crassa. *Proc Natl Acad Sci U S A* 111(4):1397-1402.

35. Bieler J*, et al.* (2014) Robust synchronization of coupled circadian and cell cycle oscillators in single mammalian cells. *Mol Syst Biol* 10:739.

36. Pariollaud M & Lamia KA (2020) Cancer in the Fourth Dimension: What Is the Impact of Circadian Disruption? *Cancer Discov*.

37. Ozturk N, Lee JH, Gaddameedhi S, & Sancar A (2009) Loss of cryptochrome reduces cancer risk in p53 mutant mice. *Proc Natl Acad Sci U S A* 106(8):2841-2846.

38. Kettner NM*, et al.* (2016) Circadian Homeostasis of Liver Metabolism Suppresses Hepatocarcinogenesis. *Cancer Cell* 30(6):909-924.

39. Lee S, Donehower LA, Herron AJ, Moore DD, & Fu L (2010) Disrupting circadian homeostasis of sympathetic signaling promotes tumor development in mice. *Plos One* 5(6):e10995.

40. Mteyrek A*, et al.* (2017) Critical cholangiocarcinogenesis control by cryptochrome clock genes. *Int J Cancer* 140(11):2473-2483.

41. Fu L, Pelicano H, Liu J, Huang P, & Lee C (2002) The circadian gene Period2 plays an important role in tumor suppression and DNA damage response in vivo. *Cell* 111(1):41-50.

42. Gu X*, et al.* (2012) The circadian mutation PER2(S662G) is linked to cell cycle progression and tumorigenesis. *Cell Death Differ* 19(3):397-405.

43. Hwang-Verslues WW*, et al.* (2013) Loss of corepressor PER2 under hypoxia up-regulates OCT1-mediated EMT gene expression and enhances tumor malignancy. *Proc Natl Acad Sci U S A* 110(30):12331-12336.

44. Mteyrek A, Filipski E, Guettier C, Okyar A, & Levi F (2016) Clock gene Per2 as a controller of liver carcinogenesis. *Oncotarget* 7(52):85832-85847.

45. Sun CM*, et al.* (2010) Per2 inhibits k562 leukemia cell growth in vitro and in vivo through cell cycle arrest and apoptosis induction. *Pathol Oncol Res* 16(3):403-411.

46. Antoch MP, Toshkov I, Kuropatwinski KK, & Jackson M (2013) Deficiency in PER proteins has no effect on the rate of spontaneous and radiation-induced carcinogenesis. *Cell Cycle* 12(23):3673-3680.

47. Hoffman AE*, et al.* (2010) Phenotypic effects of the circadian gene Cryptochrome 2 on cancer-related pathways. *BMC Cancer* 10:110.

48. Gao J*, et al.* (2013) Integrative analysis of complex cancer genomics and clinical profiles using the cBioPortal. *Sci Signal* 6(269):pl1.

49. Cerami E*, et al.* (2012) The cBio cancer genomics portal: an open platform for exploring multidimensional cancer genomics data. *Cancer Discov* 2(5):401-404.

50. Hanahan D & Weinberg RA (2011) Hallmarks of cancer: the next generation. *Cell* 144(5):646-674.

51. Kaczmarek L, Hyland JK, Watt R, Rosenberg M, & Baserga R (1985) Microinjected c-myc as a competence factor. *Science* 228(4705):1313-1315.

52. Gustafson CL & Partch CL (2015) Emerging models for the molecular basis of mammalian circadian timing. *Biochemistry* 54(2):134-149.

53. Ye R*, et al.* (2014) Dual modes of CLOCK:BMAL1 inhibition mediated by Cryptochrome and Period proteins in the mammalian circadian clock. *Genes Dev* 28(18):1989-1998.

54. McCarthy EV, Baggs JE, Geskes JM, Hogenesch JB, & Green CB (2009) Generation of a novel allelic series of cryptochrome mutants via mutagenesis reveals residues involved in protein-protein interaction and CRY2-specific repression. *Mol Cell Biol* 29(20):5465-5476.

55. Ukai-Tadenuma M*, et al.* (2011) Delay in feedback repression by cryptochrome 1 is required for circadian clock function. *Cell* 144(2):268-281.

56. van der Horst GT*, et al.* (1999) Mammalian Cry1 and Cry2 are essential for maintenance of circadian rhythms. *Nature* 398(6728):627-630.

57. Subramanian A, Kuehn H, Gould J, Tamayo P, & Mesirov JP (2007) GSEA-P: a desktop application for Gene Set Enrichment Analysis. *Bioinformatics* 23(23):3251-3253.

58. Liberzon A*, et al.* (2015) The Molecular Signatures Database (MSigDB) hallmark gene set collection. *Cell Syst* 1(6):417-425.

59. Deffie A, Wu H, Reinke V, & Lozano G (1993) The tumor suppressor p53 regulates its own transcription. *Mol Cell Biol* 13(6):3415-3423.

60. Karczewski KJ*, et al.* (2019) Variation across 141,456 human exomes and genomes reveals the spectrum of loss-offunction intolerance across human protein-coding genes. *bioRxiv*.

61. Ye Y*, et al.* (2018) The Genomic Landscape and Pharmacogenomic Interactions of Clock Genes in Cancer Chronotherapy. *Cell Syst* 6(3):314-328 e312.

62. Correia SP*, et al.* (2019) The circadian E3 ligase complex SCF(FBXL3+CRY) targets TLK2. *Sci Rep* 9(1):198.

63. Aryal RP*, et al.* (2017) Macromolecular Assemblies of the Mammalian Circadian Clock. *Mol Cell* 67(5):770-782 e776.

64. Gotoh T*, et al.* (2016) Model-driven experimental approach reveals the complex regulatory distribution of p53 by the circadian factor Period 2. *Proc Natl Acad Sci U S A* 113(47):13516-13521.

65. Gotoh T, Vila-Caballer M, Liu J, Schiffhauer S, & Finkielstein CV (2015) Association of the circadian factor Period 2 to p53 influences p53's function in DNA-damage signaling. *Mol Biol Cell* 26(2):359-372.

66. Gotoh T*, et al.* (2014) The circadian factor Period 2 modulates p53 stability and transcriptional activity in unstressed cells. *Mol Biol Cell* 25(19):3081-3093.

67. Choudhry H & Harris AL (2018) Advances in Hypoxia-Inducible Factor Biology. *Cell Metab* 27(2):281-298.

68. Semenza GL (2017) Hypoxia-inducible factors: coupling glucose metabolism and redox regulation with induction of the breast cancer stem cell phenotype. *EMBO J* 36(3):252-259.

69. Semenza GL (2013) HIF-1 mediates metabolic responses to intratumoral hypoxia and oncogenic mutations. *J Clin Invest* 123(9):3664-3671.

70. Vaughan ME, et al. (2020) Cryptochromes suppress HIF1a in muscles. *iScience*.

71. Dimova EY*, et al.* (2019) The Circadian Clock Protein CRY1 Is a Negative Regulator of HIF-1alpha. *iScience* 13:284-304.

72. Fribourgh JL & Partch CL (2017) Assembly and function of bHLH-PAS complexes. *Proc Natl Acad Sci U S A* 114(21):5330-5332.

73. Wu Y*, et al.* (2017) Reciprocal Regulation between the Circadian Clock and Hypoxia Signaling at the Genome Level in Mammals. *Cell Metab* 25(1):73-85.

74. Hogenesch JB, Gu YZ, Jain S, & Bradfield CA (1998) The basic-helix-loop-helix-PAS orphan MOP3 forms transcriptionally active complexes with circadian and hypoxia factors. *Proc Natl Acad Sci U S A* 95(10):5474-5479.

75. Attwooll C, Lazzerini Denchi E, & Helin K (2004) The E2F family: specific functions and overlapping interests. *EMBO J* 23(24):4709-4716.

76. Dong Z*, et al.* (2019) Targeting Glioblastoma Stem Cells through Disruption of the Circadian Clock. *Cancer Discov* 9(11):1556-1573.

77. Hirota T*, et al.* (2012) Identification of small molecule activators of cryptochrome. *Science (New York, N.Y.)* 337(6098):1094-1097.

78. Lee JW*, et al.* (2015) Development of Small-Molecule Cryptochrome Stabilizer Derivatives as Modulators of the Circadian Clock. *ChemMedChem* 10(9):1489-1497.

79. Miller S*, et al.* (2020) Isoform-selective regulation of mammalian cryptochromes. *Nature Chemical Biology* 16(6):676-+.

80. Oshima T*, et al.* (2015) C-H activation generates period-shortening molecules that target cryptochrome in the mammalian circadian clock. *Angew Chem Int Ed Engl* 54(24):7193-7197.

81. Thresher RJ*, et al.* (1998) Role of mouse cryptochrome blue-light photoreceptor in circadian photoresponses. *Science* 282(5393):1490-1494.

82. Lamia KA*, et al.* (2011) Cryptochromes mediate rhythmic repression of the glucocorticoid receptor. *Nature* 480(7378):552-556.

CHAPTER 5: CRY stabilizing molecules enhance the interaction between the PHR domain and the C-terminal tail of CRYs.

The candidate, Gian Carlo Parico, wrote this chapter and performed all experiments described herein. These data are unpublished as of this writing.

Acknowledgements:

We thank Tsuyoshi Hirota (University of Tokyo, Tokyo, Japan and the RIKEN Quantitative Biology Center, Osaka, Japan) for helping us conceptualize the research and gifting us with the small molecules used for this work. We thank Jennifer Fribourgh, Efrain Ceh Pavia, and Megan Torgrimson for generating critical reagents. We thank the Chemical Screening Center (University of California, Santa Cruz) and the Macromolecular Structure Function Core Facility (University of California, Santa Cruz) for access to instrumentation.

5.1 Abstract

Circadian rhythms are generated by a set of interlocked transcription-translation feedback loops that establish cell-autonomous biological timing of ~24-hours. The negative arm of the core feedback loop is mediated in part by two cryptochrome proteins, CRY1 and CRY2, that interact directly with the core circadian transcription factor CLOCK:BMAL1. Both CRY paralogs possess a conserved photolyase homology region (PHR) and intrinsically disordered C-terminal tails that are completely divergent. Previous studies have established that both the PHR and their respective C-terminal tails play a role in determining circadian timing, although the mechanism by which the disordered tails contribute to clock regulation was previously unknown. We recently showed that the tails of both CRY1 and CRY2 interact with their respective PHRs. Here, we will share current findings on how tail-binding sites on the PHR are influenced by isoform-selective ligands KL101 and TH301. The effect of the isoform-selective ligands on PHR-tail interactions suggest that the FAD-binding pocket of CRY is a conserved binding site for interacting with the C-terminal tail.

5.2 Introduction

Cryptochrome 1 and 2 (CRY1 and CRY2) are core components of the circadian clock. Both proteins repress the transcription factor CLOCK:BMAL1 to close a 24 hour feedback loop (1). While both CRYs play a similar role in repression, CRY1 and CRY2 play different roles in regulating circadian rhythms. Disrupting either *Cry1* or *Cry2* can lead to divergent effects on circadian period in mice; a *Cry1* knockout shortens circadian period, whereas a *Cry2* knockout lengthens it (2, 3). The two CRY orthologs also play different roles in physiological processes beyond circadian rhythms. DNA damage promotes stabilization of CRY1 while also promoting the degradation of CRY2, suggesting that both CRY orthologs play opposing roles in the DNA damage response pathway (4).

CRY proteins are composed of a photolyase homology region (PHR) that is tethered to an intrinsically disordered C-terminal tail. While the PHR domain is highly conserved between CRY1 and CRY2 (both share 80% identity), the tails of both CRYs are highly divergent.

However, both CRY tails share conserved functions as both bind to their respective PHR domains (5, 6). The CRY1 PHR-tail interaction is autoinhibitory and inhibits the CRY1 PHR from binding to CLOCK, but it is not clear what role the CRY2 PHR-tail interaction plays in regulating the interaction with CLOCK:BMAL1 (5). Modifications of the C-terminal tails in both CRY orthologs regulate CRY stability (7-12). The CRY1 tail stabilizes the protein by antagonizing the activity of E3 ubiquitin ligases such as Skp1-Cullin-Fbox^{FBXL3} (SCF^{FBXL3}) which stimulate proteasomal degradation of CRYs (4, 12).

Disrupting the interaction between CRY and SCF^{FBXL3} lengthens the half-life of CRYs in the cell and can extend circadian period. Molecules such as KL001 stabilize both CRY orthologs by binding to the FAD-binding pocket on the CRY PHR and inhibiting the binding of the F-box protein FBXL3, the substrate recognition unit of the SCF^{FBXL3} complex (13, 14). In contrast to KL001, the phenylpyrazole derivatives KL101 and TH301 selectively stabilize either CRY1 or CRY2: KL101 is specific to CRY1, while TH301 is moderately selective for CRY2 (i.e. more potent in stabilizing CRY2 than in stabilizing CRY1) (15). A gatekeeper tryptophan residue (W399 in CRY1 and W417 in CRY2) and its interaction with the lid loop adjacent to the FAD-binding pocket contributes to CRY1 preferentially binding to KL101 and CRY2 preferentially binding to TH301 (Supplementary Figure 2.1) (16). While both KL101 and TH301 bind to the FAD-binding pocket on the CRY PHR and stabilize CRY against thermal denaturation, removal of the C-terminal tail abolishes protection against thermal denaturation of CRY in cells (15). The selectivity of both compounds also depends on the CRY C-terminal tail such that the exon 10 region of the CRY1 tail imparts specificity for KL101, while the exon 10 of the CRY2 tail imparts selectivity for TH301 (15).

Here, we study the effect of compounds KL101 and TH301 on interactions between the CRY PHR and the CRY tail. We find that both KL101 and TH301 enhanced the affinity between the CRY PHR and CRY tail in *trans*. Unexpectedly, we found that KL101 enhances the CRY2 PHR–tail interaction despite being CRY1-selective, and that TH301 is more potent in enhancing the CRY PHR-tail interaction for both CRY orthologs, despite CRY1 being more

selective for KL101. We also determined that the exon 10 region of the CRY1 tail is necessary for either KL101 and TH301 to enhance binding between the CRY1 tail and the CRY1 PHR. These results suggest new mechanisms for how KL101 and TH301 stabilize CRY proteins and antagonize SCF^{FBXL3} function through the recruitment of the CRY C-terminal tail to the PHR.

5.3 Results

5.3.1 KL101 and TH301 enhance the CRY PHR-tail interaction.

Since the CRY selective ligands bind directly to the PHR domain but still require the C-terminal tail for activity, we wanted to determine if the ligands modulate the interaction between the PHR and the tail. We used previously established fluorescence polarization (FP) assays (5) using fluorescently labeled CRY tails and their respective PHRs saturated with their respective isoform-selective ligand (KL101 for CRY1 PHR and TH301 for CRY2 PHR). Since KL101 and TH301 were reconstituted in DMSO, we established that a 1% vol/vol DMSO weakened the interaction between the PHR and tail for both CRY1 and CRY2 (Figure 5.1) Relative to the DMSO control, we found that the CRY1-specific ligand KL101 enhanced the binding affinity between the CRY1 PHR and CRY1 tail almost 3-fold: the K_D of the CRY1 PHR-tail interaction changes from 23.2 ± 3.5 μM (with 1% vol/vol DMSO) down to 7.2 ± 1.2 μM when 1 mM KL101 is added (Figure 5.1A). Likewise, we found that the moderately CRY2-selective ligand TH301 also enhanced the binding affinity between the CRY2 PHR and the CRY2 tail, modifying the CRY2 PHR-tail affinity from 18.6 ± 6.4 μM (with 1% vol/vol DMSO) down to 7.2 ± 1.7 μM in the presence of 1 mM TH301 (Figure 5.1B).

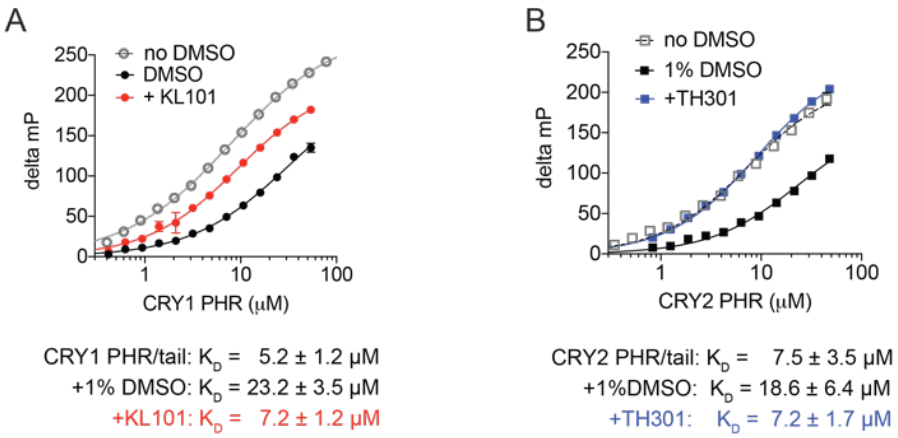

Figure 5.1. CRY selective ligands enhance binding between the PHR and tail.

(A-B) FP binding curves of fluorescently labeled CRY1 tail binding to the CRY1 PHR (A) and CRY2 tail binding to the CRY2 PHR (B). Plot shows the mean representative binding curves of duplicate samples ± sd (of n = 3 independent assays). Curve represents fit to one-site binding (Prism).

Since KL101 and TH301 bind directly to the FAD-pocket in the PHR for both CRY isoforms (15), this suggests that the KL101 and TH301 compounds could act as a small-molecule protein ligand interface stabilizer (SPLINT) or “molecular glue” between the CRY PHR and CRY tail (17, 18). Molecular glues are small molecules that bind to a protein interface and enhance interactions with other proteins at that interface (17, 18). Examples of molecular glues include the plant hormone auxin, which enhances interactions between an F-box protein TIR1 and degron sequences thus promoting degradation of TIR1 substrates (17), and also the drug rapamycin, which recruits FKBP12 near the active site of the protein kinase mTOR thus inhibiting kinase activity of mTOR (19). Since molecular glues bind directly to the protein interfaces they enhance, they could act as both agonist and antagonist. For instance, thalidomide derivatives lenalidomide and pomalidomide bind to the ubiquitin ligase substrate receptor CRBN and directly inhibits the interaction with the endogenous substrate MEIS2, but can also create a novel binding interface between CRBN and IKAROS transcription factor (20). By this logic, it might be possible that KL101 is CRY1-specific because it inhibits the

CRY2 PHR–tail interaction but still enhances the CRY1 PHR-tail interaction as a molecular glue.

Rather than acting as a molecular glue, KL101 and TH301 may also remodel the FAD-binding pocket on the CRY PHR in an isoform-specific manner and these conformational changes on the PHR may enhance the binding affinity for the C-terminal tail. For instance, the CRY1 gatekeeper residue W399 normally exhibits an “out” position (sidechain oriented away from the FAD-binding pocket) when in the apo-state, but W399 is in an “in” position (sidechain oriented towards the FAD-binding pocket) when TH301 is bound (15) (Supplementary Figure 5.1). However, TH301 is the CRY2-selective ligand, and it remains to be seen if this TH301 can also enhance the CRY1 PHR–tail interaction.

5.3.2 Both KL101 and TH301 enhance the CRY PHR–tail interaction in both CRY isoforms

To determine if the compounds enhance the CRY PHR-tail interaction in an isoform-specific manner, we repeated the ligand titration with CRY1 and CRY2 using both ligands and KL001. We titrated the compounds into a mixture containing a fixed concentration of CRY PHR and fluorescently labeled CRY tail. Both KL101 and TH301 caused a dose-dependent increase in fluorescence polarization that approached saturation (Figure 5.2) Even though KL101 is CRY1-specific for enhancing stability, KL101 is not isoform specific when enhancing the PHR-tail interaction in *trans* and can also enhance the CRY2 PHR–tail interaction. However, the CRY2-selective ligand TH301 is still more potent than KL101 in enhancing the PHR–tail interaction in CRY2 (Figure 5.2B) with a >5-fold difference in EC_{50} (TH301 has an EC_{50} = 0.63 ± 0.06 μM and KL101 has an EC_{50} = 3.3 ± 0.1 μM). Surprisingly, TH301 is also more potent than KL101 in enhancing the PHR–tail interaction for CRY1 (TH301 has an EC_{50} = 1.5 ± 0.03 μM and KL101 has an EC_{50} = 7.7 ± 2.0 μM) suggesting that both the CRY1 and CRY2 tails favor binding to moieties on TH301 or that the tails favor binding the PHR when the gatekeeper residue is in the “in” position (Figure 5.2).

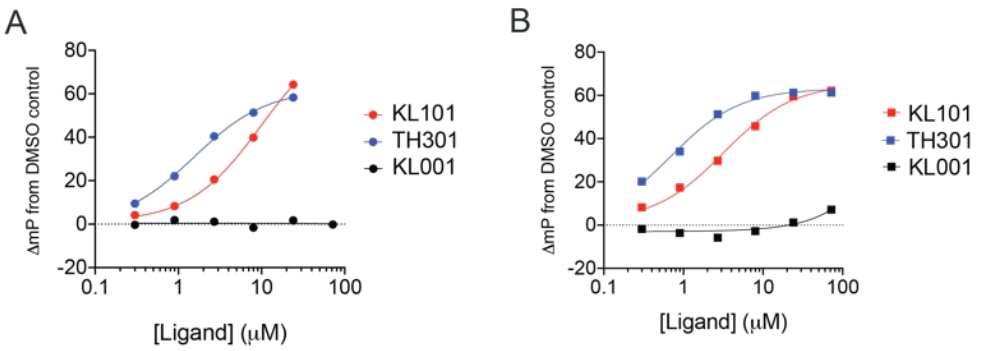

Figure 5.2. TH301 is more potent than KL101 for both CRY orthologs in enhancing interactions with the PHR

(A-B) Ligand titration of KL101 (red, circle for CRY1, square for CRY2), TH301 (blue, circle for CRY1, square for CRY2), and KL001 (black, circle for CRY1, square for CRY2) into a mixture of 5 μM CRY1 PHR and 20 nM FAM-CRY1 tail (A); a mixture of 3 μM CRY2 PHR and 20 nM CRY2 tail (B). Plot shows the mean representative titration response curves of duplicate samples ± sd (of n = 3 independent assays). Curve represents fit to response versus agonist model (Prism). For the CRY1 PHR-tail interaction, TH301 has an EC_{50} = 1.5 ± 0.03 μM and KL101 has an EC_{50} = 7.7 ± 2.0 μM, while for the CRY2 PHR-tail interaction, TH301 has an EC_{50} = 0.63 ± 0.06 μM and KL101 has an EC_{50} = 3.3 ± 0.1 μM.

While comparison of EC_{50} values suggests that TH301 is more selective for CRY2 (TH301 has an EC_{50} = 1.5 ± 0.03 μM with CRY1 and an EC_{50} = 0.63 ± 0.06 μM with CRY2), it should be noted that EC50 is an operational parameter that depends on the concentrations of CRY1 or CRY2 used and on the PHR-tail affinity for each CRY isoform. The CRY1 PHR–tail experiment used 5 μM CRY1 PHR, while the CRY2 PHR–tail experiment used 7 μM CRY2 PHR. Additionally, both isoforms exhibited slightly different PHR–tail affinities in 1% vol/vol DMSO (CRY1 PHR–tail K_D = 23.2 ± 3.5 μM; CRY2 PHR tail K_D = 18.6 ± 6.4 μM), thus making comparison of EC_{50} difficult.

KL001, another ligand that binds to the FAD-binding pocket, did not affect the CRY PHR-tail interaction for both isoforms (Figure 5.2). Even though KL001 also binds to the FAD-binding pocket to inhibit binding of FBLX3 (13), it also differs from KL101 an TH301 in that KL001 is not selective for either CRY1 or CRY2 (15). This suggests that KL101 and TH301 are selective in part due to their ability to enhance the interaction between the PHR and the divergent CRY tails.

5.3.3 CRY1 exon 10 plays an essential role in the activity of KL101 and TH301.

Since the activity of KL101 and TH301 depends on the exon 10 in the tail of either CRY isoform (15), we also performed a compound titration with a Δ10 version of the CRY1 tail to determine if exon 10 is necessary to mediate enhancement of the PHR-tail interaction by KL101. We found that enhancement of the CRY1 PHR-tail interaction is weakened when exon 10 is truncated as demonstrated by an attenuated increase in FP ratio when KL101 is added (Figure 5.3A). This also corroborates the previous finding that swapping out the exon 10 region of CRY1 blunts the half-life extension by KL101 (15). Similar to the response to KL101, removal of exon 10 from the CRY1 tail also attenuated the response to the moderately CRY2-selective ligand TH301 (Figure 5.3A)

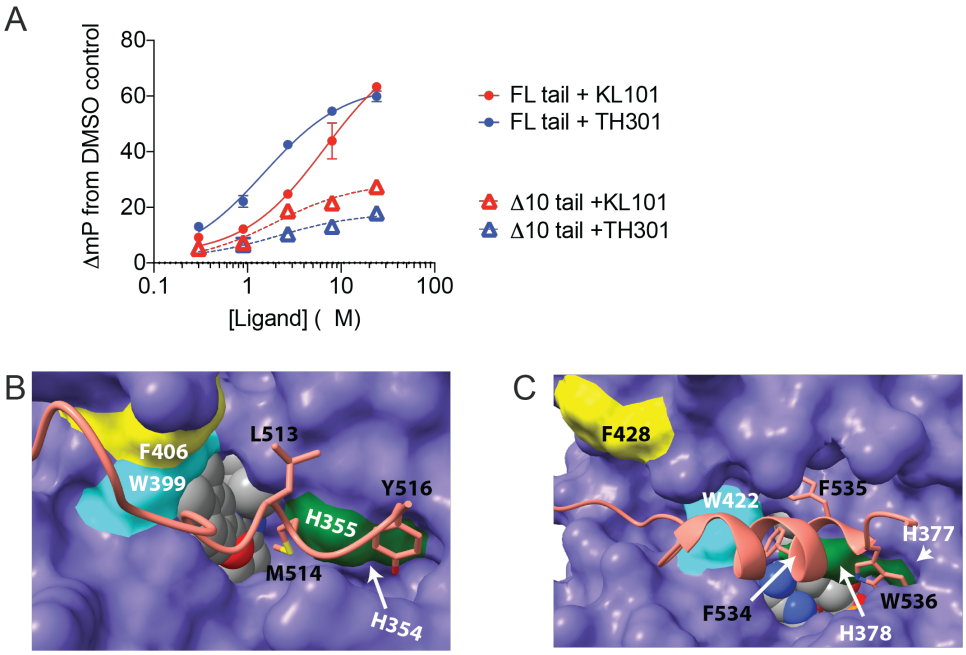

Figure 5.3. CRY1 exon 10 interacts with the FAD-binding pocket.

(A) Ligand titration of KL101 (red) or TH30 (blue) and a mixture of 5 μM CRY1 PHR and 20 nM FAM-CRY1 full-length (FL) tail (circle) or 20 nM FAM-Δ10 CRY1 tail (triangle). Plot shows the mean representative titration response curves of duplicate samples ± sd (of n = 3 independent assays). Curve represents fit to response versus agonist model (Prism). For the CRY1 PHR-tail interaction, TH301 has an EC_{50} = 1.5 ± 0.03 μM and KL101 has an EC50 = 7.7 ± 2.0 μM. ***(B)*** AlphaFold prediction for the interaction between the CRY1 tail at exon 10 (pink) and the PHR (purple) with ligand KL101 docked (from PDB 6KX6) in the FAD binding

pocket. Lid-loop residue F406 (yellow surface), gatekeeper residue W399 (cyan surface), and FAD-binding pocket residues H355 and H356 (green surface) potentially interact with the C-terminal tail ***(C)*** The dCRY tail (pink, PDB 4GU5) interacts with the dCRY PHR (purple, PDB 4GU5) at the FAD-binding pocket. Corresponding residues from mammalian CRY PHR are highlighted: lid-loop residue F428 (yellow surface), gatekeeper residue W422 (cyan surface), and FAD-binding pocket residues H377 and H378 (green surface).

While the data does not explain how CRY1 exon 10 confers ligand selectivity, they do further support the current model that the region encoded by exon 10 in CRY1 interacts with its PHR near the FAD-binding pocket. It is possible that the CRY selective ligands either interact directly with an epitope on exon 10 of the CRY1 tail or subtly remodel the CRY1 PHR such that the ligand enhances the interaction between CRY1 exon 10 and the PHR. Either alternative suggests that exon 10 on the CRY1 tail interacts near the FAD-binding pocket of CRY1, a conformation which is also predicted by AlphaFold (Figure 5.3B) (21) In the predicted model, exon 10 interacts with gatekeeper residue W399 and FAD-binding pocket residue H356, residues that also interact directly with both KL101 and TH301. AlphaFold also predicts that exon 10 interacts with lid loop residue F406; a residue that does not directly interact with either KL101 or TH301 but still controls the selectivity of these ligands depending on which CRY tail is tethered to the CRY1 PHR (16).

KL101 and TH301 play a role that is analogous to FAD in *Drosophila* CRY. The FAD co-factor bound to the FAD-binding pocket on the dCRY PHR mediates an interaction between a hydrophobic FFW motif on the C-terminal tail and the PHR at gatekeeper residue W422 and FAD-binding pocket residue H378 (Figure 5.3C) (22, 23). Neither mammalian CRY1 nor CRY2 contain an FFW motif on their respective C-terminal tails, but the human CRY1 tail has a hydrophobic FMGY (LMGY in mouse CRY1) motif within the exon 10 region that I showed binds directly to the PHR (5). AlphaFold also predicts that this motif in CRY1 exon 10 could potentially mediate an interaction with the PHR similar to how the FFW motif in dCRY interacts with the PHR. For instance, the potential interaction in mCRY1 between tail residue Y516 and FAD-binding pocket residue H355 appears to be similar to the interaction

between dCRY1 tail residue W536 and dCRY1 FAD-binding pocket residue H377.These data suggest that the FAD-binding pocket is a conserved binding site for the PHR–tail interaction.

5.3.4 The CRY selective ligands do not significantly modulate the interaction between CRY1/2 and PER2

We also determined if either KL101 or TH301 modulates binding between the CRY PHR and the CRY binding domain (CBD) of PER2 and tested whether this effect is selective for either CRY isoform. Since PER2 CBD binds in proximity to the FAD-binding pocket (24, 25), and competes with the CRY tail for binding to the CRY PHR (5), we hypothesized that KL101 and TH301 might affect CRY/PER2 binding. However, we found that even at 100 μM KL101 and TH301, neither ligand significantly affected the affinity by which both CRYs (Figure 5.4) bound to the PER2 CBD. While the binding curves suggested that TH301 (but not KL101) may enhance CRY/PER2 binding in both CRY orthologs, this effect was modest and non-selective (Figure 5.4C,D).

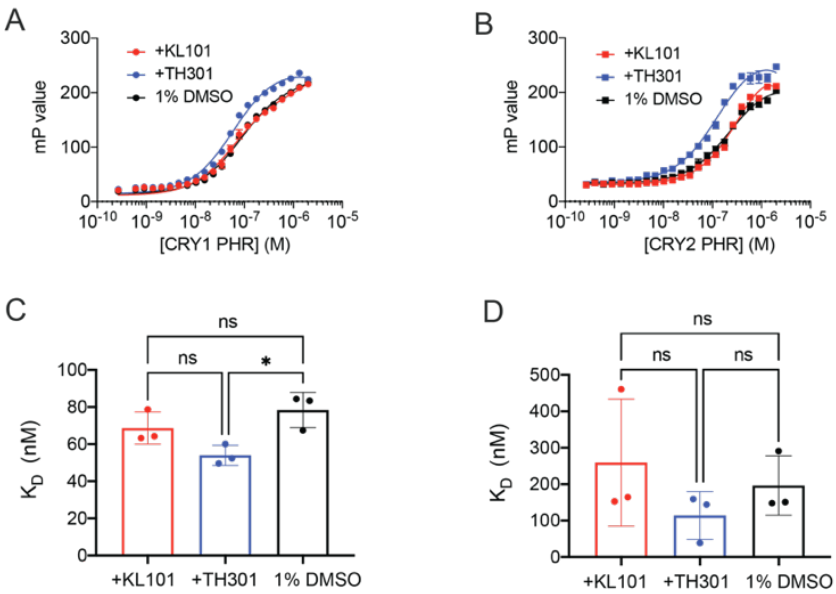

Figure 5.4. The binding affinity between CRY1/2 and PER2 CBD is not modulated by CRY binding ligands

(A-B) FP binding curves of fluorescently labeled PER2 CBD binding to the CRY1 PHR (A) and the CRY2 PHR (B) in the presence of 0.1 mM KL101 (red), 0.1 mM TH301 (blue) and 1 % vol/vol DMSO only (black). Plot shows the mean representative binding curves of duplicate samples ± sd (of n = 3 independent assays). Curve represents fit to one-site binding (Prism).

(C-D) K_D fits calculated on GraphPad Prism (one-site binding model) for 3 independent assays of PER2 binding to CRY1 PHR (C) and CRY2 PHR (D). *P < 0.05 determined by one-way unpaired ANOVA and Tukey's multiple comparison test. Non-significant differences (p > 0.05) is denoted by "ns".

5.3.5 TH301 does not modulate CRY1-CLOCK binding

The PHRs of CRY1 and CRY2 are differentiated in part through a serine loop adjacent to the secondary pocket. Previous CRY1 structures lack electron density at the serine loop and molecular dynamics simulations suggest that it is flexible (see Chapter 2 and Supplementary Figure 5.2) (22, 26, 27). By contrast, the CRY2 serine loop forms a short α-helix and is less flexible compared to the CRY1 serine loop according to molecular dynamics simulations (26, 28). These structural differences lead to differential binding such that CRY1 has a stronger affinity for CLOCK than CRY2.

Interestingly, when TH301 is bound to the FAD binding pocket of CRY1, the serine loop adjacent to the secondary pocket of CRY1 forms a short α-helix similar to the serine loop of CRY2 (Supplementary Figure 5.2) (15). This may be a result of allosteric communication between the CRY1 FAD-binding pocket. There is one other example of this type of allostery in CRY1: missense mutation p.Arg293His modifies FAD-binding pocket residue R293 and enhances CRY1 half-life (similar to TH301 and KL101) but also weakens the interaction between CRY1 and CLOCK:BMAL1 (29). Molecular dynamic simulations predict that mutating R293 to a histidine alters allosteric networks between the FAD-binding pocket and the secondary pocket, thus modulating the dynamics of the serine loop adjacent to the secondary pocket. While TH301 binds in close proximity to R293, the ligand does not directly interact with R293 or with other residues involved in this allosteric network (15, 29). However, it is still possible that TH301 affects the secondary pocket through networks not predicted by previous molecular dynamic simulations.

We hypothesized that when TH301 is bound to the FAD-binding pocket of CRY1, the serine loop is remodeled to resemble that of CRY2, thus weakening the affinity between CRY1 and CLOCK (26). This presents an potential mechanism for selectivity; even if TH301

is more potent than KL101 in enhancing the PHR–tail interaction (Figure 5.2), the stabilizing effects of TH301 might be negated by allosteric inhibition of the CRY1–CLOCK interaction. However, we found that the presence of TH301 did not affect the affinity between CRY1 and the PAS domain core of CLOCK:BMAL1 compared to a DMSO control, demonstrating that TH301 binding does not modulate the CRY1–CLOCK binding affinity (Figure 5.5).

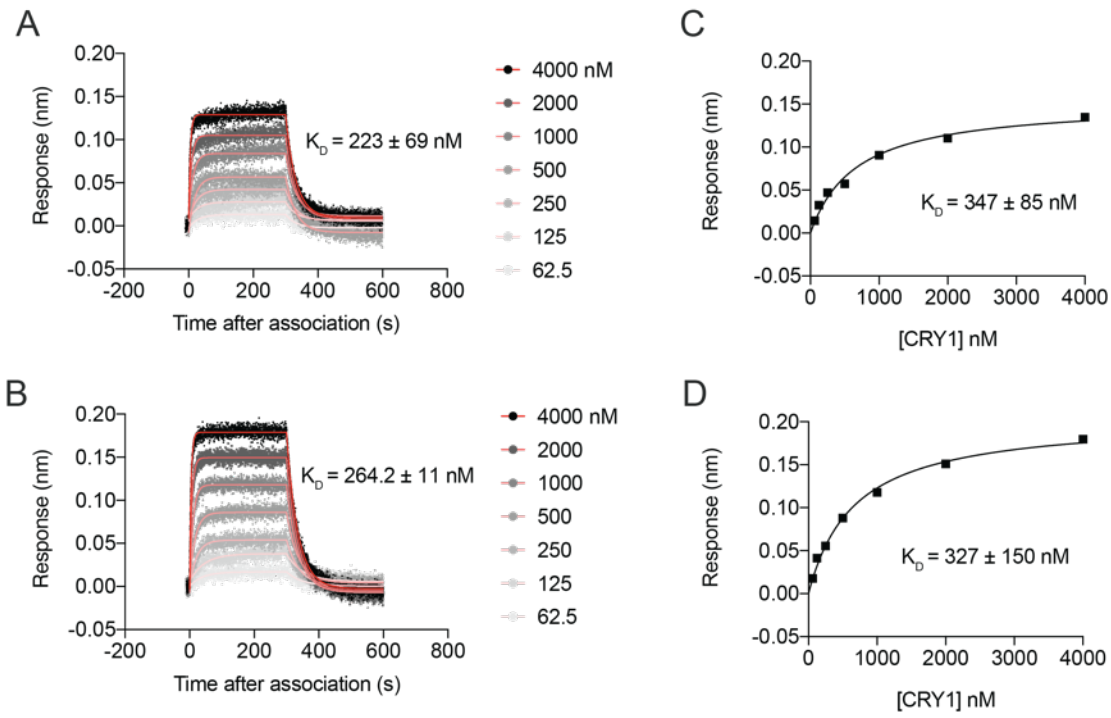

Figure 5.5. TH301 does not modulate CRY1–CLOCK binding

(A-B) BLI sensorgram for biotinylated CLOCK:BMAL1 PAS-AB titrated with CRY1 PHR at 1%DMSO with no TH301 (A, gray to black) and with 24 μM TH301 (B, gray to black). Model fit to association and dissociation over time represented by thin red line. ***(C-D)*** Steady-state analysis of BLI response versus CRY1 concentration in the absence of TH301 (C) and with 24 μM TH301 (D). Plot shows the mean representative binding curves of samples (of n = 3 independent assays). Curve represents fit to one-site binding (Prism).

5.4 Discussion

We identified a possible mechanism for how the KL101 and TH301 work synergistically with the CRY tail to regulate stability: both compounds act as a molecular glue between the PHR and the C-terminal tail to stabilize a conformation that inhibits binding between the PHR

and FBXL3. While the FAD-binding pocket is a protein-protein interaction hotspot in which small-molecule inhibitors can inhibit the formation of the CRY2-FBXL3 complex (which buries 4800 $Å^2$ of solvent accessible surface area) (28), it is also possible for the CRY tail to contribute to inhibiting the formation of the complex. For instance, PER2 binds to the CRY1 PHR near the lid-loop on a side opposite from the FAD-binding pocket and directly inhibits association of FBXL3 to that site on the CRY PHR (25). Since the CRY C-terminal tails and PER2 possibly compete for the same binding sites on the CRY PHR (5), the CRY1 and CRY2 tails might play a similar role as PER2 in inhibiting the formation of a CRY-FBXL3 complex at a site outside of the FAD-binding pocket.

KL001 can still inhibit the formation of the CRY-FBXL3 complex even without enhancing the PHR-tail interaction. We had expected KL001 to interact with the C-terminal tail since KL001 can no longer stabilize CRY when the C-terminal tail is absent (15). It is possible that KL001 and the C-terminal tail still work synergistically such that KL001 inhibits FBXL3 at the FAD-binding pocket, while the C-terminal tail binds elsewhere to inhibit FBXL3 binding on a different site on the PHR (similar to PER2). In other words, multivalent interactions may be required to inhibit binding between CRY and FBXL3. In contrast to KL001, KL101 and TH301 can both recruit the C-terminal tails to the FAD-binding pocket. Since the CRY1 and CRY2 tails are divergent, variations in how either tail binds to the PHR might lead to isoform-specific effects on FBXL3 inhibition. Lack of tail recruitment by KL001 may also explain why KL001 is non-selective while KL101 and TH301 are.

While we have identified a possible mechanism for how the CRY tail imparts a response to either KL101 and TH301, we have not identified the exact mechanisms by which the CRY tails imparts selectivity. TH301 is more potent than KL101 in enhancing the CRY1 PHR-tail interaction despite being the CRY2-selective ligand. We also rule-out that TH301 modifies either the CRY–PER interaction or the CRY1–CLOCK interaction to impart selectivity. The lack of selectivity in the PHR-tail interaction may be a consequence of looking at binding in *trans,* which lacks some of the possible restraints that would result from the C-

terminal tail being directly tethered to its PHR. Another alternative is that KL101 and TH301 each orient the CRY tail in different conformations, albeit with similar binding affinities. KL101 and TH301 orient the gatekeeper residue W399 and the lid loop in divergent ways depending on which ligand is bound to the FAD-binding pocket: KL101 orients both the gatekeeper residue and the lid loop in the “out position” (away from the FAD-binding pocket), while TH301 orients both the gatekeeper and the lid loop in the “in” position (towards the FAD-binding pocket). It is possible that the CRY1 tail works more synergistically with KL101 to inhibit FBLX3 when the gatekeeper and the lid loop are in the “out” position, while the divergent CRY2 tail works more synergistically with TH301 to inhibit FBXL3 when the gatekeeper and lid loop in the “in” position. Conversely, even though TH301 (the CRY2 selective ligand) is more potent than KL101 (the CRY1 specific ligand) in enhancing the CRY1 PHR-tail interaction, it is possible that the CRY1 PHR-tail interaction is less effective at inhibiting FBLX3 if the CRY1 gatekeeper and lid loop are oriented in the “in” position.

Further investigation of how the C-terminal tail directly interacts with the PHR may further reveal the mechanism of selectivity of KL101 and TH301. It remains to be seen if the lid loop mutations that affect the selectivity of KL101 and TH301 might also influence binding between the PHR and the tail(Figure 5.3 and Supplementary Figure 5.1) (16). For instance, CRY1 F406A blunts the response to KL101 (the CRY1 specific ligand) even though F406 does not directly interact with KL101. By contrast, F406A enhances the response to TH301 when the CRY2 tail is tethered to the PHR of CRY1 F406A (16). These data suggest an interplay between F406, the CRY-selective ligands, and the C-terminal tail. Since KL101 and TH301 appear to act as a molecular glue between the PHR and the tail, they will also aid in the study of full-length mammalian CRYs and could further enable structural and biochemical studies of the CRY PHR-tail interaction.

5.5 Materials and Methods

5.5.1 Expression and purification of recombinant proteins.

All CRY tail constructs (full length human CRY1 tail, residues 496-586; CRY1 Δ10 tail, residues 530-586; full length CRY2 tail, residues 513-592) and other proteins such as PER2 CBD (human PER2 residues 1095-1215), and Biotin Acceptor Peptide (BAP)-tagged CLOCK PAS-AB (mouse CLOCK residues 93-395) were expressed using *Escherichia coli* (*E. coli*) Rosetta2 (DE3) cells. Sortase A and BirA were expressed in BL21 (DE3) *E. coli*. Proteins were expressed as a fusion to the solubilizing tags GST (for BirA), His_6-GST (for CRY1 and PER2 constructs), His_6-NusA-XL (for BAP-tagged CLOCK PAS-AB), or His_6 (for Sortase A). Protein expression was induced at 37°C with 0.5 mM isopropyl-β-D-thiogalactopyranoside (IPTG) at an OD_{600} of ~0.8 and grown for an additional 16 hours at 18°C. Cells were centrifuged at 4°C at 3200 x g, reconstituted in 50 mM Tris pH 7.5, 300 mM NaCl, 5% (vol/vol) glycerol and 5 mM β-mercaptoethanol (BME) and lysed using a microfluidizer followed by brief sonication. After clarifying lysate on a centrifuge at 4°C at 140,500 x g for 1 hour, protein was captured using Ni-NTA affinity chromatography (Qiagen) or Glutathione Sepharose 4B resin (GE Life Sciences). After capturing protein on the relevant affinity chromatography resin, the affinity and solubility tags (e.g. His_6-GST, His_6, or GST) were cleaved using GST-TEV (on Glutathione resin) or His_6-TEV protease (on Ni-NTA resin) at 4°C overnight. Cleaved protein was then collected from the flow-through after overnight TEV cleavage. Sortase A and CRY1 tail constructs were further purified using size exclusion chromatography (SEC) in 50 mM Tris, pH 7.5, 150 mM NaCl, 10% (vol/vol) glycerol. GST-BirA was further purified using SEC in 50 mM Tris, pH 8.0, 300 mM NaCl, 1 mM dithiothreitol (DTT), 5% (vol/vol) glycerol. All other proteins (e.g. CLOCK PAS-AB) were further purified using SEC in 20 mM HEPES pH 7.5, 125 mM NaCl, 5% (vol/vol) glycerol, and 2 mM Tris(2-carboxyethyl)phosphine (TCEP). For long-term storage, small aliquots of these proteins were frozen in liquid nitrogen and stored at -70°C.

BMAL1 PAS-AB (mouse BMAL1 residues 136-441) and all CRY constructs containing the PHR domain (mouse CRY1 PHR, residues 1-491; mouse CRY2 PHR, residues 1-512) were expressed in Sf9 suspension insect cells (Expression systems) using the baculovirus expression system. His_6-tagged versions of CRYs were cloned into pFastBac HTa vectors that were later transduced into baculovirus. We used P3 virus to infect Sf9 cells at 1.2 x 10^6 cells per milliliter, which were grown for 72 hours at 27°C before harvesting.

CRY-expressing cells were centrifuged at 4°C at 3200 x g, resuspended in 50 mM Tris pH 7.5, 300 mM NaCl, 5% (vol/vol) glycerol and 5 mM BME and lysed in low concentrations of detergent (0.01% (vol/vol) Triton X-100), Pierce Protease Inhibitor EDTA-free tablets (1 tablet/50mL, Thermo Scientific), and 1 mM phenylmethylsulfonyl fluoride (PMSF) using a microfluidizer followed by brief sonication. After clarifying lysate on a centrifuge at 4°C at 140,500 x g for 1 hour, protein was captured using Ni-NTA affinity chromatography (Qiagen). Protein was further purified using ion exchange chromatography preceding SEC into CRY buffer (20 mM HEPES pH 7.5, 125 mM NaCl, 5% (vol/vol) glycerol, and 2 mM TCEP). CRY protein preps were frozen in liquid nitrogen and stored at -70°C.

BMAL1 PAS-AB expressing cells were resuspended in BMAL1 resuspension buffer (50 mM HEPES buffer pH 7.5, 300 mM NaCl, 5% (vol/vol) glycerol and 5 mM BME). Cells were lysed and clarified as described above. The soluble lysate was bound in batch-mode to Glutathione Sepharose 4B (GE Healthcare), then washed in BMAL1 resuspension buffer and eluted with 50 mM HEPES buffer pH 7.5, 150 mM NaCl, 5% (vol/vol) glycerol and 5 mM BME, 25 mM reduced glutathione. The protein was desalted into 50 mM HEPES buffer pH 7, 150 mM NaCl, 5% (vol/vol) glycerol and 5 mM BME using a HiTrap Desalting column (GE Healthcare) and the GST tag was cleaved with GST-TEV protease overnight at 4°C. The cleaved GST-tag and GST-tagged TEV protease was removed by Glutathione Sepharose 4B (GE Healthcare) and the remaining BMAL1 PAS-AB protein was further purified by Superdex75 SEC (GE Healthcare) into 20 mM HEPES buffer pH 7.5, 125 mM NaCl, 5%

(vol/vol) glycerol, and 2 mM TCEP. Purified BMAL1 PAS-AB was mixed with biotinylated CLOCK PAS-AB (below) to generate the heterodimer for binding assays.

5.5.2 Biotinylation and reconstitution of Biotin-CLOCK:BMAL1 PAS-AB.

For the biotinylation reaction, 100 μM BAP-CLOCK PAS-AB in 20 mM HEPES pH 7.5, 125 mM NaCl, 5% (vol/vol) glycerol, and 2 mM TCEP was incubated at 4˚C overnight with 2 mM ATP, 1 μM GST-BirA and 150 μM biotin. GST-BirA was removed after the reaction using Glutathione Sepharose 4B (GE Healthcare) resin and excess biotin was separated from the labeled protein by SEC. Biotin-CLOCK:BMAL1 PAS-AB heterodimer was reconstituted after labeling by adding equimolar BMAL1 PAS-AB to biotinylated CLOCK PAS-AB and verifying complex formation by SEC. Biotinylated heterodimer was quick frozen in liquid nitrogen for long-term storage at -80°C.

5.5.3 Fluorescent labeling.

For the Sortase A recognition motif, we purchased commercially synthesized peptides with N-terminal cysteines conjugated to tetramethylrhodamine (TAMRA) 5-maleimide fluorophore or a fluorescein 5-maleimide fluorophore. To fluorescently label recombinantly expressed proteins and peptides, we utilized Sortase A-mediated reactions (30) between an N-terminally fluorescein-labeled (or TAMRA-labeled) Sortase A recognition motif peptide (FAM-LPETGG) and our protein of interest (e.g., CRY1 tail, CRY2 tail, or PER2 CBD). Reactions were carried out in 50 mM Tris, pH 7.5, 150 mM NaCl, and 10 mM $CaCl_2$ using 5 μM His_6-Sortase A and 3-5x molar excess of the fluorescently labeled Sortase A recognition motif peptide relative to the protein to be labeled. Labeled protein was purified from the reaction mixture using Ni-NTA affinity chromatography (Qiagen) and/or followed by SEC. Labeled protein was characterized by fluorescent imaging on an SDS-PAGE gel using a Typhoon imager (GE Healthcare). Extent of labeling was measured through spectrophotometry and calculated using the following equation:

$$\%_{labeled} = \frac{A_{dye}}{\varepsilon_{dye} \times \left(\frac{A_{280} - (A_{dye} \times CF)}{\varepsilon_{protein}}\right)}$$

where A_{dye} is the absorbance at the maximum absorption wavelength (555 nm for TAMRA and 494 nm for fluorescein), ε_{dye} is the extinction coefficient of the dye (65,000 M^{-1} cm^{-1} for TAMRA and 68,000 M^{-1} cm^{-1} for fluorescein), and the CF is a correction factor that adjusts for the amount of absorbance at 280 nm contributed by the dye (31). We also measured molecular weights of fluorescent probe using a SciEx QTOF mass spectrometer. All probes were labeled with at least 60% efficiency.

5.5.4 Fluorescence polarization.

All FP assays were performed in 50 mM Bis-Tris Propane pH 7.5, 100 mM NaCl, 0.05% (vol/vol) Tween, 2 mM TCEP. Binding assay reactions with CRY tails contained 5% vol/vol DMSO, while binding assay reactions with PER2 CBD contained 1% vol/vol DMSO. For direct binding assays, varying amounts of CRY protein was mixed with 0.02 μM of a fluorescently labeled construct (either CRY tail or PER2 CBD). Reactions were incubated for 10 minutes at room temperature. For ligand titration assays, 0.02 μM fluorescently labeled probe (e.g., CRY1 tail, CRY2 tail, or PER2 CBD) were incubated with 5 μM CRY1 or 3 μM CRY2 PHR for 15 minutes on ice. Varying amounts of KL101 or TH301 were mixed with this reaction (all with a final concentration of 5% DMSO) and incubated for 10 minutes at room temperature. Fluorescence polarization measurements were measured on a Perkin Elmer EnVision 2103 Multilabel plate reader with excitation at 485 nm and emission at 535 nm. The equilibrium dissociation constant (K_D) and extent of non-specific binding was calculated by fitting millipolarization level (mp) to a one-site total model in GraphPad Prism using averaged mp values from assays with duplicate samples. EC_{50} values were calculated from displacement assays by fitting the mp level to Agonist versus Response model in GraphPad Prism, with averaged mp values from assays with duplicate samples. Data shown are from one representative experiment (± sd) of two independent assays.

5.5.5 Biolayer interferometry.

All BLI experiments were performed using an 8-channel Octet-RED96e (ForteBio). All BLI experiments were performed in BLI assay buffer (20 mM HEPES pH 7.5, 125 mM NaCl, 5% (vol/vol) glycerol, 2 mM TCEP, 1% (vol/vol) DMSO). (5) For each experiment, we used 8 streptavidin biosensor tips (ForteBio). All experiments began with reference measurements using unloaded streptavidin tips to establish a baseline in BLI buffer, after which non-specific CRY1 association was measured for 5 minutes in wells containing 2-fold serial dilutions of CRY1 (*e.g.* 4 μM, 2 μM, 1 μM, 0.5 μM, 0.25 μM, etc.) or a reference sample well containing no CRY, and then dissociation was subsequently measured for 5 minutes in wells containing BLI buffer. After measuring our initial reference, we repeated the same assay with fresh tips that were loaded with 1.5 – 3 μg/mL biotinylated CLOCK:BMAL PAS-AB dimer using BLI buffer that contained no BSA or Tween-20. Data were processed and fitted using Octet software v.7 (ForteBio). Before fitting, all datasets were reference-subtracted, aligned on the y-axis through their respective baselines, aligned for interstep correction through their respective dissociation steps, and finally smoothened using Savitzy-Golay filtering. For each experiment, at least 4 different concentrations were used to fit association and dissociation globally over the full range of the experiment using a 1:1 binding model in Octet software v.7 (ForteBio). Goodness of fit was determined with $\chi 2$ and $R2$ tests that conform to the manufacturer's guidelines.

5.6 Supplementary Figures

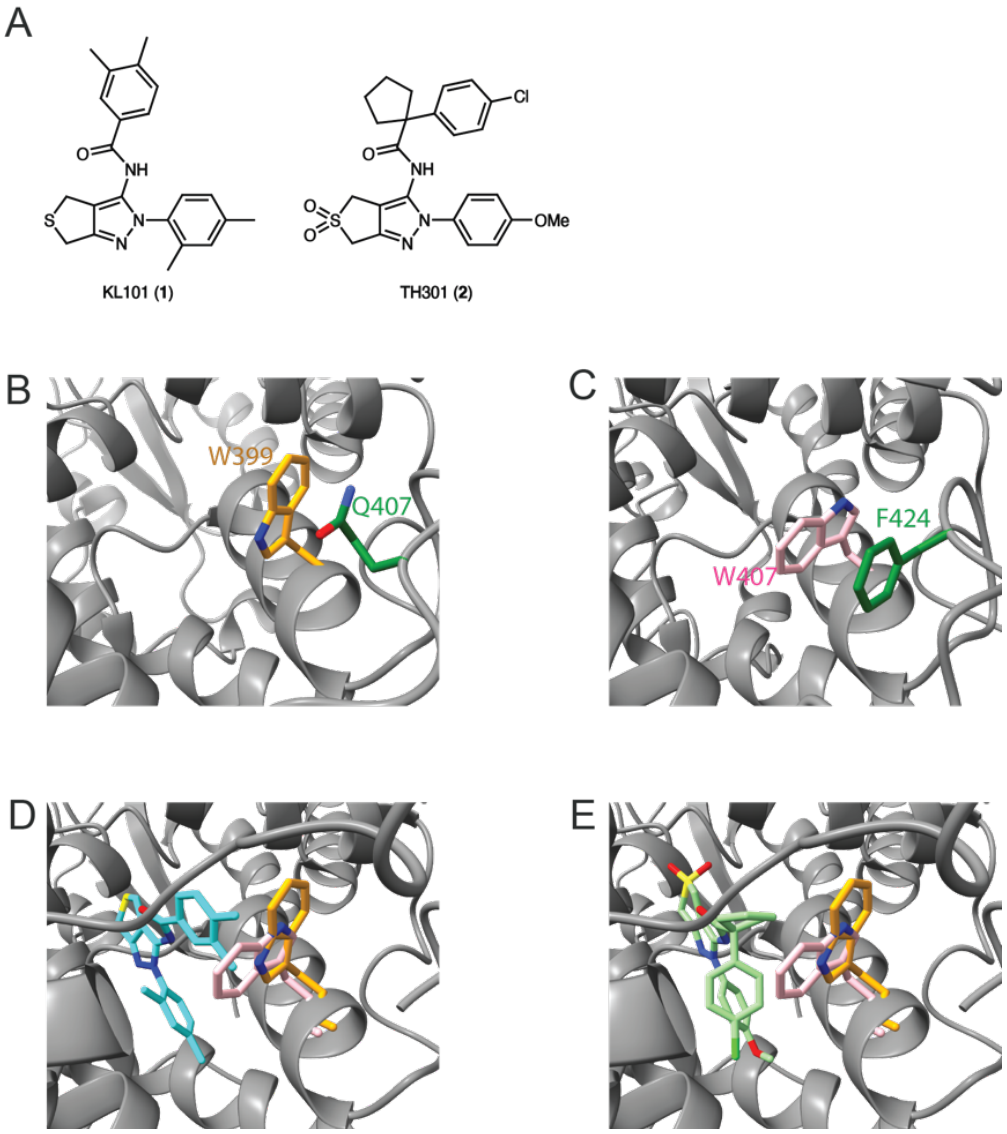

Supplementary Figure 5.1: CRY1 and CRY2 gatekeeper residues control selectivity of KL101 and TH301.

(A) Chemical structures of KL101 (1) and TH301 (2) respectively. ***(B)*** CRY1 (gray) gatekeeper residue W399 (orange) is stabilized in the "out" position (sidechain oriented away from FAD binding pocket) by an interaction with lid loop residue Q407 (green) (PDB 7D0M) (16). ***(C)*** CRY2 gatekeeper residue W407 (pink) is held is stabilized in the "in" position (side chain oriented towards the FAD binding pocket) through an interaction with lid loop residue F424 (green) (PDB 7D0N). ***(D)*** KL101 (cyan) bound in the FAD binding pocket of CRY1 (gray) would be sterically hindered by a gatekeeper residue in the "in" position (pink i.e. W407 in CRY2) but not by a gatekeeper residue in the "out" position (orange, i.e. W399 in CRY1). ***(E)*** TH301 (light green) bound in the FAD binding pocket of CRY2 favors an interaction with the gatekeeper in the "in" position (pink) rather than the "out" position (orange).

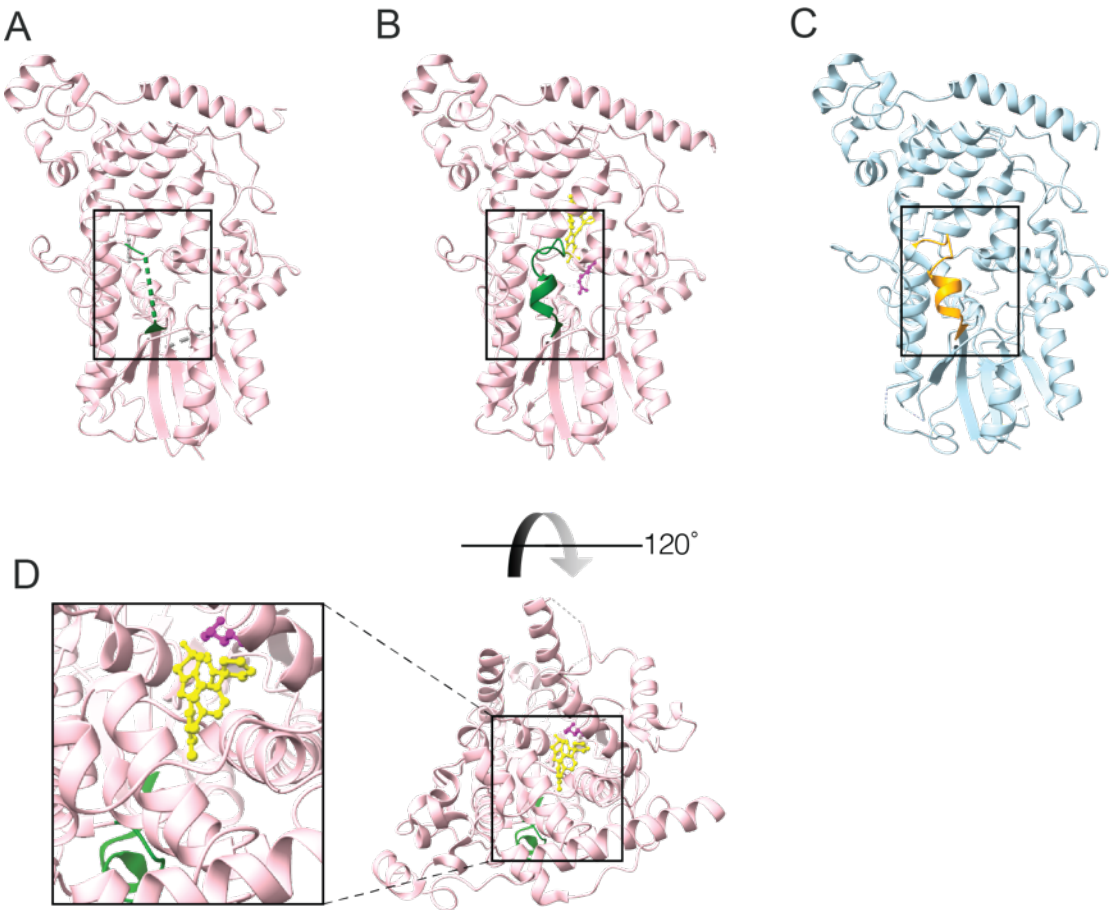

Supplementary Figure 5.2. TH301 potentially remodels the secondary pocket of CRY1.

(A) There is missing electron density corresponding to the serine loop (represented by green dashed line within black box) adjacent to the secondary pocket on the CRY1 PHR (pink, PDB 5T5X) ***(B,C)*** In crystal structures of the CRY1 PHR (pink, PDB 6KX7) bound to TH301 (yellow) the serine loop (green) adjacent to the secondary pocket forms a short helix similar to that of CRY2 (C, serine loop in orange, PHR in light blue, PDB 4I6E) (15, 28) ***(D)*** TH301 is proximal to R293 (magenta), a residue in the FAD-binding pocketed predicted to allosterically control the CRY1 secondary pocket (green).

5.7 References

1. Partch CL, Green CB, & Takahashi JS (2014) Molecular architecture of the mammalian circadian clock. *Trends in Cell Biology* 24(2):90-99.

2. van der Horst GT*, et al.* (1999) Mammalian Cry1 and Cry2 are essential for maintenance of circadian rhythms. *Nature* 398(6728):627-630.

3. Vitaterna MH*, et al.* (1999) Differential regulation of mammalian period genes and circadian rhythmicity by cryptochromes 1 and 2. *Proc Natl Acad Sci U S A* 96(21):12114-12119.

4. Papp SJ*, et al.* (2015) DNA damage shifts circadian clock time via Hausp-dependent Cry1 stabilization. *Elife* 4.

5. Parico GCG*, et al.* (2020) The human CRY1 tail controls circadian timing by regulating its association with CLOCK:BMAL1. *Proc Natl Acad Sci U S A* 117(45):27971-27979.

6. Partch CL, Clarkson MW, Ozgür S, Lee AL, & Sancar A (2005) Role of structural plasticity in signal transduction by the cryptochrome blue-light photoreceptor. *Biochemistry* 44(10):3795-3805.

7. Gao P*, et al.* (2013) Phosphorylation of the Cryptochrome 1 C-terminal Tail Regulates Circadian Period Length. *The Journal of Biological Chemistry* 288(49):35277-35286.

8. Harada Y, Sakai M, Kurabayashi N, Hirota T, & Fukada Y (2005) Ser-557-phosphorylated mCRY2 is degraded upon synergistic phosphorylation by glycogen synthase kinase-3 beta. *J Biol Chem* 280(36):31714-31721.

9. Hirano A*, et al.* (2014) In vivo role of phosphorylation of cryptochrome 2 in the mouse circadian clock. *Mol Cell Biol* 34(24):4464-4473.

10. Kurabayashi N, Hirota T, Sakai M, Sanada K, & Fukada Y (2010) DYRK1A and glycogen synthase kinase 3beta, a dual-kinase mechanism directing proteasomal degradation of CRY2 for circadian timekeeping. *Mol Cell Biol* 30(7):1757-1768.

11. Li Y, Xiong W, & Zhang EE (2016) The ratio of intracellular CRY proteins determines the clock period length. *Biochem Biophys Res Commun* 472(3):531-538.

12. Liu N & Zhang EE (2016) Phosphorylation Regulating the Ratio of Intracellular CRY1 Protein Determines the Circadian Period. *Frontiers in Neurology* 7.

13. Hirota T*, et al.* (2012) Identification of small molecule activators of cryptochrome. *Science (New York, N.Y.)* 337(6098):1094-1097.

14. Nangle S, Xing W, & Zheng N (2013) Crystal structure of mammalian cryptochrome in complex with a small molecule competitor of its ubiquitin ligase. *Cell Research* 23(12):1417-1419.

15. Miller S, *et al.* (2020) Isoform-selective regulation of mammalian cryptochromes. *Nature Chemical Biology* 16(6):676-+.

16. Miller S, *et al.* (2021) Structural differences in the FAD-binding pockets and lid loops of mammalian CRY1 and CRY2 for isoform-selective regulation. *Proceedings of the National Academy of Sciences of the United States of America* 118(26).

17. Tan X, *et al.* (2007) Mechanism of auxin perception by the TIR1 ubiquitin ligase. *Nature* 446(7136):640-645.

18. Fischer ES, Park E, Eck MJ, & Thoma NH (2016) SPLINTS: small-molecule protein ligand interface stabilizers. *Curr Opin Struct Biol* 37:115-122.

19. Yang H, *et al.* (2013) mTOR kinase structure, mechanism and regulation. *Nature* 497(7448):217-223.

20. Fischer ES, *et al.* (2014) Structure of the DDB1-CRBN E3 ubiquitin ligase in complex with thalidomide. *Nature* 512(7512):49-53.

21. Jumper J, *et al.* (2021) Highly accurate protein structure prediction with AlphaFold. *Nature*.

22. Czarna A, *et al.* (2013) Structures of Drosophila Cryptochrome and Mouse Cryptochrome1 Provide Insight into Circadian Function. *Cell* 153(6):1394-1405.

23. Levy C, *et al.* (2013) Updated structure of Drosophila cryptochrome. *Nature* 495(7441):E3-4.

24. Nangle SN, *et al.* (2014) Molecular assembly of the period-cryptochrome circadian transcriptional repressor complex. *eLife* 3:e03674.

25. Schmalen I, *et al.* (2014) Interaction of circadian clock proteins CRY1 and PER2 is modulated by zinc binding and disulfide bond formation. *Cell* 157(5):1203-1215.

26. Fribourgh JL, *et al.* (2020) Dynamics at the serine loop underlie differential affinity of cryptochromes for CLOCK:BMAL1 to control circadian timing. *Elife* 9.

27. Michael AK, *et al.* (2017) Formation of a repressive complex in the mammalian circadian clock is mediated by the secondary pocket of CRY1. *Proceedings of the National Academy of Sciences* 114(7):1560-1565.

28. Xing W, *et al.* (2013) SCF(FBXL3) ubiquitin ligase targets cryptochromes at their cofactor pocket. *Nature* 496(7443):64-68.

29. Gul S, *et al.* (2020) The Arg-293 of Cryptochrome1 is responsible for the allosteric regulation of CLOCK-CRY1 binding in circadian rhythm. *J Biol Chem* 295(50):17187-17199.

30. Theile CS, *et al.* (2013) Site-specific N-terminal labeling of proteins using sortase-mediated reactions. *Nature Protocols* 8(9):1800-1807.

31. Anonymous (2011) Calculate dye:protein (F/P) molar ratios. *Thermo Scientific. Tech Tip #31* TR0031.7(TR0031.7).

CHAPTER 6: Screening for small molecules that inhibit CRY–CLOCK binding

The candidate, Gian Carlo Parico, wrote this chapter and performed all experiments described herein. These data are unpublished as of this writing.

Acknowledgements:

We thank Atomwise gifting us with the small molecule library used for this study. We thank Jennifer Fribourgh, Efrain Ceh Pavia, and Megan Torgrimson for generating critical reagents. We thank the Chemical Screening Center (University of California, Santa Cruz) and the Macromolecular Structure Function Core Facility (University of California, Santa Cruz) for access to instrumentation.

6.1 Abstract

CRY1 and CRY2 are components of the core circadian clock that repress the transcriptional activity of CLOCK:BMAL1. The interaction between CLOCK:BMAL1 and CRY1/2 is mediated by an interaction between the secondary pocket of CRY1/2 and the PAS-B domain of CLOCK. Various mutations that affect the interaction at the secondary pocket can alter or disrupt circadian timing. Here, we present a fluorescence polarization (FP) based approach to screen for small molecules that can modulate the interaction between CRY1 and CLOCK PAS-B. Molecules that modulate CRY1–CLOCK binding could have the potential to regulate the period and/or phase-shifting properties of circadian rhythms.

6.2 Introduction

Circadian rhythms are an intrinsic 24-hour timekeeping mechanism that regulates physiology and behavior. At the core of circadian rhythms is a core feedback loop in which the basic helix-loop-helix Per-Arnt-Sim transcription factor (bHLH-PAS) CLOCK:BMAL1 drives the transcription of their own repressors Cryptochrome (CRY1 and CRY2) and Period (PER1 and PER2) (1). In mammals, over 40% of the genome exhibit oscillations in gene transcription with a period of about 24 hours (2). Since much of our physiology is regulated by circadian rhythms, disruption of circadian rhythms and/or misalignment with respect to the 24 hour solar day can lead to detrimental effects on health such as diabetes, metabolic syndrome, sleep disorders, mental illness, and cancer (3)

Unsurprisingly, there is motivation to target core circadian genes such as CRY1 and CRY2 to modulate circadian rhythms. Molecules that bind to the FAD-binding pocket in the photolyase homology region (PHR) of CRY inhibit association of the E3 ubiquitin ligase SCF^{FBXL3} and protect CRY1/2 from proteasomal degradation thus lengthening the circadian period (4-6). Beyond stabilizing CRY, it may also be possible to directly target interactions between CRY and other core circadian proteins such as CLOCK:BMAL1. CRY1 or CRY2 are recruited to the CLOCK:BMAL1 transcription factor through an interaction between the PAS-B domain of CLOCK and the secondary pocket of CRY1/2 (7). Repression of CLOCK:BMAL1

transactivation by CRY1/2 is induced when the CC-helix of the PHR binds to the transactivation domain (TAD) of BMAL1 and sequesters it from transcriptional coactivators like CBP/p300 (8).

While the CC-helix imparts CRY1 and CRY2 with the ability to directly repress CLOCK:BMAL1 through sequestration of the BMAL1 TAD, CRY–CLOCK binding at the secondary pocket also plays a significant role in regulating circadian timing by helping CRYs to stably dock onto the PAS domain core (7, 9). Point mutations in either CLOCK (in the PAS-B domain where the secondary pocket binds) or BMAL1 (in the TAD where the CC-helix binds) can each decrease repression by CRY, but mutations in both CLOCK and BMAL1 can eliminate repression completely, thus confirming an important role for the CRY–CLOCK interaction at the secondary pocket (8, 10). Mutating residues in or around the secondary pocket can also modulate the interaction with CLOCK and alter circadian timing in reconstitution assays (11-13). CRY1 and CRY2 also differ through their secondary pockets; we determined that CRY1 has a 20-fold stronger affinity than CRY2 for binding to CLOCK PAS-B (see Chapter 2) (9).

We also determined that the CRY1 secondary pocket is regulated by another region of CRY1: the intrinsically disordered C-terminal tail (see Chapter 3). A variant that deletes exon 11 (CRY1Δ11) from the CRY1 tail enhances CRY1–CLOCK binding at the secondary pocket and leads to delayed sleep phase disorder (14, 15). We found that CRY1Δ11 alleviates inhibition by the CRY1 tail and enhances CRY1–CLOCK binding (14). We also found that a peptide based on CRY1 exon 11 is sufficient to compete with CLOCK for binding to the CRY PHR, suggesting that inhibiting the CRY1–CLOCK interaction can regulate or disrupt circadian rhythms (14). In the context of CRY1Δ11 (which leads to delayed sleep phase disorder), the use of CRY1–CLOCK interaction inhibitors is analogous to restoring the inhibitory function of exon 11.

Here, we describe an approach to experimentally screen for molecules that modulate CRY1–CLOCK binding. We utilized a fluorescence polarization (FP) assay in a 384-well plate

format to simultaneously screen multiple compounds. We then followed up on potential hits using a compound titration to determine dose-response and orthogonal assays such as BLI to assess binding between CRY1 and CLOCK. Any hits detected in this assay would have the potential to be used as novel probes to dissect the role of CRY1 in regulating circadian rhythms or even as a therapeutic drug for circadian rhythm disorders and other metabolic disorders.

6.3 Results

6.3.1 Primary Fluorescence Polarization screen for CRY1–CLOCK

We hypothesized that molecules that bind to the CRY1 secondary pocket should also inhibit binding between CRY1 and CLOCK PAS-B. We collaborated with Atomwise, who computationally screened for compounds that could bind to the secondary pocket of CRY1 using their proprietary AtomNet neural network for structure-based drug design (16). For their simulations, Atomwise initially used two structures including mouse CRY1 PHR (PDB ID 5T5X) that lacks density at the serine loop adjacent to the secondary pocket and mouse CRY1 PHR bound to TH301 (PDB ID 6KX7), in which the serine loop forms a short helix similar to that of CRY2 (6, 7) .

After Atomwise identified up to ~90 top-ranking potential *in silico* hits, we sought to confirm if these small molecule compounds reduce CRY1–CLOCK binding. We used an FP-based assay that utilized 0.02 μM TAMRA-labeled CLOCK PAS-B and unlabeled 7 μM CRY1 PHR in a 384-well plate format. For positive controls, we used a 23 amino-acid peptide based on CRY1 exon 11 since we previously demonstrated that CRY1 exon 11 is sufficient to compete with CLOCK PAS-B for binding to the CRY1 PHR (14). For negative controls, we used DMSO such that all samples contained a final volume of 1 % vol/vol DMSO. The Atomwise compounds, exon 11 peptide, and DMSO were pin-transferred onto the 384-well plate containing the CRY–CLOCK mixture with a final concentration of 100 μM for each compound (or exon 11 peptide) and a final DMSO concentration of 1% (vol/vol) for all samples.

Data from the initial screen are shown in Figure 6.1. In the primary screen, the assay had a Z' factor = 0.76 (17). Only two compounds (identified through their well IDs of F07 and F10) demonstrated a decrease in fluorescence polarization >3 standard deviations from the mean. The fluorescent intensity of these compounds was also <3 standard deviations from the mean, suggesting that the decrease in FP in the primary screen was not a result of compound fluorescence.

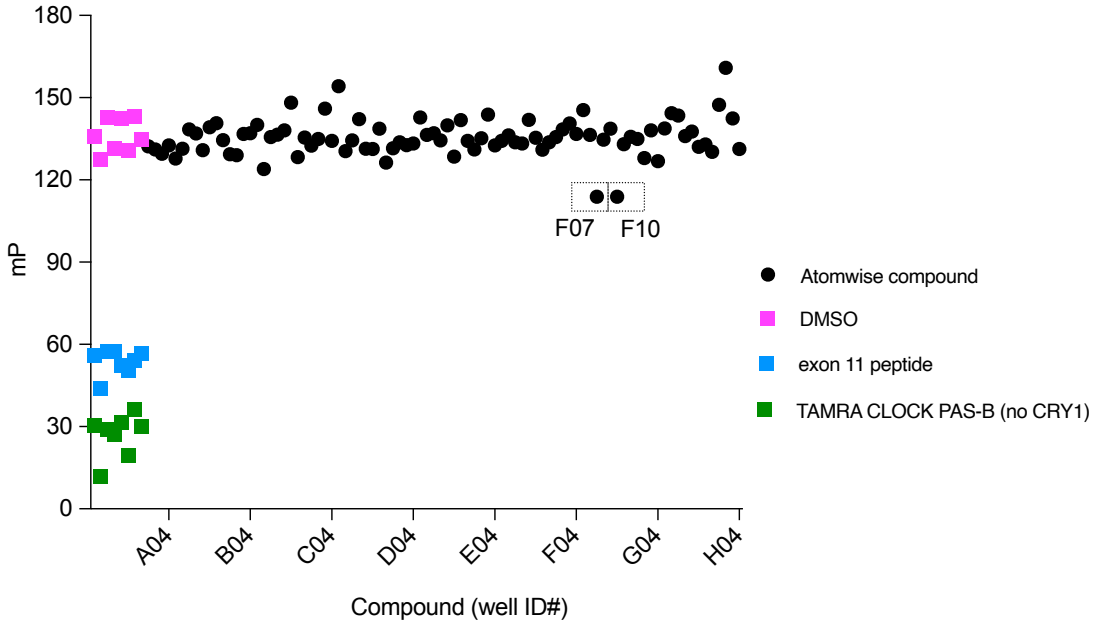

Figure 6.1. Results from primary FP screen

FP ratios for each compound (black circles) from the primary FP screen performed on compounds screened by Atomwise. DMSO (final concentration 1% vol/vol) was used as a negative control (magenta squares) and a peptide based on CRY1 exon 11 was used as a positive control (cyan squares) for CRY1–CLOCK inhibition. The addition of exon 11 causes a decrease in FP ratio approaching that of TAMRA-CLOCK PAS-B in the absence of CRY1 (green squares). Potential hits from wells F07 and F10 are boxed with dash lines.

6.3.2 Validating potential hits for CRY1–CLOCK interaction inhibitors.

To follow up on these potential hits, we performed a ligand titration with fluorescently labeled CLOCK PAS-B and CRY1. We found that the compound F10 did not exhibit a dose-dependent decrease in FP (Figure 6.2A). F07 did cause a dose-dependent decrease in FP; however, the concentrations of F07 used in the initial assay were not sufficiently high to reach saturation in the competition with CLOCK PAS-B. Further investigation suggested that this dose-dependent decrease was likely caused by the intrinsic fluorescence of F07 (Figure 6.2B). The fluorescence of F07 was not apparent in the primary screen due to the lower concentrations of compounds used. Fluorescence interference from F07 may have also affected the fluorescence polarization detected from neighboring well F10 despite the use of black 384-well plates.

To further assess if any of these potential hits inhibit CRY1–CLOCK binding, we also utilized orthogonal follow-up assays that do not rely on fluorescence. We evaluated the potential hits from F07 and F10 in a biolayer interferometry (BLI) assay that measured the association and dissociation of CRY1 with CLOCK:BMAL1 PAS-AB (Figure 6.2C-H). BLI confirmed that the compounds from F07 and F10 did not significantly change the K_D between CRY and the PAS domain core of CLOCK:BMAL1 in comparison to the vehicle.

Figure 6.2. Validation of potential hits utilize a non-orthogonal binding assay to confirm CRY1–CLOCK inhibition

(A-B) Ligand titration of potential hits into a mixture of TAMRA-CLOCK PAS-B and CRY1 depicting dose-dependent changes in FP ratio (A) and fluorescence intensity (B). Plot shows the mean representative titration response curves of duplicate samples ± sd (of n = 3 independent assays). ***(C-E)*** BLI sensorgram for biotinylated CLOCK:BMAL1 PAS-AB titrated with CRY1 PHR at 1% vol/vol DMSO dosed with 100 μM F07 (C, gray to black), F10 (D, gray to black), and no compound (E, gray to black). Model fit to association and dissociation over time represented by thin red line. ***(F-H)*** Steady-state analysis of BLI response versus CRY1 concentration in the dosed with 100 μM F07 (F), F10 (G), and no compound with DMSO at 1% vol/vol (H). Plot shows the mean representative binding curves of samples (of n = 3 independent assays). Curve represents fit to one-site binding (Prism).

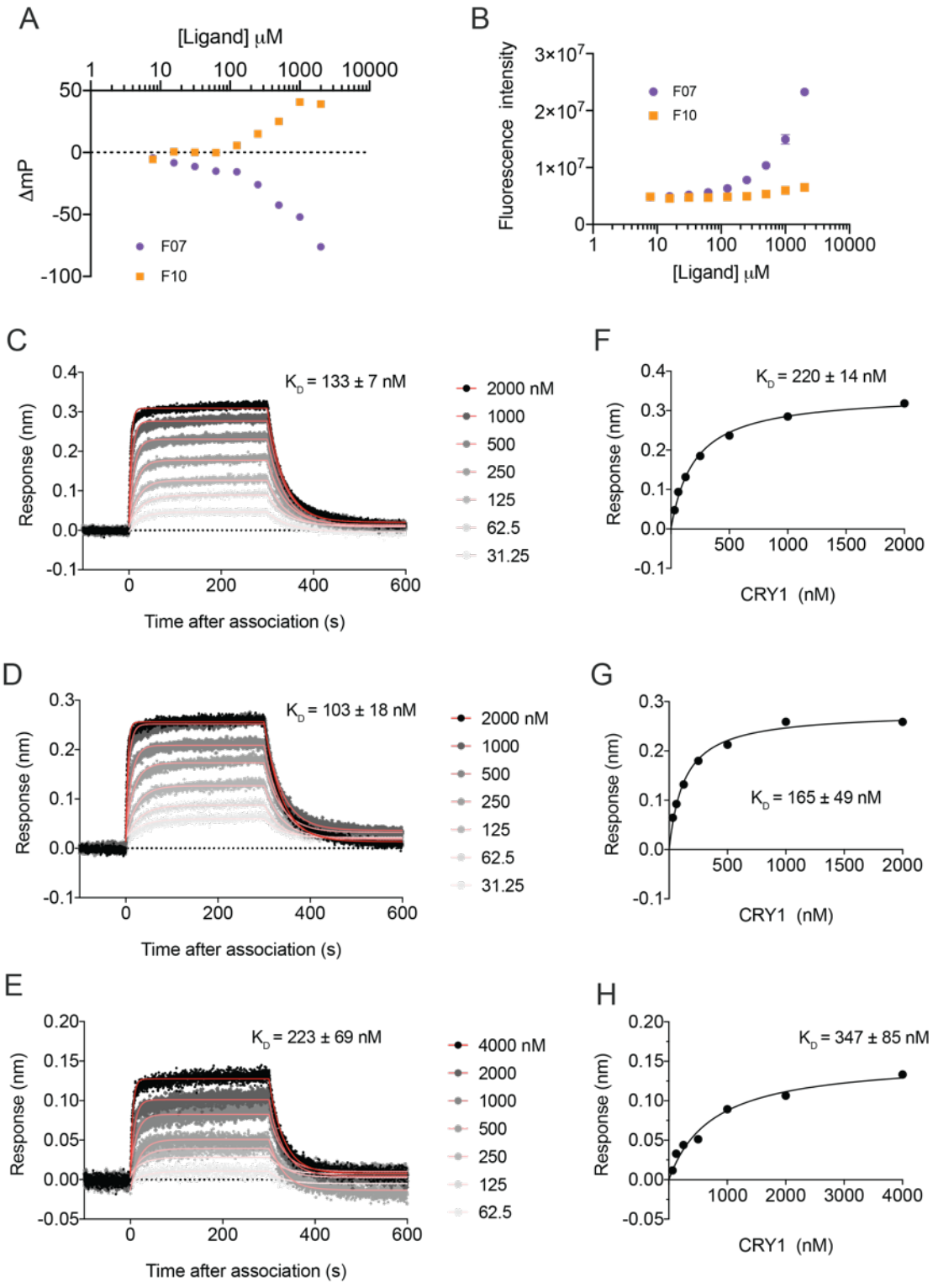
A
[Ligand] μM
1
10
100
1000
10000
50
0
-50
-100
ΔmP
F07
F10
B
Fluorescence intensity
3×10^7
2×10^7
1×10^7
0
F07
F10
1
10
100
1000
10000
[Ligand] μM
C
K_D = 133 ± 7 nM
Response (nm)
0.4
0.3
0.2
0.1
0.0
-0.1
0
200
400
600
Time after association (s)
2000 nM
1000
500
250
125
62.5
31.25
F
K_D = 220 ± 14 nM
Response (nm)
0.4
0.3
0.2
0.1
0.0
-0.1
500
1000
1500
2000
CRY1 (nM)
D
K_D = 103 ± 18 nM
Response (nm)
0.3
0.2
0.1
0.0
-0.1
0
200
400
600
Time after association (s)
2000 nM
1000
500
250
125
62.5
31.25
G
K_D = 165 ± 49 nM
Response (nm)
0.3
0.2
0.1
0.0
-0.1
500
1000
1500
2000
CRY1 (nM)
E
K_D = 223 ± 69 nM
Response (nm)
0.20
0.15
0.10
0.05
0.00
-0.05
0
200
400
600
Time after association (s)
4000 nM
2000
1000
500
250
125
62.5
H
K_D = 347 ± 85 nM
Response (nm)
0.20
0.15
0.10
0.05
0.00
-0.05
1000
2000
3000
4000
CRY1 (nM)

6.3.3 Developing an assay to screen for CRY2–CLOCK interaction inhibitors

We also explored the possibility of screening for CRY2–CLOCK interaction inhibitors in a similar FP format using CRY2 PHR and TAMRA CLOCK PAS-B. CRY2 binds the TAMRA-CLOCK PAS-B probe with a K_D of ~ 8 μM (Figure 6.3A). Whereas the CRY1 C-terminal tail and a peptide based on the exon 11 region of the C-terminal tail are sufficient to compete with CLOCK PAS-B for binding to the CRY PHR, it was previously unknown if the CRY2 C-terminal also plays a similar role in regulating the CRY PHR/CLOCK interaction. Since the CRY2 tail binds to the PHR at similar sites as the CRY1 tail (14, 18), it is possible that the CRY2 tail also inhibits the association of CLOCK PAS-B.

To evaluate if we could use the CRY2 tail or any portion thereof as a positive control for CRY2–CLOCK inhibition, we performed a titration of the CRY2 tail into a mixture of TAMRA-labeled CLOCK PAS-B and unlabeled CRY2 PHR (Figure 6.3B). We found that the CRY2 tail modestly inhibits CRY2–CLOCK binding, but the signal never attained saturation, suggesting that the CRY2 tail may not have the same autoinhibitory role as in CRY1. Since this experiment assessed the interaction of the CRY2 tail and CRY2 PHR in *trans*, we used BLI to measure the binding affinity between full-length CRY2 and the PAS domain core of CLOCK:BMAL1 (Figure 6.3C,D). We found that the affinity of full-length CRY2 for CLOCK:BMAL1 PAS-AB (K_D = 0.9 ± 0.2 μM) did not differ much from the previously published values of CRY2 PHR binding to the PAS domain core of CLOCK:BMAL1 (K_D = 1.2 ± 0.2 μM) (9). The data demonstrate that the CRY2 tail does not inhibit binding to CLOCK PAS-B, further differentiating the structure and function of CRY1 and CRY2.

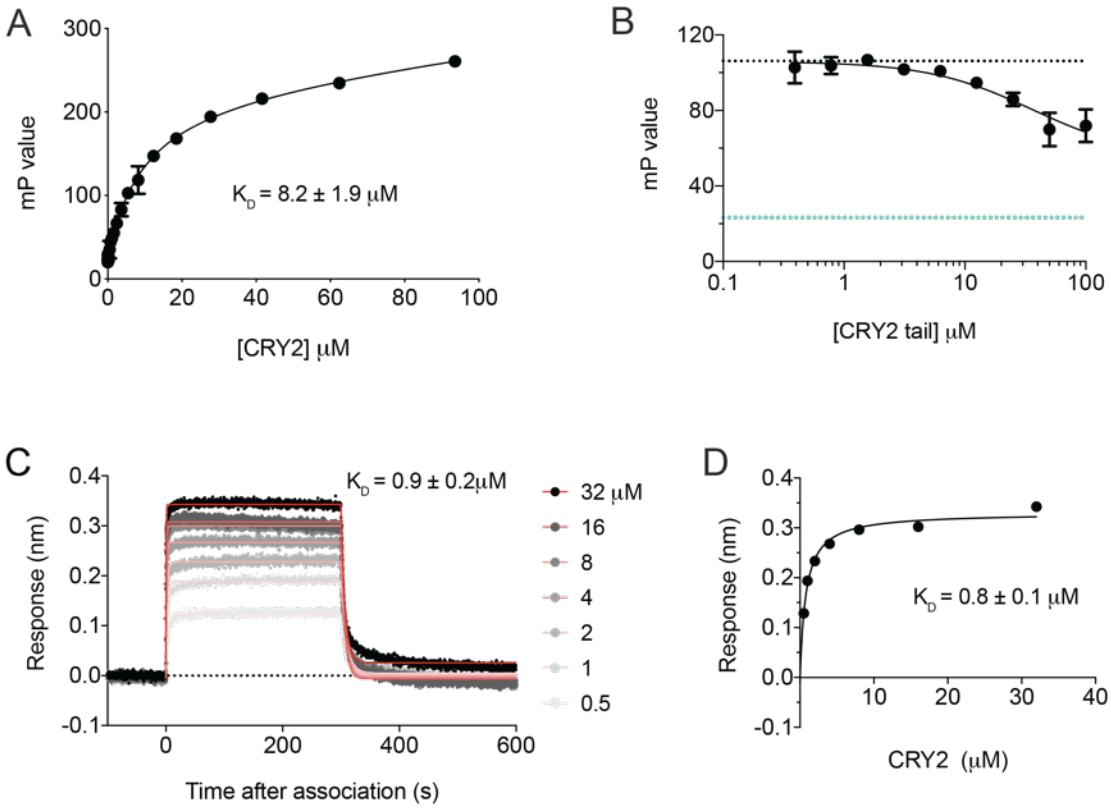

Figure 6.3. The CRY2 tail does not inhibit the interaction between CRY2 and CLOCK PAS-B

(A) FP binding curve of fluorescently labeled CLOCK PAS-B binding to the CRY2 PHR. Plot shows the mean representative binding curves of duplicate samples ± sd (of n = 2 independent assays). Curve represents fit to one-site binding (Prism). ***(B)*** FP-based equilibrium competition assay in which the CRY2 tail is titrated into a mixture of 12 μM CRY2 PHR and 20 nM fluorescently labeled CLOCK PAS-B probe. Mean FP signal of 12 μM CRY1 PHR + 20 nM CLOCK PAS-B probe is denoted by a dotted black line and the mean FP signal of isolated CLOCK PAS-B probe is denoted by a dotted cyan line. Data shown as is from one assay. Curves represent fit to one-site competitive binding model (Prism) assuming that CRY2 PHR and CLOCK PAS-B probe bind at 8.2 μM. ***(C)*** BLI sensorgram for biotinylated CLOCK:BMAL1 PAS-AB titrated with full-length CRY2 PHR (gray to black). Model fit to association and dissociation over time represented by thin red line. ***(D)***, Steady-state analysis of BLI response versus CRY2 concentration Plot shows the mean representative binding curves of samples (of n = 3 independent assays). Curve represents fit to one-site binding (Prism).

6.4 Discussion

While we have not yet identified any hits, the CRY1–CLOCK FP assay still demonstrates the feasibility of screening for circadian rhythm modulators in a non-cellular

context. The Z' score attained during the primary screen suggests that the reagents and controls used are robust and would predictably detect any potential inhibitor of the CRY1–CLOCK interaction. The work described here had also only gone as far as using BLI to validate inhibitors of CRY1–CLOCK binding; further validation of potential hits would have included co-crystallization of CRY1 (or soaking CRY1 crystals) with the ligand as well as performing cellular assays to confirm if potential hits attenuate how CRY1 represses the transcriptional activity of CLOCK:BMAL1.

We also addressed the potential to screen for compounds that modulate CRY2–CLOCK binding. One current obstacle is that we have not yet identified any positive controls to be used in an assay to screen for CRY2–CLOCK interaction inhibitors. However, inhibitors that target the CRY1 secondary pocket have the potential to dissect the differences between CRY1 and CRY2 whose functions are defined by their divergent secondary pockets (9, 13)

Inhibiting the CRY1 or CRY2 secondary pocket may also reveal if or how CRY1 represses different bHLH-PAS transcription factors other than CLOCK:BMAL1, such as HIF1α, and nuclear receptors (NRs) like PPARδ (19-22). Mutations that affect the CRY2 secondary pocket also disrupt interactions with NRs, suggesting that CRY2 secondary pocket inhibitors might have the potential to influence other physiological processes aside from circadian rhythms.

6.5 Materials and Methods

6.5.1 Expression and Purification of recombinant proteins

CLOCK PAS-B (mouse CLOCK residues 261-395), Biotin Acceptor Peptide (BAP)-tagged CLOCK PAS-AB (mouse CLOCK residues 93-395), and CRY2 tail (mouse CRY2 residues 513-592) were expressed using *Escherichia coli* (*E. coli*) Rosetta2 (DE3) cells. Sortase A and BirA were expressed in BL21 (DE3) *E. coli*. Proteins were expressed as a fusion to the solubilizing tags GST (for BirA), His_6-NusA-XL (for CLOCK PAS-B and BAP-tagged CLOCK PAS-AB), His_6-GST (for CRY2 tail constructs) or His_6 (for Sortase A). Protein

expression was induced at 37°C with 0.5 mM isopropyl-β-D-thiogalactopyranoside (IPTG) at an OD_{600} of ~0.8 and grown for an additional 16 hours at 18°C. Cells were centrifuged at 4°C at 3200 x g, reconstituted in 50 mM Tris pH 7.5, 300 mM NaCl, 5% (vol/vol) glycerol and 5 mM β-mercaptoethanol (BME) and lysed using a microfluidizer followed by brief sonication. After clarifying lysate on a centrifuge at 4°C at 140,500 x g for 1 hour, protein was captured using Ni-NTA affinity chromatography (Qiagen) or Glutathione Sepharose 4B resin (GE Life Sciences). After capturing protein on the relevant affinity chromatography resin, the affinity and solubility tags (e.g. His_6-GST, His_6, or GST) were cleaved using GST-TEV (on Glutathione resin) or His_6-TEV protease (on Ni-NTA resin) at 4°C overnight. Cleaved protein was then collected from the flow-through after overnight on-column TEV cleavage. Sortase A was further purified using size exclusion chromatography (SEC) in 50 mM Tris, pH 7.5, 150 mM NaCl, 10% (vol/vol) glycerol. GST-BirA was further purified using SEC in 50 mM Tris, pH 8.0, 300 mM NaCl, 1 mM dithiothreitol (DTT), 5% (vol/vol) glycerol. All other proteins (e.g. CLOCK PAS-B, CLOCK PAS-AB) were further purified using SEC in 20 mM HEPES pH 7.5, 125 mM NaCl, 5% (vol/vol) glycerol, and 2 mM Tris(2-carboxyethyl)phosphine (TCEP). For long-term storage, small aliquots of these proteins were frozen in liquid nitrogen and stored at -70°C.

BMAL1 PAS-AB (mouse BMAL1 residues 136-441) and all CRY constructs containing the PHR domain (mouse CRY1 PHR, residues 1-491; mouse CRY2 PHR, residues 1-512) were expressed in Sf9 suspension insect cells (Expression systems) using the baculovirus expression system. His_6-tagged versions of CRYs were cloned into pFastBac HTa vectors that were later transduced into baculovirus. We used P3 virus to infect Sf9 cells at 1.2 x 10^6 cells per milliliter, which were grown for 72 hours at 27°C before harvesting.

CRY-expressing cells were centrifuged at 4°C at 3200 x g, resuspended in 50 mM Tris pH 7.5, 300 mM NaCl, 5% (vol/vol) glycerol and 5 mM BME and lysed in low concentrations of detergent (0.01% (vol/vol) Triton X-100), Pierce Protease Inhibitor EDTA-free tablets (1 tablet/50mL, Thermo Scientific), and 1 mM phenylmethylsulfonyl fluoride (PMSF) using a

microfluidizer followed by brief sonication. After clarifying lysate on a centrifuge at 4°C at 140,500 x g for 1 hour, protein was captured using Ni-NTA affinity chromatography (Qiagen). Protein was further purified using ion exchange chromatography preceding SEC into CRY FP buffer (50 mM Bis-Tris Propane pH 7.5, 100 mM NaCl, 0.05% (vol/vol) Tween, 2 mM TCEP). CRY protein preps were stored on ice at 4°C or frozen in small aliquots with liquid nitrogen and subjected to only one freeze/thaw cycle after storage at -70°C. If kept on ice, CRY proteins were used within 7 days.

BMAL1 PAS-AB expressing cells were resuspended in BMAL1 resuspension buffer (50 mM HEPES buffer pH 7.5, 300 mM NaCl, 5% (vol/vol) glycerol and 5 mM BME). Cells were lysed and clarified as described above. The soluble lysate was bound in batch-mode to Glutathione Sepharose 4B (GE Healthcare), then washed in BMAL1 resuspension buffer and eluted with 50 mM HEPES buffer pH 7.5, 150 mM NaCl, 5% (vol/vol) glycerol and 5 mM BME, 25 mM reduced glutathione. The protein was desalted into 50 mM HEPES buffer pH 7, 150 mM NaCl, 5% (vol/vol) glycerol and 5 mM BME using a HiTrap Desalting column (GE Healthcare) and the GST tag was cleaved with GST-TEV protease overnight at 4°C. The cleaved GST-tag and GST-tagged TEV protease was removed by Glutathione Sepharose 4B (GE Healthcare) and the remaining BMAL1 PAS-AB protein was further purified by Superdex75 SEC (GE Healthcare) into 20 mM HEPES buffer pH 7.5, 125 mM NaCl, 5% (vol/vol) glycerol, and 2 mM TCEP. Purified BMAL1 PAS-AB was mixed with biotinylated CLOCK PAS-AB (below) to generate the heterodimer for binding assays.

6.5.2 Biotinylation and reconstitution of Biotin-CLOCK:BMAL1 PAS-AB.

For the biotinylation reaction, 100 μM BAP-CLOCK PAS-AB in 20 mM HEPES pH 7.5, 125 mM NaCl, 5% (vol/vol) glycerol, and 2 mM TCEP was incubated at 4˚C overnight with 2 mM ATP, 1 μM GST-BirA and 150 μM biotin. GST-BirA was removed after the reaction using Glutathione Sepharose 4B (GE Healthcare) resin and excess biotin was separated from the labeled protein by SEC. Biotin-CLOCK:BMAL1 PAS-AB heterodimer was reconstituted after labeling by adding equimolar BMAL1 PAS-AB to biotinylated CLOCK PAS-AB and verifying

complex formation by SEC. Biotinylated heterodimer was quick frozen in liquid nitrogen for long-term storage at -80°C.

6.5.3 Fluorescent labeling.

For the Sortase A recognition motif, we purchased commercially synthesized peptides with N-terminal cysteines conjugated to tetramethylrhodamine (TAMRA) 5-maleimide fluorophore or a fluorescein 5-maleimide fluorophore. To fluorescently label recombinantly expressed proteins and peptides, we utilized Sortase A-mediated reactions (23) between an N-terminally fluorescein-labeled (or TAMRA-labeled) Sortase A recognition motif peptide (FAM-LPETGG) and CLOCK PAS-B. We labeled CLOCK PAS-B right after purification via SEC (i.e., without a freeze/thaw cycle). Reactions were carried out in 50 mM Tris, pH 7.5, 150 mM NaCl, and 10 mM $CaCl_2$ using 5 μM His_6-Sortase A and 3-5x molar excess of the fluorescently labeled Sortase A recognition motif peptide relative to the protein to be labeled. Labeled protein was purified from the reaction mixture using Ni-NTA affinity chromatography (Qiagen) and/or followed by SEC. Labeled protein was characterized by fluorescent imaging on an SDS-PAGE gel using a Typhoon imager (GE Healthcare). Extent of labeling was measured through spectrophotometry and calculated using the following equation:

$$\%_{labeled} = \frac{A_{dye}}{\varepsilon_{dye} \times \left(\frac{A_{280} - \left(A_{dye} \times CF\right)}{\varepsilon_{protein}}\right)}$$

where A_{dye} is the absorbance at the maximum absorption wavelength (555 nm for TAMRA and 494 nm for fluorescein), ε_{dye} is the extinction coefficient of the dye (65,000 M^{-1} cm^{-1} for TAMRA and 68,000 M^{-1} cm^{-1} for fluorescein), and the CF is a correction factor that adjusts for the amount of absorbance at 280 nm contributed by the dye (24). We also measured molecular weights of fluorescent probe using a SciEx QTOF mass spectrometer. All probes were labeled with at least 60% efficiency.

6.5.4 Primary Fluorescence Polarization screen

We prepared an FP assay mixture with 0.02 μM of TAMRA labeled CLOCK PAS-B and 7 μM CRY1 PHR in 50 mM Bis-Tris Propane pH 7.5, 100 mM NaCl, 0.05% (vol/vol) Tween, 2 mM TCEP. We used a multichannel pipette to dispense into 384-well black square-well plates (Corning) at 20 μL/well. Compounds or controls were pin transferred using a 200 nL pin tool (PerkinElmer) to a final concentration of 100 μM and 1% DMSO. After incubation with compounds or DMSO, we measured fluorescence polarization and fluorescence intensity using a Perkin Elmer EnVision 2103 Multilabel plate reader with excitation at 485 nm and emission at 535 nm.

For equilibrium competition assays, 0.02 μM fluorescently labeled probe (CLOCK PAS-B, or CRY2 tail) were incubated with unlabeled CRY PHR for 30 minutes on ice. Varying amounts of inhibitor were mixed with this reaction and incubated for 10 minutes at room temperature. Fluorescence polarization measurements were measured on a Perkin Elmer EnVision 2103 Multilabel plate reader with excitation at 485 nm and emission at 535 nm. The equilibrium dissociation constant (K_D) and extent of non-specific binding was calculated by fitting millipolarization level (mp) to a one-site total model in GraphPad Prism using averaged mp values from assays with duplicate samples. IC_{50} values were calculated from displacement assays by fitting the mp level to a one-site competitive binding model in GraphPad Prism, with averaged mp values from assays with duplicate samples. Data shown are from one representative experiment (± sd) of three independent assays.

6.5.5 Biolayer interferometry.

All BLI experiments were performed using an 8-channel Octet-RED96e (ForteBio). We used BLI assay buffer (20 mM HEPES pH 7.5, 125 mM NaCl, 5% (vol/vol) glycerol, 2 mM TCEP) with all conditions at a final DMSO concentration of 1% vol/vol. For conditions with small molecule inhibitors, we added each inhibitor to the BLI assay buffer to establish a baseline reference before association and during dissociation. For each experiment, we used 8 streptavidin biosensor tips (ForteBio). All experiments began with reference measurements

using unloaded streptavidin tips to establish a baseline in BLI buffer, after which non-specific CRY association was measured for 5 minutes in wells containing 2-fold serial dilutions of CRY1 (*e.g.* 4 μM, 2 μM, 1 μM, 0.5 μM, 0.25 μM, etc.) or a reference sample well containing no CRY, and then dissociation was subsequently measured for 5 minutes in wells containing BLI buffer. After measuring our initial reference, we repeated the same assay with fresh tips that were loaded with 1.5 – 3 μg/mL biotinylated CLOCK:BMAL PAS-AB dimer using BLI buffer that contained no BSA or Tween-20. Data were processed and fitted using Octet software v.7 (ForteBio). Before fitting, all datasets were reference-subtracted, aligned on the y-axis through their respective baselines, aligned for interstep correction through their respective dissociation steps, and finally smoothened using Savitzy-Golay filtering. For each experiment, at least 4 different concentrations were used to fit association and dissociation globally over the full range of the experiment using a 1:1 binding model in Octet software v.7 (ForteBio). Goodness of fit was determined with $\chi 2$ and $R2$ tests that conform to the manufacturer's guidelines.

6.6 References

1. Partch CL, Green CB, & Takahashi JS (2014) Molecular architecture of the mammalian circadian clock. *Trends in Cell Biology* 24(2):90-99.

2. Zhang R, Lahens NF, Ballance HI, Hughes ME, & Hogenesch JB (2014) A circadian gene expression atlas in mammals: implications for biology and medicine. *Proceedings of the National Academy of Sciences of the United States of America* 111(45):16219-16224.

3. Bass J & Lazar MA (2016) Circadian time signatures of fitness and disease. *Science* 354(6315):994-999.

4. Hirota T*, et al.* (2012) Identification of small molecule activators of cryptochrome. *Science (New York, N.Y.)* 337(6098):1094-1097.

5. Miller S*, et al.* (2020) An Isoform-Selective Modulator of Cryptochrome 1 Regulates Circadian Rhythms in Mammals. *Cell Chem Biol* 27(9):1192-+.

6. Miller S*, et al.* (2020) Isoform-selective regulation of mammalian cryptochromes. *Nature Chemical Biology* 16(6):676-+.

7. Michael AK*, et al.* (2017) Formation of a repressive complex in the mammalian circadian clock is mediated by the secondary pocket of CRY1. *Proceedings of the National Academy of Sciences* 114(7):1560-1565.

8. Xu H*, et al.* (2015) Cryptochrome 1 regulates the circadian clock through dynamic interactions with the BMAL1 C terminus. *Nature Structural & Molecular Biology* 22(6):476-484.

9. Fribourgh JL*, et al.* (2020) Dynamics at the serine loop underlie differential affinity of cryptochromes for CLOCK:BMAL1 to control circadian timing. *Elife* 9.

10. Sato TK*, et al.* (2006) Feedback repression is required for mammalian circadian clock function. *Nature genetics* 38(3):312-319.

11. Chan AB*, et al.* (2021) CRY2 missense mutations suppress P53 and enhance cell growth. *Proc Natl Acad Sci U S A* 118(27).

12. Nangle SN*, et al.* (2014) Molecular assembly of the period-cryptochrome circadian transcriptional repressor complex. *eLife* 3:e03674.

13. Rosensweig C*, et al.* (2018) An evolutionary hotspot defines functional differences between CRYPTOCHROMES. *Nature Communications* 9(1):1138.

14. Parico GCG*, et al.* (2020) The human CRY1 tail controls circadian timing by regulating its association with CLOCK:BMAL1. *Proc Natl Acad Sci U S A* 117(45):27971-27979.

15. Patke A*, et al.* (2017) Mutation of the Human Circadian Clock Gene CRY1 in Familial Delayed Sleep Phase Disorder. *Cell* 169(2):203-215.e213.

16. Wallach I, Dzamba M, & Heifets A (2015) AtomNet: A Deep Convolutional Neural Network for Bioactivity Prediction
in Structure-based Drug Discovery. *arxiv*.

17. Zhang JH, Chung TD, & Oldenburg KR (1999) A Simple Statistical Parameter for Use in Evaluation and Validation of High Throughput Screening Assays. *J Biomol Screen* 4(2):67-73.

18. Partch CL, Clarkson MW, Ozgür S, Lee AL, & Sancar A (2005) Role of structural plasticity in signal transduction by the cryptochrome blue-light photoreceptor. *Biochemistry* 44(10):3795-3805.

19. Dimova EY*, et al.* (2019) The Circadian Clock Protein CRY1 Is a Negative Regulator of HIF-1alpha. *iScience* 13:284-304.

20. Jordan SD*, et al.* (2017) CRY1/2 Selectively Repress PPARdelta and Limit Exercise Capacity. *Cell Metab* 26(1):243-255 e246.

21. Kriebs A*, et al.* (2017) Circadian repressors CRY1 and CRY2 broadly interact with nuclear receptors and modulate transcriptional activity. *Proc Natl Acad Sci U S A* 114(33):8776-8781.

22. Vaughan ME*, et al.* (2020) Cryptochromes Suppress HIF1alpha in Muscles. *iScience* 23(7):101338.

23. Theile CS*, et al.* (2013) Site-specific N-terminal labeling of proteins using sortase-mediated reactions. *Nature Protocols* 8(9):1800-1807.

24. Anonymous (2011) Calculate dye:protein (F/P) molar ratios. *Thermo Scientific. Tech Tip #31* TR0031.7(TR0031.7).

CHAPTER 7: Conclusions and Future directions

The candidate, Gian Carlo Parico, wrote this concluding chapter.

It's about time? It's about time …

7.1 Conclusions

Protein-protein interactions between CRY and CLOCK:BMAL1 are analogous to interlocking gears of a 24-hour timing mechanism. The orthologs CRY1 and CRY2 each interact with the transcription factor CLOCK:BMAL1 at multiple interfaces to induce repression and close a transcription-translation feedback loop (1). The CRY coiled-coiled (CC) helix binds to the transactivation domain (TAD) of BMAL1 to induce repression (2). Studies on the CRY CC-helix–BMAL1 TAD interaction helped establish a model in which the tighter CRY binds to the BMAL1 TAD, the longer circadian period becomes (2).

In addition to the CC-helix, the CRY secondary pocket makes contacts with CLOCK:BMAL1 through the PAS-B domain of CLOCK (3). The secondary pocket dictates functional differences between CRY1 and CRY2. As described in Chapter 2 of this dissertation, we determined that the affinity between CRY1 and the CLOCK:BMAL1 PAS domain core is 20-fold stronger than the affinity between CRY2 the CLOCK:BMAL1 PAS domain core (4). As a result of this difference in binding affinities, CRY1 reconstitutes circadian rhythms with a longer circadian period in cells compared to rhythms reconstituted by CRY2 (5). As was previously established in earlier work from our lab with BMAL1 TAD (2), these data suggest a model in which the tighter the CRY secondary pocket interacts with CLOCK PAS-B, the longer circadian period becomes (Figure 7.1).

In Chapters 3 and 4, we determined how two disease-related mutations, CRYΔ11 (a prevalent variant that causes delayed sleep phase disorder) and CRY2 D347H (a mutation that has been detected in multiple tumors) affect CRY–CLOCK binding and alter circadian timing. CRY1Δ11 exhibits an enhanced affinity for CLOCK PAS-B and also extends circadian period in human patients thus conforming to the model that relates CRY–CLOCK binding affinity with circadian timing (Figure 7.1) (6, 7). By contrast, CRY2 D347H (and mouse analog CRY2 D325H) exhibits a weaker affinity for CLOCK and fails to restore rhythms in reconstitution assays of cell-autonomous circadian rhythms (8). While it does not quite fit the model that relates CRY–CLOCK binding affinity to length of circadian period, CRY2 D347H

further confirms the importance of the CRY–CLOCK interaction in generating and regulating circadian rhythms.

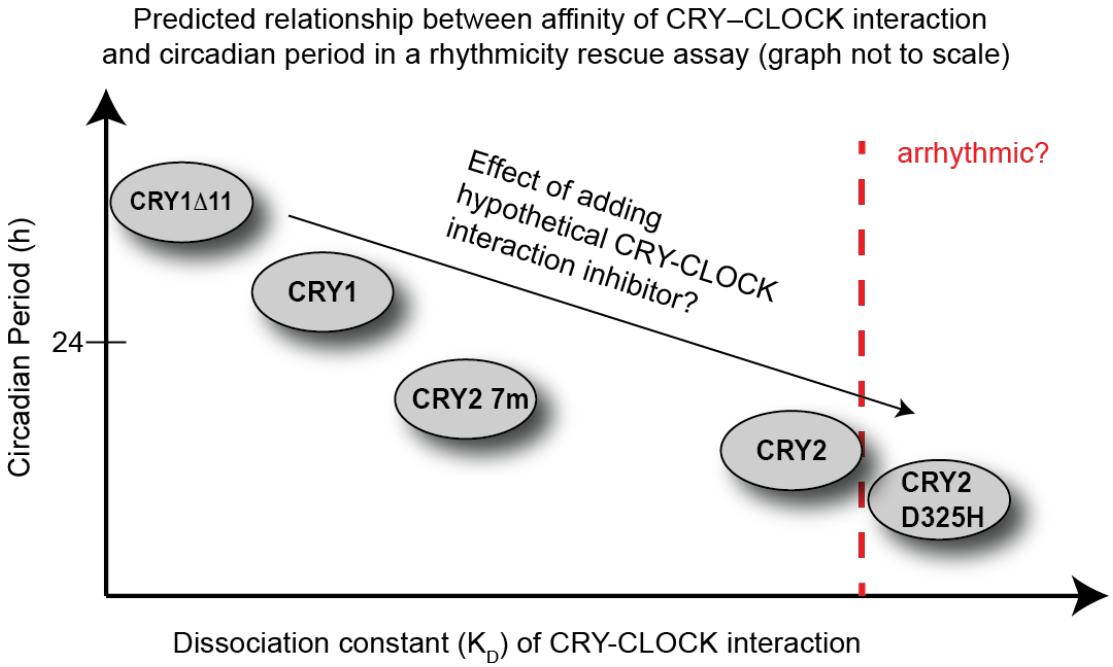

Figure 7.1. The tighter CRY binds to CLOCK PAS-B, the longer circadian period becomes.

Different variants of CRY1 or CRY2 are plotted onto a graph (not to scale) to depict a relationship between the CRY-CLOCK binding affinity and circadian period. CRY2 7m (CRY2 A61G/S64N/S394E/V396M/R379K/D400E/F408W) mutates residues around the secondary pocket and enhances CRY2 affinity for CLOCK PAS-B while also extending period (relative to wild-type CRY2) in cell-autonomous circadian rhythm rescue assays (4, 5).

While CRY2 D347H modifies a residue on the secondary pocket to modulate the CRY2–CLOCK interaction, CRY1Δ11 modifies a different domain of the CRY1 molecule: the intrinsically disordered C-terminal tail. CRY1Δ11 is a splice site mutation that skips and deletes exon 11, thus removing a 24 amino acid residue segment from the CRY1 tail. In addition to the C-terminal tail, all CRYs also possess a conserved photolyase homology region (PHR) where the secondary pocket and CC-helix are located. While the PHR is the necessary and sufficient component for binding CLOCK:BMAL1 to generate circadian

rhythms (9), modifications of the C-terminal tail (including but not limited to CRY1Δ11) also control circadian timing (5, 9-14). In Chapter 3, we determined that the CRY1 C-terminal tails binds to the PHR and that exon 11 is necessary and sufficient to compete with CLOCK PAS-B for binding to the PHR (Figure 7.2A) (6). Since CRY1Δ11 lacks the auto-inhibitory module exon 11, we verified that CRY1Δ11 has an enhanced affinity for CLOCK PAS-B and that CRY1Δ11 is a stronger repressor of CLOCK:BMAL1 than wild-type CRY1 (6). This suggests that the molecular mechanism by which CRY1Δ11 causes delayed sleep phase disorder fits our model: increasing the CRY–CLOCK binding affinity leads to an increase in circadian period.

In addition to the CRY1 tail regulating the secondary pocket on the PHR, we also determined that the CRY1 and CRY2 tails interact with the FAD-binding pocket on the PHR (Figure 7.2A,B). CRY1-specific ligand KL01 and CRY2-selective TH301 bind to the FAD-binding pocket to inhibit binding of ubiquitin ligase substrate receptor FBXL3 thus stabilizing CRY (15). In Chapter 6, I determined that the CRY-selective ligands enhance the PHR–tail interaction, likely near or at the FAD-binding pocket. In Drosophila CRY (dCRY), a light-controlled PHR–tail interaction (mediated by FAD in the FAD-binding pocket) inhibits binding of TIMELESS, one of the core circadian corepressors in Drosophila, in the absence of light (Figure 7.2) (16-18). Despite playing different roles, there is a conserved function in cryptochromes: the PHR–tail interaction creates an autoinhibited conformation that inhibits binding with other proteins. In CRY1, the tail binds to the PHR to inhibit interactions with CLOCK at the CRY1 secondary pocket (via exon 11) and the tail likely inhibits FBXL3 binding to the CRY1 FAD-binding pocket (via exon 10) (Figure 7.2A). By contrast, the CRY2 tail does not inhibit CLOCK binding (see Chapter 7), but the CRY2 tail might also inhibit FBXL3 binding at the CRY2 FAD-binding pocket (Figure 7.2B).

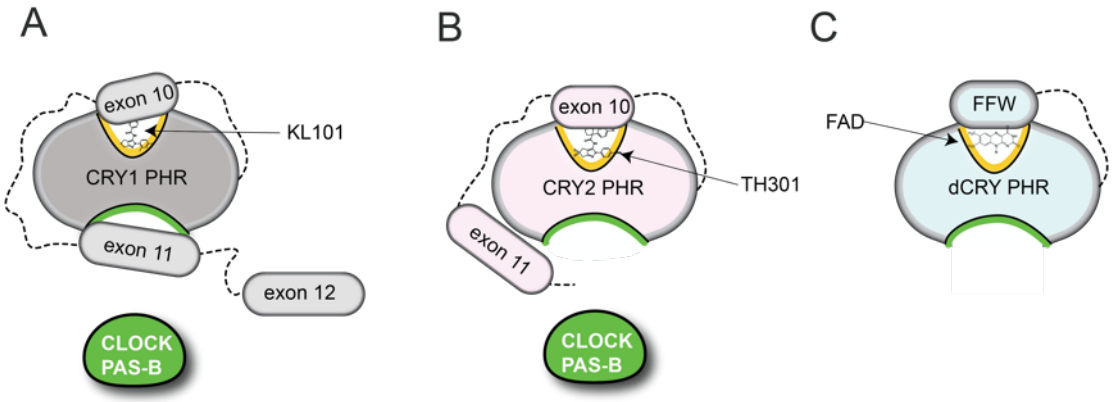

Figure 7.2. PHR-tail interactions are conserved across cryptochromes

(A) Mammalian CRY1 tail (dashed line) interacts with the CRY1 PHR (gray) at different sites: exon 10 interacts with the FAD-binding pocket (yellow cavity) to inhibit FBXL3 binding and exon 11 interacts with the secondary pocket (green cavity) to inhibit binding of CLOCK PAS-B. KL101 in the FAD-binding pocket enhances the exon 10–PHR interaction. ***(B)*** Mammalian CRY2 tail (dashed line) interacts with CRY2 PHR (pink) with exon 10 potentially interacting at the FAD-binding pocket (yellow cavity). TH301 in the FAD-binding pocket enhances the exon 10-PHR interaction. The CRY2 tail does not inhibit CRY2–CLOCK binding. ***(C)*** An FFW motif on the Drosophila (dCRY) tail interacts with the dCRY PHR and the FAD co-factor at the FAD-binding pocket (yellow cavity).

Core circadian co-repressor PER2 also plays a large role in regulating CRY function. PER2 is an “equalizer” for CLOCK binding: while CRY1 has a ~20 fold stronger affinity than CRY2 for CLOCK, CRY1:PER2 only has a ~3 fold stronger affinity than CRY2:PER2 (4). We also found that PER2 competes with the CRY tail for binding to the PHR, suggesting that PER2 and the CRY1 and CRY2 tails have overlapping binding sites on the PHR (6). Since PER2 associates with CRY1 at specific phases during the circadian cycle (19), this implies that CRY1 is temporally regulated through the formation of a CRY1:PER2 complex that weakens both the CRY1–CLOCK interaction and the CRY1 PHR–tail interaction.

Identification of key protein-protein interactions with and within CRYs enable new strategies for modulating circadian rhythms. We established a model in which the tighter CRY binds to CLOCK PAS-B, the longer circadian period becomes. The CRY–CLOCK interaction can thus be targeted to modulate circadian rhythms. Some of the structural models generated in Chapter 2 can be used to computationally screen for molecules that can bind to the CRY

secondary pocket and potentially inhibit binding of CLOCK. In Chapter 6, I describe a strategy for screening molecules that can modulate CRY1–CLOCK binding, likely by binding to the CRY1 secondary pocket. This approach was made more practical by the discovery that a peptide based on exon 11 is a positive control for CRY1–CLOCK inhibition. In conclusion, increased understanding of the biochemical interactions of core circadian proteins will bring us closer to finding novel therapeutic strategies for circadian rhythm disorders and beyond.

7.2 Future Directions

7.2.1 Determining the structure of full-length mammalian cryptochromes

There are currently no structures of mammalian CRY1 or CRY2 that demonstrate how the PHR and the tail interact. Possible reasons include spontaneous proteolysis of the CRY tail during preparation of CRY crystals or that the C-terminal tail may be too disordered to crystallize. As an alternative approach to crystallography, we utilized nuclear magnetic resonance (NMR) spectroscopy to probe the CRY1 tail in solution and determine how it interacts with the PHR at the amino-acid residue level (6). Unfortunately, while we have some insight into regions on the tail that may bind to the PHR, we have not been able to map tail interaction sites definitively on the PHR, as there are practical limitations in directly probing the CRY PHR by NMR due to its size (~55 kDa) and expression of the recombinant protein in Sf9 cells. Finally, mass-spectrometry based methods such as hydrogen-deuterium exchange mass spectrometry or cross-linking mass spectrometry might also yield low resolution structures of full-length cryptochromes.

Despite the obstacles in studying full-length cryptochromes, the recent discovery of the CRY-binding ligands KL101 and TH301 may aid in structural studies that probe the CRY PHR-tail interaction (15). We recently determined that KL101 and TH301 enhances the binding affinity between the PHR and the tail. It could be possible that KL101 or TH301 can orient the the tail in a more stable conformation amenable for structure determination and/or further protect the tail from proteolysis while bound to the PHR.

While structural determination of full-length CRY1 or CRY2 remains difficult, the predicted structures from the AlphaFold Protein Structure Database might also aid in generating testable hypotheses for how the CRY tail binds the PHR (20). While NMR can map binding sites on the CRY1 tail (but not the PHR), AlphaFold predictions can recommend novel point mutations at the PHR that can potentially affect PHR–tail binding rather than using a more brute-force approach with mutagenesis. However, AlphaFold still presents a high predicted aligned error with regards to the relative positions between the tail and the rest of the CRY1 molecule (Figure 7.3) (20). Therefore, biochemical mapping and mutagenesis should still be performed in the context of previous experimental work. For instance, AlphaFold predicts that a region within exon 10 ("LMGY") interacts with specific residues near or at the FAD-binding pocket (Figure 5.3B). Even though there is a low confidence score for AlphaFold predicting the CRY1 tail conformation, my NMR spectroscopy studies also suggested that the LMGY region within exon 10 is an epitope for binding to the CRY1 PHR (6). Additionally, AlphaFold also predicts that LMGY region also interacts with residues on the PHR that are modified by KL101 or TH301 (15). Since I verified that exon 10 is essential for the activity of KL101 and TH301, then it is possible to mutate those specific sites on the PHR (or tail) and confirm if these mutants affect the PHR–tail interaction.

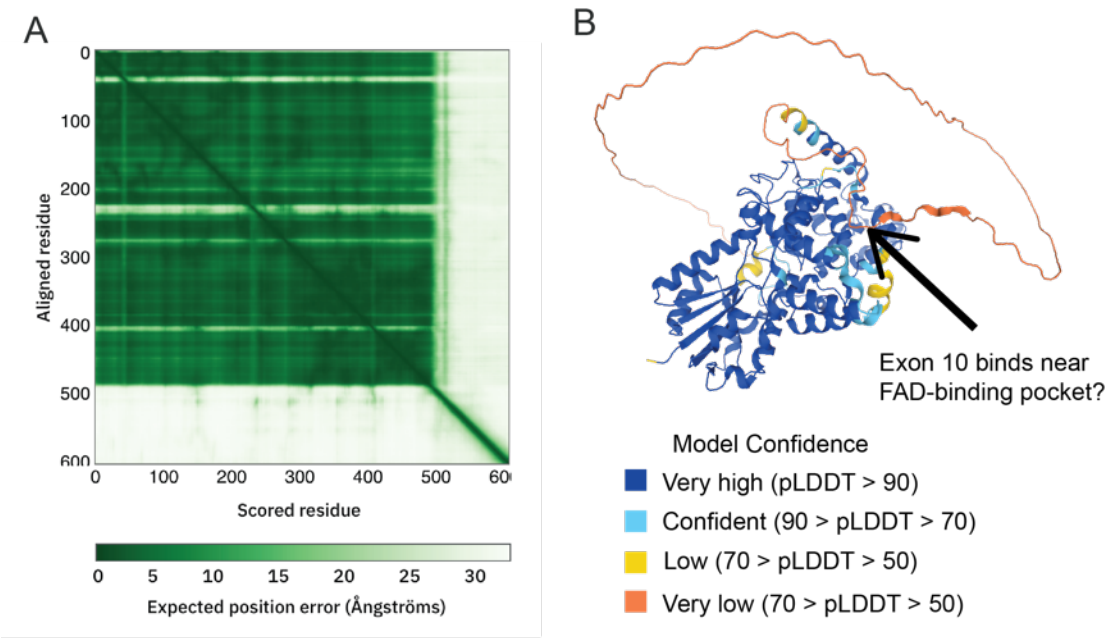

Figure 7.3. Analysis of the AlphaFold prediction for mCRY1

(A) Predicted aligned error maps that indicates expected position error at residue x if the predicted and true structures were aligned on residue y. Residues within the PHR (residues 1-491) present low expected position error relative to other residues within the PHR, while residues on the tail (residues 492-610) present high expected position error relative to all other residues on the mCRY1 structure (20). ***(B)*** Model confidence of the AlphaFold prediction for mCRY1. AlphaFold has a high confidence score for the PHR (blue, very high pLDDT, predicted local distance test) but a very low confidence score for the tail (orange, very low pLDDT) (20).

7.2.2 Identification of molecules that target the PAS domains of CLOCK:BMAL1

In Chapter 6, I described a strategy to screen for small molecules that can modulate CRY1–CLOCK binding. While we initially screened compounds that were computationally predicted to bind to the CRY1 secondary pocket, it might also possible for CRY1–CLOCK interaction inhibitors to bind to the PAS-B domain of CLOCK instead. PAS domains contain an internal cavity or pocket that can potentially bind a ligand (21). Based on the crystal structures of the CLOCK:BMAL1 bHLH PAS-AB heterodimer (22), CLOCK PAS-B has an internal cavity with a volume of about 146.6 $Å^3$. While the predicted volume might be too small to bind a drug, the flexibility of the CLOCK PAS-B domain may also allow the cavity to expand and accommodate binding of a small molecule ligand (Figure 7.4A) (23).

As a hub of protein-protein interactions in the core circadian loop, CLOCK PAS-B makes significant interactions with proteins other than just CRY1/2. The formation of the CLOCK:BMAL1 heterodimer is partially mediated by an interaction between CLOCK PAS-B and BMAL1 PAS-B (22). The isolated PAS-B domains of CLOCK and BMAL1 can also form a heterodimer (3). Modulating the interaction between the PAS domains of CLOCK and BMAL1 through mutation or inhibition by small molecules could affect the transcriptional activity of CLOCK:BMAL1 and affect circadian timing (22, 24).

There are various approaches to discover new ligands that can bind within PAS domains and modulate their interactions with other proteins. Ligands that regulate transcriptional activity of hypoxia inducible factor 2α - ARNT (HIF2α:ARNT), a bHLH-PAS transcription factor related to CLOCK:BMAL1, do so by binding within the HIF2α PAS domain and modulating the interaction with the PAS domain of its binding partner ARNT (24-27). These HIF2α binding ligands were discovered using techniques such as NMR spectroscopy and thermal shift assays, and there is ongoing work to apply these techniques to probe CLOCK PAS-B and BMAL1 PAS-B (Figure 7.4B,C). Furthermore, the placement of cysteine residues proximal to the internal cavities of CLOCK PAS-B and BMAL1 PAS-B also makes these proteins candidates for covalent tethering approaches (Figure 7.4D), a method that leverages mass spectrometry to screen for weakly binding ligands that covalently react to cysteine residues on a protein target (28). Overall, these strategies could potentially yield new chemical tools to modulate circadian rhythms.

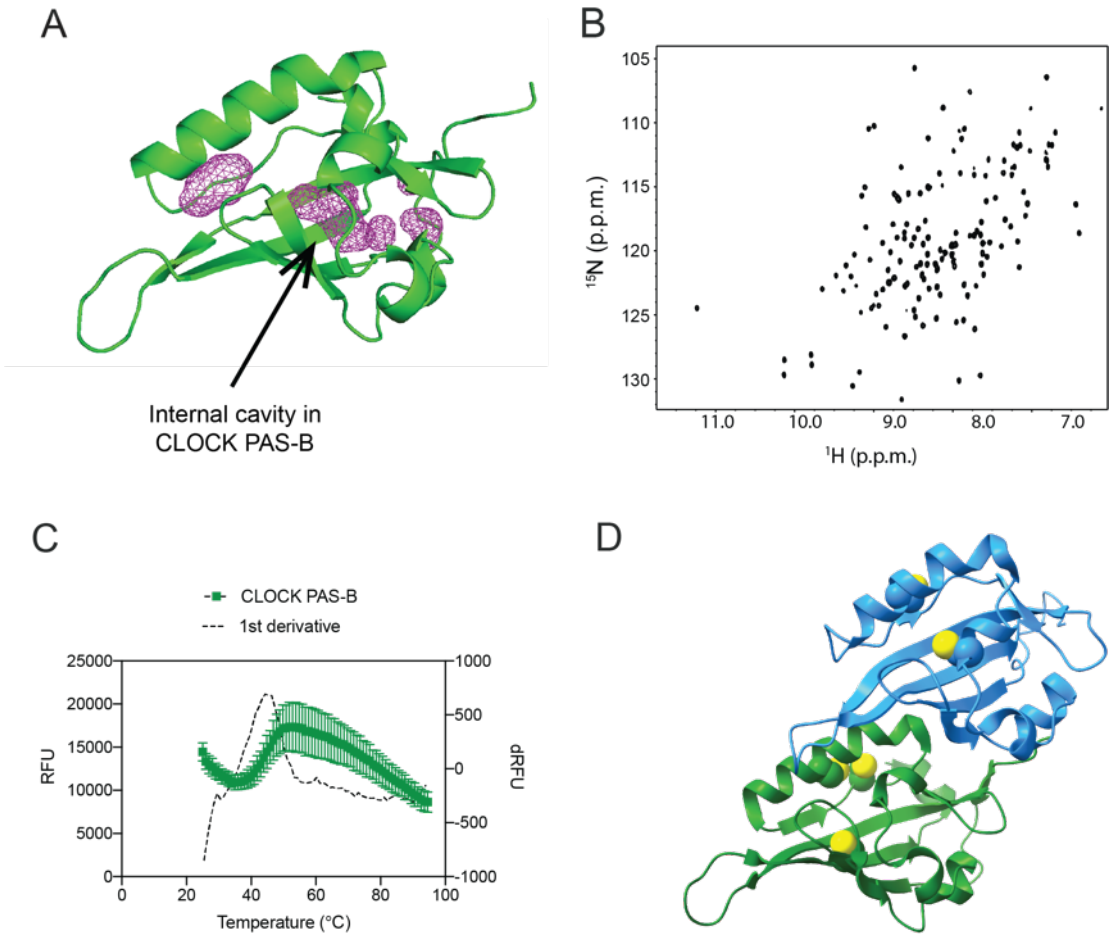

Figure 7.4. Various methods to detect ligands that bind CLOCK:BMAL1 PAS domains.

(A) Crystal structure of CLOCK PAS-B (green, PDB 4F3L) highlighting an internal cavity (pink mesh) with a calculatd volume of 146.6 Å^3. ***(B)*** HSQC NMR spectrum of CLOCK PAS-B (Figure adapted from Michael, et al.) ***(C)*** Example of a protein melt assay using CLOCK PAS-B (green) measuring fluorescence of SYPRO orange (RFU, relative fluorescence units) versus temperature and the first derivative of fluorescence versus temperature (black dashed line) denoting T_m = 44°C. ***(D)*** Structures of BMAL1 PAS-B (blue, PDB ID 4F3L) and CLOCK PAS-B (green) highlighting cysteine residues (yellow) adjacent to internal cavities and/or protein interaction interfaces.

7.3 References

1. Sato TK*, et al.* (2006) Feedback repression is required for mammalian circadian clock function. *Nature genetics* 38(3):312-319.

2. Xu H*, et al.* (2015) Cryptochrome 1 regulates the circadian clock through dynamic interactions with the BMAL1 C terminus. *Nature Structural & Molecular Biology* 22(6):476-484.

3. Michael AK*, et al.* (2017) Formation of a repressive complex in the mammalian circadian clock is mediated by the secondary pocket of CRY1. *Proceedings of the National Academy of Sciences* 114(7):1560-1565.

4. Fribourgh JL*, et al.* (2020) Dynamics at the serine loop underlie differential affinity of cryptochromes for CLOCK:BMAL1 to control circadian timing. *Elife* 9.

5. Rosensweig C*, et al.* (2018) An evolutionary hotspot defines functional differences between CRYPTOCHROMES. *Nature Communications* 9(1):1138.

6. Parico GCG*, et al.* (2020) The human CRY1 tail controls circadian timing by regulating its association with CLOCK:BMAL1. *Proc Natl Acad Sci U S A* 117(45):27971-27979.

7. Patke A*, et al.* (2017) Mutation of the Human Circadian Clock Gene CRY1 in Familial Delayed Sleep Phase Disorder. *Cell* 169(2):203-215.e213.

8. Chan AB*, et al.* (2021) CRY2 missense mutations suppress P53 and enhance cell growth. *Proc Natl Acad Sci U S A* 118(27).

9. Khan SK*, et al.* (2012) Identification of a Novel Cryptochrome Differentiating Domain Required for Feedback Repression in Circadian Clock Function. *Journal of Biological Chemistry* 287(31):25917-25926.

10. Gao P*, et al.* (2013) Phosphorylation of the Cryptochrome 1 C-terminal Tail Regulates Circadian Period Length. *The Journal of Biological Chemistry* 288(49):35277-35286.

11. Hirano A*, et al.* (2014) In vivo role of phosphorylation of cryptochrome 2 in the mouse circadian clock. *Mol Cell Biol* 34(24):4464-4473.

12. Li Y, Xiong W, & Zhang EE (2016) The ratio of intracellular CRY proteins determines the clock period length. *Biochem Biophys Res Commun* 472(3):531-538.

13. Liu N & Zhang EE (2016) Phosphorylation Regulating the Ratio of Intracellular CRY1 Protein Determines the Circadian Period. *Frontiers in Neurology* 7.

14. Papp SJ*, et al.* (2015) DNA damage shifts circadian clock time via Hausp-dependent Cry1 stabilization. *Elife* 4.

15. Miller S*, et al.* (2020) Isoform-selective regulation of mammalian cryptochromes. *Nature Chemical Biology* 16(6):676-+.

16. Busza A, Emery-Le M, Rosbash M, & Emery P (2004) Roles of the Two Drosophila CRYPTOCHROME Structural Domains in Circadian Photoreception. *Science* 304(5676):1503-1506.

17. Dissel S*, et al.* (2004) A constitutively active cryptochrome in Drosophila melanogaster. *Nature Neuroscience* 7(8):834-840.

18. Rosato E*, et al.* (2001) Light-dependent interaction between Drosophila CRY and the clock protein PER mediated by the carboxy terminus of CRY. *Curr Biol* 11(12):909-917.

19. Koike N*, et al.* (2012) Transcriptional Architecture and Chromatin Landscape of the Core Circadian Clock in Mammals. *Science (New York, N.Y.)* 338(6105):349-354.

20. Jumper J*, et al.* (2021) Highly accurate protein structure prediction with AlphaFold. *Nature*.

21. Vreede J, van der Horst MA, Hellingwerf KJ, Crielaard W, & van Aalten DM (2003) PAS domains. Common structure and common flexibility. *J Biol Chem* 278(20):18434-18439.

22. Huang N*, et al.* (2012) Crystal structure of the heterodimeric CLOCK:BMAL1 transcriptional activator complex. *Science (New York, N.Y.)* 337(6091):189-194.

23. Loving KA, Lin A, & Cheng AC (2014) Structure-based druggability assessment of the mammalian structural proteome with inclusion of light protein flexibility. *PLoS Comput Biol* 10(7):e1003741.

24. Doruk YU*, et al.* (2020) A CLOCK-binding small molecule disrupts the interaction between CLOCK and BMAL1 and enhances circadian rhythm amplitude. *J Biol Chem* 295(11):3518-3531.

25. Key J, Scheuermann TH, Anderson PC, Daggett V, & Gardner KH (2009) Principles of ligand binding within a completely buried cavity in HIF2alpha PAS-B. *J Am Chem Soc* 131(48):17647-17654.

26. Scheuermann TH*, et al.* (2009) Artificial ligand binding within the HIF2alpha PAS-B domain of the HIF2 transcription factor. *Proc Natl Acad Sci U S A* 106(2):450-455.

27. Wu D*, et al.* (2019) Bidirectional modulation of HIF-2 activity through chemical ligands. *Nat Chem Biol* 15(4):367-376.

28. Erlanson DA*, et al.* (2000) Site-directed ligand discovery. *Proc Natl Acad Sci U S A* 97(17):9367-9372.